DEVOLOPMENT OF NOVEL BIOACTIVE SCAFFOLDS FOR HARD TISSUE REPLACEMENT

By

KAPIL CHOPRA

A thesis submitted to the
University of Manchester
for the degree of
Doctor of Philosphy
in the
Faculty of Engineering and Physical Sciences

2007

Manchester Materials Science Centre
University of Manchester

ProQuest LLC.
789 East Eisenhower Parkway
P.O. Box 1346
Ann Arbor, MI 48106 – 1346

(ET6LX)

X

Th 30520

TABLE OF CONTENTS

LIST OF FIGURES

LIST OF TABLES

ABSTRACT

This thesis presents an investigation of the use of a novel fabrication technique to produce three-dimensional porous scaffolds with controlled geometry and interconnections that may be used as load bearing implants. The work is presented in two parts. First, the fabrication of composite scaffolds and moulds for ceramic scaffolds; and second, a study of the adhesion of osteoblasts on these scaffolds. Bioactive glass LG112 and polyethylene glycol diacrylate (PEGDA) composite scaffolds were fabricated using stereolithography with a 40 vol.% fraction of ceramic loading. Stereolithography was also used to fabricate moulds for gel casting LG112 suspensions, to produce glass-ceramic scaffolds. All scaffolds had controlled geometry, with all interconnected channels of the same size.

Both composite and glass-ceramic scaffolds were then tested for cell attachment using human osteoblasts. Attachment of cells was characterised using light, scanning electron and confocal microscopy. It was found that the cells adhered and spread well on glass-ceramic scaffolds, and spread throughout the entire scaffold with time, producing extracellular matrix and leading to mineralisation. Cell attachment proved unsuccessful with composite scaffolds. This was caused by the toxic effects of uncured photoinitiator present in the system, and hence cells were not able to attach to the surface.

The principal aim of this study was to determine the feasibility of using stereolithography to fabricate three dimensional scaffolds for use in high load bearing applications. The scaffolds demonstrated similar mechanical properties to human trabecular bone, but were not as stiff or strong as cortical bone. This means that the materials used in this study have proven that 3-D scaffolds fabricated using this technique can only be used for non-load bearing applications at this stage.

DECLARATION

No portion of the work referred to in this thesis has been submitted in support of an application for another degree or qualification of this or any other university or other institute of learning.

COPYRIGHT STATEMENT

(i) Copyright in text of this thesis rests with the author. Copies (by any process) either in full, or of extracts, may be made only in accordance with instructions given by the author and lodged in the John Rylands University Library of Manchester. Details may be obtained fromthe Librarian. This page must form part of any such copies made. Further copies (by any process) of copies made in accordance with such instructions may not be made without the permission (in writing) of the author.

(ii) The ownership of any intellectual property rights which may be described in this thesis is vested in the University of Manchester, subject to any prior agreement to the contrary, and may not be made available for use by third parties without the written permission of the University, which will prescribe the terms and conditions of any such agreement.

(iii) Further information on the conditions under which disclosures and exploitation may take place is available from the Head of School of the School of Materials.

ACKNOWLEDGEMENTS

First of all, I would like to thank my supervisors Dr. Julie Gough and Dr. Paul Mummery for their invaluable support and advice over the last three years. Thanks also to Prof. Brian Derby for the discussions on Stereolithography.

I would also like to thank Prof. David Wood and Dr. Nigel Bubb from the Dental School, Univerisity of Leeds, for providing the bioactive glass.

A special thanks to Mr. Andrew Wallwork for the support he gave me throughout my PhD, along with Dr. Rachel Saunders who helped me will cell work. Thanks to all my friends especially Divya and B.B.Singh who kept pushing me to get things done, the E13 crew, who made this a great experience, and last but certainly not the least, I would like to thank my parents for their support and understanding.

1. Introduction

A *Biomaterial* is a non-viable material used in medical devices intended to interact with biological systems. Biomaterials may be distinguished from other materials in that they possess a combination of properties (chemical, mechanical, physical and biological) that render them suitable for safe, effective and reliable use within a physiological environment (Park *et al.*, 1992).

Biomaterials have many applications and are extremely important in the field of medical research. Modern technology has made it possible to replace body parts with artificial materials that have been diseased or damaged or for cosmetic reasons. The development of synthetic materials and their employment in tissue engineering has become an alternative to bone grafting materials, and in the past few years, increasing attention has been given to composites made of polymers and ceramics.

A new type of ceramic bone replacement material was developed by Larry Hench over 30 years ago known as bioactive glass (Jones *et al.*, 2001). Bioactive glasses are synthetic materials mainly consisting of calcium, phosphorus, silicon and sodium, although many variations of these constituents are present. These bioceramics are not resorbed but undergo corrosion, which means the material slowly degrades and is finally completely dissolved (Jones *et al.*, 2001).

There are several types of bioceramics that are being investigated for tissue engineering including University of Limerick bioactive glass, LG112. This thesis describes the manufacture and characterisation of porous three-dimensional scaffolds to be used as load-bearing bone implants, made using bioactive material (LG112 glass-ceramic). A solid free-form fabrication technique known as Stereolithography was implemented to manufacture these porous scaffolds with controlled internal geometry to facilitate cell growth and differentiation.

2. Literature review

The main objective of this research is to fabricate porous scaffolds of controlled geometry using a bioactive material, using novel free-form fabrication techniques and to study their mechanical properties in order for them to be used as load-bearing implants.

When developing engineered materials for medical applications, it is important to have an understanding of the natural material that the synthetic one is designed to replace. Therefore this chapter will begin by considering the roles that natural bone has to fulfil; looking at the way Nature has devised a complex composite structure to provide suitable mechanical and biological properties to meet these demands. It is also important to understand its regenerative abilities and the way it responds to injury.

Another aspect would also be to consider the circumstances under which a bone implant might be required and the mechanical and biological properties the material should possess. The body's reaction to foreign materials within a bony defect and the interactions between the natural and synthetic material will also be discussed. The techniques that are used to secure these implants in place and their inadequacies, which lead to clinical problems, are also presented. At this point the concept of using bioactive materials will be introduced, as an alternative to the current procedures and materials. Emphasis will be placed specifically on bioactive glass-ceramics, which are the focus of this study.

The potential advantages of techniques used to fabricate custom-made implants with controlled geometry and internal architecture will be discussed, with particular attention given to gel casting and stereolithography. Upon fabrication of these scaffolds, their mechanical properties will also be studied demonstrating their potential to be used as load-bearing implants. Finally, a brief introduction to cell culture is provided for cellular attachment and differentiation on the scaffolds.

2.1. Natural bone

Bone is a specialised form of dense connective tissue that serves as the primary structural material for a range of vertebrates. As the precise structure and properties of bone have adapted to suit each particular species, this literature review will focus primarily on human bone.

2.1.1. Functions of Human Bone

Human bone has four main functions (Martini, 1995):

- To provide structural support for the body against external forces.
- To act as a lever system to transfer the magnitude and directions of the forces generated by skeletal muscles and ligaments.
- To provide protection for vital internal organs and delicate tissues.
- To act as a mineral reserve – 97% of the body's calcium is stored in bone.

2.1.2. Composition and Structure of Human Bone

Bone is a composite material containing both organic (35%) and inorganic (65%) components (Martin et al., 1998). The organic components include cells such as osteoblasts, osteocytes and osteoclasts, and 'osteoid', which consists of a collagenous framework set within a glycosaminoglycan gel. This gel contains specific glycoproteins (e.g. osteocalcin) which strongly bind calcium. The collagen is secreted by osteoblasts and self-assemble into bundles of interlacing fine parallel fibrils. There are twenty eight different types of collagen in mature bone, each determined by the particular sequence of amino acids in its molecules, although those of Type I are by far the most abundant (Boyd *et al.*, 1956). The specialised support cells reside either on the surface of bone or within small cavities (lacunae) within the bone.

The structure of collagen is based on the helical arrangement of three non-coaxial, helical polypeptides, stabilised by inter-chain hydrogen bonds (figure 2-1). Three of these, coil around a central axis leading to a triple helix structure, commonly referred to as tropocollagen (Vincent, 1982). The tropocollagen molecules have an inherent tendency to combine together to form microfibrils, by bonding head to tail with molecules in neighbouring files. Many of these microfibrils become aligned in a staggered fashion, overlapping by a quarter of their length to form a cross-striated collagen fibril.

Tropocollagen molecules are 260 nm long, with a gap between the head of one molecule and the tail of the next. This gap is referred to as the "hole region", which has a characteristic 64 nm periodicity (Wainwright *et al.*, 1976). This gap is significant in

mineralised tissues as the deposition of mineral phases are said to be controlled in this region (Wainwright *et al.*, 1976).

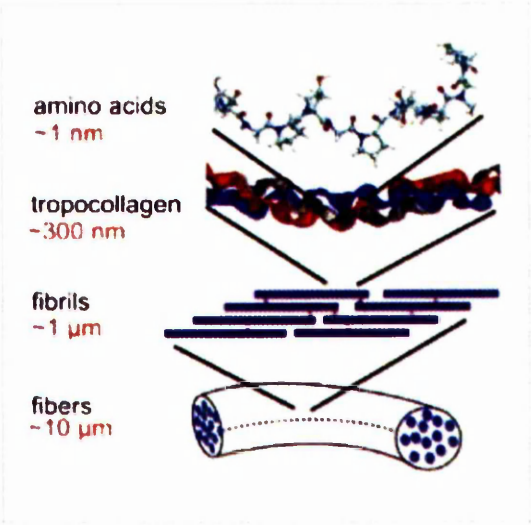

Figure 2-1 Components of Collagen fibres (http://www.sciencedaily.com/images/2006/11/061114190020.jpg).

The inorganic mineral component of bone tissue is predominantly calcium phosphate [$Ca_3(PO_4)_2$], which accounts for almost two-thirds of the weight of bone. It interacts with calcium hydroxide [$Ca(OH)_2$] to form crystals of hydroxyapatite (HA) [$Ca_{10}(PO_4)_6(OH)_2$] in a wet environment. Apatite is usually referred to as crystalline but some amorphous mineral may co-exist (Currey, 1984). These crystals are hexagonal prisms, approximately 5 x 20 x 40 nm (Katz *et al.*, 1973) in size and are arranged in parallel layers that traverse the collagen fibrils (Weiner and Traub, 1986). As the crystal particles are significantly larger than the diameter of a single collagen fibril, the crystal layers span several adjacent collagen fibrils.

These collagen fibres provide an organic framework for the deposition of hydroxyapatite crystals (figure 2-2). These crystals form small platelets and rods that are locked into the collagen fibres. The result is a protein – crystal combination with properties intermediate between those of collagen and those of pure mineral crystals (Martini, 1998). It is thought that the mineral is initially deposited in the gaps between the tropocollagen molecules i.e. in the quarter stagger, i.e. resulting in the initial mineralisation having a 64 nm periodicity (Berthet-Colominas and White, 1979). The basis of this conclusion is that it is highly

probable that in some way the particular conformation of the collagen molecule allows it to act as a nucleation site, permitting the precipitation of mineral, which without the presence of the energetically favourable sites, could not come out of solution (Currey, 1984). Later, the mineral is deposited all over the collagen fibrils and to some extent within them, with specific alignment with the collagen fibrils. Finally, mineral is deposited between the fibrils, in the amorphous and tenuous ground substance.

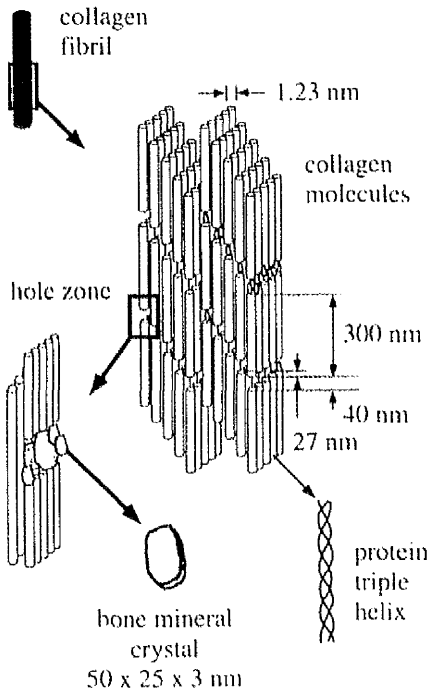

Figure 2-2 Arrangement of collagen molecules and bone mineral within a collagen fibril (Weiner et al., 1998).

It is these collagen fibrils organised into fibres which are typically laid down parallel to one another to produce mature (lamellar) bone. Lamellar bone is formed of numerous stacked layers composed of many collagen fibres parallel to other fibres in the same layer. The fibres run in opposite directions in alternating layers, assisting in the bone's ability to resist torsion forces. At periods of repair or growth, bone is rapidly formed and the fibres are randomly arranged in an irregular, loosely inter-twined pattern and this is called woven bone. After a break, woven bone quickly forms and is gradually replaced by slow-growing lamellar bone. The collagen in woven bone is fine fibred with a diameter of 0.1 μm (Currey, 1984), which is orientated randomly. The fibres are in a three dimensional network instead of being confined within lamellae (Swanson, 1971). As in most bone,

woven bone also contains osteocytes and blood vessels, which are imprisoned in cavities (lacunae) and connect via delicate processes in channels (canaliculi) to neighbouring osteocytes and ultimately to blood channels (Figure 2-3).

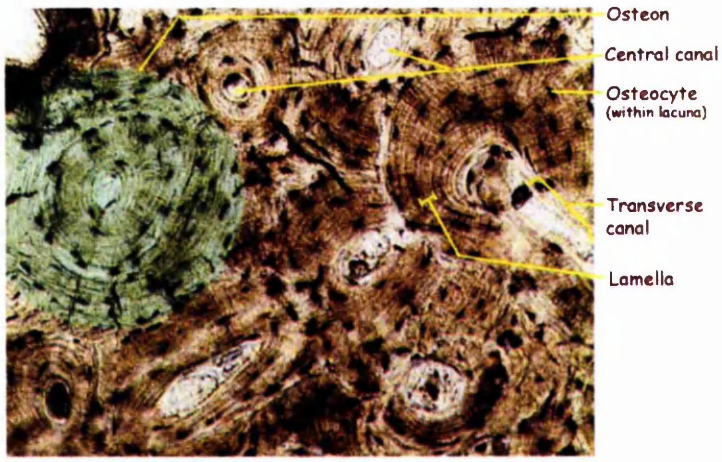

Figure 2-3 Scanned electron micrograph of compact bone (http://www.lionden.com/MicroBone.jpg).

At the next higher order of structure, a bone can be characterised as a porous material, and whilst the porosity of mature bone can vary between 5-95%, the majority of bone can be considered as being either compact (low porosity) or spongy (high porosity) bone (figure 2-4).

It is the compact bone that consists of a large number of closely packed, irregularly spaced cylinders of bone, termed osteons or Haversian systems, which can be seen in figure 2-3. These structures are made up of a central osteonic (Haversian) canal approximately 200 μm in diameter which contains blood vessels and some nerves, surrounded by concentric rings (lamellae) of bony tissue, with collagen fibres of successive lamellae running at approximately right angles to those in the previous one.

Spongy (trabecular) bone consists of a 3-dimensional pattern of branching plates or struts (trabeculae) approximately 100 μm thick (Martin, 1999). There are no Haversian canals in these structures as they are too thin to contain any osteons. Instead the spaces between the trabeculae are occupied by connective tissue or bone marrow.

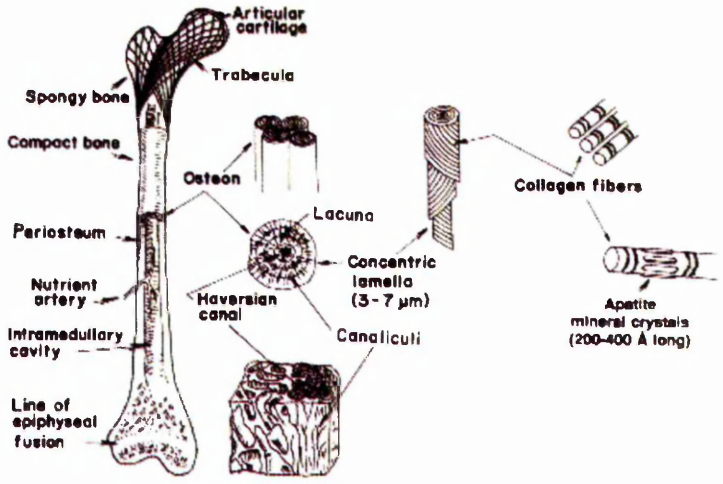

Figure 2-4 Organisation of a typical bone (Park and Lakes, 1982).

2.1.3. Mechanical Properties of Human Bone

The presence of hydroxyapatite crystals within the osteoid matrix results in a material with properties intermediate between those of collagen and those of the mineral crystals. The HA crystals give bone its characteristic hardness and rigidity, preventing damage to the bundles of collagen fibres. However, being ceramics, they are relatively inflexible, brittle and have poor impact resistance. They have good resistance to compression, but are susceptible to failure when exposed to bending, twisting or sudden impacts. It is the organic components, particularly collagen, which are responsible for the flexibility of bone. They can easily withstand bending and twisting, but have poor compressive strength (Martini, 1998).

The exact mechanical properties of bone are difficult to define, being determined by a number of factors including orientation of collagen fibres, degree of mineralisation, and porosity (Martini, 1998). The mechanical properties of a natural fibre composite depend on many parameters such as fibre strength, modulus, fibre length and orientation, in addition to the fibre-matrix interfacial bond strength i.e. the structure of the composite. In particular, they depend on the shape of the inhomogeneties, on the volume fraction occupied by them, and the interface between the constituents (Martini, 1998).

The strength of bone depends (as with most other materials), on the loading regime (i.e. tension, compression and flexion) and the rate of loading. Bone is also anisotropic which leads to the mechanical properties of bone being dependant on the orientation of the bone

structure with respect to the direction of the applied force. Thus, bone is stronger and stiffer in the longitudinal direction, i.e. parallel to the long axis of the osteons, than in the transverse direction. Bone is stronger in compression than in tension, and is weakest in shear. Table 2-1 summarises the ranges of strengths of compact bone reported by Yaszemski *et al.*, (1996) compiled from a number of sources.

Table 2-1 Mechanical properties of femoral compact bone (Yaszemski et al., 1996).

Loading Mode		**Ultimate Strength (MPa)**	**Elastic Modulus (GPa)**
Longitudinal	Tension	78.8 – 151	17 – 20
	Compression	131 – 224	17 – 20
	Shear	53.1 – 70	3.3
Transverse	Tension	51 – 56	6 – 13
	Compression	106 – 133	6 – 13

The material properties of bone are greatly influenced by its apparent density, which is the mass of bone divided by the bulk volume. Compact bone has an apparent density of approximately 1.8 gcm^{-3}, and is significantly stronger and stiffer than spongy bone, whose density varies between 0.1 to 1.0 gcm^{-3} (Yaszemski *et al.*, 1996). The strength of trabecular bone varies widely over the range of different densities. The strength varies as the square of the apparent density, and the modulus varies as the cube of the apparent density (Deligianni *et al.*, 1991). The strength and modulus are both sensitive to the rate of loading. This is a manifestation of the viscoelastic nature of bone. Midrange values for trabecular bone strength and modulus that can serve as design goals for replacement materials are 5 -10 MPa strength and 50 -100 MPa modulus (Ratner *et al.*, 1996). The modulus or strength of compact bone is affected proportionally more, by changes in porosity than spongy bone (Yaszemski *et al.*, 1996).

Although the mineral content of bone is more consistent than its porosity, changes in mineralisation have a greater effect on the mechanical properties of bone. Loss of

mineralisation (or bone mineral density as in osteoporosis) results in a weaker and less stiff structure with an increased risk of fracture (Wright *et al.*, 1977).

Osteonal compact bone has been found to be weaker and less stiff than primary bone (Rilley *et al.*, 1974). It is thought that this results from the formation of Haversian systems, which replace the highly mineralised bone matrix, and the subsequent increase in canals also increases the porosity of the structure. However its fracture toughness and fatigue resistance are superior. This has been attributed to the interfaces between lamellae and osteonal cement lines trapping and dispersing cracks into longitudinal directions, thus preventing growth of traverse cracks which may have otherwise led to fracture (Piekarski, 1970).

Bone is viscoelastic, with the strength and modulus both being sensitive to the rate of loading. Increased strain rates have been shown to reduce ductility of compact bone loaded in compression, but increase the modulus and strength (McElhaney, 1996).

The age and health of the individual may also affect the mechanical properties of their bones. McCalden *et al.* (1993) found the tensile strength of the human femur to be approximately 120 MPa at the age of 20, but to decrease to approximately 65 MPa by the age of 95. This was due to the increase in porosity of bone, as the mineral content was not affected. The strength of the tibia however did not exhibit such a marked decrease with age (Burnstein *et al.*, 1976).

2.1.4. Bone development and remodelling

Bone is formed by specialised cells known as osteoblasts, which are thought to derive from osteogenic stem cells. The cuboidal cells synthesise and release the proteins and other organic components of the bone matrix in a process known as 'osteogenesis'. Following production of osteoid, most osteoblasts return to an inactive state at the surface of bone, having adopted a flattened and more spindle-like shape. Some osteoblasts however become trapped within the bone, residing in small cavities (lacunae) (Figure 2-5). These cells, which are then known as osteocytes, account for most of the cell population and are thought to be involved in the mineralisation process and participate in the repair of damaged bone. The lacunae are connected by canaliculi, narrow channels containing long

cytoplasmic process that allow adjacent osteocytes to communicate with each other and receive nutrients (Martini, 1998).

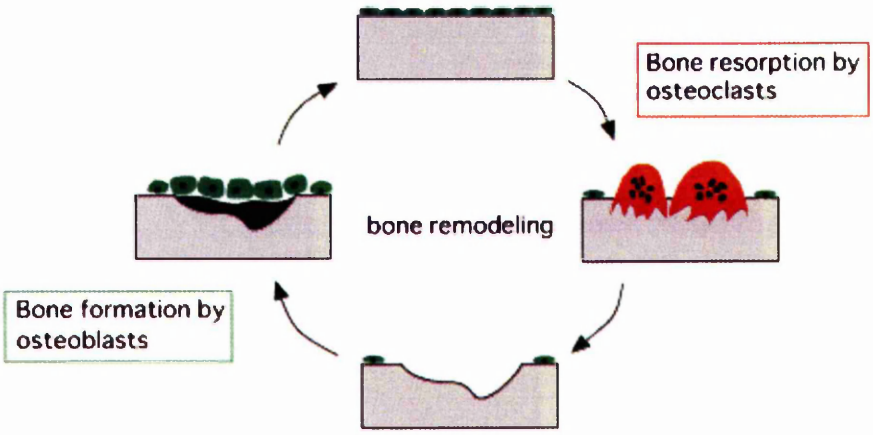

Figure 2-5 Deposition of bone matrix by osteoblasts and resorption by osteoclasts (http://www.endotext.org/parathyroid/parathyroid1/figures/figure5.jpg).

Mineralised bone is resorbed by giant multi-nucleated cells called osteoclasts, which are thought to be derived from hemopoietic stem cells in the bone marrow. They secrete acids and proteolytic enzymes which dissolve the bone matrix and release the stored minerals in a process known as osteolysis.

In healthy, mature bone, a delicate balance between the activities of the osteoblasts and osteoclasts allows the organic and mineral components of the bone matrix to be continually recycled and remodelled, without affecting the overall mass of bone (Currey, 1984). This process allows bones to maintain or change shape and size during growth. An imbalance in remodelling leads to metabolic bone diseases such osteoporosis, which usually occur with ageing.

Bone remodelling is thought to be controlled by cytokines and growth factors, which affect the production and activity of bone cells. These include transforming growth factor beta (TGFß) and insulin-like growth factors (IGFs) that stimulate the formation and activity of osteoblasts, and interleukin-1, -3 and -6 that stimulate resorption. The equilibrium between the activities of the two types of cells can also be changed in response to systemic hormones and mechanical stimuli. If a bone remains immobile for a significant period of

time, rapid bone loss occurs due to increased osteoclastic activity. However, weight-bearing or other activities that cause more stress than normal to be applied, increases osteogenic activity and hence results in an increase in bone mass. This phenomenon is known as Wolff's law of bone remodelling (Bronzino, 1995).

2.1.5. Fracture Repair

Despite its strength, bone may crack or even break if subjected to extreme loads, sudden impacts or stresses from unusual directions. The damage produced constitutes a fracture. A useful consequence of the constant remodelling of bone is its ability to repair itself following a minor injury. The process of fracture healing can be thought of as three overlapping stages: *inflammation, repair,* and *remodelling* (Ratner *et al.*, 1996). The sequence and duration of each stage is influenced by local factors such as the degree of local trauma, type of bone affected, and presence or absence of infection as well as more general systemic factors such as age, hormones and nutrition (Ratner *et al.*, 1996).

Inflammation

In even a small fracture, many blood vessels are broken and extensive bleeding occurs. A large clot, or fracture hematoma, soon closes off the injured vessels and leaves a fibrous meshwork of fibrin in the damaged area. The disruption of circulation kills osteocytes around the fracture, broadening the area affected. Platelets in the blood attach to the fibrin clot and release vasoactive mediators, growth factors and other cytokines, which attract inflammatory cells to the fracture site. Polymorphonuclear leucocytes, macrophages and mast cells remove necrotic bone and tissue debris. This process takes place between the time of injury to 24-72 hours. This is followed by the stimulation of proliferation of the cells necessary for repair of bone (Ratner *et al.*, 1996).

Repair

During the reparative stage, osteoblasts begin to create a bridge between the bone fragments on either side of the fracture. As the repair progresses, osteoblasts continue to proliferate and begin to lay down new bone matrix. A soft bridging callus of fibroblasts and osteoblasts in a collagen rich matrix forms into which new blood vessels grow. Ossification of the matrix leads to the formation of new woven bone. The reparative stage normally takes place from 2 days to 2 weeks from injury (Ratner *et al.*, 1996).

Remodelling

Osteoclasts and osteoblasts then remodel the region for a period ranging from 4 months to well over a year. When the remodelling is complete, and the callus has stopped increasing in size, only living compact bone will remain. During this phase the woven bone undergoes sequential resorption and deposition, gradually being converted to more organised lamellar bone. The repair may be "good as new", with no indications that a fracture ever occurred, or the bone may be slightly thicker and stronger than normal at the fracture site (Ratner *et al.*, 1996).

However, natural bone repair is not always possible and this is why biomaterials are required to replace damaged or defective bone. This is achievable by implantable biomaterials or by tissue engineering, which can be defined as a process involving the controlled *in vitro* and *in vivo* growth of living tissues and organs on three-dimensional support structures (scaffolds). It is built upon the basic cell biology of host cells and the variety of signals that control their behaviour. Tissue engineering uses synthetic or naturally derived, engineered biomaterials to replace damaged or defective tissues, such as bone and skin (Liu *et al.*, 2007).

2.2. Biomaterials as Bone Replacement Materials

Biomaterials are synthetic materials used for biomedical applications to replace part of a living system or to function in intimate contact with living tissue. The most obvious requirement of any biomaterial is that it must be able to perform the function or functions that necessitated its insertion. Biomedical implants are used to resolve pathologies that cannot be corrected either by the natural healing process or traditional surgical intervention.

The success of a biomaterial in the body depends on factors such as the material properties, design, biocompatibility of the material, in addition to the skill of the surgeon, age and health of the patient and the activities of the patient, which are not under the control of the engineer. It is not, however, sufficient for the implant to simply reside or survive in the body. Implants designed to replace lost or damaged bone must regain the mechanical function of the bone by restoring skeletal continuity at the site of disease or injury. They must also stay functional for a reasonable period of time. Our expectations from implants are increasing, and it is no longer sufficient for an implant to alleviate pain and restore

some function for a few years – 15 years or more are now generally expected (Jones *et al.*, 2001). As they are implanted in the body and thus only accessible by major surgery, they must be able to survive and remain functional for this time, ideally without revision operations.

Although, as has been seen in the previous section, bones are able to regenerate themselves to repair voids up to a certain size, this is only true to a certain extent. If the defect is too large, a soft connective tissue scar is produced, which impairs bone stability and can potentially lead to further fracture of the bone. Bone is one of the most commonly transplanted materials, second only to blood transfusions. Therefore a bone replacement material is used to fill the fracture space and bridge the defect, thus regaining continuity between bone tissues.

Before we consider the materials currently used as bone replacement materials and discuss their suitability for this application, it is important to ascertain the properties that are important in a biomaterial specifically intended for use as a replacement for human bone.

2.2.1. Requirements of a bone replacement material

All medical implant materials have to fulfil many criteria before they can be used in the body due to its harsh environment. Whenever any foreign material is introduced into the body environment, a series of reactions occur. The magnitude of effect may range from mild irritation to inflammation or even death. Any implant material must be biocompatible, that is, it must produce a minimum degree of inflammation and toxicity. Products resulting from reactions with body fluids must be tolerated by surrounding tissue so that normal tissue reactions are unimpaired. Biocompatibility is a function of the location of the implant, as well as of its chemistry and shape (Callister, 2000).

Body fluids consist of approximately 1 wt% NaCl in addition to other salts, which makes the environment of the implants highly corrosive, and may cause crevice attack, pitting, and fretting, which can lead to corrosion cracking and fatigue (Callister, 2000). These can all lead to premature failure of the implant. Another adverse consequence of corrosion is the generation of corrosion products, which may be toxic and can interfere with normal

body functions. Most corrosion products are excreted from the body, but some may accumulate in specific organs (Callister, 2000).

Another important factor is the demonstration of appropriate functional characteristics, which means that the implant must perform as the tissue for which it substitutes. Thus, a biocompatible material is used which disrupts normal body functions as little as possible. Therefore, the material is meant to cause no thrombogenic, toxic, allergic or inflammatory response when the material is placed *in vivo*. The material must not stimulate changes in plasma proteins and enzymes or cause an immunologic reaction, nor can it instigate carcinogenic, mutagenic, or teratogenic gross tissue change effects (Zakaria, 2007).

In order to implant a material, the surgeon has to make an incision into the tissue first, along with removal of diseased tissue. The success of the entire operation depends on the kind and degree of tissue response, and hence body response to the material. This is an important aspect of biocompatibility. The response of the body towards implants varies widely according to the host site and species, the degree of trauma imposed during implantation, and all of the variables associated with a normal wound healing process. Then again, the chemical composition and micro and macrostructure of the implants induce different body responses.

When considering bone implants, one needs to consider the extensive forces that originate due to gravity alone i.e. forces transmitted as a result of muscular actions such as walking. These forces are complex in nature and fluctuate with time in magnitude, in direction, and in rate of application. Thus, mechanical characteristics such as modulus of elasticity, yield strength, tensile strength, fatigue strength, fracture toughness, and ductility are all important considerations and should ideally match that of natural bone. However, for the purpose of design goals for replacement materials, strengths of 5-10 MPa or 100-150 MPa and moduli of 100-150 MPa or 10-20 GPa are required for replacement of trabecular bone and cortical bone respectively [Bauer and Schills, 1999].

Another problem that can arise from a new implantation is the resorption of existing, surrounding bones, which is caused by a disproportionate amount of the load being borne by the implant, effectively shielding the surrounding bone from stresses. This is caused by inferior implant design and leads to dissolution of bone (osteolysis), which can lead to

loosening of the implant providing discomfort to the patient and necessitating a surgical revision. This can be partially relieved by designing implants with curved surfaces to prevent stress concentrations (NIH Consensus, 2001).

The methods used to manufacture the implants and secure them into the defect must also be considered. The replacement material should be easily formed into complex shapes, and must be able to be implanted quickly with minimal damage to the surrounding tissues or the surface of the material. Skeletal morphology can vary significantly between patients, and therefore, in order for minimal skeletal adaptation to be necessary, the material must be readily modifiable either prior to surgery or during implantation.

Fixation of the material into the defect is very important, as loosening between the material and surrounding bone is currently the main reason for skeletal implant failure. One of the ways to minimize loosening is by using rough surfaces on implants, which help to increase the rate at which bone bonds to such a surface. Alternatively, the surface of the implant may need to be completely smooth, to prevent the concentration of bacteria and increase fatigue resistance. Thus, a compromise must be reached. The implanted material should also allow bone to bond and grow at its surface, a process known as 'osseointegration' (Kawahara *et al.*, 2003). This process can be improved by using bioactive materials such as various glass-ceramics, where bioactivity refers to the ability of certain materials to form a direct physicochemical bond with bone (explained in section 2.2.3) (Cehreli *et al.*, 2003). Ideally, a material that acts as an osteoconductive scaffold is required to ensure maximum fixation of the implant (Vrouwenvelder, 1993). Osteoconduction supports ingrowth of bone into a 3-dimensional structure, therefore providing maximum integration of the surrounding natural bone into the implanted material. To achieve this, a fully interconnected porous matrix is required to allow resorption and new bone formation. By using a porous implant the interfacial area between the implant and the tissue is increased, thereby reducing the movement of the device in the tissue. Although still the subject of much debate, pores in the range of 100 to 600 μm are required for mechanically strong bone ingrowth (Klawitter *et al.*, 1971). A minimum pore size of 100 μm is necessary for cell penetration, tissue ingrowth and vascularisation. Re-establishment of vascularisation is required for the delivery of nutrients, cellular precursors, and the removal of metabolic wastes and necrotic debris. High porosity can however, adversely affect the mechanical

strength and reliability of implants, which is an important consideration if the material is intended for use in load bearing applications.

Table 2-2 Ideal material properties for a scaffold to replace trabecular bone (Bauer, 1999; Whang and Healey, 2001).

Compression Yield Strength (representing trabeculae)	5-10 MPa
Compression Elastic Modulus (representing trabeculae)	100-150 MPa
Pores	> 350 μm
Macroporosity	> 50%

Ideally the material should be resorbable, initially re-establishing the mechanical integrity of the injured skeleton, but then gradually resorbing as natural bone is produced. It is important that the material resorbs in such a way that only non-toxic degradation products are produced that can be easily excreted or metabolised via normal physiological mechanisms. This would eradicate the need for further surgery to remove things such as bone plates and screws at a later stage.

A biocompatible material does not adversely affect the biological environment within which it is placed, either by irritating the surrounding structures, provoking an abnormal inflammatory response, inciting allergic or immunologic reactions, or causing cancer. At the same time the material itself is not adversely affected by the surrounding host tissues and fluids. However, this does not necessarily mean that there should be no response, i.e. the material should be completely inert. As will be seen later, no biomaterial is completely inert – there will always be some kind of reaction between the implant and tissues. Moreover, many materials are currently being developed with the intention of producing a "specific" response (Ratner *et al.*, 1996). Four general categories of materials that are suitable for implants can be defined, depending on the type of interfacial reaction that occurs when they are implanted – *bioinert, bioactive, resorbable and biodegradable.*

Bioinert materials act as a structural connection between the living bone and the surrounding tissue, without any adverse affects. An example of this is alumina (Al_2O_3),

which is one of the most commonly used bioinert materials. The tissue response to a bioinert implant is encapsulation with a non-adherent fibrous tissue, which isolates it from the surrounding bone (Cao *et al.*, 1996). The ideal scenario would be for the material to be covered by bone tissue rather than a fibrous layer, but this is rarely the case. A thick fibrous layer reflects poor biocompatibility. A number of factors influence the thickness of the fibrous layer including the conditions of the implant, host tissue, and motion and fit at the interface (Cao *et al.*, 1996). However due to their good biocompatibility, high strength, and excellent corrosion and wear resistance, bioinert materials have been the focus of implant materials where porous structures provide an interlock to diminish motion between the bones artificially and naturally made (Hing *et al.*, 1995).

A bioactive material is one that elicits a specific biological response at the interface of the material, which results in the formation of a bond between the tissues and the material (Hench *et al.*, 1972). This is the newest approach to the problems relating to interfacial attachment of implants. The concept of bioactive materials is intermediate between resorbable and bioinert materials (Figure 2-6). Bioactive materials are primarily glasses and glass-ceramics, where a fibrous tissue does not form around the implant, as with bioinert materials, but instead a silica hydrogel layer forms on their surface that, fuelled by consuming calcium and phosphate ions from the surrounding body fluid, allows subsequent crystallisation of an apatite-like phase (Hench, 1994). As the composition and structure of this apatite is very similar to that of hydroxyapatite found in bones, osteoblasts are able to proliferate and differentiate to produce both apatite and collagen on this layer, allowing the bone to come in direct contact with the implant via its surface apatite layer without the intervention of the fibrous tissue layer, and form a bond with the bone (Hench, 1994). This allows the development of a much greater interfacial adhesive strength. This phenomenon of bioactivity will be discussed further in later sections (section 2.2.3).

Resorbable materials are extreme versions of bioactive materials and have sufficiently high surface bioactivity that the material can dissolve or resorb and is replaced by the surrounding tissue (Wilson and Hench, 1993). Examples of such a materials are tricalcium phosphate, porous hydroxyapatite, calcium phosphate salts, certain bioglasses and polyurethane. To be successful biomaterials, resorbable materials should be able to maintain the strength and stability of the interface during degradation and replacement, and have a similar resorption rate to the repair rates of body tissues. It is also important

dissolution occurs without toxicity or rejection. Thus, resorbable materials are predominantly used in temporary procedures such as stitches.

Biodegradable materials are derived by transforming compounds that are present in nature to structural plastics. Organic molecules are polymerised to form strong fibres and solid compounds (Yetkin et al., 2000). When these polymers are implanted in patients, they degrade and are eliminated from the body over a period of time. Moreover, the employment of biodegradable materials with long degradation kinetics maintains bioactive elements at the site of implantation long enough to guide the process of tissue growth, providing a temporal match between kinetic degradation and tissue maturation. Biodegradable materials are used in orthopaedic surgery mostly for the fixation of fractures (Yetkin et al., 2000). The mechanical properties of the materials permit them to be used with fractures where the loading is relatively low. Therefore, they have mainly been used for treating small-bone fractures such as ankle fractures (Yetkin *et al.*, 1993).

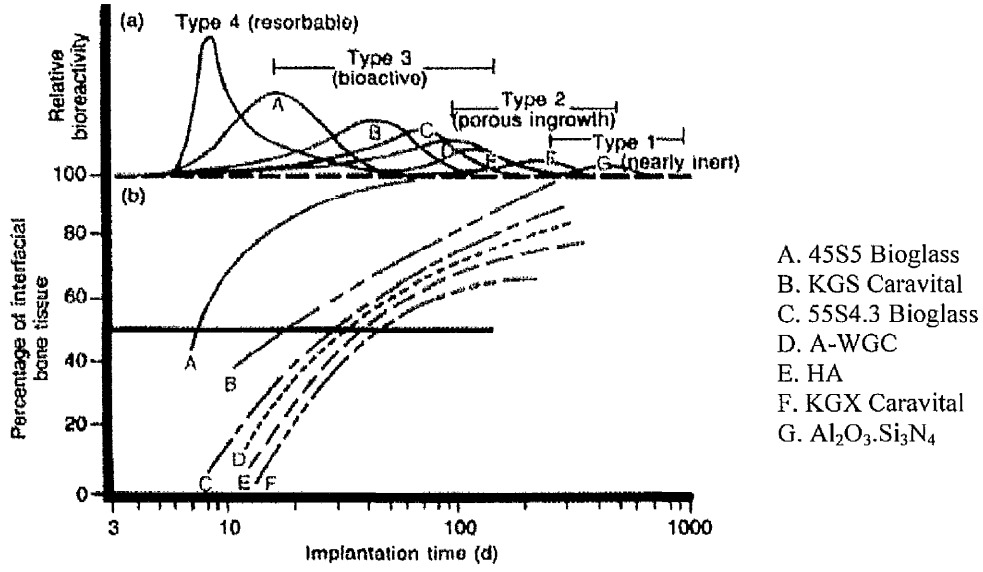

Figure 2-6 Bioactivity spectrum for various bioceramic implants, (a) Relative rate of bioreactivity, (b) Time dependence of formation of bone bonding at an implant interface (http://bg.ic.ac.uk/lectures/hench/bioglass/cal3.htm).

2.2.2. Types of Bone Replacement Materials

The cellular component of any engineered product describes the type of tissue graft being used. The most favoured replacement of human bone tissue is known as an *autograft*. This procedure involves taking bone fragments from an undamaged area of the patient's body and transplanting it into the damaged area. The obvious benefit of this approach is there is little potential for rejection, and the bone fragments can replicate the structure of human bone. However, the drawbacks of this process are the limited volume of available bone, the additional surgery required and the pain caused by removing bone from an undamaged area. Often the newly formed bone will not take the exact shape of the original bone (Damien *et al.*, 1990).

The use of *allografts* alleviates the problem of additional surgery on the patient, as the bone tissue is taken from a donor rather than the patient. However, this introduces several problems such as greater chance of rejection by the body, as well as the risk of transfer of infectious diseases such as HIV and hepatitis (Paul, 1992).

Metals

It is these concerns over the use and availability of autogenous and allogenic bone graft materials that have resulted in the development of artificial materials. The most common of these are rigid metal plates made of stainless steel, cobalt-chromium alloys and titanium alloys, which have the advantages of a long clinical history, are reasonably cheap, and are easy to produce and shape. The plates are usually formed to the approximate morphology of the implant site prior to implantation, and then adapted intra-operatively by the surgeon who manually bends the plate into the exact shape and fixes it to existing bone by means of retaining screws (Riden, 1998). Drawbacks of this procedure include the large differences in the mechanical properties between the metal implants and bone, which can cause stress-shielding, reduction of blood supply at the implantation site, the potential for corrosion, wear and debris formation (Breme *et al.*, 1998). A metal implant would also not have the desired effect of filling the void with a structure that would encourage tissue re-growth and revascularisation. But the reasons that metal implants have been the most popular choice over the past 100 years is because of their inertness, adequate ductility and elasticity, and high compressive and tensile strength (Breme *et al.*, 1998).

Synthetic Polymers

Synthetic polymers are the most diverse class of biomaterial due to their wide variety of compositions, properties and forms. They are easily shaped at low cost and can be produced as films, fibres, emulsions, powder, fluids, porous scaffolds and even coatings on other materials. Polymers are currently used in a wide variety of biomedical implants, but their use in orthopaedic applications has generally been limited due to insufficient stiffness and strength. However, where they have proved successful is as one of the articulating surface components in joint prosthesis, and for fixation as a structural interface between the implant component and bone tissue. Ultrahigh molecular weight polyethylene (UHMWPE), is used as acetabular component in artificial hip joints as a load bearing material (figure 2-7). Self-curing acrylic bone cements based on polymethyl methacrylate, PMMA, are the other major use of polymers in orthopaedic applications (Brown *et al.*, 1999).

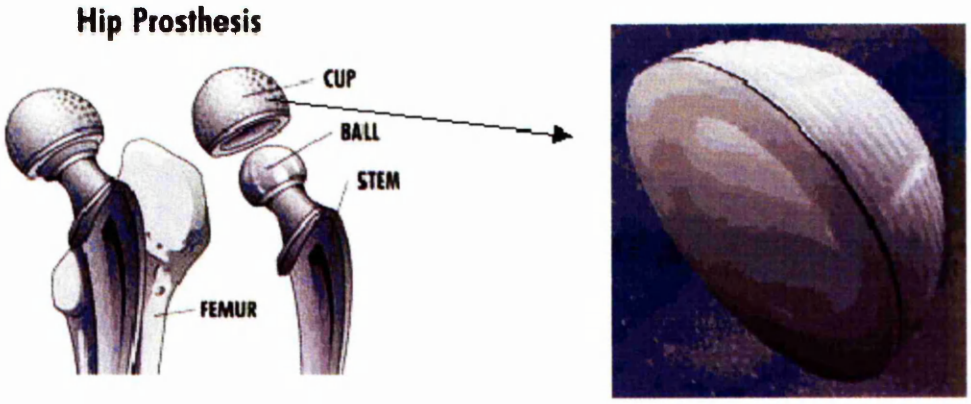

Figure 2-7 Acetabular cup used in a hip prosthesis made from UHMWPE (http://economy.mse.uiuc.edu/figure/hyq2.gif).

The potential to use polymers as bone replacement materials arises from their ability to be tailored into a desired shape to suit a particular need, and their ability to undergo controlled degradation. The former can be achieved by combining different monomers to form copolymers, or from the incorporation of chemical additives, and controlling the extent of polymerization or cross-linking between adjacent chains (Brown *et al.*, 1999). The degradation of the polymers goes through phases of dissolution, hydrolysis, and enzyme degradation. It is essential that the breakdown products are non-toxic, and the bi-products are excreted through the normal physiological pathways. Biopolymers in use should have high initial strength and a controlled reduction in mechanical properties. A large number of

polymers have been investigated for potential use in this area such as poly(L-lactic acid) (PLLA), polycaprolactone (PCL), poly(α-hydroxyacid), poly(glycolic acid) (PGA), and poly(lactic-co-glycolic acid) (PLGA) (Yangpeng *et al.*, 2007; Williamson *et al.*, 2006; Athanasiou *et al.*, 1998). These materials have proven biocompatibility and a long history as degradable sutures and bone plates. However, their potential use as bone replacement materials is limited by their low stiffness and strength.

Ceramics

Ceramics have the most similar composition to that of the mineral components of bone and this makes them the ideal material to be used as implants, as they are well tolerated by tissues, with negligible foreign body reactions and demonstrate good resistance to the corrosive nature of body fluids (Jarcho, 1981). They are low in density, hard-wearing and demonstrate high strength under compressive load. However it is primarily the brittleness of ceramics that precludes their wide use at present.

Ceramics used for implantation are termed bioceramics, and can be biologically inactive (e.g. alumina, zirconia), resorbable (e.g. tricalcium phosphate), bioactive (e.g. hydroxyapatite, bioactive glasses, and glass-ceramics), or porous for tissue ingrowth (e.g. hydroxyapatite-coated metals), as shown in Figure 2-6. It is the bioactive materials that are the topic of the current study, due to their ideal properties of bonding directly with bone. Thus, these bioactive materials are going to be discussed further with particular emphasis on bioactive glass-ceramics and glasses.

2.2.3. Bioactive materials

The importance of achieving secure fixation of the implant to the bone was discussed in section 2.2.1. The chance of achieving this is increased by using bioactive materials. A bioactive material is defined as a material that elicits a specific biological response at the interface of the material, which results in the formation of a bond between the tissues and the material (Hench *et al.*, 1972). A number of compositions of glasses, ceramics, glass-ceramics and composites now exist that have been shown to bond to bone (Kokubo, 1993).

Materials that exhibit bioactive behaviour can be divided into two distinct classes – Class A and Class B (Hench, 1994). Class A materials are osteoproductive and this type of

bioactivity occurs when a material elicits both an intracellular and an extracellular response at its interface. Class B materials are osteoconductive, providing a biocompatible interface along which bone migrates. This type of bioactivity occurs when a material elicits only an extracellular response at its interface.

A Class B material will bond to hard tissue, and a Class A then it will bond to both soft and hard tissue. An example of a Class A material is 45S5 Bioglass®, and a Class B material is synthetic hydroxyapatite (Hench, 1991).

2.2.3.1. Hydroxyapatite

Hydroxyapatite was the first bioactive material, and is also the primary mineral component of bone and teeth, representing 43% of bone weight. Artificial HA has the chemical formula $Ca_{10}(PO_4)_6(OH)_2$ and has a calcium to phosphate ratio (Ca:P) of 1.67. When compared to the chemical formula of natural bone, $Ca_{8\ 3.1.7}(PO_4)_{4.3}\ (CO_3)_1\ (HPO4)_{0.7}\ (OH,CO_3)_{0.3\ 1.7}$ (where 3.1.7 denotes the number of calcium ions that might be present in a particular lattice) it can be seen that they are very similar (Wilson and Hench, 1993). As hydroxyapatite is present in bone, it was an obvious choice of a material to investigate for bioactivity and for use as implants. In the early seventies, hydroxyapatite was suggested for use as bone and tooth implants and by the middle of that decade dense, sintered hydroxyapatite was being produced. Although one major drawback of using hydroxyapatite as an implant material is that it has very low strength, it is used for small, non-load bearing applications such as replacement bones in the ear (Grotte, 1998). The structure of hydroxyapatite is shown in Figure 2-8.

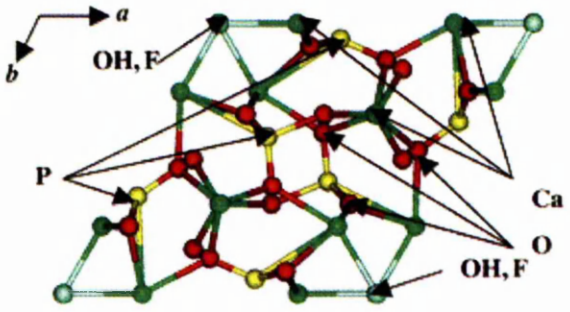

Figure 2-8 Structure of Hydroxyapatite (OH) and Fluorapatite (F) (http://www.rsc.org/ej/CC/2001/b104850n/b104850n-f1.gif).

2.2.3.2. Fluorapatite

An alternative to HA is fluorapatite, where the hydroxyl ion in the apatite lattice is exchanged with fluorine that fits better as it is smaller in size. This leads to fluorapatites being chemically and thermally more stable (Guida *et al.*, 2002). Fluorine is quite commonly used in the dental industry and is also found in toothpastes, as it prevents caries. Bioactive glasses have been produced with fluorine as one of its constituents that lead on to a fluorapatite glass-ceramic upon heating (Hill *et al.*, 1991).

2.2.3.3. Bioactive glasses

Hench devised the first bioactive glass at the University of Florida in 1969 (Hench *et al.*, 1972). A certain compositional range of bioactive glasses containing SiO_2, Na_2O, CaO and P_2O_5 were the first materials to demonstrate bioactive behaviour. Their key features were:

- Less than 60 mol% SiO_2
- High Na_2O and high CaO content
- High CaO/ P_2O_5 ratio

One aspect that makes bioactive glasses different from other bioactive ceramics is the possibility of controlling a range of chemical properties and rate of bonding to tissues. The most reactive glass compositions develop a stable, bonded interface with soft tissues, as shown by Wilson *et al.* (1984).

Many of the glasses in this system are based on the composition of the well-studied Bioglass® 45S5 which contains 45 wt% SiO_2, which acts as the glass network former, and has a 5 to 1 molar ratio of Ca to P. It is very important to get the compositions of the glass right, as small variations can have major effects. As little as 3 wt% of alumina in other glasses can prevent the glass-ceramic bonding to bone (Hench, 1991). It has also been stated that alumina also minimises the solubility of the glass by producing a passive layer, which may inhibit bonding (Jallot *et al.*, 2000). The addition of CaF_2 initiates the formation of fluorapatite, a denser bioactive material than hydroxyapatite.

Bioglass® has been used in the form of middle ear devices, implants for the orbital floor, and endosseous ridge maintenance devices. Whilst bioactive glasses undergo rapid surface

reaction, which leads to fast tissue bonding, their mechanical properties are relatively poor, demonstrating low strength and fracture toughness due to an amorphous three-dimensional glass network (Jones *et al.*, 1995).

The mechanism of bone bonding with the implant is also highly dependant on the exact compositions of the constituents. Hench and co-workers have studied a series of the four component system of oxides, silicon, sodium, calcium and phosphorous with a constant 6 wt% P_2O_5 content (Wilson and Hench, 1993). This is illustrated in the ternary diagram (Figure 2-9), where area A shows the bioactive compositions which bond to bone, and area B shows glasses that are nearly inert and form a fibrous capsule at the tissue-implant interface.

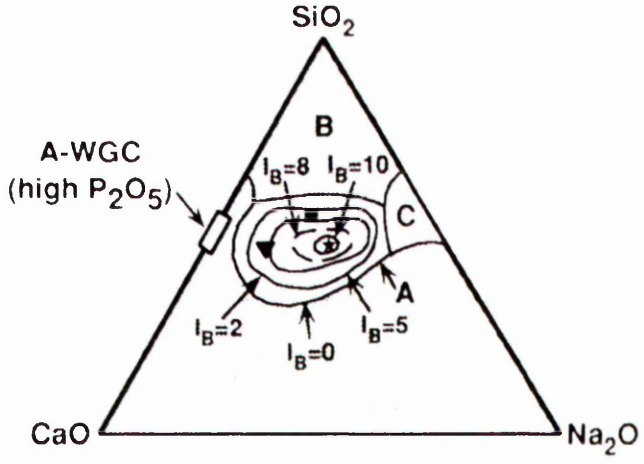

Figure 2-9 Compositional dependence (in weight %) of bone bonding of bioactive glasses and glass-ceramics where area A shows the bioactive compositions which bond to bone, and area B shows glasses that are inert (http://bg.ic.ac.uk/lectures/hench/bioglass/cal3.htm).

The ability of certain bioactive glasses and glass-ceramics to bond to bone has been attributed to the formation of a hydroxycarbonate (HCA) layer in the surface of the material when in contact with body fluids. Bonding occurs due to a sequence of reactions, which have been described by Jones *et al.* (2001) as follows:

Stage 1 – Rapid exchange of Na^+ and Ca^{2+} with H^+ or H_3O^+ from the solution causing hydrolysis of the silica groups, which form silanols (SiOH) :

$$Si\text{-}O\text{-}\ Na^+ + H^+ + OH^- \longrightarrow Si\text{-}OH^+ + Na^+_{(aqueous)} + OH^-$$

This stage is usually diffusion controlled and exhibits a $t^{-1/2}$ dependence. The pH of the solution increases as a result of H^+ ions in the solution being replaced by cations.

Stage 2 – The cation exchange increase the hydroxyl concentration of the solution, which leads to an attack on the silica glass network. Soluble silica is lost in the form of $Si(OH)_4$ to the solution, resulting from the breaking of Si-O-Si bonds and the continued formation of sianols at the glass solution interface:

$$\text{Si-O-Si} + H_2O \longrightarrow \text{Si-OH} + \text{OH-Si}$$

Stage 3 – Condensation and repolymerisation of SiO_2 rich surface layer, depleted in cations:

$$\text{-Si-OH} + \text{HO-Si-} \longrightarrow \text{-Si-O-Si} + H_2O$$

Stage 4 – Migration of Ca^{2+} and PO_4^{3-} groups to the surface through the SiO_2 rich layer, forming a $CaO\text{-}P_2O_5$ rich film on top of the SiO_2 rich layer. Growth of this amorphous $CaO\text{-}P_2O_5$ rich film follows by incorporation of soluble calcium and phosphates from solution.

Stage 5 – Crystallisation of the amorphous $CaO\text{-}P_2O_5$ film by incorporation of OH^-, CO_3^{2-}, or F^- anions from solution to form a hydroxycarbonate apatite (HCA) layer.

These are the first five stages in the process of complete bonding of a bioactive material to bone, occurring on the material side of the interface and not depending on the presence of tissues. Therefore, studies have been conducted to study the sequence of events *in vitro* using simulated body fluid (SBF) containing similar ion concentrations to that of human blood plasma. A schematic illustrating the mechanism of apatite formation on the surface of $CaO\text{-}SiO_2$-based glasses and glass-ceramics in the human body can be seen in figure 2-10 (Hench, 1991).

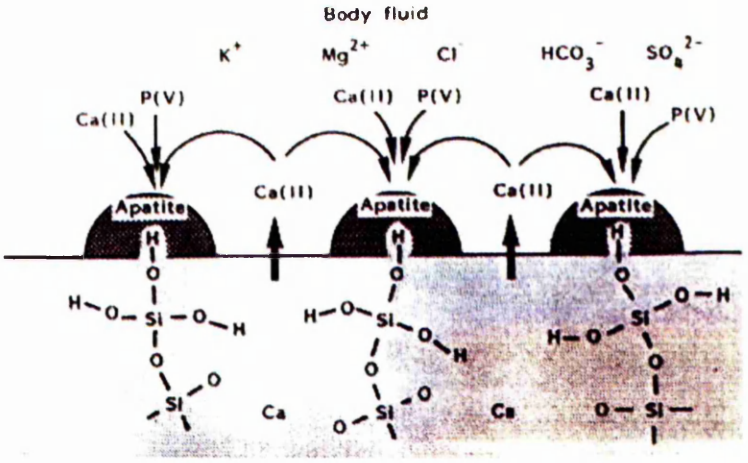

Figure 2-10 Schematic illustration of the mechanism of apatite formation on the surface of CaO-SiO_2-based glasses and glass-ceramics in the human body (Kokubo, 1993).

It must be noted that stages 1 to 5 summarise the time dependent changes of only a single phase amorphous material. If one desires to understand a multiphase bioactive implant, such as polycrystalline sintered hydroxyapatite or a bioactive composite, it is necessary to establish the time dependant surface changes for each phase and each interface between the phases.

Stages 1 to 5 result in the formation of a hydroxycarbonate apatite (HCA) crystal layer on the implant surface. However for the implant to bond to tissues, stages 6 to 11 are necessary, as described below (Jones *et al.*, 2001):

Stage 6 – Adsorption and desorption of biological growth factors in the HCA layer to activate differentiation of stem cells.
Stage 7 – Action of macrophages to remove debris from the site allowing cells to occupy the space.
Stage 8 – Attachment of stem cells on the bioactive surface.
Stage 9 – Differentiation of stem cells to form bone growing cells, such as osteoblasts.
Stage 10 – Generation of extracellular matrix by the osteoblasts to form bone.
Stage 11 – Crystallisation of inorganic calcium phosphate matrix to enclose bone cells in a living composite.

All stages are shown in figure 2-11 (Hench, 1998).

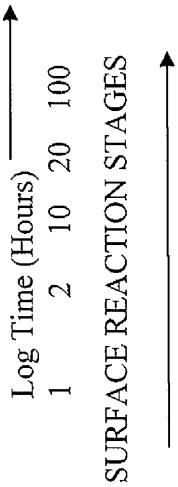

11	Crystallisation of Matrix
10	Generation of Matrix
9	Differentiation of Stem Cells
8	Attachment of Stem Cells
7	Attachment of Macrophages
6	Adsorption of biological moieties in HCA layer
5	Crystallisation of Hydroxycarbonate apatite (HCA)
4	Adsorption of amorphous Ca + PO4 +CO3
3	Polycondensaton of SiOH + SiOH ⟶ Si-O-Si
1 & 2	Formation of SiOH bonds
	Bioactive Glass

Figure 2-11 Sequence of interfacial reactions involved in forming a bond between bone and bioactive glasses.

2.2.4. Bioactive Glass-Ceramics

Glass-ceramics are a class of ceramic material formed through the controlled crystallisation of a base glass (Holand *et al.*, 2002). Crystallisation is achieved by subjecting the base glass to a carefully regulated heat-treatment schedule, resulting in the nucleation and growth of crystal phases within the glass. The resulting glass-ceramic consists of at least one glass phase and one crystal phase and superior mechanical properties to those of the base glass from which it was formed. The reason for this as stated by Thompson *et al.* (1980) is that, unlike glass which is amorphous, crystalline ceramics contain structural discontinuities or grain boundaries at points where the crystals meet, which act as an impediment for fracture propagation by causing deflection, branching, or splitting of cracks.

Crystallisation is the process whereby an ordered structure is produced from a disordered phase, usually from a melt or dilute solution. It can be classed as a *nucleation* and *growth* process. Nucleation involves the formation of regions of longer atomic order than are normally present in the liquid phase. Submicroscopic nuclei are formed in the base glass, which grow into macroscopic crystals to form a polycrystalline ceramic. Nucleation may be either homogeneous or heterogeneous. In homogeneous nucleation, the resulting crystals are of the same constitution as the nuclei that initiated their formation, whereas in heterogeneous nucleation the crystals are often chemically quite different. Homogeneous

nucleation occurs when a new phase develops in the absence of any foreign boundaries (e.g. substrates) as a result of local fluctuations of density and kinetic energy. This is extremely difficult to achieve experimentally as there must be no dust particles in the material that would result in nucleation becoming heterogeneous. Homogeneous nucleation tends to occur at high degrees of supersaturation or supercooling of the liquid phase (McMillian, 1979).

The majority of crystallisation that occurs within glass-ceramics is heterogeneous, which involves phase boundaries, special catalysts, and foreign substrates that are distinct from the parent phase. This results from situations when the driving forces causing the formation of a new phase are stronger than those required by the parent phase for its transformation into a crystal (McMilian, 1979).

The second step in the crystallisation process is growth, whereby the crystal nuclei grow by the addition of further chains. Usually the rates of the two stages of crystallisation vary with temperature as shown in figure 2-12 (a) and in order for crystallisation to proceed at a reasonable rate the glass has to first be held a temperature around T_N to induce nucleation and then held at a higher temperature (around T_G) to allow crystal growth at the nucleation sites.

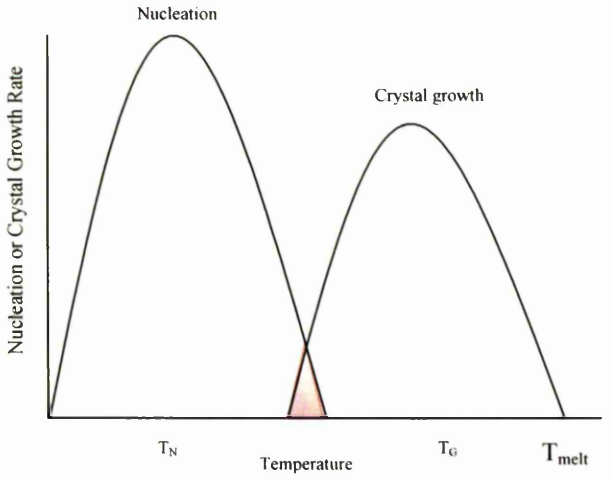

(a)

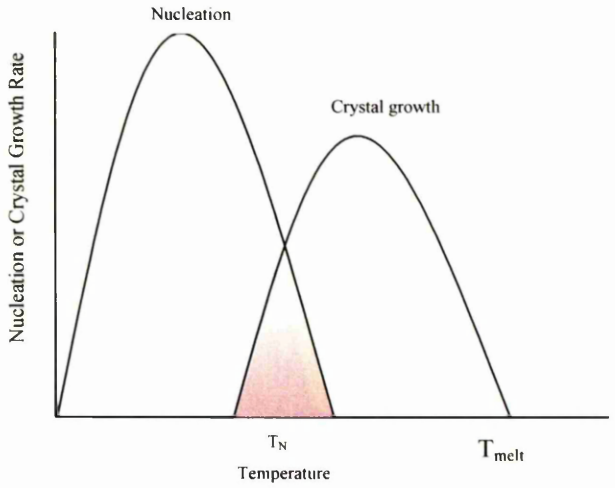

(b)

Figure 2-12 Crystallisation of a glass (a) Negligible overlap of nucleation and growth-rate curves leading to a two-stage heat treatment; (b) overlapping nucleation and growth curves leading to a single-stage heat treatment (Rawlings, 1993).

However, there are a few glass-ceramics which have overlapping rate curves (figure 2-12 (b)) that can be crystallised by a single heat treatment.

A glass-ceramic is not fully crystalline; typically at least 50% and as much as 98% of volume may be crystalline (Rawlings, 1993). In order to produce a material with good mechanical strength, a fine grained microstructure is usually required and therefore it is desirable to produce a glass-ceramic that contains small, closely interlocked crystals. To

achieve this, efficient nucleation is needed producing a large number of small crystal nuclei rather than a small number of relatively coarse ones. Once the glass has been nucleated, the temperature is raised to allow crystal growth of the nuclei. Careful control must be exercised over the rate of temperature rise as a heating rate that is too rapid may cause deformation or cracking of the glass-ceramic to occur. This results from the generation of stresses in both the glass phase and the crystal phases as a result of a difference in their densities and the volume change which accompanies crystallisation (McMillian, 1979). With slower heating this should not occur since stresses are relieved by viscous flow of the glass phase.

An idealised heat treatment schedule for a glass-ceramic is shown in figure 2-13. The initial stage involves heating the glass from room temperature to the nucleation temperature and holding at this temperature for a suitable period of time, usually from 0.5 to 2 hours. The point at which the nucleation rate is at its optimum, the degree of crystal nuclei formation is at its greatest resulting in the production of a maximum possible number of crystals and thus the optimum mechanical properties for that material.

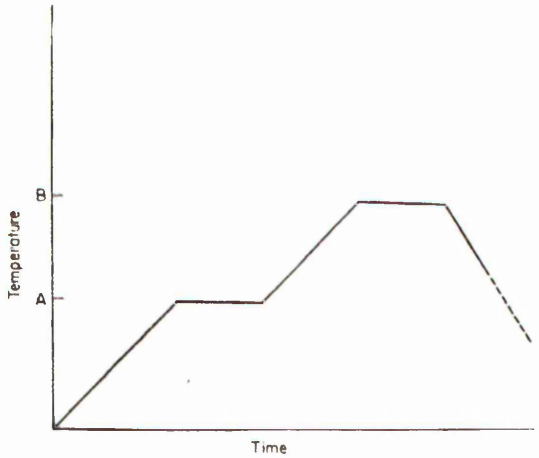

Figure 2-13 Idealised heat-treatment schedule for a glass-ceramic (McMillian, 1979).

Following nucleation, the temperature of the glass is raised further to allow crystal growth to occur at a controlled rate up to a point where maximum crystallisation can be achieved without causing deformation of the material. It is held at this maximum crystallisation temperature for a period of at least 1 hour, although longer holds are often used to increase the degree of crystallinity in the glass-ceramic (McMillian, 1979).

This two stage heating regime is considered optimum as it allows crystal nuclei to be generated in the glass at temperatures below those at which major crystalline phases could grow at a significant rate (McMillian, 1979).

The process of controlled crystallisation is termed ceramming. If uncontrolled crystallisation occurs, which is most likely on the surface, there will be a small number of large crystals due to a reduced number of nuclei available, and thus a decrease in mechanical properties (Stewart, 1990). The conventional production route for a glass-ceramic is to fabricate the component whilst in the glassy state by casting or forming and then to crystallise. This is so that nucleation on the free surfaces does not occur to any extent, as this can result in elongated orientated crystals and poor mechanical properties (Rawlings, 1993).

A number of bioactive glass-ceramics have been developed, containing apatite as a crystal phase. Two of these are apatite-wollastonite (A-W) developed by Kokubo *et al.* (1982), and apatite-mullite (A-M) developed by Hill *et al.* (1991). Whilst the presence of an apatite phase allows tissue bonding to occur, both glass-ceramics contain at least one other crystal phase designed to act as a reinforcing agent to improve the mechanical properties of the material.

2.2.4.1. Apatite Wollastonite (A-W)

Apatite-Wollastonite (A-W) glass-ceramic was developed by Kokubo and is now produced under the trade name of Cerabone®. They are the most widely used two- phase glass-ceramics and are based on the SiO_2-P_2O_5-CaO-MgO system with a very small amount of CaF_2. The material contains ß-wollastonite ($CaO{\cdot}SiO_2$) and crystalline oxyfluorapatite (Ca_{10} $(PO_4)_6$ (O,F_2)), with its high strength being attributed to the presence of the chain phase wollastonite. Wollastonite tends to surface nucleate on A-W glass-ceramics, hence processing can be difficult to produce complex geometries, as A-W glasses cannot be cast. Their main uses are as artificial vertebrae, intervertebral spacers, sinous process spacers and iliac spacers (Kokubo *et al.*, 1993). They have a reported bending strength of 215 MPa, which is almost twice that of dense sintered hydroxyapatite and even higher than that of human cortical bone (160 MPa), in an air environment (Kokubo *et al.*, 1993). They also have a compressive strength of 1080 MPa and fracture toughness of 2 $MPa{\cdot}m^{1/2}$. When

loaded in an aqueous environment, this glass-ceramic shows a decrease in mechanical strength (Kokubo *et al.*, 1993).

2.2.4.2. Apatite Mullite (A-M)

Apatite-mullite glass-ceramics were developed by Hill *et al.* (1991) and are based on the SiO_2-Al_2O_3-P_2O_5-CaO-CaF_2 system, which crystallises to form an apatite phase (fluorapatite) and mullite ($3Al_2O_3.2SiO_2$) upon heating. The microstructure of this glass-ceramic consists of interlocking apatite and mullite crystals that have a high length to diameter aspect ratio. During fracture these needle-like crystals are pulled out resulting in high fracture toughness. As a result, apatite-mullite glass-ceramics have achieved bend strength in excess of 250 MPa and fracture toughness of 2.5 $MPa{\cdot}m^{1/2}$ (Freeman *et al.*, 2003). A typical microstructure consisting of elongated apatite crystals is shown in figure 2-14. The high fluorine content in these glasses facilitates amorphous phase separation, leading to bulk nucleation. They therefore have an advantage over apatite-wollastonite glass-ceramics as the two stage crystallisation process of crushing and sintering is not required.

Figure 2-14 Scanning electron micrograph of a fracture surface showing elongated apatite crystals with a high length to diameter aspect ratio (Rafferty et al., 2000).

The nucleation and crystallisation behaviour of this set of materials is affected by both the fluorine content and the calcium-to-phosphate ratio of the glass. If fluorine is not present, no apatite phases are formed. Fluorine reduces the glass transition temperatures and peak crystallisation temperatures by disrupting the glass network and replacing bridging oxygens with non-bridging fluorines (Rafferty *et al.*, 2000). Glasses with a calcium-to-

phosphate ratio of 1.67, which corresponds to apatite, have been shown to undergo bulk nucleation by holding the latter glass compositions for an hour at a temperature close to the glass transition temperature (Clifford *et al.*, 2001).

LG112 (University of Limerick Glass 112), an apatite-mullite glass-ceramic is based on the formula $4.5SiO_2$ - $3Al_2O_3$ – YP_2O_5 - 3CaO - $1.51CaF_2$ where the parameter Y=1.6, determining the Ca:P ratio to be 1.41 (Freeman *et al.*, 2003), making it phosphate rich. Studies have been conducted on this glass-ceramic, by implantation into a rat femur to assess its ability to bond to bone tissue (Freeman *et al.*, 2003). The glass was studied in the glassy state (designated LG112g), following crystallisation to principally apatite (LG112a), and as a mixed apatite and mullite phase (LG112m). Both the base glass and the resulting glass-ceramic were implanted into bone, and backscattered images of the implanted materials are shown in figure 2-15 (a) and (b) respectively. In figure 2-15 (a), a fibrous capsule layer can be seen around the implanted material. However in figure 2-14 (b), excellent osteointegration is seen with the formation of mineralised bone in direct contact with the implant. It was therefore concluded that prior to heat treatment the glass demonstrates no signs of bioactive bonding. However after heat treatment and crystallisation, this composition of apatite-mullite glass-ceramic is bioactive. LG112 has a reported nucleation temperature of 660°C and a ceramming temperature of 893°C for transformation into an apatite phase, and 1040° for the ceramming of the mullite phase (Freeman *et al.*, 2003).

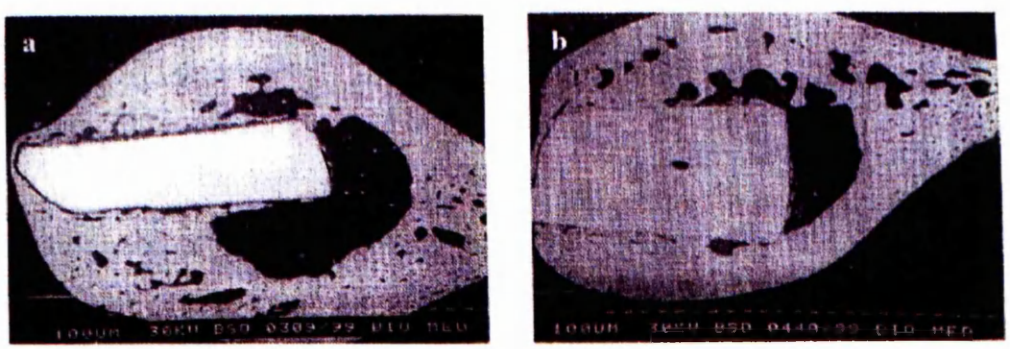

Figure 2-15 (a) Backscattered image of LG112 implanted without heat treatment; (b) and after heat treatment (Freeman et al., 2003).

The difference in the osseointegration of the three different classes of LG112 as discussed earlier is also shown as bar chart (figure 2-16).

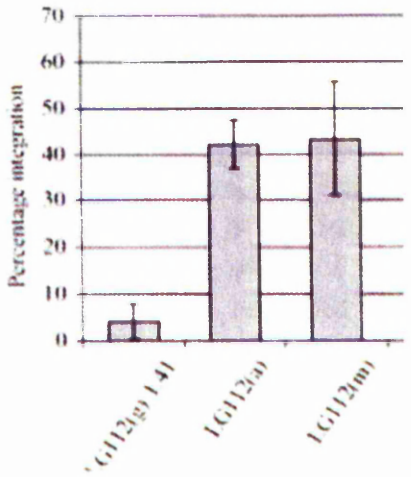

Figure 2-16 Percentage osteointegration of LG112 in the apatite form of the materials (a), in its glassy state (g), and mixed apatite-mullite form (m) (Freeman et al., 2003).

It is evident from the graph that the glassy state is a poor integrator with bone, whereas the apatite and, apatite and mullite state of LG112 are good integrators, with not much difference between the two.

To enhance the properties of ceramics they are often used as composite materials with polymers. These can improve certain properties of implant materials such as composite materials have been developed in an attempt to solve the problem of elastic moduli mismatch and stress shielding of bone. Attempts to mimic the natural structure of bone have led to composites containing hydroxyapatite with collagen to be studied by a number of groups (Du *et al.*, 1998; Marouf *et al.*, 1990). Although these materials are generally tough, they tend to have lower strength than natural bone possibly due to the poor wet tensile strength of reconstituted collagen (Tenhuisen *et al.*, 1995). Synthetic polymers such as polyethylene, have been combined with bioactive ceramics, such as synthetic hydroxyapatite to produce bioactive composites with elastic moduli closer to that of natural bone (Bonfield, 1998).

2.3. Biomedical Polymers and Composites

Polymers have been used in the augmentation and repair of the human body with much success for years. As for other biomaterials, the basic design criteria for polymers used in the body call for compounds that are biocompatible, processable, sterilisable, and capable of controlled stability or degradation in response to biological conditions. The reasons for designing an implant that degrades over time often go beyond the obvious desire to eliminate the need for retrieval. A bioabsorbable implant can increase ultimate bone strength by slowly transferring load to the bone as it heals (Katz, 2001). For drug delivery, the specific properties of various degradable systems can be precisely tailored to achieve optimal release kinetics of the drug or active agent (Katz, 2001).

With regards to using polymers as implant materials, they can be categorised into four types (Vert, 1992):

- **Biodegradable** – polymer materials that break down *in vivo*, into macromolecular particles, although there is no evidence to say they have been eliminated from the body.

- **Bioresorbable** – polymeric materials which do degrade but in addition show resorbtion, whereby the products are removed via natural pathways. This may be due to degradation, which results in simple by-products that can be filtered or resorbed into the body's system. Therefore, bioresorption is a description of a material that is totally removed from the body with no side effects.

- **Bioerodable** – this refers to solid polymeric materials or devices which show surface degradation compared to bulk degradation as is generally seen in polymers. Only the surface of the device is degraded.

- **Bioabsorbable** – when a polymer dissolves into body fluids without the chains of the polymer being cleaved, or a decrease in molecular mass. A bioabsorbable polymer may be bioresorbable if the polymer chains, which have been absorbed, can then be eliminated via natural pathways.

The possibility of manufacturing biodegradable/bioresorbable composites for use as bioactive matrices to guide and support tissue ingrowth has been investigated using a variety of polymers, due to their very different properties. Examples of this are poly (D-L-lactic acid) (PDLLA)/Bioglass composites, poly (lactic-co-glycolic acid) (PLGA)/Bioglass composites and high density polyethylene (HDPE)/Bioglass composites (Verrier *et al.*, 2004; Maquet *et al.*, 2003; Wang *et al.*, 1998). An ideal biodegradable polymer for medical applications would have adequate mechanical properties to match the application, would not induce inflammation or other toxic response, would be fully metabolised once it degrades, and would be sterilisable and easily processed into a final end product with an acceptable shelf life.

2.3.1. Polyethylene Glycol based polymers

Polyethylene glycol (PEG) is also referred to as polyethylene oxide (PEO), polyoxyethlene (POE), or polyoxirane. They are made up of a simple monomer unit; $HO\text{-}(CH_2CH_2O)_n - CH_2CH_2OH$, where n corresponds to the molecular weight of the polymer being under 20,000 (PEG) and over 20,000 (PEO). When the monomer has a molecular weight less than 1000, it is a colourless viscous liquid. However higher molecular weights have a waxy white solid appearance. PEGs are noted for being biocompatible, non-toxic, and water soluble (Table 2-3). It is these properties that make it applicable for many biomedical applications. Although PEGs do not degrade in the biological environment, below a certain molecular weight they can be eliminated via excretion (Harris, 1992).

Table 2-3 Properties of Polyethylene glycol (Harris, 1992).

Properties of PEG that make it a suitable biomaterial
• Soluble in water, toluene, methylene chloride and many other organic solvents • Insoluble in ethyl ether, hexane and ethylene glycol • Insoluble in water at elevated temperatures • Solubility controlled by making derivatives • Forms complexes with metal cations • Highly mobile: large exclusion volume in water • Can be used to precipitate proteins and nucleic acids • Forms two phase systems and aqueous solution of other polymers • Non toxic and FDA approved for internal consumption • Hospitable for biological materials • Causes cell fusion at high concentrations • Weakly immunogenic

PEG and PEG-based polymers have been widely used in the form of hydrogels for biomedical applications such as contact lenses, wound bandages, bioadhesives, artificial skin and cell immobilisation. It has also been noted that PEGs have been used to develop protein-resistant surfaces. This is due to its remarkable efficiency in impeding other polymers from an aqueous environment, leading to protein rejection (Harris, 1992). This is the main reason for using PEG based polymers as their surface chemistry can be altered to make them biocompatible or inhibit attachment of biomolecules.

Polyethylene glycol diacrylate (PEGDA) and dimethacrylate (PEGDMA) are copolymers that use PEGs as their main chain, and the acrylate groups provide functionality allowing cross-linking of the polymer. In general, polymer degradation is accelerated by greater hydrophilicity in the backbone or end groups, greater reactivity among hydrolytic groups in the backbone, less crystallinity, greater porosity, and smaller finished device size (Alexis, 2005).

2.3.2. Photoinitiated Polymerisation

Photoinitiated polymerisation is that initiated by light, normally ultraviolet (UV) radiation, and is an attractive material processing method due to its high polymerisation rates at room temperature, solvent-free processing, low energy input, spatial and temporal control of the

initiation process, and chemical versatility (Decker, 1996). The route to polymerisation depends on the processing technique. Factors that must be considered are the effects of processing and any chemical additives will have on cell attachment and proliferation.

The UV spectrum of radiation has wavelengths ranging from 400–100 nm. This range is divided into three categories depending on how intense the transmitted waves are. UV-A (400-315 nm) is the least strong of the three, but there is concern over its long term exposure and is mainly used for polymerisations. UV-B (315-280 nm) is very damaging to the skin and eyes, and can cause sunburn leading to skin cancer. UV-C (280-100 nm) is the strongest and most dangerous type of ultraviolet light and is the one absorbed by the ozone layer in the atmosphere. Ultraviolet arcs that transmit the full range of UV light can also be used for polymerisation reactions, to achieve faster rates of reaction, but one of the problems associated with these is the heat generated which can lead to surface distortion.

UV curing is a process that changes a multifunctional monomer into a crosslinked polymer by a chain reaction initiated by reactive species which are generated by UV irradiation. When a photoinitiator system is exposed to the UV light, an interaction occurs which leads to the chemical re-arrangement of the photoinitiator molecule. The chain reaction after initiation is that of conventional polymerisation, except that a much higher rate of initiation can be achieved by intense radiation (Decker, 1996). When a free radical photoinitiator is exposed to UV light, it absorbs the energy to generate free radicals. These free radicals react with the monomer and chain polymerisation occurs, until the system is no longer subjected to the UV light.

Free radical photoinitiators are the most important commercial photoinitiators due to their high reactivity and easy synthetic method. An example of a free radical photoinitiator is 2,2-dimethoxy – 2 – phenylacetophenone (DMPA), which has a chemical structure:

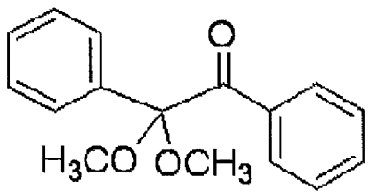

Another common photoinitiator used is IRGACURE 1173, which has a chemical structure:

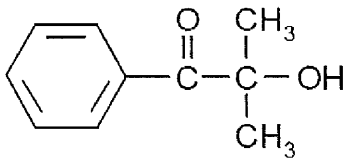

Both these photoinitiators are widely used in biomedical applications and have been known to be non-toxic at low concentrations (Rimmet *et al.*, 2007; Pierre *et al.*, 2006). Rimmet *et al.* (2007) used IRGACURE 1173 for producing hydrogels for corneal implants and proved their affinity for stromal cell attachment.

2.4. Porous Scaffolds

For many tissue engineering applications, a scaffold is required that can act as a template and guide for cell proliferation, cell differentiation and tissue growth. The internal architecture of the scaffold also has a direct impact on the mechanical behaviour of the implant. A scaffold must exhibit a number of properties to make it a viable option for use in the body. The design must cater for the needs of the organ/tissue to be regenerated and induce a similar environment to that found in that area of the body. Knesser *et al.* (2001) have been studying the differentiation function of hepatocytes (liver cells) which have been transplanted and believe that the ability of the cells to function, and differentiate are in fact influenced by the three-dimensional scaffold architecture.

Ideally, the design of a scaffold needs to be highly porous, to allow the interaction of body fluids with seeded cells in the implant. With regards to the design of the scaffold, it must have structural integrity and a degree of reproducibility. These can be controlled by the use of materials and the processing routes. The porosity is required to have characteristic length scales in the order of, or larger than cellular dimensions. This would allow vascularisation of the implant.

Polymers comply with many of the criteria required from materials to form scaffolds and act as extracellular matrices for cell differentiation and proliferation. In addition, they can be light in weight, biocompatible, biodegradable and their mechanical properties can be matched to that of many natural body materials.

2.4.1. Porous Scaffolds as Bone Implants

The physical characteristics for development of porous scaffolds as bone implants requires precise control of the porous volume of the biomaterial, as well as the mean pore and interconnection sizes. The desirable characteristic of these biomaterials are: biocompatibility i.e. not to provoke any unwanted tissue response to the implant, and at the same time to possess the right surface chemistry to promote cell attachment and function; and biodegradability i.e. degradable into non-toxic products, leaving the desired living tissue. These characteristics are possessed by both natural and synthetic polymers and ceramics. Most synthetic polymers degrade via chemical hydrolysis and are insensitive to enzymatic processes so that their degradation does not vary from patient to patient (Lu and Mikos, 1996).

An example of a tissue compatible polymer used as a scaffold is Poly (ε-caprolactone) (PCL). The presence of hydrolytically-unstable aliphatic-ester linkage causes the polymer to be biodegradable. The homopolymer has a degradation time of the order of 2 years, which can be altered by copolymerization (Lu and Mikos, 1996).

The regeneration of specific tissues aided by synthetic materials has been shown to be dependant on the porosity and pore size of the supporting three-dimensional structure (Cima *et al.*, 1991). A large surface area favours cell attachment and growth, whereas a large pore volume is required to accommodate and subsequently to deliver to a cell mass. The surface area/volume ratio of porous materials depends on the density and average diameter of the pores. Depending on the envisioned application, the pore size must be carefully controlled, which is dependant on the cell type. Klawitter *et al.* (1971) have suggested that the pore sizes required for regeneration of bone should be between 100 – 600 μm (see Table 2-4).

Table 2-4 Studies defining optimal pore size for bone regeneration (Whang and Healy, 2001).

Scaffold pore size (μm)	Porosity (%)	Mineralise tissue ingrowth
Type I: 2-6 μm	33.5	No tissue ingrowth
Type II: 15-40 μm	46.2	No bone ingrowth, fibrous tissue ingrowth
Type III: 30-100 μm 80% pores < 100 μm	46.9	50 μm of bone ingrowth, osteoid and fibrous tissue ingrowth
Type IV: 50-100 μm 63% pores < 100 μm	46.9	20 μm of bone ingrowth by 11 weeks and 500 μm of ingrowth by 22 weeks, osteoid and fibrous tissue ingrowth
Type V: 60-100 μm 37% < 100 μm	48	600 μm of bone ingrowth by 11 weeks and 1500 μm of ingrowth by 22 weeks, osteoid and fibrous tissue ingrowth
≤ 100 μm	35.3	Not statistically different from untreated controls
≤ 200 μm	51	Not statistically different from untreated controls
≤ 350 μm	73.9	Statistically significant more bone than all other groups

Flautre *et al.* (2001) studied HA ceramic using poly methylmethacrylate microbeads as the porous agent, and found that the best osteoconduction result was achieved with a mean pore size of 175 – 260 μm with the means of a 130 μm interconnection size. It was observed that increasing the mean pore size to 260-350 μm reduced the occupied bone tissue volume within the scaffold by 10% after 12 weeks, and by 20% when the pore size was increased to 350-435 μm. The size of the interconnected pores was set to 130 μm before implantation in order to immediately encourage the cells and fibroconnective tissue of the bone host to be recolonised by bone tissue as fast as possible.

The interconnectivity of the pores is a very important consideration. Cell migration would be inhibited if the pores were not interconnected even if the matrix porosity is high (Moone and Baldwin, 1996). Mass transport is one of the most significant challenges in tissue engineering.

A further concern is the change in the effective pore structure with time *in vivo*. If the matrix is biodegradable the average pore size will increase and bottlenecks in the continuity of the pore structure will open with time (Cohen and Yoshioka, 1991). If the matrix does not degrade, its effective pore size may be reduced by *in vivo* events such as

the invasion of fibrous tissues into the pores. Strong cell adhesion and spreading often favour proliferation while rounded cell morphology is required for cell specific function. Thus a polymer scaffold must act as a suitable substrate to maintain differentiated functions without hindering proliferation (Lu and Mikos, 1996).

2.4.2. Fabrication of Porous Scaffolds

There are a variety of techniques that can be used to fabricate a scaffold. To fabricate a scaffold, the major requirement of any proposed processing technique is to use a biocompatible material, without compromising its biocompatibility during processing. The processing technique should also allow the manufacture of scaffolds with controlled porosity and pore size, which are both very important factors in tissue regeneration. Thus, choosing the correct technique is very important since the fabrication method can determine the ultimate properties of the implant. Some of these techniques are discussed in detail.

2.4.2.1. Selective Laser Sintering

Selective Laser Sintering (SLS) consists of a roller which spreads powder over the surface of a build cylinder. During each cycle the cylinder moves down one layer thickness to accommodate the new layer of powder. Subsequently the powder delivery system supplies a measured quantity of powder for each layer.

A laser beam is then focused and projected over the surface of this tightly compacted powder to selectively melt and bond it to form a layer of the object. For plastic parts the fabrication chamber is maintained at a temperature just below the melting point of the powder, thus allowing a minimum amount of laser energy required to sinter the object layers. This greatly speeds up the process. The temperatures required to sinter ceramics are extremely high, therefore the ceramic powders are normally coated with a polymer binder. The laser melts the binder, which bonds the layers together forming a green object.

After the object is fully formed, excess powder is simply brushed away and final manual finishing may be carried out. Thus allowing the green ceramic object to be fired in a

conventional furnace. Supports are not required with this method since overhangs and undercuts are supported by the solid bed of excess powder.

Several polymer-based systems have been developed to fabricate ceramic objects, although the resultant green bodies are highly porous. Infiltrating these porous ceramic objects with metal, resin or inorganic colloidal suspensions improve their structural strength (Nelson *et al.*, 1995 and Subramanion *et al.*, 1995).

However, this technique has some disadvantages such as rough surface finish, porosity of parts, the first layers may require a base anchor to reduce thermal effects (e.g. curl), part density may vary and material changes require cleaning of machine.

Manufacturing ceramic components by SLS is significantly more problematic than fabricating either polymeric of metallic parts, mainly due to the thermal shock inherent in the sintering process. Crawford *et al.* (1997), however, have successfully processed a calcium phosphate material suitable for bone implants, and Goodridge *et al.* (2006) have fabricated apatite-mullite glass-ceramics using SLS with a strength similar to that of cancellous bone, and a porous structure which was suitable for the ingrowth of bone.

2.4.2.2. Fibre Bonding

A number of textile technologies have been applied to design and fabricate highly porous scaffolds (Hutmacher, 2001). Fibres are used in this process as they provide a large surface area to volume ratio and hence act as a desirable scaffold matrix. The process begins with immersing a fibre in a premixed polymer solution in solvent. The solvent is then evaporated, leaving an interpenetrating network of fibres in a polymer matrix which when heated to slightly above the melting point of the fibres, bond at their network junctions. Finally the polymer is dissolved, leaving a porous scaffold of bonded fibres (Mikos *et al.*, 1994).

Although fibre bonding techniques produce highly porous scaffolds, the use of solvents make this technique undesirable as small amounts of solvent remaining within the scaffolds can be toxic to cells if not removed completely. In order to extract these chemicals, the constructs must be vacuum dried for several hours, making it difficult to be used immediately in a clinical setting.

2.2.4.3. Solvent-casting and particulate leaching

This process utilises a salt dispersed in a polymer-solvent solution. The solvent is evaporated and then the polymer/salt composite is heated above the melting point of the polymer and then cooled down. The salt is leached out by immersing the scaffold in distilled water and the porous polymer matrix with pore sizes between 50-150 μm can be obtained (Mikos, 1994). The drawbacks of using this technique are that only a limited thickness of pores can be achieved and the use of solvents can prove toxic to cells.

2.4.2.4. Laminated Object Manufacturing (LOM)

Laminated Object Manufacturing (LOM) uses a laser beams to cut out the outline of each layer of an object from thin sheets of material, usually paper, but polymers, metals or composites may also be used (Klosterman *et al.* 1998). The undersides of these sheets are coated with a heat-sensitive adhesive that bonds them to the previous layer when a heated roller is passed over.

The paper is unwound from a feed roll onto the stack with the first layer bonded to the next using a heated roller, which activates the adhesive. The profiles are then traced by an optics system that is mounted on an X-Y stage. Excess paper is cut away to separate the layer from the web. Waste paper is wound on a take-up roll. The method is self-supporting for overhangs and undercuts. Areas of cross sections, which are to be removed in the final object, are heavily crosshatched with the laser to facilitate removal. Figure 2.17, illustrates the principal commercial version of LOM systems.

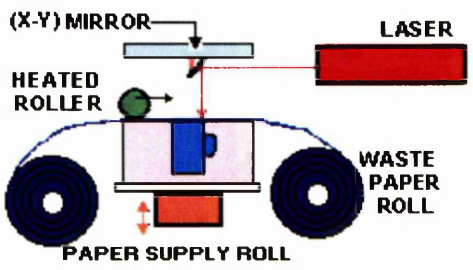

Figure 2-17 Schematic of Laminated Object Manufacturing.

Creating ceramic objects by LOM differs slightly in detail. Green tapes of ceramic powder in binder are prepared by conventional tape casting. These are cut to shape with a laser. Again, the shaped tapes correspond to each layer (slice) of a CAD image, and are loaded in place on top of each other. The lamination process is achieved through simultaneous application of temperature and pressure, to improve the interlayer bond. LOM of ceramic objects was first achieved by Griffith *et al.* (1994) who fabricated Al_2O_3 with properties similar to those expected from conventional processed material.

One of the main advantages of LOM is accuracy, with models contructed to ±127 μm, and due to the use of sheet material, they do not shrink or distort (Yan and Gu, 1996). However, difficulties arise in the production of hollow parts or parts with undercuts. There is also a large amount of scrap generated. The produced parts have limited applications as functional prototypes due to poor shear strength resulting from the layering of adhesive and material (Yan and Gu, 1996).

2.4.2.5. Gel Casting

Gel casting is a new ceramic forming process in which a slurry of ceramic powder in a solution of organic monomers is cast into a mould. It can be used to fabricate complex shapes which are not possible to achieve using other techniques such as injection moulding and slip casting. During this process, a concentrated slurry of ceramic powder is poured into a mould and allowed to polymerise *in situ* to form a strong, crosslinked polymer-solvent gel that holds the ceramic particles in place (Omatete *et al.*, 1991).

The monomer solution consists of a solvent, a chain forming monomer, a chain branching monomer, and a free radical initiator. The most commonly used chain formers are methacrylamide (MAM), hydroxymethylacrylamide (HMAM), methoxy poly(ethylene glycol) monomethacrylate (MPEGMA), isobornyl acrylate (IBA) and N-vinyl pyrrolidone (NVP). These monomers can also be used in conjunction with each other. The most commonly used branching monomers are methylene bisacrylamide (MBAM), propoxylated neopentoglycol diacrylate (PNPGDA) and poly(ethylene glycol) dimethacrylate (PEGDMA). The initiator used being ammonim persulfate (APS) and tertramethylethylene diamine (TEMED) is used as a catalyst to accelerate the polymerisation reaction by breaking down the APS faster.

Gel casting has been used as a successful way to produce scaffolds for use as implants. Chu *et al.* (2002) used gel casting to produce porous HA implants, using a 1:1 mixture of PNPGDA and IBA and suspending the HA in the monomer solution. Benzoyl peroxide (BPO) was used as the initiator which was added to the slurry, and cast into a mould to be cured at 85° C for 1 hour. The binder and the mould were burnt out thereafter, to be left with a 3-dimensional HA implant with controlled geometry. A flowchart of the gel casting process is shown below (figure 2-18).

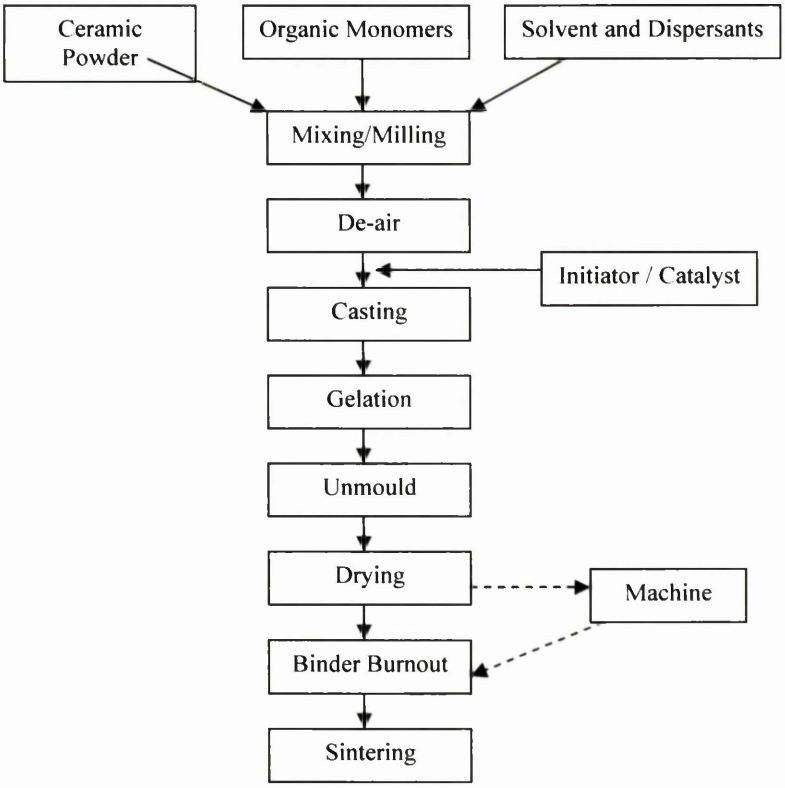

Figure 2-18 Flowchart of the gel casting process (Janney, 1998).

A modified form of gel casting process was also used by Limpanuphap (2002) to produce a composite scaffold of PEGDMA and hydroxyapatite, where the procedure for gel casting was the same but the polymer was not burned out, hence giving the scaffold a higher structural integrity. The mould used was fabricated by Ink jet printing.

Ramay *et al.* (2003) used the same process of gel casting to produce HA implants using polymer foam as the scaffold materials. The foams could be produced with controlled pore sizes but not controlled internal architecture. The components of the gel casting process

were the reactive organic monomers: monofunctional acryamide and difunctional methylenebisacrylamide. APS and TEMED were used as the initiator and catalyst respectively. Surfanol was used as a surfactant to stabilize the slurry which was mixed with deionised water. The solution was then cast into polyurethane foams, which were burnout at a rate of 1°C/min to 600 °C subsequent to polymerisation. Some of the scaffolds produced are shown in figure 2-19.

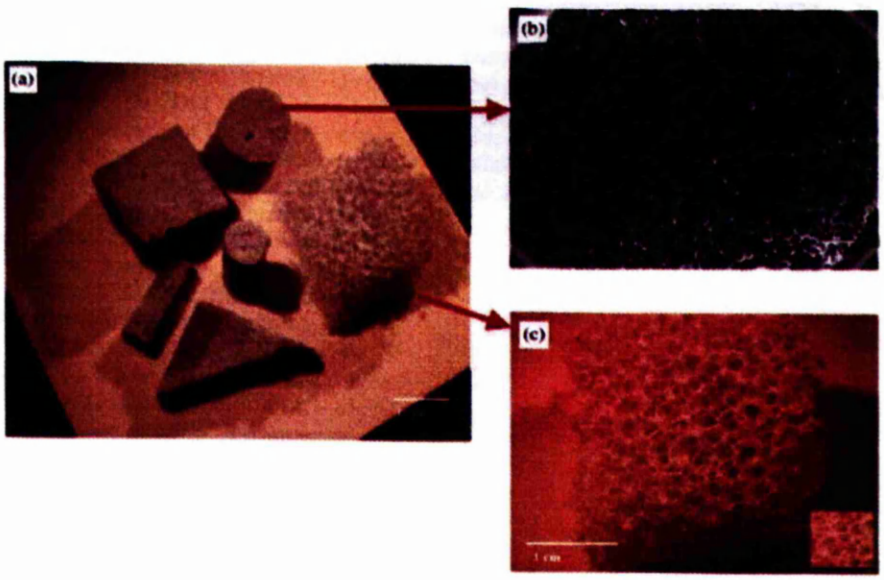

Figure 2-19 Optical micrographs of (a) HA scaffolds of different shapes; (b) and (c) macroporous structures of HA scaffolds fabricated using combined gel casting and polymer foam methods (Ramay and Zhang, 2003).

2.4.2.6. Three-Dimensional Printing

Three-dimensional printing (3DP) was developed at the Massachusetts Institute of Technology (MIT) and shown schematically in figure 2-20. The process uses powdered materials which are thinly spread over the surface of a powder bed and levelled by a roller. A multi-channel jetting head selectively deposits a liquid adhesive onto the layer of powder according to data from a computer model, and the powder particles become bonded in these areas. On completion of a layer, the piston that supports the powder bed lowers the work piece by a distance equivalent to one layer thickness, and the next layer of powder is spread over the previously formed layer. The process is repeated until the entire part is formed within the powder bed. Any overhangs, undercuts, or internal volumes in the

part are supported during the build cycle by the surrounding unbound powder. Once all layers have been completed, the object is elevated and any unbound powder is removed leaving a relatively low-density "green part". Heat treatment is used to enhance the bonding of the glued powder (Lee, 2005).

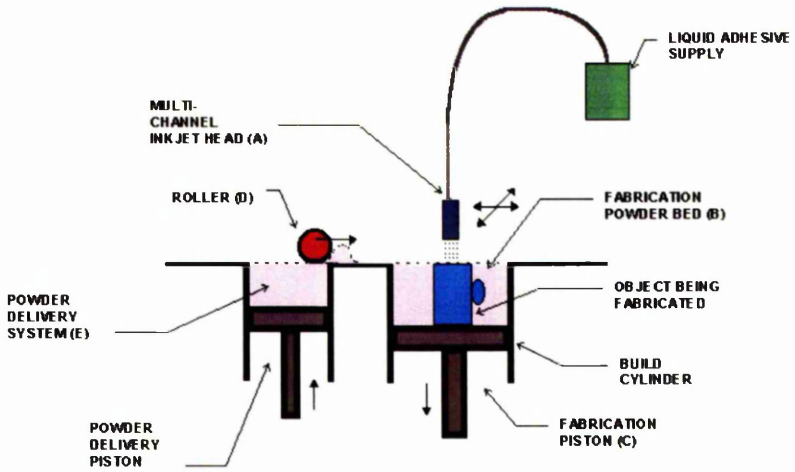

Figure 2-20 Schematic diagram of 3DP.

3DP is a particularly versatile method as it can be used to process any material that can be obtained as a powder, including ceramics, metals, polymers and composites. There is also the ability to control local material composition, as different materials can be dispensed from different printer heads. There are limitations however on resolution, fragility of parts, surface finish and materials available (Lee, 2005).

2.4.2.7. Inkjet Printing

Another technique similar to this is the direct printing of 3-dimensional structures using a "drop on demand" system, where the droplets are forced onto a platform and then built upon (Yeong, 2005). This is a slow technique but can be exceptionally accurate. It uses a printer head that squirts out small particles through a nozzle, and has the ability to form the fine network that is essential in bioengineering. The accuracy of the method is partly due to a milling step after each layer deposition, which is where a cutter smoothes every layer after deposition. However, using hot molten particles requires that there is some sort of support in the system. This is provided by another printer head, which fills in the outline of the object formed by the first printer head. A cutter is then moved over the surface to give

a smooth finish again. These support materials are often waxes, which can be removed at a later stage by melting or dissolving (Figure 2-21).

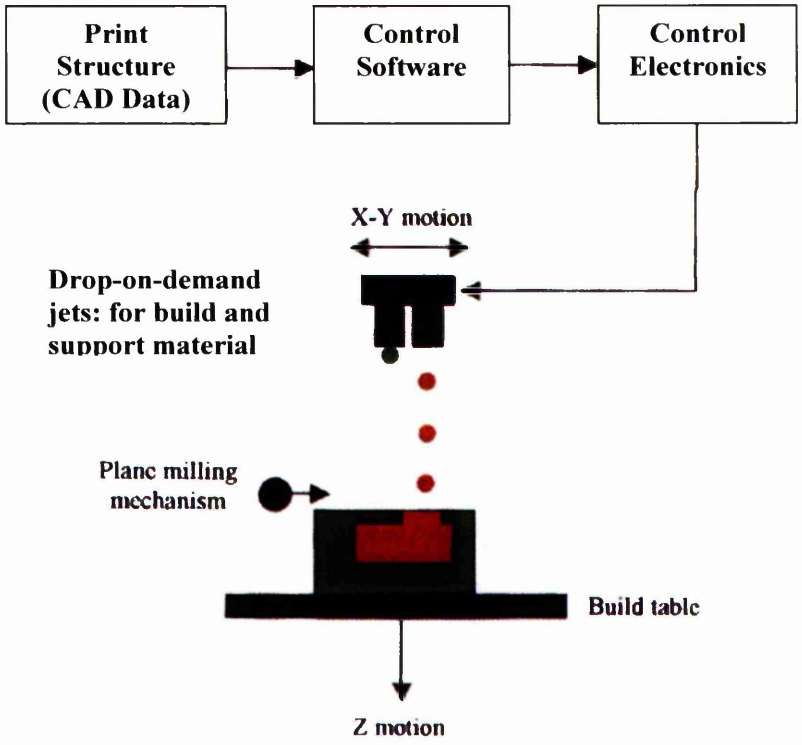

Figure 2-21 Schematic of drop-on-demand printing (Limpanuphap, 2004).

The main advantage of inkjet printing is the ability to produce extremely fine resolution and surface finishes. However the technique is very slow for large objects, and there is a very limited selection of materials that can be used with this technique.

2.4.2.8. Stereolithography

Stereolithography (SLA) was originally developed by Kodama (1981) and is a widely used technology in the field of rapid prototyping. It is a photopolymerisation process that uses a laser beam to selectively draw or print cross sections of a model on a photocurable resin surface.

The main feature of rapid prototyping technologies is the selective creation of material, layer by layer, producing a part directly from CAD data. This in turn is converted into a STL data format that is a faceted version of the surface of the model.

Commercial SLA machines e.g. Viper Si2, 3D systems produce plastic prototypes from epoxy resins by photopolymerisation of a liquid monomer with a UV laser (figure 2-22). The laser generates a small, intense beam which is moved by a computer-controlled optical scanning system across the top of the vat containing the liquid resin. The first step is curing a thin (250 μm) layer by drawing the cross-section on the surface of the resin with the laser (Griffith and Halloran, 1996). The part is attached by supports to an elevator platform beneath the surface of the resin. When the first layer is completed, an elevator lowers the part deeper into the vat, covering it with the resin contained in the vat. Levelling and recoating systems establish the thickness and flatness of the liquid layer. When the resin surface is stable, the laser draws the next layer of the part. As each layer is drawn, it adheres to the previous layer, creating a solid part. Repeating these steps many times builds up the 3-dimensional plastic part which then undergoes the necessary clean up and post-curing process.

During the photopolymerisation method the resin does not reach full solidification; therefore after building in the SLA, the part is put into an UV oven to be cured up to 100% and to complete the polymerisation process (post-curing process). The machine used for the post processing is called a Post Curing Apparatus (PCA) (figure 2-23). However, under this process, the presence of shrinkage and distortion is one of the major sources of error in the stereolithography process.

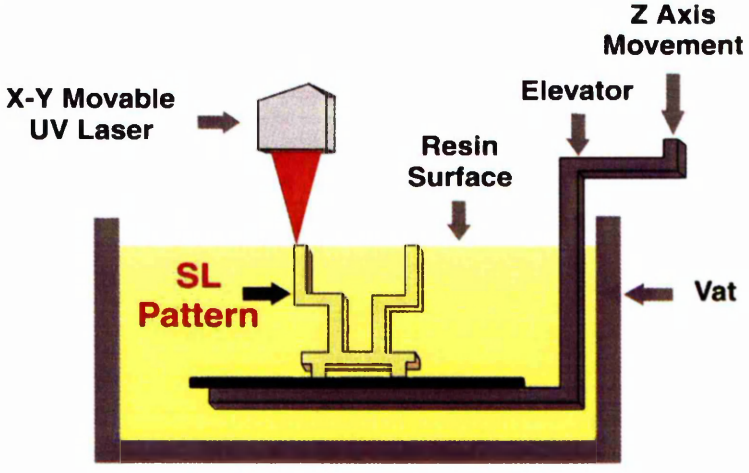

Figure 2-22 Schematic of a Stereolithography apparatus (SLA)(Courtesy of 3d systems).

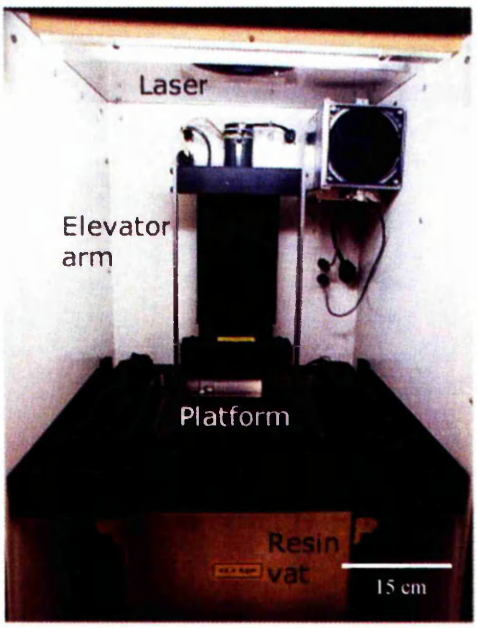

(a)

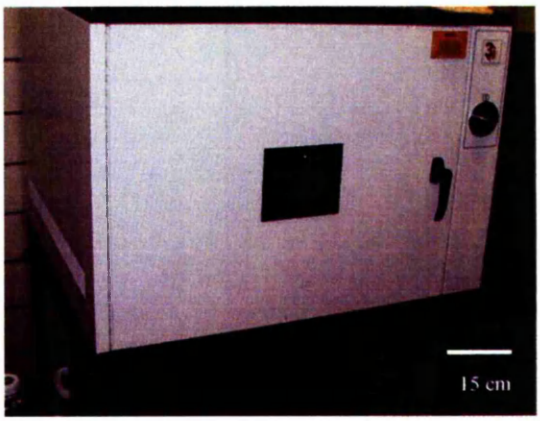

(b)

Figure 2-23 (a) Stereolithography apparatus, and (b) shows the post-curing apparatus (PCA).

Investigating the curing behaviour of photopolymers in the stereolithography process is very important as the resulting shrinkage leads to strains of considerable magnitude (Zhou *et al.*, 1999). To reduce the amount of time taken at the post curing stage, many variables need to be considered prior to the manufacturing process. Some of these are layer thickness, Z-level wait, sweep period, overcure, blade gap, hatch spacing, dip velocity and dip acceleration (Zhou *et al.*, 1999)..

Each of these variables affects the output part quality. The primary control factors out of these are: -

- Layer thickness – the thickness of each slice of the part building on the previous layer.
- Hatch spacing – defined as the distance between the centrelines of adjacent parallel hatch vectors.
- Overcure – refers to the depth that the laser cures past the layer thickness.
- Blade gap – allows the vertical separation between the bottom of the recoater blade and the top of the previous (cured) layer to be increased per sweep.

- Position on the build plane – the build plane can be partitioned as inner, middle and outer (from the centre to the edge) of the platform.

These factors affect the dimensional and geometrical accuracy, and surface roughness of the final parts, individually or interactively.

For over a decade, stereolithography has been the predominant freeform fabrication technique. Stereolithography has been more recently modified to the fabrication of ceramic parts (Dufuad and Corbel, 2002). The process then entails formulating a suspension of fine ceramic particles in an appropriate photosensitive resin. The green body is obtained by selectively curing the resin that acts as temporary binder. Subsequent thermal processing of the part burns-out the photopolymer binder and sinters the particles to high density. For ceramic processing purposes it is desirable to maximise the solid volume fraction of particle in the resin in order to limit shrinkage and part distortion during curing, binder burnout and sintering. This assumes the development of carefully-tailored formulations wherein the various components have been matched to one another in order to also fulfil additional requirements in terms of recoating properties and reactivity (Griffith and Halloran, 1996).

Griffith and Halloran (1996) have reported the fabrication of ceramic parts by SLA. Suspensions of alumina, silicon nitride and silica particles loaded in UV photocurable monomer have been used in the SLA. Curing of the monomer resulted in binding of ceramic particles to form a green body. The binder was thence removed by pyrolysis and the ceramic parts sintered. Levy *et al.* (1997) also used the same technique to produce HA scaffolds for orbital floor prosthesis. These HA scaffolds offer superior cosmetic appearance for bone graft applications compared to conventional techniques. Matsuda and Mizutani (2002) have developed a biodegradable, photocurable copolymer, acrylate-endcapped poly(e-caprolactone-co-trimethylene carbonate), which can be used with the SLA apparatus.

2.4.2.8.1. Advantages of Freeform Fabrication over other techniques

When fabricating polymer scaffolds, several factors have to be considered, not only the geometrics of the scaffold but also the degradation effects of the synthetic polymers.

Polymers often release acidic by-products over time after being implanted, which reduce the pH, and create a highly acidic environment adjacent to the scaffold. Such an environment, may adversely affect cellular functions (Kohn *et al.*, 2002). These changes can also affect bone-remodelling processes (Wake *et al.*, 1998) along with eliciting an inflammatory response and inducing bone resorption.

Conventional scaffold fabrication techniques are incapable of precisely controlling pore size, pore geometry, spatial distribution of pores and construction of internal channels within the scaffold. Scaffolds produced by solvent-casting cannot guarantee interconnection of pores because this is dependant on whether the adjacent salt particles are in contact, which also makes controlling the pore size difficult (Hutmacher, 2001). For solvent casting, it has been reported that only 10-30% of the pores were interconnected (Mooney *et al.*, 2000) Non-woven fibre meshes have poor mechanical integrity. Some of these techniques also use organic solvents during the process which are a risk of toxicity and carcinogenicity to cells.

In addition, these techniques produce scaffolds that are foam structures, upon which cells are seeded and expected to grow into the scaffold. However, this approach only results in the growth of the tissues of less than 500 μm from the external surface (Ishaug-Riley *et al.*, 1997). This is probably caused by the diffusion constraints of the foam, in which the cells cannot migrate deep into the scaffold because of lack of nutrients and oxygen, and insufficient removal of waste products (Figure 2-24).

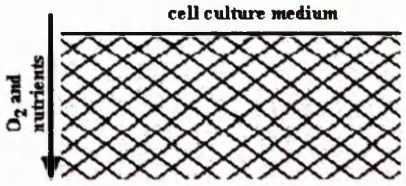

a) Tissue engineering scaffold which is an open-cell foam structure. Oxygen and nutrients are supplied from the liquid cell culture medium.

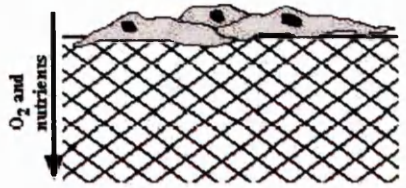

b) Cell seeding on scaffold.

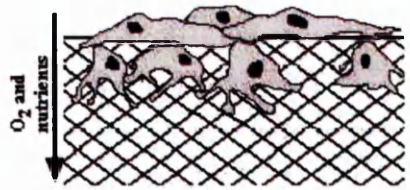

c) Cells start to proliferate and migrate into the pores of the scaffold.

d) The cells fully colonise the pores and start to lay down their own extracellular matrix.

e) The top layer of cells consumes most the oxygen and nutrients in addition to limiting the diffusion of these components, thus reducing the amount available for pioneering cells migrating deep into the scaffold. Eventually, cellular migration is halted due to the lack of oxygen and nutrients supply. The layer of cells that can survive on the diffusion of oxygen and nutrients from the medium is called the cellular penetration depth (Dp).

Figure 2-24 Schematic diagram showing the diffusion constraints of tissue engineering scaffolds which are foam structures (Sachlos et al., 2003.)

The cell colonisation at the periphery acts as an effective barrier to the diffusion of oxygen and nutrients into the scaffolds. Furthermore, for bone tissue engineering, the consumption of oxygen and nutrients on the surface of the scaffold leads to mineralisation, which further limits the mass transfer to the interior of the scaffold (Martin *et al.*, 1998). Thus, cells are only able to survive close to the surface.

It is due to these reasons that tissue engineering scaffolds need to embrace the techniques of solid freeform fabrication such as Stereolithography, which has the ability to construct a controlled geometrical scaffold with pore sizes and interconnected channels, which are able to provide oxygen and nutrients within the scaffold and remove waste products.

2.4.2.8.2. Ceramic Composite Stereolithography

For ceramic composite stereolithography, an acrylate monomer suspension with at least 50% volume loading of glass-ceramic particles is required to ensure green body integrity while maintaining a "pourable" viscosity to aid in the viscosity process (Wu *et al.*, 2005). The monochromatic UV laser (325 nm) photopolymerises successive two-dimensional patterns of specified thickness, onto the surface of this suspension which has photoinitiators mixed within. Each photopolymerised layer adheres to the previous layer beneath by an excess dose of energy (overcure), allowing the fabrication of complex three-dimensional structures. For this suspension to be successful in a SLA, the 50-60% loading of glass-ceramic by volume must have a relatively low viscosity. To operate in a SLA tank, the ceramic suspension must be at least as fluid as conventional SLA resins (viscosity less than 3000 mPa·s) for proper flow during recoating of the new layer and not source any resistance (Griffith and Halloran, 1996).

Apart from this, factors that need to be considered are influence of exposure conditions, powder characteristics (nature, particle size), and the formulation of the reactive system (photoinitiator concentration, nature of the curable monomer) on the cured depth and width, and on the dimensional resolution (Chartier *et al.*, 2002).

The critical parameters in SLA that take these factors into account and fabricate a product that is suitable are Depth of Penetration, D_p, which is the rated penetration distance of the resin or the distance which the laser intensity is reduced by e^{-1}, and Cure Depth, C_d, which is the desired cure depth.

They are related through the Jacobs equation where E_0 and E_{crit} are the maximum energy (mJ/cm^2) delivered by the laser to the surface of the resin and the critical exposure energy for polymerisation, respectively.

$$C_d = D_p \ln\left(\frac{E_0}{E_{crit}}\right) \qquad \text{Equation 2-1}$$

This is an important equation for the SL process and is called the working curve of the laser. D_p and E_{crit} are parameters dependant on the resin, which makes it possible to calculate the maximum exposure that is necessary to generate a cure depth, C_d. It is also possible to calculate the maximum cured lined width, L_w, by the expression,

$$L_w = B\sqrt{\frac{C_d}{2D_p}} \qquad \text{Equation 2-2}$$

where $B = 2W_0$ (W_0 is the laser spot diameter) (figure 2-25).

However, the introduction of glass-ceramic particles in these suspensions adds a level of complexity because the laser may be scattered by the suspensions instead of being absorbed by the photoinitiator (Griffith *et al.*, 1997). This situation reduces the cure depth and the overall build speed. The SLA makes layers 150 – 200 μm thick when using the normal resin. Therefore, it is necessary that the cure depth of the highly loaded glass-ceramic suspensions is equal to or greater than 150 – 200 μm in order to fabricate a product with enough structural integrity in a sufficient amount of time (Griffith *et al.*, 1997).

The addition of glass-ceramic particles causes the laser to scatter, thus limiting the penetration of the UV radiation into the suspension, reducing the cure depth and the overall build speed. The reason for the degradation in performance is that such colloidal systems strongly scatter light due to the difference in refractive index between the particles and the dispersing medium.

Taking the particles volume, size and scattering properties into account, equation 2-1 can also be clarified using the Beer-Lambert law, where,

$$C_d \quad \alpha \quad \frac{d}{\phi\beta\left(n_{ceramic} - n_{resin}\right)^2} \ln\left(\frac{E_0}{E_{crit}}\right) \qquad \text{Equation 2-3}$$

This states that cure depth is proportional to the average particle size (d) and the logarithm of the exposure (E_0) and inversely proportional to the volume fraction of ceramic (Φ). The materials scattering ability is described as a function of the refractive index difference between the ceramic and the resin.

Therefore, the cure depth is inversely proportional to $\Delta n^2 = (n_{cer} - n_{resin})^2$, where n is the refractive index of each phase, and β is related to the particle size and wavelength of the radiation.

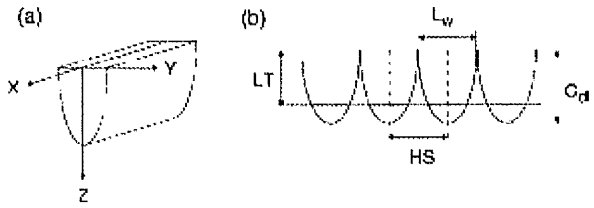

Figure 2-25 (a) Parabolic cylinder shape of the cured line; (b) cross-sectional view of cured lines (Campanelli, 2007).

A high cure depth requires a high density of energy whereas a high resolution requires a low density of energy. Therefore, a compromise has to be reached to reduce the time of fabrication and to obtain a good dimensional resolution. Several parameters such as photoinitiator concentration, powder concentration, the mean particle diameter and the nature of the powder will have an effect on obtaining an appropriate product (Chartier *et al.*, 2002).

2.4.2.8.3. Influence of Photoinitiator

Chartier *et al.* (2002) tested two different ceramic powders, with different photoinitiator concentrations, ranging from 0.3 to 1 wt % based on the monomer weight. They found no significant influence of the photoinitiator concentration on the cure depth of the samples. Nevertheless, a higher concentration (> 2 wt %) led to a loss of reactivity, due to the laser beam being absorbed by the quickly polymerised surface.

Delmotte *et al.* (2003) used two different initiators with different concentrations and showed that using 0.5 wt % of benayldimethylketal leads to a slightly larger depth of cure than the acylphosphine oxide (~ 100μm) (figure 2-26). Mixing the two initiators bis(2,4,6-trimethylbenzoyl) phenophosphine oxide (BAPO) with hydroxyketone demonstrated the best reactivity, but this was accompanied by extensive shrinkage and layer deformation. Consequently, the photoinitiator type and content both influence the cure depth and the texture of the polymerised layer.

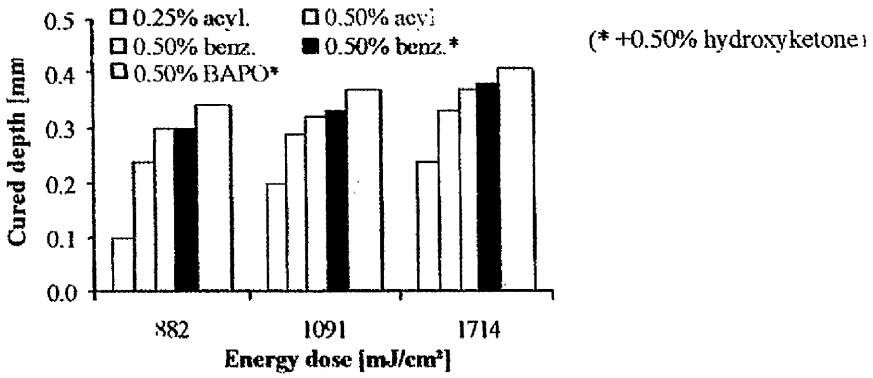

Figure 2-26 Effects of different initiators on cure depth (Delmotte et al., 2003).

2.4.2.8.4. Influence of powder concentration and mean particle size

Cure depth and width decrease as the concentration of the powder increases. This was shown by Chartier *et al.* (2002) where concentrations of ceramic powder ranging from 25 – 60% were used and polymerised at different densities of energy. At the highest density of energy (6.36 J/cm^2), a difference of 600 μm is observed in the cure depth at 25% concentration and 60% concentration. This is obviously due to the higher concentration of powder scattering the laser and thus not achieving a higher cure depth, but the mean particle size also plays a role in this. The bigger the particle size, the higher the cure depth achieved. Similarly, there is an influence of the refractive index difference between the powder and the monomer. As the difference between refractive index of the powder and monomer increases, the cross sectional dimensions decrease.

After the successful fabrication of scaffolds, the next step is to check for their compatibility with cells. The geometry of the scaffold in achieving satisfying cell proliferation and differentiation rates is also likely to be a very important factor.

2.5. Cells

The cell is the fundamental unit of life. Cells are small, membrane-bound compartments filled with a concentrated aqueous solution of chemicals. Cells have certain functions in common, including synthesis and sorting of components, interaction with the environment, energy conversion, and maintenance of their molecular and structural order. In addition, most cells can move, grow, and reproduce. Each cell is at least somewhat self-contained and self-maintaining: it can take in nutrients, convert these nutrients into energy, carry out specialised functions, and reproduce as necessary. Each cell stores its own set of instructions for carrying out each of these activities.

2.5.1. Cell culture

Cell culture is the process by which cells are grown under controlled conditions. The historical development and methods of cell culture are closely interrelated to those of tissue culture and organ culture. Cell culturing is carried out to check the viability of specific cells to a surface. These experiments establish the biocompatibility of the scaffolds, and more over the constituents the scaffolds are made from. These tests finally establish if a material is suitable to be used *in vivo* and if it is able to produce extracellular matrix and essential proteins required for cell growth.

Cells can be isolated from tissues for *ex vivo* culture in several ways. The most common way is to obtain small pieces of tissue, which can be placed in growth media, and the cells that grow out are available for culture. This method is known as explant culture.

Cells that are cultured directly from an animal or person are known as primary cells. With the exception of some derived from tumours, most primary cell cultures have limited lifespan. After a certain number of population doublings cells undergo the process of de-differentiation, and stop dividing, while generally retaining viability (Stanulis-Preger, 1987).

Cells are grown and maintained at an appropriate temperature and gas mixture (typically, 37°C, 5% CO_2) in a cell incubator. Culture media can vary widely for each cell type, and variation of conditions for a particular cell type can result in different phenotypes being expressed.

Aside from temperature and gas mixture, the most commonly varied factor in culture systems is the culture medium. Recipes for culture media can vary in pH, glucose concentration, growth factors, and the presence of other nutrient components. The growth factors used to supplement media are often derived from animal blood, such as calf serum.

Adherent cells can be grown on tissue culture plastic, which may be coated with extracellular matrix components (e.g. collagen or fibronectin) to increase its adhesion properties and provide other signals needed for growth.

As cells generally continue to divide in culture, they generally grow to fill the available area or volume. This can generate several issues:

- Nutrient depletion in the growth media
- Accumulation of apoptotic/necrotic (dead) cells
- Cell-to-cell contact can stimulate cell cycle arrest, causing cells to stop dividing (contact inhibition)
- Cell-to-cell contact can stimulate promiscuous and unwanted cellular differentiation

These issues can be dealt with by using tissue culture methods that rely on sterile techniques. These methods aim to avoid contamination with bacteria or yeast that will compete with mammalian cells for nutrients and/or cause cell infection and cell death. Manipulations are typically carried out in a laminar flow cabinet to exclude contaminating micro-organisms. Antibiotics can also be added to the growth media.

Amongst the common manipulations carried out on culture cells are media changes, and passaging cells.

The purpose of media changes is to replenish nutrients and avoid the build up of potentially harmful metabolic by-products and dead cells. In the case of suspension cultures, cells can be separated from the media by centrifugation and be resuspended in fresh media. In the case of adherent cultures, the media can be removed directly by aspiration and replaced.

Passaging or splitting cells involves transferring a small number of cells into a new vessel. Cells can be cultured for a longer time if they are split regularly, as it avoids the

senescence associated with prolonged high cell density. Suspension cultures are easily passaged with a small amount of culture containing a few cells diluted in a larger volume of fresh media. For adherent cultures, cells first need to be detached by using a mixture of trypsin-EDTA. A small number of detached cells can then be used to seed a new culture.

In an appropriate medium and given suitable physical conditions cells in culture will grow at a characteristic rate as long as growth is not influenced by, for example, the concentration of nutrients becoming limiting or by a build-up of toxic metabolic products. In batch culture (eg. a tube or flask of broth) nutrient supply is limited and growth cannot continue indefinitely. When the growth of such a culture is followed over a period of time three distinct phases of growth are seen; namely lag, exponential, and stationary phase (figure 2-27) (McAteer and Davis, 2002).

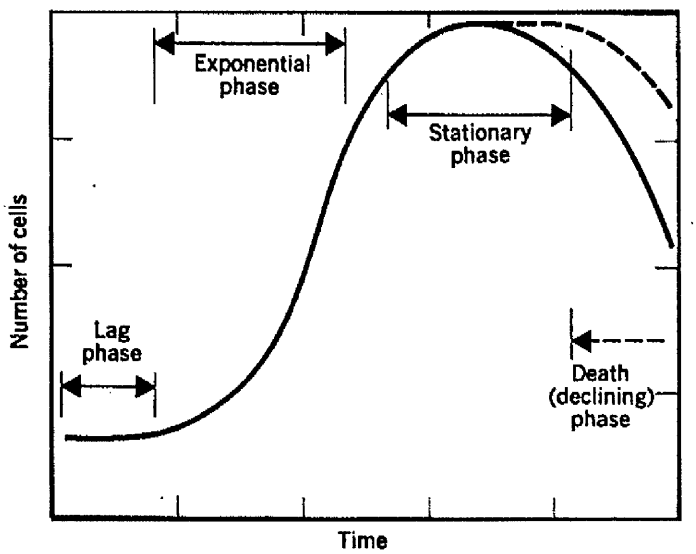

Figure 2-27 Growth phases of cells in culture.

The lag phase is the period when a suspension of cells is seeded into a fresh medium and growth does not occur immediately. The length of the delay, or lag, in growth depends on the cell type and the seeding density. During this period the cells undergo physiological readjustment enabling them to utilise substrates in the new medium (McAteer and Davis, 2002).

In the exponential phase, cells increase exponentially in number and are considered to be at their healthiest. Cells enter a period of balanced growth, during which all constituents of cells increase by the same proportion over the same time interval and the population

doubles in a definite and constant time. The length of the exponential phase is affected by the seeding density, rate of cell growth, and the saturation density of the cell line (McAteer and Davis, 2002).

At the stationary phase, the cell proliferation rate slows down and levels off as the cell population reaches confluency. Confluency is the term used when cells are present throughout the media after proliferation. Eventually the cells stop growing, because some nutrient becomes exhausted. The cells may continue to divide and their daughter cells may be released into the medium. At the end of this stage comes the declining phase, where the number of cells dramatically decreases due to uncompensated cell death (McAteer and Davis, 2002).

2.5.2. Extracellular Matrix (ECM)

Extracellular matrix (ECM) is any material part of a tissue that is not part of any cell. It is the defining feature of connective tissue. It is any material produced by cells and secreted into the surrounding medium, but usually applied to the non-cellular portion of animal tissues. The ECM of connective tissue is particularly extensive and the properties of the ECM determine the properties of the tissue. In broad terms there are three major components: fibrous elements particularly collagen; elastin; and space filling molecules (usually glycosaminoglycans). The matrix may be mineralised to resist compression (as in bone) or dominated by tension resisting fibres (as in tendon). The extracellular matrix of bone is composed of 90% collagenous proteins (Type I collagen 97% and Type V collagen 3%) and of 10% non-collagenous proteins (NCP) (osteocalcin 20%, osteonectin 20%, bone sialoproteins 12%, proteoglycans 10%, osteopontin, fibronectin, growth factors, bone morphogenetic proteins, etc.). All these proteins are synthesized by osteoblasts and most are involved in adhesion. *In vitro*, other proteins such as fibronectin or vitronectin have been shown to be involved in *in vitro* osteoblast adhesion (Anselme, 2000).

2.5.3. The Cytoskeleton

The cytoskeleton is a cellular scaffolding holding all other organelles within the cytoplasm. It is a dynamic structure that maintains cell shape, and also has been known to protect the

cell, enable cell movement, and plays important roles in both intra-cellular transport (the movement of vesicles and organelles) and cellular division (Cooper and Hausman, 2004).

The cytoskeleton contains various filaments which provide the cells cytoplasm with structure and shape.

Actin is the major cytoskeletal protein of most cells. It is mostly concentrated just beneath the plasma membrane, as it keeps cellular shape, forms cytoplasmatic protuberances (like pseudopodia and microvilli), and participates in some cell-to-cell or cell-to-matrix junctions and in the transduction of signals. Other filaments which are thicker and are more stable than actin filaments, are the heterogeneous constituents of the cytoskeleton. They organize the internal tri-dimensional structure of the cell (they are structural components of the nuclear envelope). They also participate in some cell-cell and cell-matrix junctions.

Focal adhesions are specific types of large macromolecular assemblies through which both mechanical force and regulatory signals are transmitted. More precisely, focal adhesions can be considered as sub-cellular macromolecules that mediate the regulatory effects (e.g. cell anchorage) of extracellular matrix (ECM) adhesion on cell behaviour (Chen, 2003). Focal adhesions are in a state of constant flux: proteins associate and disassociate with it continually as signals are transmitted to other parts of the cell, relating to anything from cell motility to cell cycle. On the cytoplasmic side of focal adhesions, integrins interact with cytoskeletal proteins that function in the attachment of bundles of actin filaments to these regions.

2.5.4. Cell Adhesion

Cell adhesion is the binding of a cell to another cell or to a surface or matrix (figure 2-28). Cellular adhesion is regulated by specific adhesion molecules that interact with molecules on the opposing cell or surface. Such adhesion molecules are also termed receptors and the molecules they recognise are termed ligands. Cell adhesion generally involves protein molecules at the surface of cells, so the study of cell adhesion considers cell adhesion proteins and the molecules that they bind to. After cells contact surfaces (passive adhesion), cells are always dynamically altering their cell membrane and its morphology to

optimise interactions and to stabilise the cell-material surface interface (active adhesion), both physiochemically and biologically (Okano *et al.*, 1995).

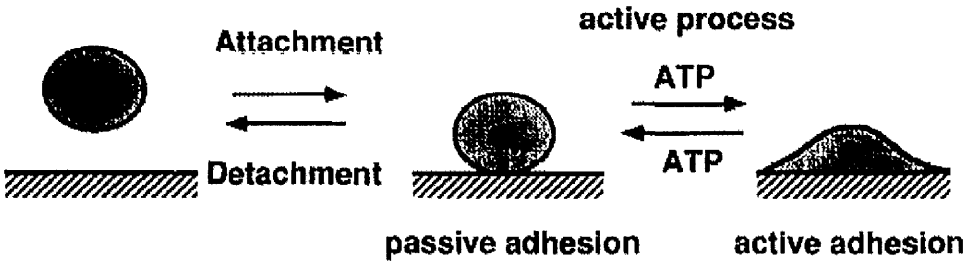

Figure 2-28 Mechanism of cell attachment and detachment from material surfaces.

Human osteoblasts interaction with a substrate can normally be characterised by four stages, where (1) protein is adsorbed on to the surface, (2) the rounded cells make contact, (3) cells attach to the surface, and (4) cells start spreading. Several studies have been conducted on hydroxyapatite materials and their interaction with osteoblasts, and their behaviour has always shown positive results making them ideal materials for reconstruction of bone (Howlett *et al.*, 1994; Rizzi *et al.*, 1999; Specchia *et al.*, 2002).

2.6. Aims and Objectives

Several research groups have used three-dimensional free form fabrication techniques to build porous scaffolds for a variety of uses. Stereolithography (SLA) stands out from the other rapid prototyping techniques with regards to controlling the geometry and internal architecture, to produce three-dimensional scaffolds.

LG112 glass-ceramic is a bioactive material, which has received very little attention in the field of load bearing implants, and for this reason LG112 will be used in this study to fabricate a three-dimensional scaffold with controlled porosity and internal architecture using SLA.

The principal aim of this study is to determine the feasibility of using stereolithography as a technique, to fabricate three-dimensional porous scaffolds, for use as load bearing implants.

The scaffolds will be fabricated in two ways: directly by means of the SLA using a suspension of bioactive glass-ceramic LG112 and PEGDA (258) monomer to produce a composite scaffold, where the matrix gives the scaffold extra structural integrity; and by gel casting a LG112 suspension into moulds fabricated using the SLA, to produce glass-ceramic scaffolds following sintering.

Successful fabrication of scaffolds will be followed by a study of their mechanical properties. As these materials will be used as tissue engineering scaffolds, their biocompatibility and cell viability will also have to be studied. This will be performed on 3-dimensional scaffolds using human osteoblasts, as they are the primary cells responsible for bone formation.

3. Materials and Methods

From the materials available for use in biomedical applications, discussed in Chapter 2, it was decided that an apatite-mullite glass ceramic will be investigated further for load bearing implants. The glass-ceramic selected is LG112 (University of Limerick Glass 112), with a composition of $4.5SiO_2$ - $3Al_2O_3$ – $1.6P_2O_5$ - 3CaO - $1.51CaF_2$. As discussed earlier, LG112 has been shown to exhibit bioactive properties following heat treatment and crystallisation, forming a direct physical bond with tissue *in vivo*.

3.1. Powder Preparation

LG112 was produced using the following reagents and compositions, to give a ~ 500g batch.

Reagent	SiO_2	Al_2O_3	P_2O_5	$CaCO_3$	CaF_2
Mass	102.7g	116.2g	172.5g	114g	44.8g

Whilst most of the reagents are available in the form specified, CaO is formed by the decomposition of $CaCO_3$ during heating.

Each reagent was weighed out (Sartorius Roughing balance, 3.1 kg x 0.1 g, PT3100) and placed in a plastic container with P_2O_5 being added last due to its reactivity with air. An agitating bar was added to the closed container, and the reagents were mixed in a rotary mill for one hour. The resulting powder mixture was transferred into a high-density mullite crucible (Dyson PC2988 LJD SM7), and placed on a vibrator to compact the powder down as much as possible. The crucible was then placed in an electric furnace (1600 °C, I Temp 15/16, Pyrotherm) at a temperature of 1550 °C for 2 hours. After 1 hour the crucible was briefly removed from the furnace, and the glass swirled to aid homogenisation, before being returned to the furnace for a further hour. After this time, the crucible was removed and the glass melt was shock quenched by pouring directly into a water tank, in a slow circling motion. This shock quenching was used to rapidly cool the material before it had the chance to crystallise, and the circular motion helped to spread out the glass so that large masses of glass which would have taken longer to cool down and may have then crystallised, were prevented from forming.

A suction pump was used to retrieve the resulting glass frit from the water tank and collect it in a sieve. This was left in a drying cabinet for 30 minutes to remove all moisture from the glass. The dried glass was then placed in a puck and ring to be pulverised in a Gy-Ro Rotary Mill for 120 seconds. The glass powder was then placed in the furnace, which was heated to 1300 °C at a heating of 1 °C. This allowed the glass to go through various phase transitions in order to form a multi-phase apatite-mullite glass-ceramic. The resulting glass-ceramic was ground again and sieved through a series of mesh sizes, placed on a shaker (Octagon Digital) for 90 minutes, to separate it out into five particle sizes – 0-38 μm, 38-45 μm, 45-90 μm, 90-1 mm and >1 mm. The latter two particle size ranges were ground again to the first three particle size ranges.

3.2. Powder Refinement

Stirred-ball attrition mills are widely used for fine grinding of various materials because of the fast, efficient fine grinding and simple operation. This procedure was used in this investigation to reduce the size of glass particles in the 90 μm to 1 mm range and to obtain a more uniform particle size distribution. The method involves subjecting the bioactive glass to friction, impact, and compression forces, by grinding the feed between a media and the ceramic walls of the chamber by using a stirrer.

Before milling the glass particles, the powder was first mixed at a ratio of 2:3 with distilled water. Two to three drops of a surfactant (Dispex A40) were then added to the slurry and stirred for 2 minutes. The slurry was transferred into the ceramic walled chamber of the attrition mill, and filled to the top with the Zirconia beads (MGO stabilized, XR-10, 1.4-1.7 mm). The attrition mill was set at 600 rpm to accelerate the media balls by the motion of the stirrer for a period of 16 hours.

When the required particle size distribution was achieved (measured on a Malvern Particle sizer, Section 3.3), the glass powder had to be separated from the water and the zirconia beads. This was attained by the Freeze-Drying Process.

Firstly, the glass powder was separated from the zirconia media by using a sieve and the beads were washed with more distilled water to liberate them from the powder. The resulting solution was transferred into a round bottom flask, which was then connected to

the rotating shaft of the Shell Freezer (manufactured by Edwards, New Jersey) and pre-frozen for 15 hours. When the solution was completely frozen, it was connected to a vacuum drier (Micro Modulyo, Edwards, New Jersey), which removed the moisture from the flask, leaving completely dried powder.

3.3. Particle Size Determination

Particle size distributions were determined by means of laser light diffraction (Mastersizer plus, Malvern Instruments, Malvern UK), where light scattering is used to determine the particles size. The particle size distribution is determined by measuring the scattered light intensity as a function of scattering angle. Figure 3-1 shows a simplified schematic version of the particle size analyser. A laser beam illuminates a group of particles, which are dispersed in a liquid. Light scattered by the particles, and the incident beam of light, are focused onto an optical detector array, which measures the angular distribution of scattered light. Each point on the array collects a single angle of scattered light, from all the particles in the beam; and the angular resolution is independent of the sample volume size. The detector array sums all of the scattered light distributions from individual particles in the ensemble. This composite distribution is mathematically inverted to obtain the particle size distribution, using a theoretical model for the scattering process. The most widely used model is based on Mie theory (Trainer, 2001). Using a mathematical deconvolution procedure the volumetric particle size distribution is determined that best fits the measured pattern. This method relies on the fact that all particles scatter light at a range of angles which are characteristic of their size.

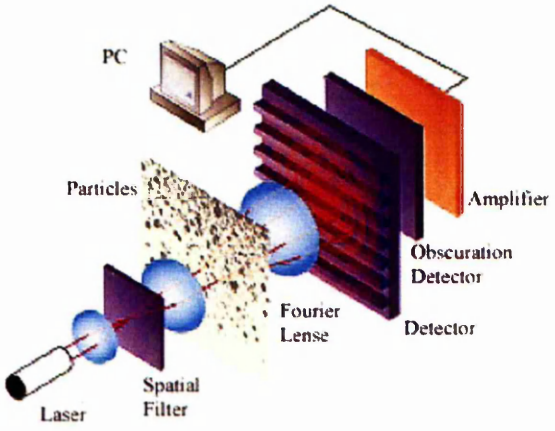

Figure 3-1 Schematic of the Malvern Particle Size Instrument (http://www.malvern.com/ProcessEng/images/diagrams.gif).

The experiments were carried out by mixing LG112 bioactive glass in a liquid carrier of water and a poly-acrylic acid dispersant (Dispex A40) was used as dispersing agent. A low energy ultrasonic probe with a maximum output of 19 kHz was employed to de-agglomerate the powders and the experiment was repeated five times.

3.4. X-Ray Diffraction (XRD)

XRD was used in this investigation to confirm the amorphous structure of the LG112 powder and to observe if any impurities or crystal structures were present. XRD is a non-destructive method that uses the properties of crystal lattices to diffract monochromatic X-ray radiation.

Each mineral is defined by a crystal lattice with characteristic diffraction properties, which can be resolved by x-rays. This is described by Bragg's Law:

$$n\lambda = 2d\sin\theta \qquad \text{Equation 3-1}$$

The *d*-spacing is the lattice plane distance, which show up as relative peak heights on the diffractogram in a fixed relationship to θ which is the incident angle between the x-ray beam and the lattice plane. λ is the wavelength of the x-rays and n is the order of the reflection.

XRD patterns were collected using a Philips powder X-ray diffractometer (PW 1830 generator, Philips Analytical, Cambridge), which is equipped with a copper monochromator with CuK_α radiation (λ = 1.5406 Å), from incident angles 10° to 80°. The phases present were then compared to the standard patterns from the Joint Committee for Powders Diffraction Standards (JCPDS) indices.

3.5. Pycnometery

The specific density of LG112 bioactive glass powder was determined using a liquid pycnometer. The pycnometer used is a precision piece of glassware that consists of several portions: a flask; thermometer assembly; degassing and filling apparatus (figure 3-2). The volume of the flask fitted with a side arm and stopper, may be accurately determined from

the mass of distilled water it holds at a particular temperature. The stopper is a capillary tube with a ground glass bottom that fits suitably into the ground glass arm of the bottle. Since the volume of the container may be accurately determined using the density of water, the entire experiment involves only the determination of weights.

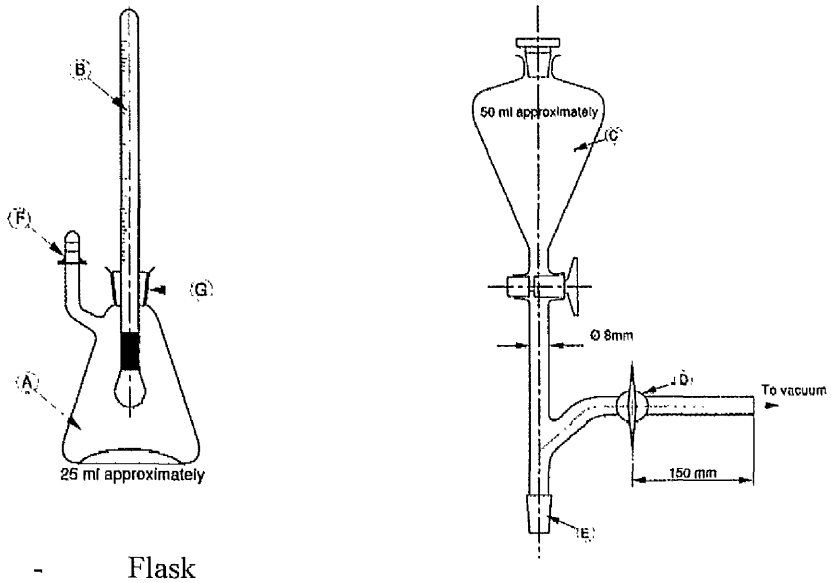

A - Flask
B - Thermometer
C - Tap Funnel
D - Side arm with tap
E - Conical ground glass joint
F - Ground glass cover
G - Socket

Figure 3-2 Schematic of a pycnometer set.

3.6. Scanning Electron Microscopy (SEM)

SEM was used in this investigation to examine the particle size range of LG112 glass-ceramic before and after the glass-ceramic was attrition milled, and to observe the general shape of the particles. A two-dimensional composite slip of LG112 and PEGDA was also observed under the SEM to look for particle distribution. At a later stage, the scaffolds produced were also observed under the SEM for their surface characteristics and cell attachment.

The SEM (figure 3-3) consists of condenser lenses, which form a fine probe; a demagnified image of the electron source focused on the specimen. When the electron

strikes the specimen surface it generates secondary electrons, which are very low energy electrons. As the specimen easily absorbs them, only those generated close to the surface reach the detector. One of the signals produced by the incident electron beam is collected, amplified and used as the input signal to a cathode ray tube (CRT). The CRT scan is synchronized with the scan on the specimen and hence the magnification obtained is simply the ratio of the two scan sizes (Goodhew *et al.*, 2001). By varying the scan on the specimen between a few millimeters and few microns, magnifications between ten and several thousand are obtained. Secondary electrons along with back scattered electrons were used in this study to observe the surfaces of different scaffolds.

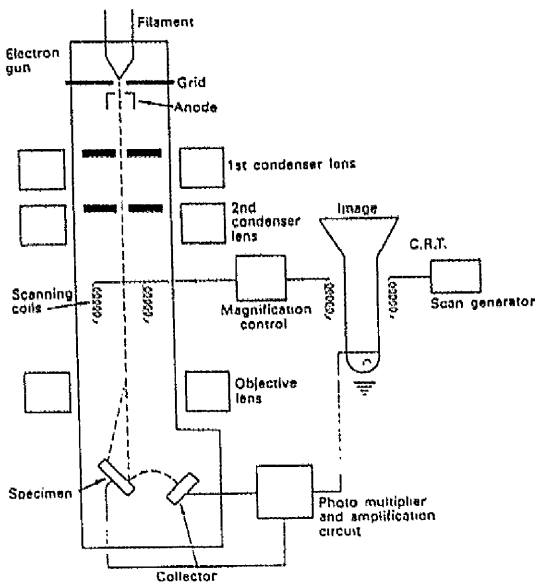

Figure 3-3 The main components of a SEM (http://mse.iastate.edu/microscopy/path.html).

The glass-ceramic powder was sprayed onto an aluminium stub and sputter coated with gold for 2 minutes (Edwards sputter coater S150, Tokyo, Japan). The stub was then silver painted to provide a conducting path to ground in order to scatter secondary electrons. Thereafter, the specimen was placed into a scanning electron microscope (JEOL, JSM6300, Tokyo, Japan), which operated at 20.0 kV, under a high vacuum atmosphere inside its chamber. The experiment was conducted five times to get accurate sizes of the particles.

For the LG112/PEGDA composite slip, the sample first had to be ground using silicon carbide paper with grit size 125 μm working up to 6.5 μm and then polished on 1 μm

polishing pad using diamond paste. Thereafter, the sample was coated in the same manner as the powder and observed under a SEM.

For cell attachment to be observed under the SEM, the cells had to be fixed and dehydrated prior to gold coating. This will be explained in detail in section 3.10.3.

3.7. Thermo Gravimetrical Analysis

Thermogravimetric Analysis (TGA) is performed on samples to determine changes in weight in relation to change in temperature. Such analysis relies on a high degree of precision in three measurements: weight, temperature, and temperature change.

The analyser usually consists of a high-precision balance with a pan loaded with the sample. The sample is placed in a small electrically heated oven with a thermocouple to measure the temperature accurately. The atmosphere may be purged with an inert gas to prevent oxidation or other undesired reactions. A computer is used to control the instrument.

Analysis is carried out by raising the temperature gradually and plotting weight against temperature.

The thermal analysis instrument used was the STA 449C Jupiter (NETZSCH), which is designed to measure simultaneously the mass changes (TG) and the calorimetric effects (Differential Thermal Analysis) at both high and low temperature (25°C - 1500°C). The TG technique measures the temperature induced changes in sample mass. The TG technique may be used to study the dehydration, decomposition and thermal stability of solids, to determine their oxidation behaviour, which characterise the production processes of ceramics.

The DTA technique measures the difference in temperature between the sample and a reference material. DTA employs two heated chambers; one holds the specimen and the other a reference material. The two chambers are heated or cooled together at the same constant rate and thermocouples compare the temperature differences between the two chambers. When an endothermic or exothermic transition occurs in the material, the energy

change causes a temperature difference between the sample and reference, which is recorded on a chart. DTA curves provide information on the temperature range wherein a process takes place and allow calculation of the value of the enthalpy change (ΔH).

A small amount of LG112 powder was weighed (5 mg ± 0.5 mg) and placed into a standard alumina DTA pan. The pan with the sample was then placed into the DTA chamber along with another empty reference pan. One thing to be noted is that the sample must make good thermal contact with the sample platform to achieve optimum conduction throughout the sample.

The sample was subjected to the following conditions under the DTA machine: -

- Baseline run from 0 °C to 1300 °C.
- Equilibration at 25 °C.
- Ramp test at 10 °C/min to 1200 °C.

TGA was used to examine the amorphous LG112, to determine the temperatures at which phase transitions occur. In addition the decomposition temperatures of the epoxy resin from the SLA and the monomer carrier IBA/PNPGDA for the glass-ceramic scaffold were also determined. All samples were tested three times to get accurate results.

3.8. Scaffold Preparation

Out of the many different ways discussed in section 2.4.2 to fabricate scaffolds, stereolithography was the chosen method to produce hard tissue replacement scaffolds in this study. This technique offers both reliability and repeatability, and can be used to produce different shapes with controlled geometry and interconnected pores.

The SLA was used to fabricate two different types of scaffolds; a glass-ceramic/polymer composite scaffold and a sintered glass-ceramic scaffold. Different techniques were employed in fabricating these using the same apparatus. To fabricate both types of scaffolds, their relevant suspensions with different volume fractions and different viscosities had to be formulated first.

3.8.1. Suspension for Composite Scaffold

To fabricate composite scaffolds of LG112 bioactive glass, PEG based polymers were chosen as a matrix, due to their common use in biomedical applications. Polyethylene glycol diacrylate (PEGDA) with a molecular weight of 258 was selected, due to its relatively low viscosity, which is an essential requirement for use in the SLA. As explained in section 2.4.2.7, the resin sits in the vat of the machine without any movement or mixing. Hence, the only way to ensure a uniform section is lasered, is by inducing shear thinning by the depression of the elevator into the vat, and by the recoating process. The same principle had to be applied when the LG112/PEGDA suspension was being formulated, regulating the viscosity and keeping it under 3000 mPa·s (Griffith *et al.*, 1996).

3.8.1.1. Suspension Characterisation

A concentric cylinder rheometer (DV-III, Brookfield, Middleboro, MA, USA) (Figure 3-4) was employed to establish two things. First, which dispersant resulted in the lowest viscosity at a constant concentration of glass-ceramic powder, at low shear rates; and secondly, to establish the maximum loading of ceramic powder into the monomer without reaching the maximum threshold of a SLA resin, namely Accura SI-40.

A small volume unit connected to a re-circulating oil bath maintains the temperature and allows measurement of the experimental volumes. The suspensions were measured between 25 – 30 °C, simulating the working conditions of the SLA. The suspension was subjected to steady shear rates between 10 – 100 s^{-1} by incrementing the rotational speed of the spindles, which in turn provides detailed information on the flow characteristics of the suspension. As the suspension reaches higher viscosities, smaller spindles are used to maximise the range of shear rates achievable.

For maximum dispersion of ceramic into the monomer, it is necessary to add a dispersant. Jakubauskas concluded that effective steric stabilisation is achieved by using surfactants that anchor to the particle interface at one end, but the other end is free to move in the solvent (Jakubauskas, 1997). A low viscosity, highly loaded suspension can be achieved using a ratio of long and short chain dispersants. Therefore, different dispersants were to be investigated to check their compatibility with the bioactive glass and the PEGDA.

Limpanuphap and Derby (2002) who had worked with similar systems using hydroxyapatite and PEGDA found Variquat CC-55 (Quaternary Ammonium Acetate) and Emphos CS1361 (Aromatic Phosphate Ester) to be suitable dispersants. Therefore, three suspensions using 5 vol.% bioactive glass in PEGDA, with 5 wt.% (of the ceramic powder) dispersant were prepared using Variquat, Emphos and a 1:1 mixture of Variquat and Emphos.

Viscosity measurements were taken for all three suspensions, and Variquat proved to be the most compatible dispersant with our suspension, showing the lowest viscosity.

After a suitable dispersant had been chosen, the next step was to find the maximum ceramic loading that could be achieved, keeping the viscosity of the suspension at a minimum at very low shear rates. The fact that the suspension would shear thin was irrelevant due to the nature of the equipment being used to fabricate scaffolds.

Five solutions with ceramic volume loading ranging from 10 – 50 % were prepared, and rheometry was conducted to observe viscosity changes in the suspensions. As the ceramic loading increases, the viscosity of the suspension would increase, but this experiment was conducted to establish the threshold of the loading level at which a maximum loading is achieved at a suitable viscosity for the SLA.

The composite suspension of PEGDA with a 40 vol.% loading of LG112 bioactive glass ceramic powder was prepared with Variquat (5 wt.% of the ceramic powder). The slurry was then added to a mixing container which was filled one third with 3:2:1 ratio of 10 mm, 6 mm, and 3 mm diameter Yittria stabilised Zirconia media. The suspension was then placed in a vibratory mill for 20 hours which homogenised the slurry into a low viscosity suspension. IRGACURE 1173 (2-hydroxy-2-2-methyl-1-phenyl-1-propanone) was used as a photoinitiator for polymerisation (1 wt.% of the monomer) in the SLA.

3.8.1.2. Window Panes

To establish an appropriate photoinitiator and concentration of initiator, a test known as "window panes" was conducted. Window panes are used to find the correct settings the (Cure depth, C_d and Critical exposure to induce polymerisation, E_c) needed for input into

the computer software, which are dependant on the particular resin to be used. These in turn led to better resolution of the final product.

Window panes were used to determine which photoinitiator out of IRGACURE 1173 and DMPA (2,2 – dimethoxy – 2 – phenyl acetophenone) would be more suitable in the SLA machine, and what concentration of photoinitiator was necessary to induce the reaction without overcuring or undercuring the layers.

The window panes test entails the machine making five different windows with 203, 254, 304, 355 and 406 microns cure depth at different energy intensities. This is done so that the machine can be calibrated to a particular resin, as each resin has different characteristics and properties. In particular the inclusion of particles greatly affects the cure depth.

The two different initiators were used in concentrations ranging from 0.2 – 3.0 wt.%. The cure depth of each window was measured using Vernier callipers (Mitsuyo, Japan). The data for the thicknesses of each window pane along with their corresponding exposure of laser data were input into a program known as WINDOWPANE™ Report. Through a series of calculations within the program, it calculates the correct C_d and E_c values, which are subsequently used to make another set of window panes. The thickness of these window panes are measured again and the program correlates this data to what the actual thicknesses of the window panes should be, giving a final value for the C_d and E_c.

Different concentrations of ceramic powder ranging from 0 – 40 vol.% were used in the window panes test, to determine if it was feasible to reach to the maximum loading of ceramic without affecting the shape or resolution of the scaffold.
The initiator that produced window panes with equivalent thickness to that of the SLA resin was chosen.

Two composite scaffolds were fabricated with external dimensions of 8 mm x 8 mm x 8 mm, but with 400 μm and 600 μm holes throughout the structure (Figure 3-4). Upon complete fabrication, these scaffolds had a range of sizes due to the effects of the cleaning process resulting in holes ± 150 μm to the intended size.

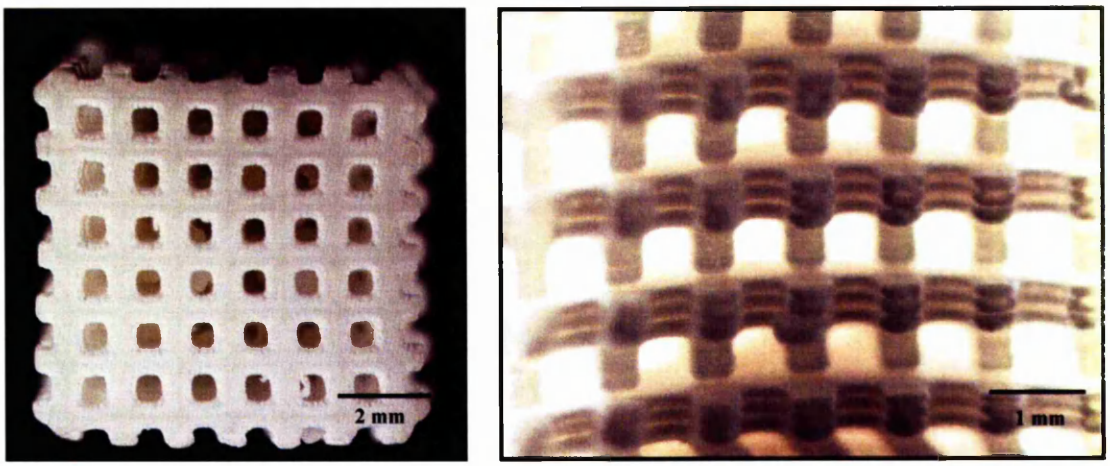

Figure 3-4 Images of a composite scaffold.

This was achieved by modifying the machine by substituting the original vat with a much smaller vat and replacing the elevator with a stationary platform. This meant that unlike conventional SLA, the recoater blade could not be used to remove excessive resin from the cured resin, instead only the dipping action of the elevator would ensure removal of excess uncured resin from the surface (figure 3-5).

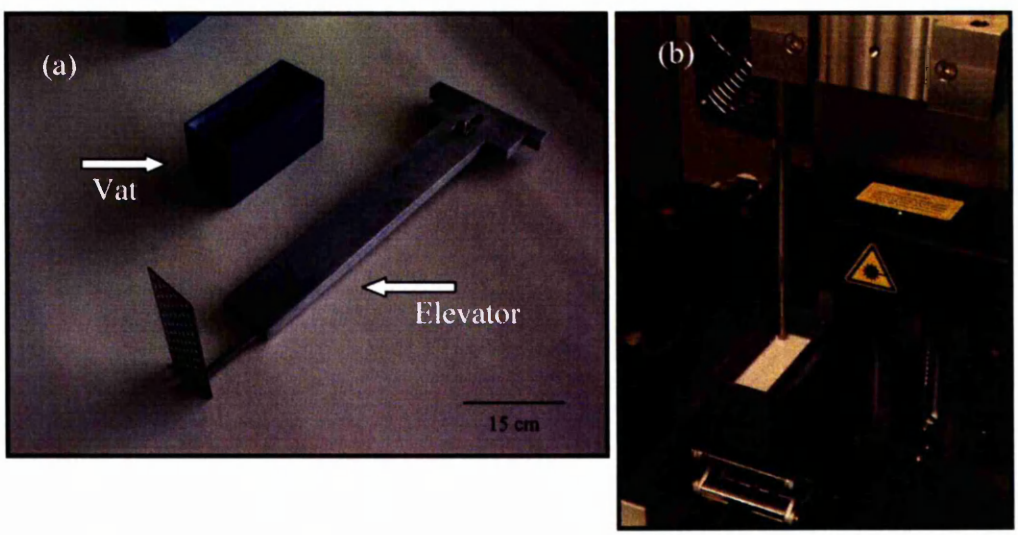

Figure 3-5 (a) the modified vat and elevator, and (b) the elevator and resin installed in the SLA.

Once the complete scaffold had been fabricated, the supports from the base of the scaffold were removed and the scaffold washed with ethanol to remove any excessive resin within the pores of the scaffold. Thereafter, the scaffold was placed in a beaker of water in a sonic bath for 1 hour, with continuous rotations of water, with intervals of high pressure air outlets blown onto the scaffold to force out any resin stuck within the pores. Once the scaffold had been cleaned thoroughly, it was placed in the post curing apparatus for 3 hours, to ensure complete polymerisation.

3.8.2. Suspension for Glass-Ceramic Scaffold

The suspension used to prepare a glass-ceramic scaffold was based on the work done by Chu *et al.* (2002) where two monomers; Isobornyl acrylate (IBA) and Propoxylated neopentoglycol diacrylate (PNPGDA), were mixed in the ratio 1:1 by weight.

Similar to the method reported in section 3.7.1.1, rheometry was conducted to establish the maximum loading of ceramic in the carrier. The results were not required to correlate with that of the SLA resin because a different method was used to fabricate these scaffolds. Glass-ceramic scaffolds were to be fabricated by gel casting ceramic suspensions into moulds formed by the SLA. The only factor that had to be taken into account with regards to the viscosity was that the suspension should be free flowing, in order for it to be poured into a mould without blocking any pores, so that a homogeneous scaffold could be produced using the gel casting method.

In the 1:1 solution of IBA and PNPGDA, 50 vol.% LG112 powder with 5 wt.% Variquat was mixed in a vibrating mill. After 20 hours the suspension was homogenised and 1 wt.% Benzoyl peroxide (BPO) was added as a thermal initiator. The suspension was de-aired in a sonic bath for 1 hour to remove any air particles trapped within, after which it was poured into a mould formed by the SLA. Two different types of moulds were fabricated on the SLA with different size holes. The moulds had walls on each of its 4 sides but were left open on the top and bottom face, for the suspension to be poured in. This suspension was then placed in a tight fit box, to hold the suspension.

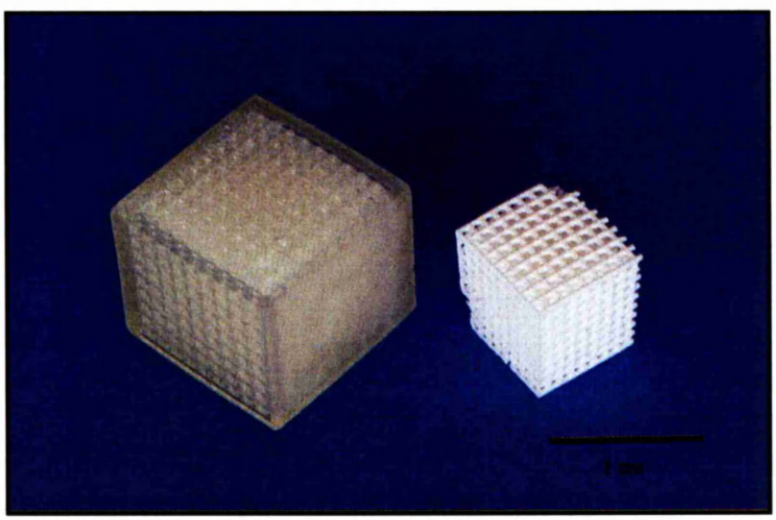

Figure 3-6 A mould fabricated on the SLA and a resulting glass-ceramic scaffold.

The box was then placed in a vacuum oven, for the mould to be de-aired again (1 hour) after which the temperature was set to 80 °C for 30 minutes, until the contents within the mould had gelled. After air cooling for 1 hour, the walls of the box were ground on 800 μm silica grit paper. This was performed prior to the burnout process, in order for the scaffold to have open pores on all six faces. After grinding, the mould was placed in a furnace to burnout the epoxy mould and the polymer holding the ceramic, to end up with a sintered glass-ceramic scaffold. The polymer binder and epoxy resin were burnt off at 550 °C for 2 hours, after which the glass-ceramic was left to sinter at 1200 °C for 2 hours (figure 3-6).

Two glass-ceramic scaffolds were produced using this technique with the same external dimensions (7.2 mm x 7.2 mm x 6 mm) but with different interconnected pore sizes (400 μm and 600 μm). The moulds for the glass-ceramic scaffolds were made on the SLA using the epoxy resin that is generally used with the machine. High resolution moulds were made on the SLA, as the recoater blade can be used with the conventional elevator and platform on the machine. After completion the moulds were cleaned thoroughly repeating the steps described earlier in Isopropanol and DOWANOL TPM (Tri (propylene glycol) methyl ether), after which they were cured in the post curing apparatus for 2 hours.

3.9. Dilatometry

A dilatometer is an instrument used to measure thermal expansion and dilation in solids and liquids. The thermal expansion coefficient (α) of the sample is defined as the rate of change of sample length with respect to the change in its temperature. Thermal expansion is a measurement of entropy of a body which reacts to changes in its volume. Dilatometry was conducted on a pellet of glass-ceramic to calculate the shrinkage of the material upon sintering to a temperature of 1200°C.

Dilatometers consist of a heat source, usually a furnace (temperatures from 25°C to 2000°C) with a temperature distribution (rising temperature, constant temperature, changing temperature) that can be adjusted. A connecting rod dilatometer was used in this case, where the same is placed in a furnace and the connecting rod transfers the thermal expansion to a strain gauge, which measures the shift. Since the measuring system (connecting rod) is exposed to the same temperature as the sample and thereby expands, a

relative value is produced which is converted by the machine to give the amount of shrinkage and the rate of shrinkage.

For this experiment, a cyclindrical rod shaped glass-ceramic pellet was made with a diameter of 5 mm and a length of 10.49 mm. The system was calibrated using standards of Poco graphite and silver to temperatures of 1600°C in atmospheres of argon and air. The heating rate of the machine was set to 120°C/hr upto a temperature of 1200°C.

3.10. Mechanical Testing of Scaffolds

The mechanical testing of both glass-ceramic and composite scaffolds was conducted using an Instron 5569 (Buckinghamshire, UK) machine with the scaffolds tested in the direction they were built on the SLA. A compressive force was then applied to the upper surface of the scaffolds using a 1 kN load cell at a constant crosshead displacement rate of 1 mm/min until failure occurred. The compressive load and the sample length were recorded at 0.1 second intervals during compression. Using these data, the stress and strain were calculated and plotted against one another. The initial compressive modulus, an indication of the extent of compressive deformation in a scaffold for a given load, was obtained from the linear portion of the stress versus strain curve.

3.11. Cell Culture Analysis

To study cell attachment and proliferation on the composite and glass-ceramic scaffolds, primary human osteoblasts were used as they are responsible for bone formation. They also produce osteoid, which is composed mainly of Type I collagen. Osteoblasts also are also responsible for mineralisation of the osteoid matrix.

3.11.1. Materials and Chemicals

For osteoblast studies, cell culture medium, serum and cell culture reagents were obtained from Gibco Invitrogen Ltd (Paisley, UK). Costar and Nunc tissue culture plates were obtained from Fisher Scientific (Loughborough, UK). Eppendorf tubes were obtained from Eppendorf UK Limited (Cambridge, UK). Alamar Blue was obtained from BioSource Invitrogen Ltd (Paisley, UK). DAPI and Phalloidin fluorescent stains, Live/Dead Viability

assay kit, and collagen-I antibody stains were all obtained from Molecular Probes Invitrogen Ltd (Paisley, UK). Sircol soluble collagen assay was obtained from Biocolor Ltd (Newtownabbey, Ireland). Alizarin Red S was obtained from Sigma (Dorset, UK). Other chemicals used in cell culture, unless specified, were obtained from Sigma (Dorset, UK).

3.11.2. Cell Culture

Human primary osteoblasts (HOBs) (supplied by Colin Scotchford, University of Nottingham) were cultured in Dulbecco's Modified Eagles Medium (DMEM) supplemented with 10% foetal bovine serum (FBS) with 1% antibiotic (streptomycin and penicillin) and 2.5 mg ascorbic acid. They were incubated at 37°C in a humidified incubator with 5% CO_2. After culturing for 3-4 days, the cells were routinely subcultured by trypsinisation using trypsin-EDTA at 37°C. The resulting cell suspension was then centrifuged at 1500 rpm to pellet the cells. After centrifugation, the supernatant was discarded and warm medium was added to the tube containing the pellet, and the cells were dispersed in the suspension using a pipette. This suspension was then ready to be used for the cell attachment study by diluting to obtain a desired cell concentration. The cells used in the experiments were between 4^{th} and 30^{th} passages. Every time a new cell line with a high passage number was used, the phenotype of the osteoblasts was confirmed in order to avoid any discrepancies in the results.

3.11.3. Cell attachment

Four different substrates were used for cellular studies. The first two scaffolds were fabricated using the SLA, and were a polymer/bioactive glass composite, with the same external dimensions and but comprised of 400 and 600μm holes (hereby these scaffolds will be known as COMP 400 and COMP 600 respectively).

The remaining two scaffolds were made by gel-casting and were a sintered glass-ceramic scaffold with 400 and 600 μm holes (now known as CER 400 and CER 600).

Preliminary tests for cell attachment were conducted using a pellet made of bioactive glass and a composite slip, to determine cell attachment. Firstly, the substrates were placed in a

24-well plate and were sterilised for 30 minutes under UV light. Osteoblasts were trypsinised as above and a cell suspension of 1 x 10^5 was carefully placed on each scaffold (2 ml), immersing them completely. After incubation for a predetermined time, the substrates were gently rinsed twice with Dulbecco's Phosphate Buffered Saline (PBS), and then the cells were fixed with 1.5 % glutaraldehyde in 0.1 M phosphate buffer for 30 minutes at 4°C. The substrates were then rinsed with PBS, after which they were dehydrated through a series of different ethanol concentrations (50%, 70%, 90% and 100% ethanol), taking care to prevent cells from drying out between concentrations. A final drying step was performed using Hexamethyldisilisane (HMDS). After the cells were fixed onto the surface of the substrates, they were sputter coated with gold to be viewed under the SEM for cell attachment.

3.11.3.1. Cell attachment using conditioned media

Conditioned media was prepared using CER 600 and COMP 600. Apart from the scaffolds, two-dimensional polymer/bioactive glass composite slips were also fabricated using the SLA (1cm^2). Another two-dimensional composite slip was also fabricated, but this was achieved by using a conventional UV box with a 15 watts UV tube light. Of the 2-D composite slips fabricated on the SLA, one of them was washed in PBS for 24 hours. All samples were then incubated in culture media for 24 hours, after which the media was used as conditioned media. The conditioned media was used to observe any toxic effects from products leaching out from the substrates during the incubation period. To determine this effect, the cells were placed into a well plate with the conditioned media and incubated for 48 hours at 37°C in humidified air with 5% CO_2 and were observed using an inverted optical microscope.

3.11.4. Cell Attachment Observations

3.11.4.1. Inverted Light Optical Microscopy

This technique allows the observation of cells, present in the culture plates covered in media, allowing a continuous examination of the cells during the cell attachment stage. A

Leica DMIL (with Spot Insight Colour Camera, Leica Microsystem (UK), Milton Keynes, UK) was used to observe the cells.

3.11.4.2. Scanning Electron Microscopy

Due to the opaque nature of the substrates and scaffolds used, an inverted light microscope could only be used to observe the cells on the transparent culture plates. As the light could not pass through the scaffolds, SEM had to be used to observe the cells on the surface of the scaffolds. This technique also provided higher resolution images. The process with which the cells were fixed onto the scaffolds has been explained in section 3.10.3.

3.11.4.3. Fluorescence Microscopy

A Fluorescence Microscope is a light microscope used to study properties of organic or inorganic substances using the phenomena of fluorescence instead of, or in addition to, reflection and absorption. In fluorescence microscopy, the sample itself is the light source. The technique is used to study specimens which can be made to fluoresce. The specimen is illuminated with light of a specific wavelength (or wavelengths) which is absorbed by the fluorophores, causing them to emit longer wavelengths of light (of a different colour than the absorbed light). The illumination light is separated from the much weaker emitted fluorescence through the use of an emission filter. The sample can either be fluorescing in its natural form like chlorophyll and some minerals, or treated with fluorescing chemicals. Typical components of a fluorescence microscope are the light source (Xenon or Mercury arc-discharge lamp), the excitation filter, the dichroic mirror (or dichromatic beam splitter), and the emission filter (figure 3-7). The filters and the dichroic are chosen to match the spectral excitation and emission characteristics of the fluorophore used to label the specimen. One aspect that needs be considered is that fluorophores lose their ability to fluoresce as they are illuminated in a process called photobleaching. Special care must be taken to prevent photobleaching through the use of chemicals or by minimising illumination.

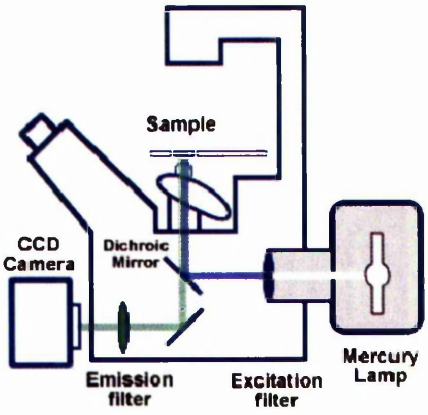

Figure 3-7 Schematic of a Fluorescence Microscope (http://www.bris.ac.uk/depts/Synaptic/info/imaging/figs/fluomicro.gif).

3.11.4.3.1. Live/Dead Viability/Cytotoxicity Assay for mammalian cells

A Nikon Eclipse 50i microscope with Lucia software (version 4.82, Laboratory Imaging Ltd.) was used to observe the cell attachment on the surface of both types of scaffolds; CER and COMP. A live/dead viability assay kit was used for this procedure. The assay is used to measure cell viability. It is a two-colour fluorescence assay that simultaneously determines;

- Live cell number – live cells have intracellular esterases that convert non-fluorescent, cell permeable calcein acetoxymethyl (calcein AM) to the intensely fluorescent calcein. The cleaved calcein is retained within the cells and fluoresces green at a wavelength range of 494 - 517 nm.
- Dead cell number – dead cells have damaged membranes, and the chemical ethidium homodimer-1 (EthD-1) enters damaged cells and fluoresces when bound to nucleic acids. EthD-1 produces a bright red fluorescence in damaged or dead cells within the range of 528 - 617 nm.

Live and dead cell numbers are calculated from standard curves with known numbers of live and dead cells. The data from this assay are typically presented as: -

- Percent live cells – calculated as the number of live cells divided by the number of total cells at each time point.

- Percent survival – calculated as the number of live cells at each time point divided by the number of live cells at 0 hours.

Calcein and EthD-1 can be viewed simultaneously with a conventional fluorescein longpass filter. The calcein can be viewed with a standard fluorescein bandpass filter and EthD-1 can be viewed with filters for propidium iodide dye. The reagents are prepared by mixing 20 µl of the supplied 2 mM EthD-1 stock solution to 10 ml of sterile PBS, and 4 µl aliquot of the supplied 4 mM calcein AM solution to the EthD-1 solution made in 10 ml of PBS.

Both sets of CER and COMP scaffolds were UV sterilised for 30 minutes in 24 well-plates prior to cell culture. Each well containing the scaffolds was seeded with 4×10^4 cells/ml of cells, and then incubated in a 5% CO_2 incubator for 2 days to allow cell attachment. The scaffolds seeded with cells were then washed with PBS to remove cells that were unattached to the scaffolds. Then the scaffolds were moved to a new well plate and covered with the live/dead reagent. The well plates were left in the incubator for 10 minutes after which they were ready to be observed under the fluorescence microscope with a green (live cells) and red (dead cells) filter. Glass cover slips were used as a 2D control to compare the cell growth in comparison with 3D scaffolds.

3.11.4.3.2. DAPI/Phalloidin staining of F-actin

DAPI or 4',6-diamidino-2-phenylindole dihydrocholride is a nucleic acid stain, which preferentially stains DNA. It is used extensively in fluorescence microscopy to visualise cell nuclei. Since DAPI will pass through an intact cell membrane, it is used to stain live and fixed cells. It fluoresces blue, which stands out in vivid contrast to green or red fluorescent probes of other structures. For fluorescence microscopy, DAPI is excited with ultraviolet light. When bound to double-stranded DNA its absorption maximum is at 358 nm and its emission maximum is at 461 nm.

Phalloidin binds specifically at the interface between F-actin subunits, locking adjacent subunits together. Phalloidin, a bicyclic heptapeptide, binds to actin filaments much more tightly than to actin monomers, leading to a decrease in the rate constant for the

dissociation of actin subunits from filament ends, which essentially stabilizes actin filaments through the prevention of filament depolymerisation (Cooper, 1987).

Cell morphology and actin organization was examined using the two stains under a fluorescence microscope. Culture media was removed from the well plate and scaffolds rinsed twice in PBS. The cells were then fixed with formaldehyde (3.7%), followed by rinsing in PBS. Cells were permeabilised with 0.1% Triton X100 for 20 minutes and rinsed again with PBS. Samples were then immersed for 30 minutes in PBS containing 1% bovine serum albumin (BSA). This solution was removed, and the actin filaments were then stained with FITC-conjugated phalloidin (10 μg/ml) in PBS for 20 minutes at 4°C. After another rinse of PBS, the scaffolds were stained with DAPI (10 μg/ml) and were then ready to be observed under the microscope. Glass cover slips were used as a 2D control to compare the cell growth with 3D scaffolds.

3.11.4.3.3. Collagen-I Antibody Staining

Type I collagen provides a structural framework for connective tissues and plays a central role in the temporal cascade of events leading to the formation of new bone. Osteoblasts were seeded on scaffolds to observe collagen production for varying time points (7, 14 and 21 days). After each time point, the scaffolds were washed three times with pre-warmed PBS and then the cells were fixed with 4% formaldehyde solution in PBS for 30 minutes. Scaffolds were then washed three times with PBS containing 1% BSA, and thereafter the primary antibody (Polyclonal Rabbit Anti-Mouse Immunoglobulin) was added and incubated at 37°C for 1 hour. After another wash in PBS containing 1% BSA, the FITC conjugated secondary antibody (produced in rabbit) was added and incubated for 1 hour at room temperature. Excess secondary antibody was removed using PBS with 1% BSA, and the scaffolds were immersed in DAPI for 5-10 minutes. The samples were then ready to be viewed under the fluorescence microscope with a blue filter for the cell nuclei and the red filter for collagen I.

3.11.4.4. Confocal Microscopy

Confocal microscopy is an imaging technique used to increase micrograph contrast and/or to reconstruct 3-D images. In a conventional confocal microscope, the sample is flooded with light and all parts in the optical path are excited and thus fluoresce (same as a

fluorescence microscope). The advantage of using confocal is that it eliminates the out-of-focus information and produces a higher contrast image.
Cell morphology was conducted on scaffolds (CER and COMP), which had been stained with DAPI and Phalloidin, to obtain higher resolution images.

3.11.5. Quantitative assays

3.11.5.1. Alamar blue cell proliferation assay

Alamar blue is a non-toxic aqueous dye that is used to assess cell viability and cell proliferation. The oxidised, non-fluorescent blue dye (resazurin) is reduced to a pink fluorescent dye (resorufin) in the medium by cell activity (likely to be by oxygen consumption through metabolism) (O'Brien *et al.*, 2000). As cell concentrations increase, the number of metabolic pathways also increase leading to a higher amount of fluorescence measured.

As Alamar blue is non-toxic, it does not alter the viability of cells cultured for various time points and the cells under study can be returned to culture. Proliferation measurements with Alamar blue are performed spectrophotometrically by absorption measurements supplemented with cell culture media at two different wavelengths. A calibration curve is used to convert the measured fluorescence into a cell number.

3.11.5.1.1. Calibration curve

A calibration curve is a plot used to determine the instrumental response, to that of changing concentrations of the substance to be measured. The calibration curve for Alamar blue was determined by taking different known concentrations of cells in culture media and measuring their fluorescence. The cell concentrations were increased logarithmically from 1×10^3 to 1×10^6 cells/ml and suspended homogeneously. 100 µl of each cell suspension were then added to a 24-well plate and supplemented with 900 µl of fresh culture media. To this, 200 µl of 12.5 mg/l Alamar blue was added and the samples were incubated at 37°C with 5% CO_2 for 2 hours. Subsequent to the incubation, 200 µl of solution was transferred to a 96-well plate and the fluorescence measured using a Fluostar Optima fluorescence plate reader (BMG Latech) at wavelengths of 530 nm (excitation wavelength) and 590 nm (emission wavelength).

3.11.5.1.2. Alamar blue assay

After obtaining the calibration curve, cells were ready to be seeded onto four types of scaffolds; CER 400, CER 600, COMP 400 and COMP 600. 4 x 10^4 cells/ml were seeded onto each scaffold very carefully, in order to maximise cell attachment to the surface of the scaffold, rather than the bottom of the well plate. After cells had been incubated for 7, 14 and 21 days, the well plate was supplemented with 2 ml of fresh media to which 400 µl of 12.5 mg/l Alamar blue solution was added. The cells were then incubated for 2 hours at 37°C with 5% CO_2. 200 µl of the solution was then removed and transferred to a 96 well plate and the fluorescence measured.

T-Test analysis for two samples assuming equal variance was conducted on all samples with a confidence level of 0.05 %.

3.11.5.2. Sircol Soluble Collagen Assay

The Sircol assay is a quantitative dye-binding method for the analysis of acid-soluble collagens extracted from mammalian tissues. A Sircol soluble collagen assay kit which can determine salt-soluble, acid-soluble and pepsin-soluble forms of mammalian collagens, Types I to IV, was used in this experiment.

3.11.5.2.1. Calibration curve

A calibration standard curve was also calculated for the collagen assay. Aliquots of 0, 5, 10, 25 and 50 µl of the collagen standard were taken and placed in eppendorf tubes. All five tubes were adjusted to 100 µl by adding 0.5 M acetic acid. 1 ml of Sircol dye reagent was then added to each tube, and the contents mixed by using a mechanical shaker for 30 minutes. The eppendorf tubes were subsequently placed in a centrifuge for 10 minutes at 10,000 rpm, after which the unbound dye was decanted, retaining the collagen bound dye. To recover the bound dye, 1 ml of the Sircol dye release reagent was added and mixed vigorously. 200 µl of the samples was then placed in a 96-well plate and the colour absorbance of the alkali dye solution was measured using a spectrophotometer at a wavelength of 540 nm.

3.11.5.2.2. Collagen assay

For the collagen assay, the same procedure for cell seeding and different time points as described in section 3.10.5.1.2 was applied. Control glass cover slips were used at each time point, to monitor cell attachment and proliferation.

After culturing the cells for 7, 14 and 21 days, the media from the well plates was removed, and the scaffolds were gently rinsed with PBS. 500 µl of 0.5 M acetic acid was then added to each well, and the samples were incubated overnight at 4°C. After incubation, 10 µl of the solution from each well was placed into an eppendorf tube, and the contents of each tube were adjusted to 100 µl with 0.5 M acetic acid. A blank was also used that just contained 100 µl of acetic acid. Thereafter, the same procedure was applied as explained in section 3.10.5.2.1 and the fluorescence was measured in a spectrophotometer at 540 nm.

3.11.5.3. Alizarin Red S Mineralisation Assay

Alizarin red staining determines quantitatively by colorimetry, the presence of calcific deposition by cells of an osteogenic lineage. As such it is an early stage marker (days 10-16 of in vitro culture) of matrix mineralisation, a crucial step towards the formation of calcified extracellular matrix associated with true bone (Gregory, 2004).

The assay was conducted on 5 different sets of substrates. All four scaffold types were used to check for calcification, along with a pellet of LG112 bioactive glass powder, which was used as the control where no cells were seeded. This was because LG112 bioactive glass contains a high amount of calcium, which the alizarin red could stain. This could then be compared to the amount of calcification caused as a direct result of osteoblast seeding.

Osteoblasts were seeded on to the substrates for a period of 10 days with continuous changes of media, to keep the cells nourished with nutrients. After culturing the cells, the substrates were washed twice with warm PBS and then fixed in ice-cold 70 % ethanol for 1 hour. The samples were subsequently rinsed twice with distilled water and then stained with 40 mM Alizarin Red-S (pH 4.2) for 5 minutes at room temperature, after which the samples were rinsed five times with distilled water. The substrates were then washed with PBS for 15 minutes with continuous rotations to remove most of the non-specific stain not

associated with calcium mineral deposits. The cells were then destained with 1 ml of 10 % cetylpyridinium chloride (CPC) for 30 minutes with rotation at room temperature. 200 µl of the solution was then placed in a 96-well plate and the absorbance was measured in a spectrophotometer at a wavelength of 562 nm.

3.11.6. High Performance Liquid Chromatography (HPLC)

HPLC is a form of column chromatography and is used to separate components of a mixture by using a variety of chemical interactions between the substance being analysed and the chromatography column. This technique was conducted to find any leachants that were released from the SLA fabricated composite scaffolds.

A Dionex P680 HPLC pump was used to quantify the results to find out chemicals leaching into the culture media, obstructing cellular attachment. A 20 µl sample was injected onto a Macherer-Nagel C18 column of length 250 mm, internal diameter 4.6 mm, and particle size 5 µm at a flow rate of 1 mL/min. The gradient used was 37.7 % acetonitrile in water for 15.43 minutes, being constant prior, and then increasing to 50.8 % acetonitrile in water at 23.30 minutes.

Four samples were tested in the HPLC; (1) Initiator, (2) Culture Media, (3) PEGDA monomer, and (4) Culture media with composite scaffold. These solutions were chosen to check if there was any amount of monomer or initiator leaching out into the system i.e. the culture media.

4. Results and Discussion

The first step in the fabrication of scaffolds was the production of LG112 bioactive glass. After glass production, vigorous grinding steps had to be performed to reduce the particle size, to make it applicable in suspensions. After quenching the melting LG112 glass in a water bath, the glass pieces were first dried and then the glass was placed in a puck and ring to be pulverised in a Gy-Ro rotary mill for 120 seconds, after which they were sieved into different size fractions. Sieving resulted in the majority of glass particles ranging from 30 – 100 μm.

4.1. SEM of LG112 Glass Powder

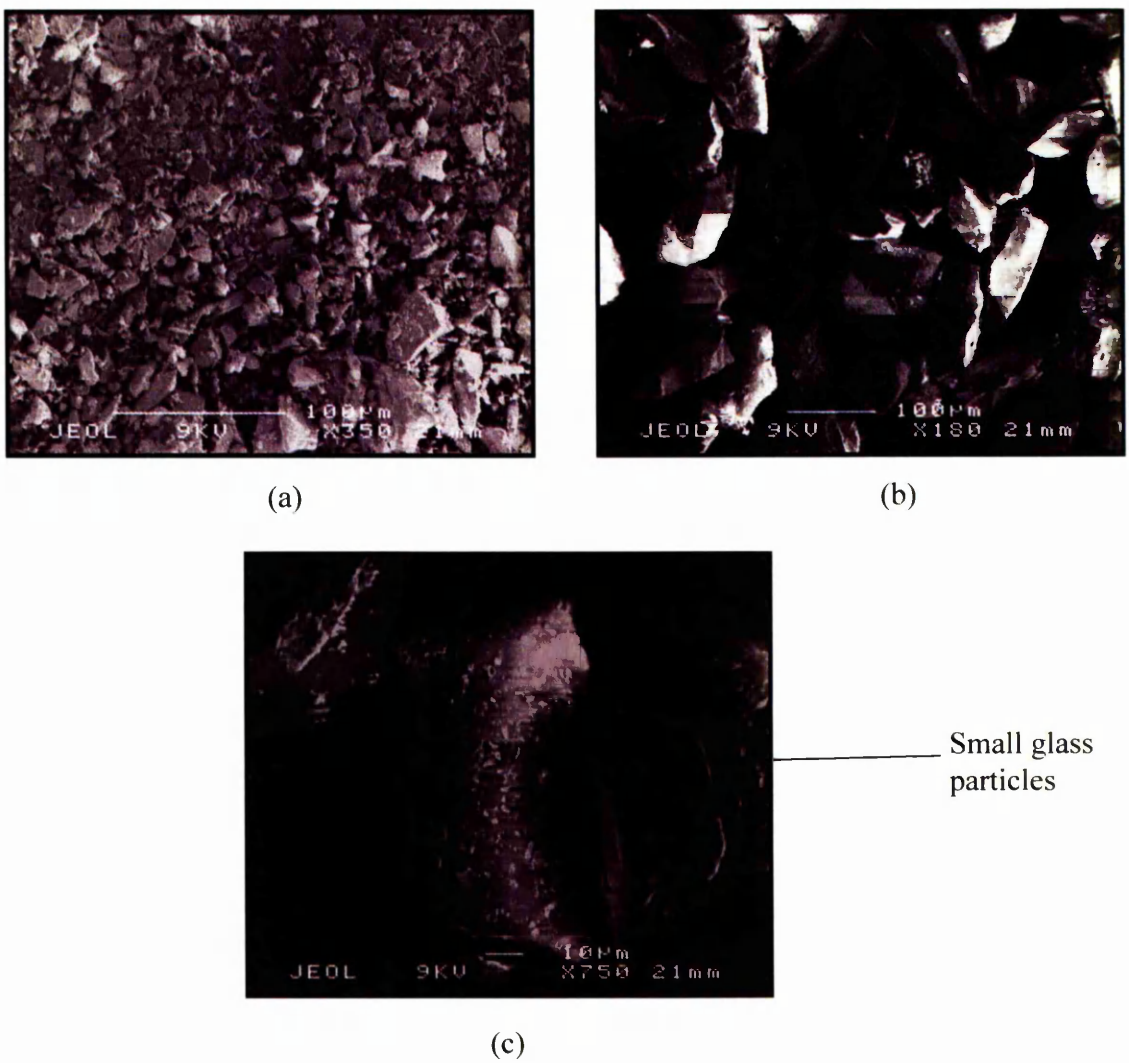

(a) (b) (c)

Figure 4-1 Scanning electron micrographs showing the distribution of different sized glass particles after gy-ro crushing.

As can be seen from figure 4-1(a), sieving of the glass particles gave particle sizes below the 38 μm range, whereas (b) and (c) show glass particles ranging from 45 – 90 μm. Glass powder obtained by crushing led to angular particles, but this process was an intermediate step in bringing the size of the particles below 5 μm.

LG112 glass particles were to be used in the direct and indirect fabrication of scaffolds using stereolithography. Hence, to be able to use the glass powder with such a technique it was very important to get the particle size of the glass below 5 μm. This was achieved by attrition milling the glass a number of times. Smaller glass particles enabled a better mixing of the particles in the monomers for both direct SLA work and indirect (gel casting) fabrication of scaffolds.

Attrition milling was conducted on the glass particles for 16 hours, during which the glass particles were ground by the frictional forces between the milling media and the ceramic walls of the container. The particle sizing of the glass was then performed to verify the correct size had been obtained. If this was not the case, then the glass was attrition milled again until the target size was achieved.

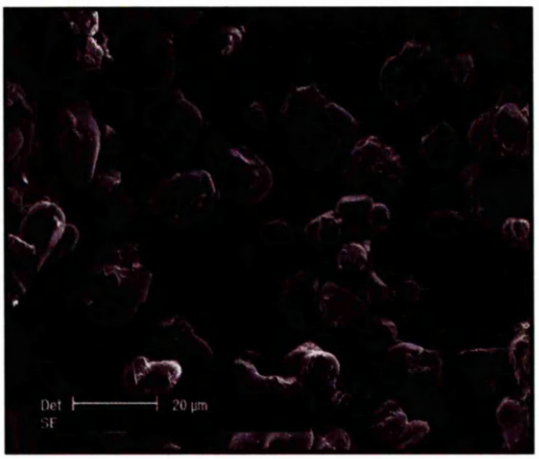

(a)

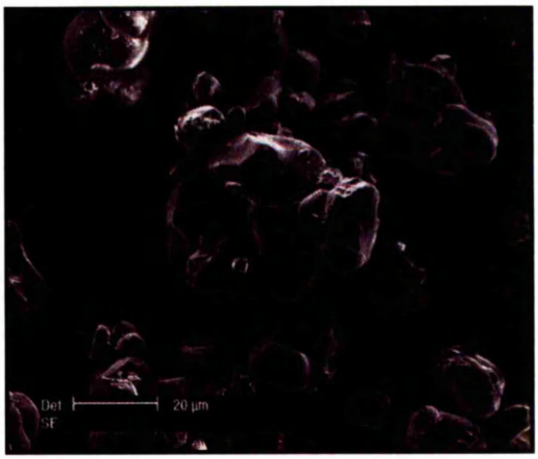

(b)

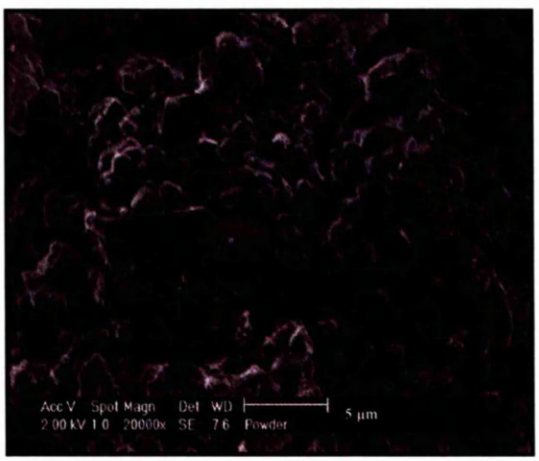

(c)

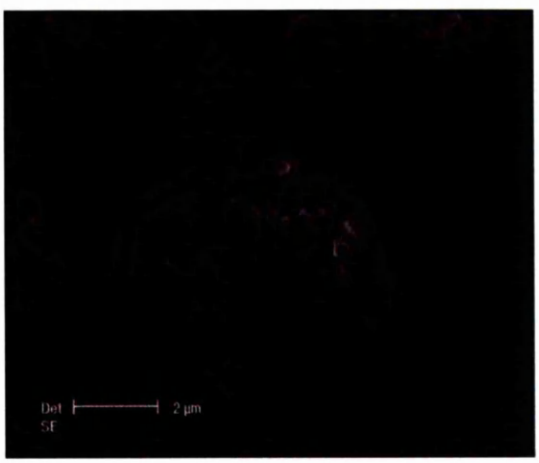

(d)

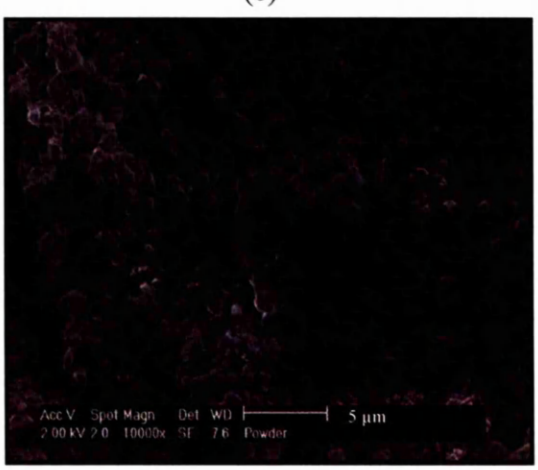

(e)

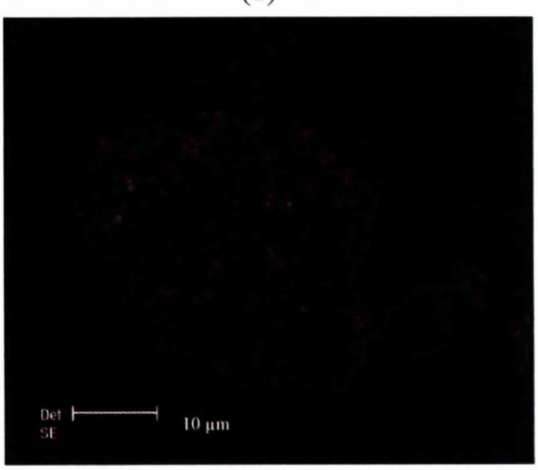

(f)

Figure 4-2 (a) and (b) show an intermediate stage in the attrition milling process producing particle sizes of approximately 20 – 30 microns, and (c) and (d) show further milling of the glass powder to achieve glass particles below 5 microns, (e) and (f) show agglomeration of the small glass particles.

It can be observed from the attrition milled glass that the particle morphology has changed from being angular to rounded. Although angular particles technically have a better packing arrangement as compared to spherical particles, the bigger size of the angular particles would have hindered the achievement of a high particle loading in the monomers. This would have thence led to an inhomogeneous slurry being produced, leading to poor scaffolds.

One problem that can be seen from figure (e) and (f) is the agglomeration of the fine glass particles. When dispersing the glass particles in monomers, this could again lead to an inhomogeneous slurry with all the particles together rather than dispersed throughout the resin. To combat this problem, an appropriate dispersant was employed (section 4.6.1).

4.2. Particle Size Distribution

Particle size distributions of LG112 glass powder received after production (gy-ro crushing) and after attrition milling were conducted. The results show a bimodal distribution for the glass particles before being attrition milled (figure 4-3 (a)) where 90 % of the particles have a mean size of 204 μm and 10 % of the particles have a mean size of 11 μm.

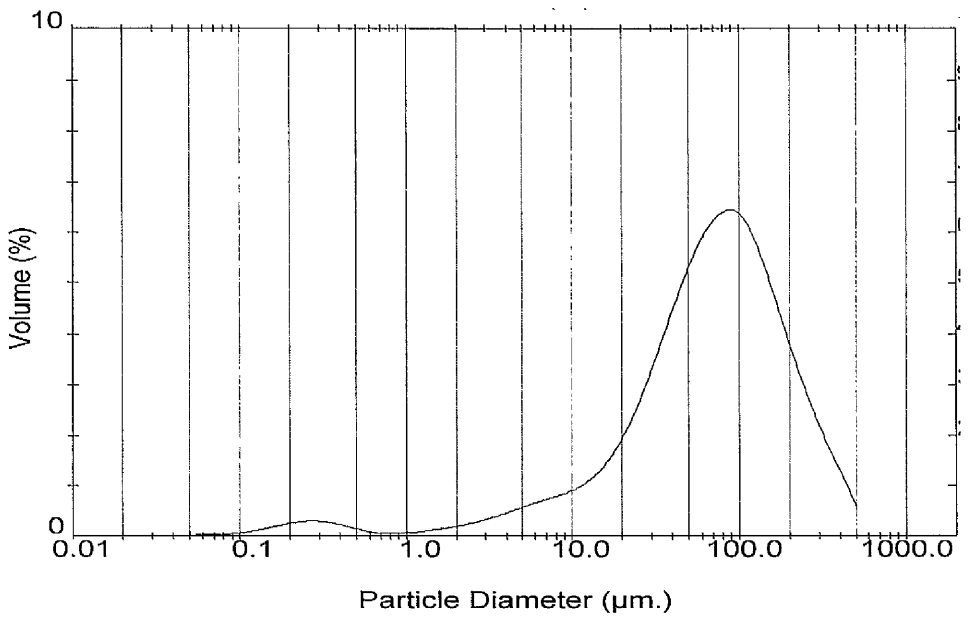

Figure 4-3 (a) Particle size distribution before attrition milling showing a bimodal distribution.

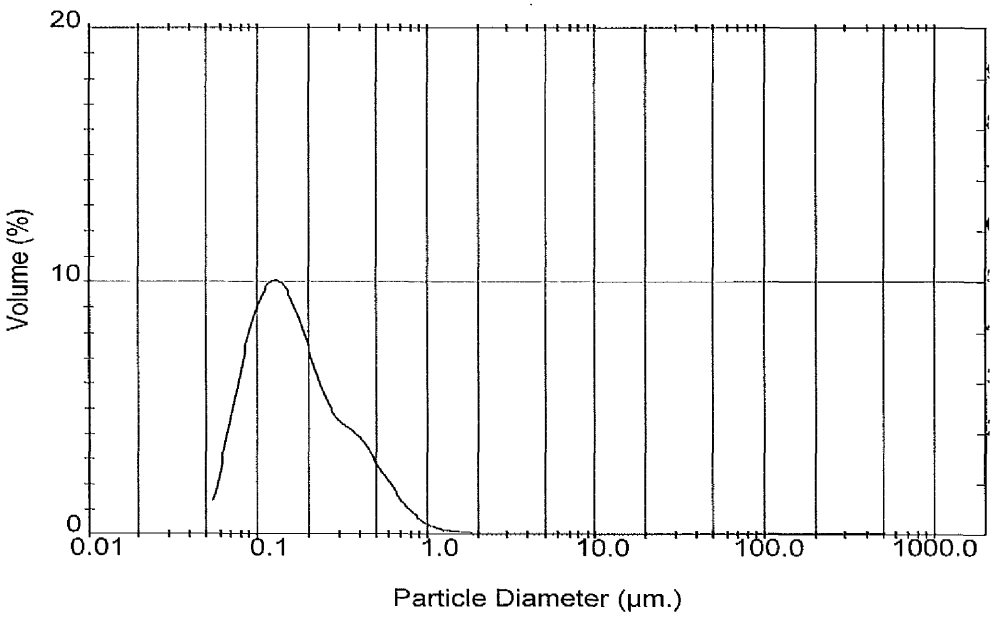

Figure 4-3 (b) Particle size distribution after attrition milling.

Figure 4-3 (b) shows the glass particle size distribution after being attrition milled to obtain the target size of below 5 µm. The graph clearly shows that all particles fall below 1 µm, with 90 % of the particles having a mean size of 0.44 µm. For this size to be achieved the glass had to be milled several times.

4.3. SEM of LG112/PEGDA Composite

Preliminary studies were conducted to observe the behaviour of the glass particles mixed into a monomer. A 30 vol.% loading of LG112 was mixed in PEGDA (258) monomer, and polymerised into a mould made out of two glass slides joined together. The LG112/PEGDA composite was then viewed using SEM to examine the particle distribution within the polymer.

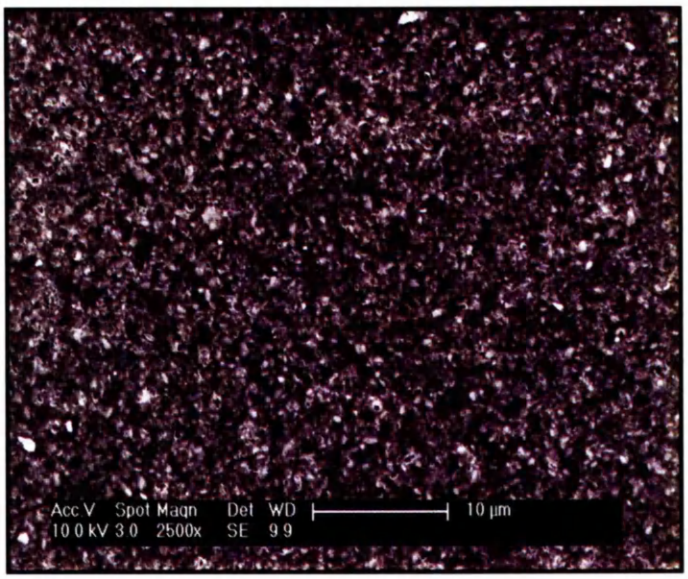

Figure 4-4 Scanning electron micrograph of 30 vol.% LG112 powder (white) in PEGDA (dark) matrix.

Figure 4-4 shows a SEM image of the composite, where the LG112 glass particles are shown in white and the polymer matrix is represented by the dark colour. This image illustrates the homogeneity of the glass particles within the polymer matrix and also the size of the particles to be ~ 1 µm.

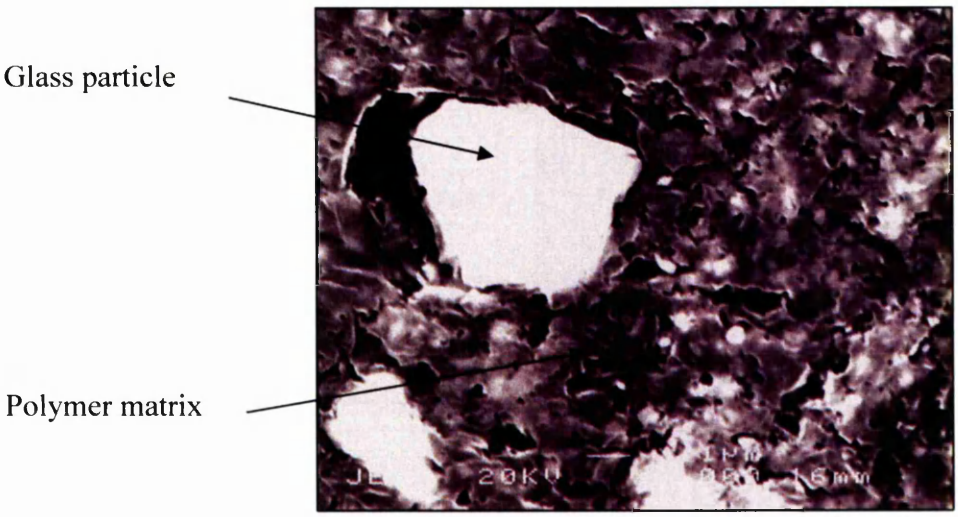

Figure 4-5 Scanning electron micrograph showing a higher magnification image of the glass particle incorporated within the polymer matrix.

Figure 4-5 shows the porous structure of the polymer matrix which has the glass particles evenly dispersed. The polymerisation of the monomer leads to small gaps (1 μm) present between the interface of the glass particles and the polymer itself, but this does not affect the structure as a whole due to any type of dislodgement or loosening.

This test was conducted to get an understanding of how well the glass particles would mix with the monomer. The preliminary results have shown that the targeted particle size of the glass mix homogeneously with the monomer. Hence, the processing route using < 5 μm glass particles with a suitable dispersant mixed in a monomer is a viable route for making ceramic suspensions.

4.4 XRD of LG112 Glass Powder

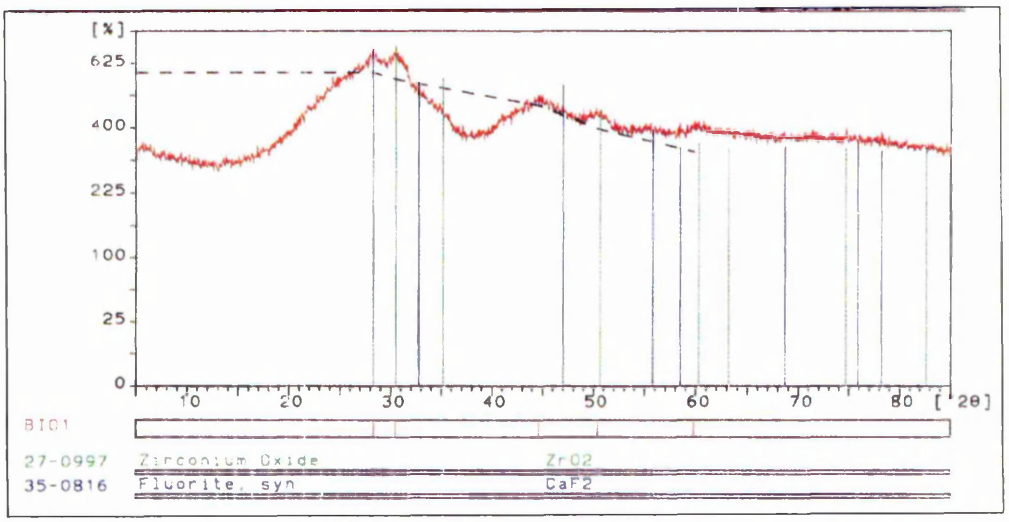

Figure 4-6 XRD trace of attrition milled LG112 glass powder.

As we can see from figure 4-6, the glass powder has a completely amorphous structure, apart from showing two very small crystalline region peaks. The first peak maybe due to some fluorite still present in the glass, which could be because CaF_2 did not fuse properly with the other components of the glass upon heating in the furnace or upon quenching some crystallisation occurred. The second peak is caused due to zirconium oxide, which would have contaminated the glass powder while it was being attrition milled. Grinding of the powder at high RPM with small zirconia balls, could have resulted in some of the beads being ground themselves.

4.5. Pycnometery

The specific density of LG112 bioactive glass was calculated using a pycnometer with the following relation : -

$$Ps = \frac{(m_2 - m_1)p_k}{V\,x\,p_k + m_2 - m_3} \qquad \text{Equation 4-1}$$

where,

V – pycnometer volume

m_1 – weight of empty pycnometer

m_2 – weight of pycnometer with dry sample

m_3 – weight of pycnometer with the sample and distilled water

p_k – density of distilled water

The specific density of bioactive glass LG112 was calculated to be 2.5 gcm^{-3}. To make sure there was no change in the specific density of the glass, the density of the glass was also calculated at 890 °C and 1040 °C; the phase transformation temperatures and the density was found to be within ± 0.2 gcm^{-3}.

This value was used for all further calculations for the percentage volume fractions of the ceramic powder in resins, used to fabricate scaffolds.

4.6. Thermo Gravimetrical Analysis

DTA was carried out on unsintered LG112 to determine the temperatures at which phase transitions occur. From the DTA trace (figure 4-7), the glass transition temperature, T_g, is seen to occur at approximately 675°C. The second peak, represents the apatite crystallisation temperature at around 875°C. The third peak representing the mullite crystallisation occurs at around 1100°C.

Hill *et al.* (1991) (section 2.2.4.2), reported a nucleation temperature of 660°C, apatite phase at 893°C and mullite phase at 1040°C for LG112. Hence, there is about 20°C difference in the apatite phase change and about 60°C difference for the mullite phase. The reason for this could be the difference in the manufacturing method of the glass. As stated

in Section 3.1, the crucible is left in the furnace for a period of 2 hours at a temperature of 1550°C. However, the mullite crucibles often leak at such high temperatures, therefore after about 1 hour the melt was taken out and quenched, to prevent any loss of material in the furnace. This shorter time could have lead to the constituents of the crucible not bonding completely and hence giving a change in the phase transition temperatures. Even though the crucibles were not placed in the furnace for 2 hours, it was ensured that all constituents in the crucible had thoroughly mixed and fused with each other.

The thermo gravimetric (TG) (figure 4-7) trace shows that approximately 12 % loss in mass is seen when the sample is heat treated up to 1200°C. Some loss of material is a common occurrence at such high temperatures.

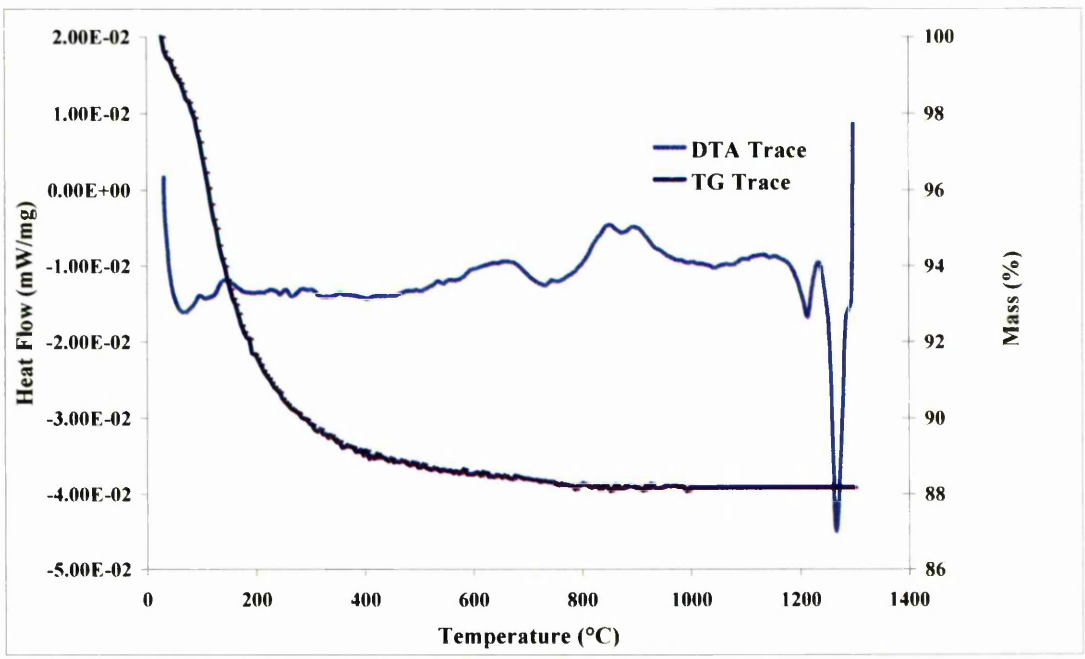

Figure 4-7 TGA trace for LG112 glass powder.

TGA was also conducted on a 1:1 ratio of IBA and PNPGDA (figure 4-8), to calculate the burnout temperature of the polymer during the sintering process of the glass-ceramic scaffold. The polymer starts to burn-off at 250 °C and starts losing mass at that point (20 % mass loss). Complete burn-off is achieved at temperatures up to 350 °C.

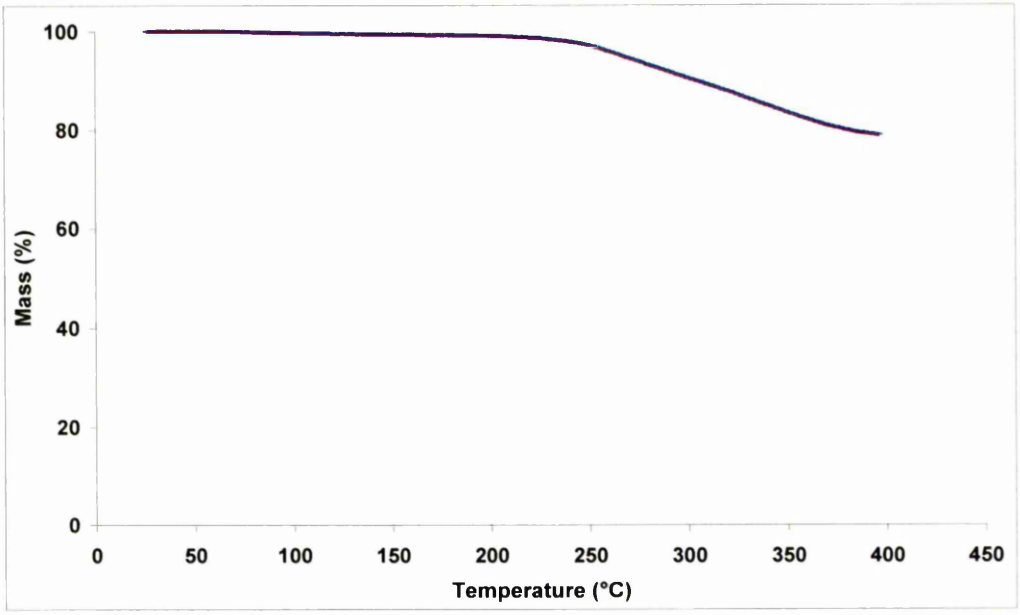

Figure 4-8 TGA trace for IBA/PNPGDA monomer mix.

The epoxy resin used by the SLA to fabricate moulds for gel casting was also tested in the same manner to determine the burn-off temperature. This was found to be approximately 200 °C, with mass loss at about 350 °C (figure 4-9).

Thus, the burn-off of the epoxy resin and the polymer binder (IBA/PNPGDA) can be performed by holding the temperature at 350 °C for 2 hours, after which the glass-ceramic can be allowed to sinter at 1200 °C.

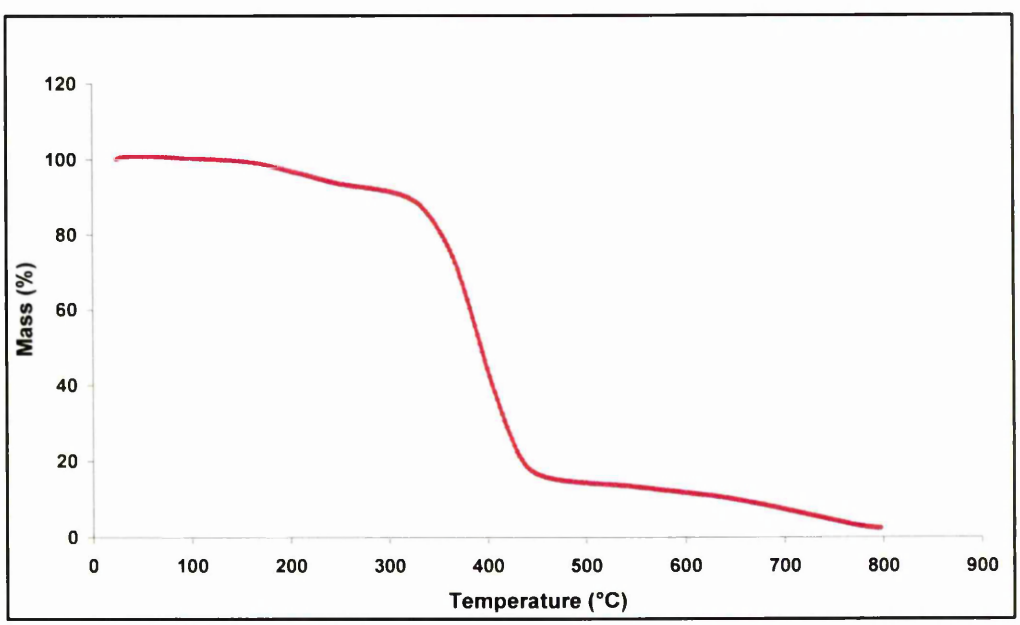

Figure 4-9 TGA trace for epoxy resin used with the SLA.

4.7. Scaffold Fabrication

4.7.1. Composite Scaffolds

The composite scaffolds were fabricated on the SLA and are known as COMP scaffolds throughout this study. To make the scaffolds, a suspension of bioactive glass powder in a monomer was prepared, maintaining the loading of the glass-ceramic powder at a maximum, whilst keeping the viscosity of the suspension to a minimum.

Limpanuphap (2004) had tested a variety of dispersants to aid in the successful mixing of hydroxyapatite ceramic powder into PEGDA 258. Out of the dispersants tested, two were observed to have better results in reducing the viscosity of the suspensions. Hence, a solution with 5 vol.% LG112 in PEGDA 258 monomer was tested with three different dispersants; Variquat, Emphos and a 1:1 mix of Variquat and Emphos. The dispersant was used according to the weight of ceramic powder added to the suspension resulting in a homogeneous mixture (5 wt.% of the ceramic powder).

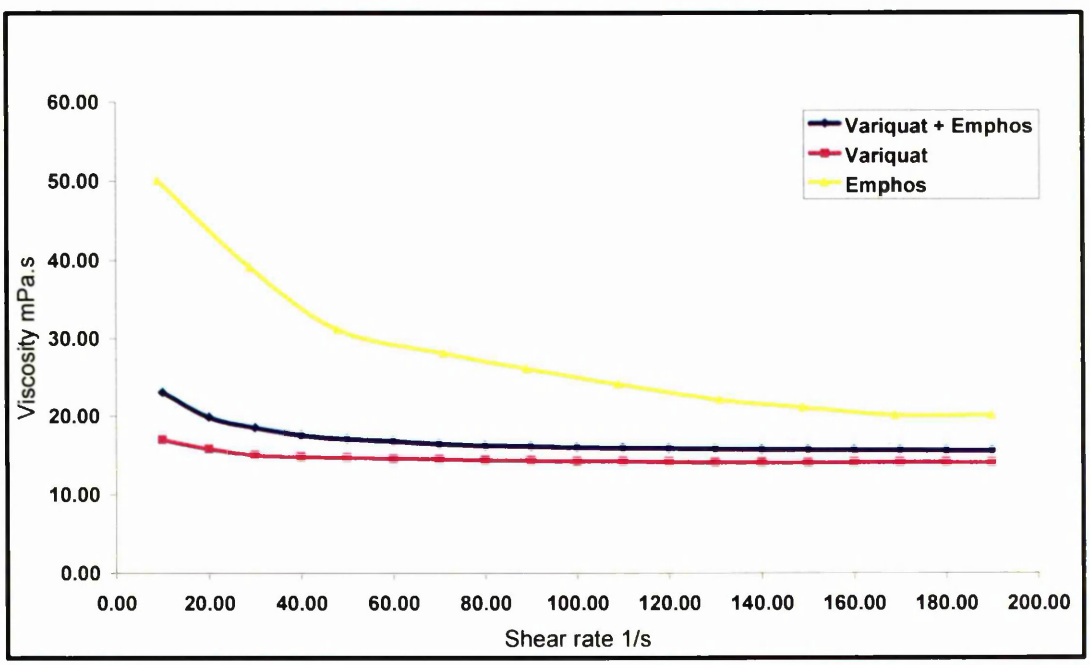

Figure 4-10 Effect of using different dispersants on the viscosity of the suspension

It can be seen from figure 4-10, that the lowest viscosity suspension was achieved by using Variquat.

After a suitable dispersant had been chosen, the maximum loading of solid achievable was determined using rheometry. Five suspensions with ceramic volume fractions ranging from 10 – 50% were prepared and their changes in viscosity were observed with increasing shear rates.

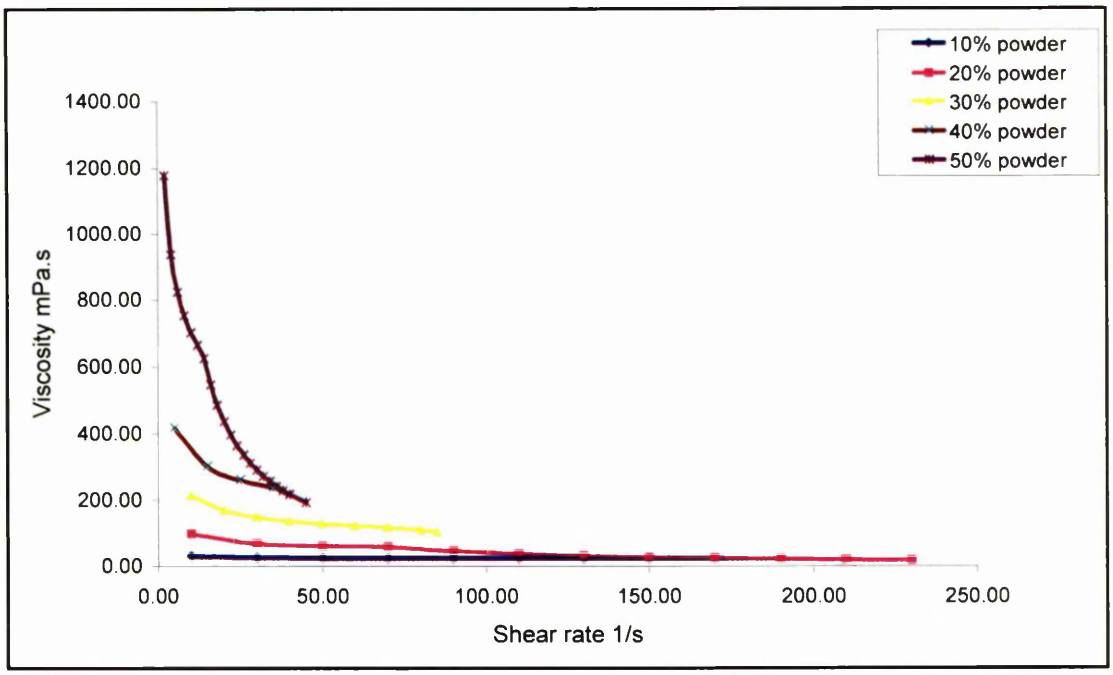

Figure 4-11 Viscosity vs shear thinning of ceramic slurry in PEGDA at different concentrations of glass powder.

As expected, figure 4-11, shows that the viscosity increases with volume fraction of the ceramic. As the concentrations of the powder increases from 10 – 40 %, there is a steady increase in the viscosities of the suspensions. However, on increasing from 40 – 50 % there is a very large increase in viscosity (800 mPa.s).

This experiment was conducted to establish the threshold of the loading level at which the maximum solid loading could be achieved with an appropriate viscosity that corresponds to that of the SLA resin.

The rheometer was also used to determine the viscosity of the SLA epoxy resin, so that a comparison between the two resins can be established. Figure 4-12, shows the viscosity of the epoxy resin to be 600 mPa.s at a shear rate of $15s^{-1}$. It has been stated by Griffith *et al.*

(1996) that shear rates of $15s^{-1}$ (in the SLA) are produced by the recoater blade and the rest is achieved by the dipping action of the platform into the vat. This factor had to be considered when choosing the optimum loading of solid. The modified SLA (explained in Section 3.7.1.2) for the bioactive glass resin used in this study does not have the use of the recoater blade incorporated within it. The only shear produced in the modified SLA is through the dipping action of the platform into the vat of resin.

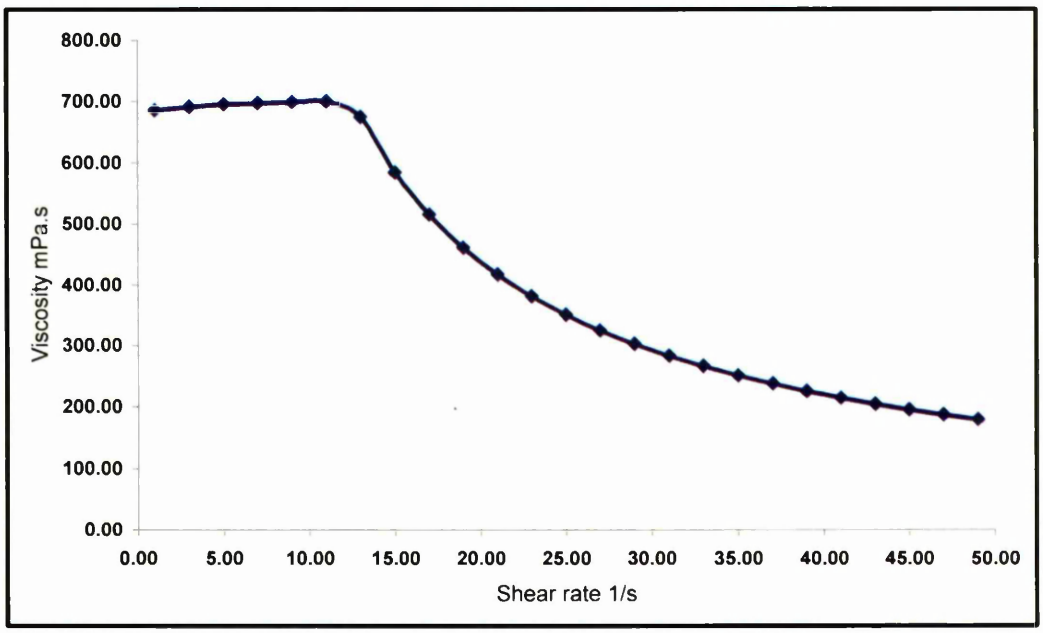

Figure 4-12 Viscosity of the epoxy resin at low shear rates.

Figure 4-13 shows the viscosity of the different suspensions at a shear rate of 15 s^{-1}, to correspond to that of the platform dipping action. The graph has a linear relationship up to a loading of 40%, after which there is a dramatic increase in the viscosity.

Therefore, the maximum loading that the modified SLA would be able to process effectively was 40 vol.%. This value of maximum ceramic loading was then confirmed using the window panes test.

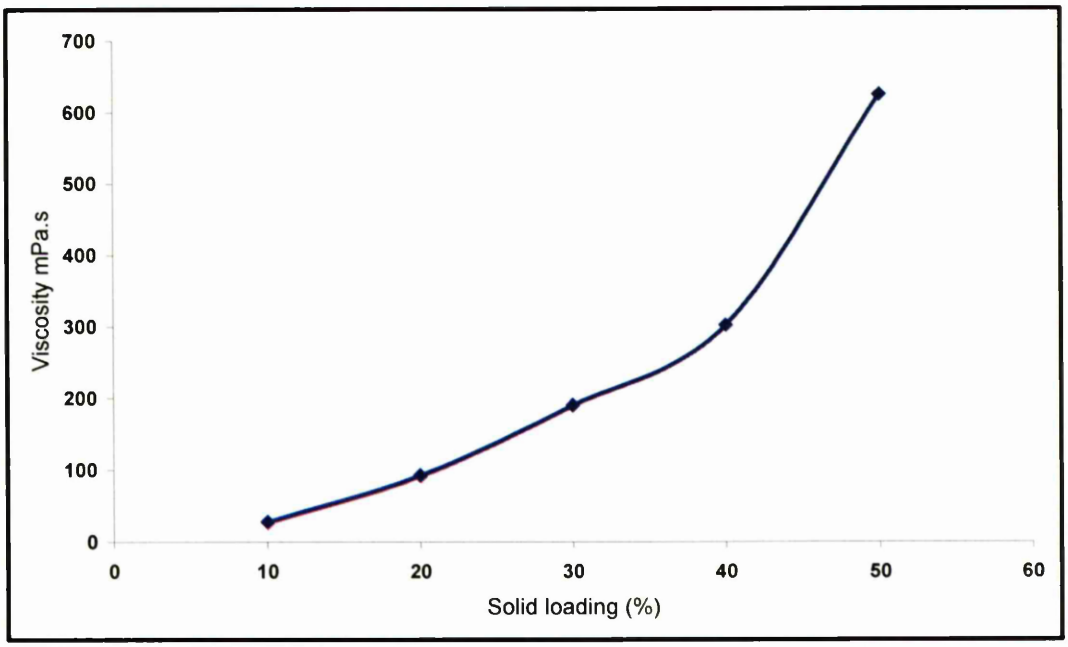

Figure 4-13 Viscosity of different loading suspensions at a shear rate of $15s^{-1}$.

Although the results so far showed that 40 vol.% was the maximum amount of loading that would lead to a suitable scaffold being produced by the SLA, a trial of a scaffold made with 50 vol.% was also fabricated using the SLA. This scaffold had major problems caused by over curing of the layers, which resulted in a solid block rather than a scaffold with controlled channels within the structure. The high volume fraction of ceramic loading in the suspension was causing the UV laser to cure excessively, which resulted in the blocking of channels in the scaffold. This also led to difficulties in removing the excess resin lodged within, which meant that interconnections were blocked. Upon post curing the scaffold, the result was a solid block of composite.

4.7.1.1. Window Panes

Window panes were produced on the SLA using the bioactive glass resin, to establish the extent to which the SLA could fabricate a product whilst maintaining the final shape and resolution. The E_c (critical exposure) and D_p (depth of penetration) values for pure PEGDA were obtained, increasing the loading of powder in increments of 10% up to 40 vol.%.

The window panes program made five different windows with different depths, as explained in section 3.8.1.2. Window panes were created using the varying values of E_c and D_p, until the correct cure depth was achieved to get the best resolution product.

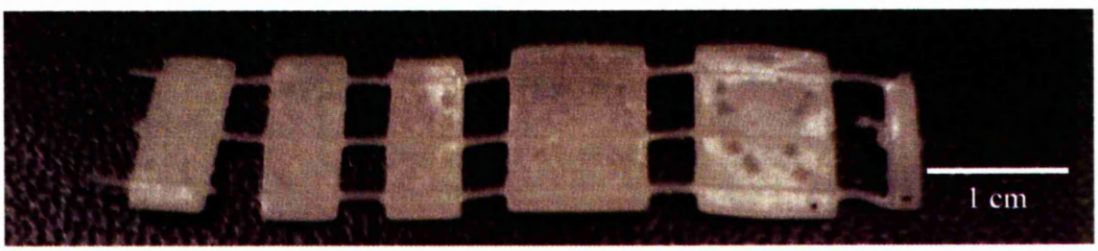

Figure 4-14 Set of window panes produced using the SLA using a glass-ceramic suspension.

The cure depth of the window panes from left to right should be 203, 254, 304, 355 and 406 microns (figure 4-14). The cure depth of each window pane is established by E_c and D_p values that are used to control the processing, and these values change depending on the solid loading in the suspension. Increasing the loading of ceramic particles in the suspension leads to refraction of the laser as it hits the resin, consequently giving differing cure depths.

Thus, as the loading of powder is increased, the E_c and D_p values have to be calculated to compensate for the higher number of ceramic particles the laser can scatter from. The refractive indices of the PEGDA and bioactive glass are both ~ 1.5. Hence, when the laser hits the surface of the suspension, the laser will refract at the same angle for both materials, leading to a more uniform polymerisation on impact.

The basis on which E_c and D_p are calculated have already been explained in section 2.4.2.7.2. The values for E_c and D_p calculated by the system relate directly to a particular suspension, where the particle size and concentration of the glass particles, and the

concentration of initiator is taken into account. Each suspension leads to different values for E_c and D_p which lead to the best possible end product.

Exposure	Measured Cure Depth	AccuMax Results			Result Status	
25.1	0.00800	Dp:	0.0070	inches	Measurement Range:	Valid
33.4	0.01000		(7.0	mils)	Pearson Correlation:	Valid
44.4	0.01200	Ec:	8.0	mJ/cm^2	AccuMax Curve:	Valid
59.1	0.01400	Correlation:	100.0%		Results are Valid	
78.7	0.01600					

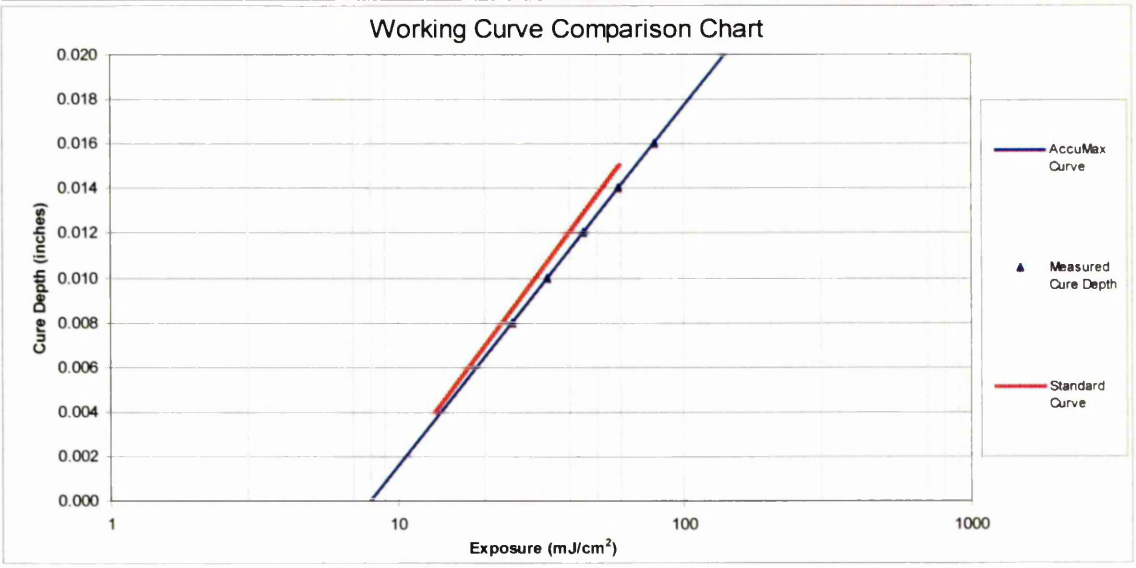

Figure 4-15 The working curve when pure PEGDA was used.

The analysis routine produces a working curve, which consists of three curves.

- Measured curve
- Standard curve
- Accumax curve

Firstly, to start the program random values for E_c and D_p are input into the software. This in turn produces five windows which are all measured for cure depth manually using Vernier callipers. It is from these values of cure depth of the window panes that the software calculates a new E_c and D_p value using the working curve.

The D_p is calculated from the slope of the measured curve, and the E_c is calculated from the intercept value of the measured curve and D_p. These results are then correlated to the

software's calculations and a validation of the results is provided. If the results are valid, a correlation over 99 % is achieved and the true values of E_c and D_p are obtained for that particular suspension.

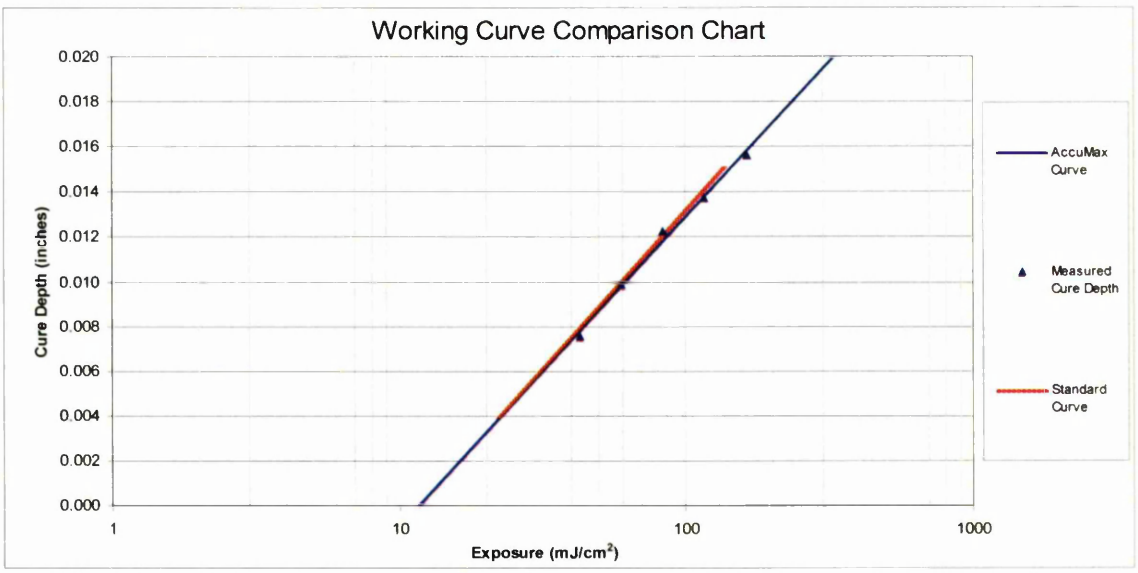

Figure 4-16 The working curve for PEGDA with 10 vol.% LG112 loading.

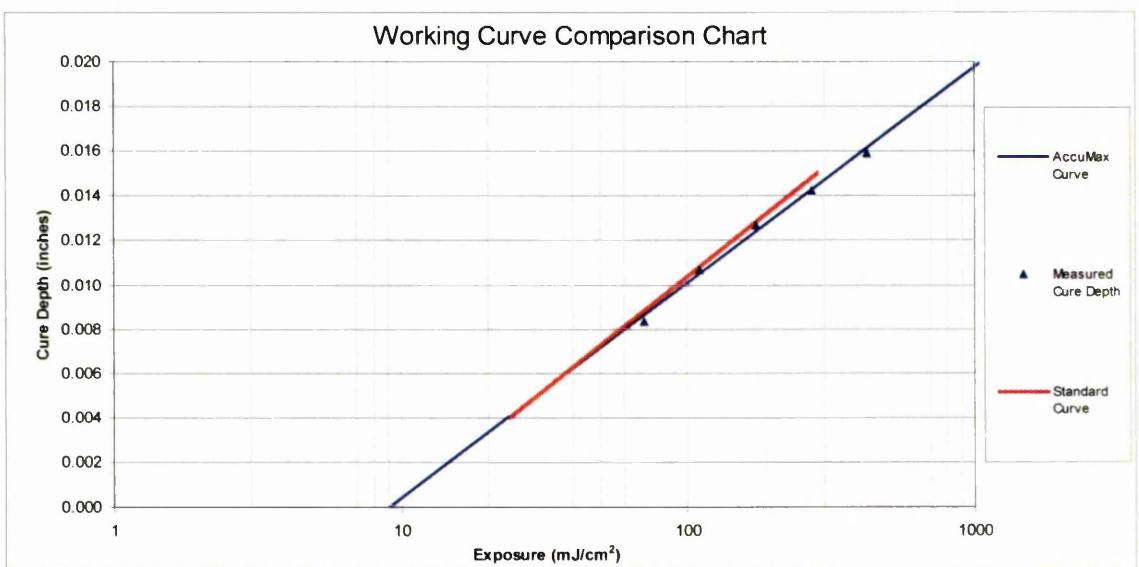

Figure 4-17 The working curve for PEGDA with 20 vol.% LG112 loading.

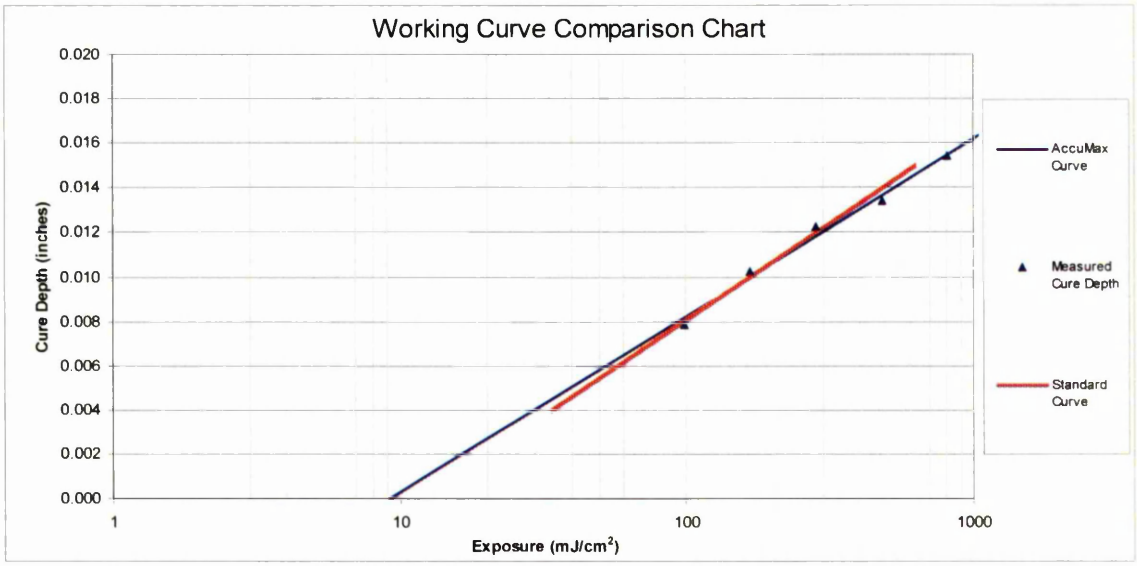

Figure 4-18 The working curve for PEGDA with 30 vol.% LG112 loading.

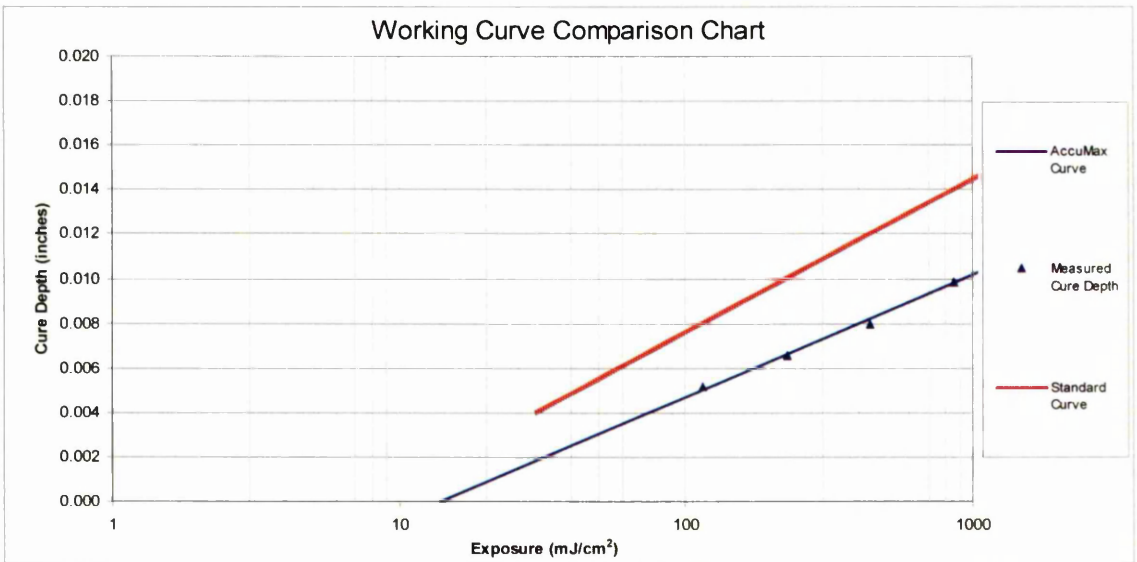

Figure 4-19 The working curve for PEGDA with 40 vol.% LG112 loading.

Table 4-1 The Ec and Dp values for suspensions at different concentrations.

Percentage loading of LG112 in PEGDA	E_c (mJ/cm^2)	D_p (mils)
0	8	177.8
10	11.7	152.4
20	9.1	106.7
30	9.1	86.4
40	13.9	60.9

The E_c and D_p values calculated represent the parameters required by the SLA to obtain good resolution scaffolds at different concentrations of solid loading. These values ensure that factors such as concentration of initiator, volume fraction of ceramic loading and particle size are taken into account when producing window panes. Table 4-1 shows that the depth of penetration (D_p) of the laser decreases as the volume fraction of ceramic increases. This is because the higher number of particles in the suspension leads to a higher scattering of the UV laser thus achieving the same cure depth. The critical exposure (E_c) generally increases with a higher loading of ceramic particles. This is due to the increased number of particles hindering the polymerisation process and as E_c is the exposure required to induce polymerisation, a higher dose is required to get the process started. The reason that a clear increasing trend cannot be seen for the values of E_c with an increase in volume fraction of ceramic could be attributed to the suspension not being homogeneous. The settling of particles at the bottom of the vat would lead to the suspension not being truly representative of the volume fraction of ceramic present. This would in turn give a lower value for E_c. This is proven by the fact that to produce a window pane with a cure depth of 406 μm, a laser exposure of 78.7 mJ/cm^2 was required for PEGDA without any ceramic loading (figure 4-15). Increasing the volume fraction of ceramic to 40 vol.% required an exposure of 1657.1 mJ/cm^2 to produce the same window pane (figure 4-19). This clearly proves the relation of increasing laser exposure, with increase in volume fraction of ceramic in the resin.

After the maximum loading of glass powder had been established (40 vol.%), a comparison between two photoinitiators (IRGACURE 1173 and DMPA) was conducted by taking a 40 vol.% loading of ceramic powder in PEGDA and adding different concentrations of photoinitiator. The laser on the SLA has a wavelength of 354 nm, thus

IRGACURE 1173 and DMPA were both chosen as they have an absorption peak at 331 nm and 338 nm respectively. The values for E_c and D_p were kept constant throughout the experiment at 8 mJ/cm^2 and 3 mils. Figures 4-20 and 4-21 show the effect of percentage initiator used on the cure depth of the window panes.

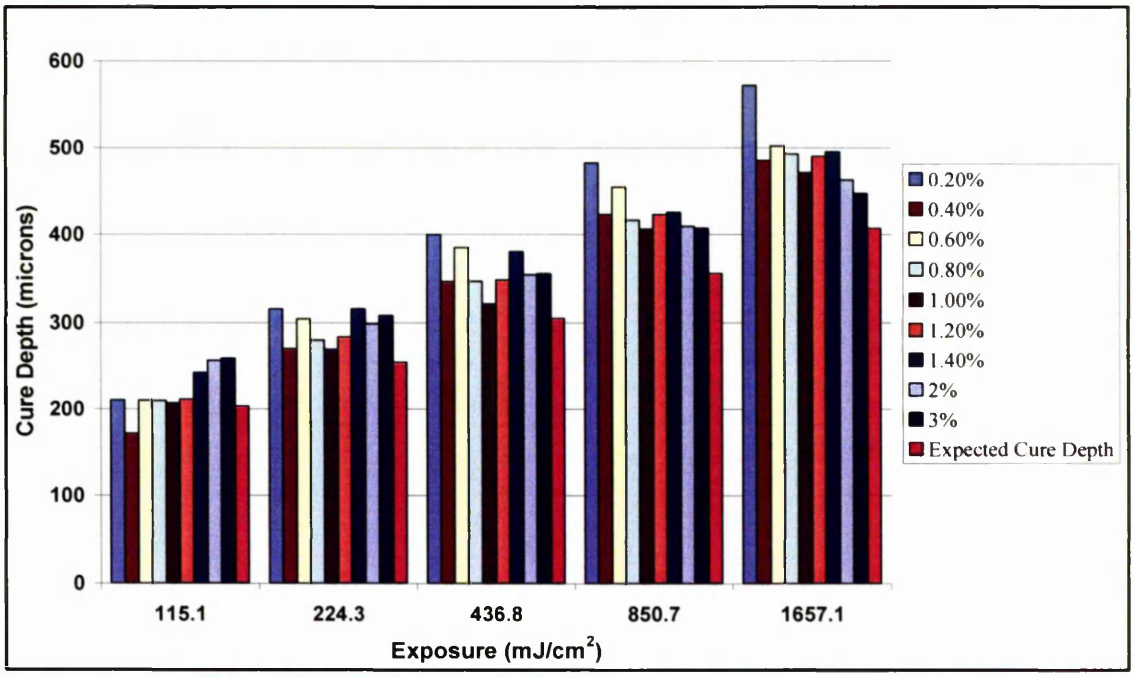

Figure 4-20 The effect of using different concentrations of IRGACURE on the cure depth.

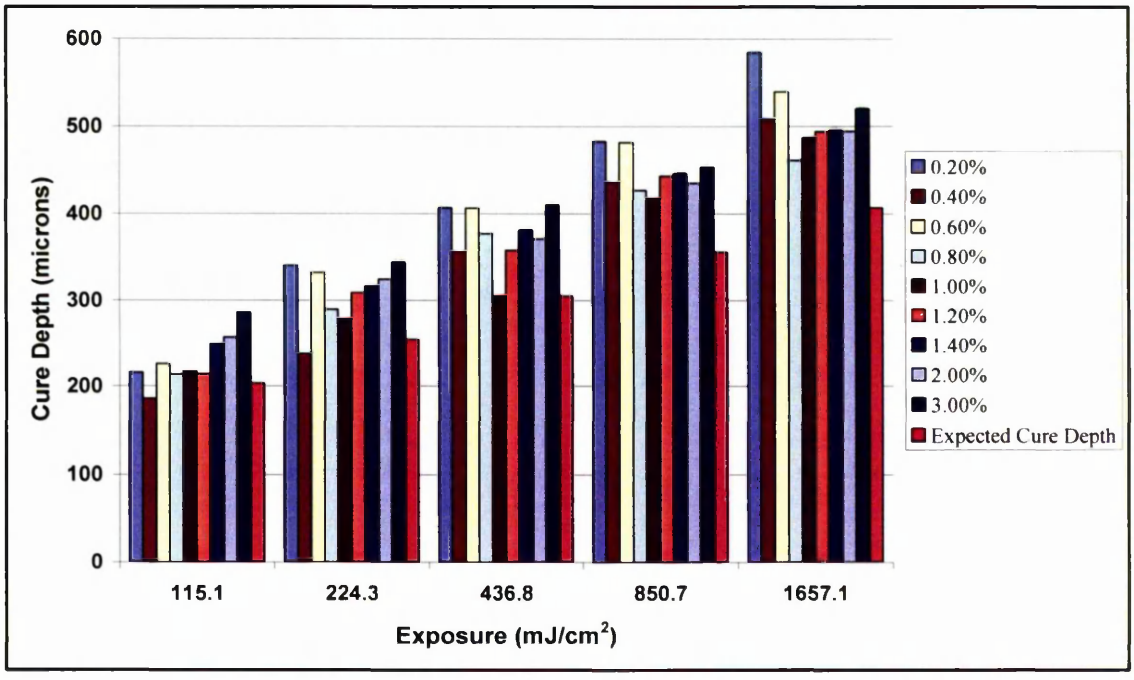

Figure 4-21 The effect of using different concentrations of DMPA on the cure depth.

For both initiators, 1 wt.% initiator seems to be the closest to the expected cure depth required by the SLA. The results on the bar chart at each of the exposures all seem to be very close to each other, but observing the final product and texture of each of the separate window panes determined the correct concentration of initiator to be used. For both initiators, this concentration was found to be 1 wt.%.

Usually a very low percentage of 0.2 wt.% is used when photopolymerising with UV initiators. This is normally the case for pure resins without any ceramic loadings. In this case, a higher percentage of initiator is required because a high loading of ceramic particles in the resin prohibits complete polymerisation at lower initiator concentrations. Regardless of the concentration of ceramic loading, the window panes test ensures cure depth to be consistent and repeatable over a range of exposures. All other concentrations of photoinitiator are not consistent in producing all five window panes to the expected size at different exposures apart from 1 wt.%.

Although both initiators give similar results, IRGACURE 1173 was chosen as a suitable photoinitiator for the SLA. This is because it provides more consistent results throughout the range of exposures in the window panes test. It also comes in a liquid form (DMPA is a powder), making it easier to fabricate a more homogeneous suspension.

For these reasons, the modified SLA bioactive glass resin was prepared with 40 vol.% bioactive glass in PEGDA (258), with 5 wt.% Variquat and 1wt.% IRGACURE. These were all mixed together using a vibrating mill and zirconia balls for 12 hours, to achieve a homogeneous mixture with low viscosity.

4.7.1.2. Optical Microscopy

After establishing optimum parameters for the suspension, the modified SLA was used to fabricate two scaffolds with external dimensions of 8 mm x 8 mm x 8 mm, but with varying size holes, i.e. 400 μm and 600 μm. Both scaffolds had the same size struts (500 μm). For efficient transportation of nutrients to the cells and vascularisation, scaffolds need to have channels which are able to provide the cells with nutrients and provide a route to remove waste products. For this reason, the holes in the scaffold have to be over 350 μm in size as stated by Whang and Healey (2001). As this is the first time this technique is being used to produce scaffolds to be used as bone implants, the size of the holes has been chosen to prove that controlled geometry can be achieved.

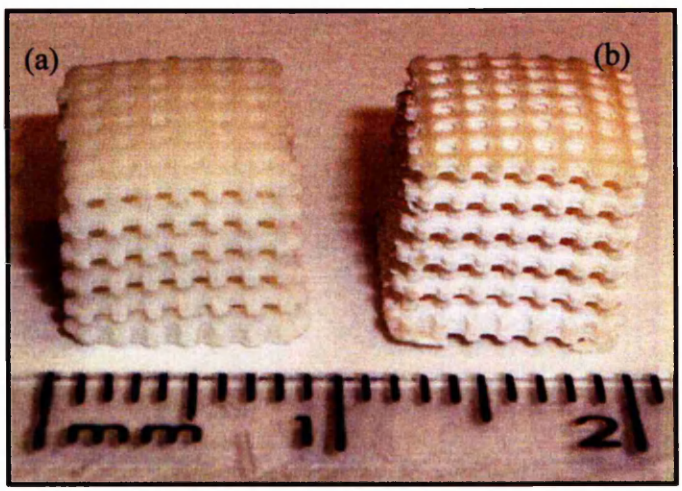

Figure 4-22 (a) uncured scaffold and (b) after being cured in the post curing apparatus.

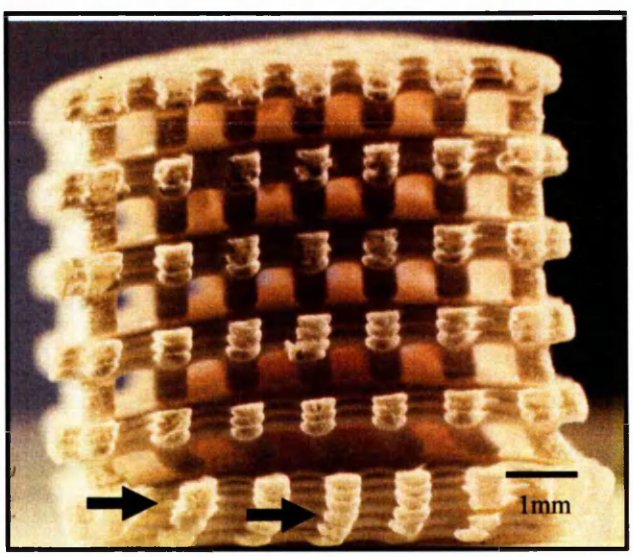

Figure 4-23 Individual layers of the scaffold at a higher magnification with shifted layers at the bottom (arrow).

Figure 4-22(a) shows the scaffold after removal from the SLA and cleaning to remove the excess resin trapped within it. Figure 4-22(b) shows the scaffold after it has been placed in the PCA for 3 hours, to completely cure the scaffold. This leads to a very small, almost negligible shrinkage (~2%) of the scaffold, which keeps distortion to a minimum and not many changes occur in the structure of the scaffold.

A clear difference can be seen in the colour of the two scaffolds. The precured scaffold is also much softer and ductile as the layers have been cured just enough to bond to each other on the SLA. After curing in the post curing apparatus the scaffold is much harder as it has predominantly cured.

Figure 4-23 shows a higher magnification image of the composite scaffold, where the individual layers can be clearly seen. A slight U-shape at the base of each layer is also visible. This is for two reasons: distortion of the scaffold during the cleaning process, where the scaffold has to be handled with care; and blowing air through the holes of the scaffold to remove the dislodged resin, which leads to some distortion in the shape of the scaffold. This is reinforced in the PCA if the scaffold is overcured.

Figure 4-23 also shows the loss of registration of the layers at the base of the scaffold. This can sometimes lead to a complete shift of the layers, thus blocking the holes of the scaffold. This is caused by the supports that are laid on the platform prior to the base of the scaffold. The supports are six thin structures joining the platform to the scaffold, to aid scaffold removal after fabrication. The thin supports are very fragile and are prone to movements in the machine, e.g. when the platform dips into the resin. If the dipping action is too fast, the supports move and thus the whole structure is compromised. The dipping action of the elevator set to be slow would counteract this problem, but then very low shear rates will be achieved causing problems of both over curing and under curing on the surface of each layer. Thus, a medium pace was used to alleviate both problems.

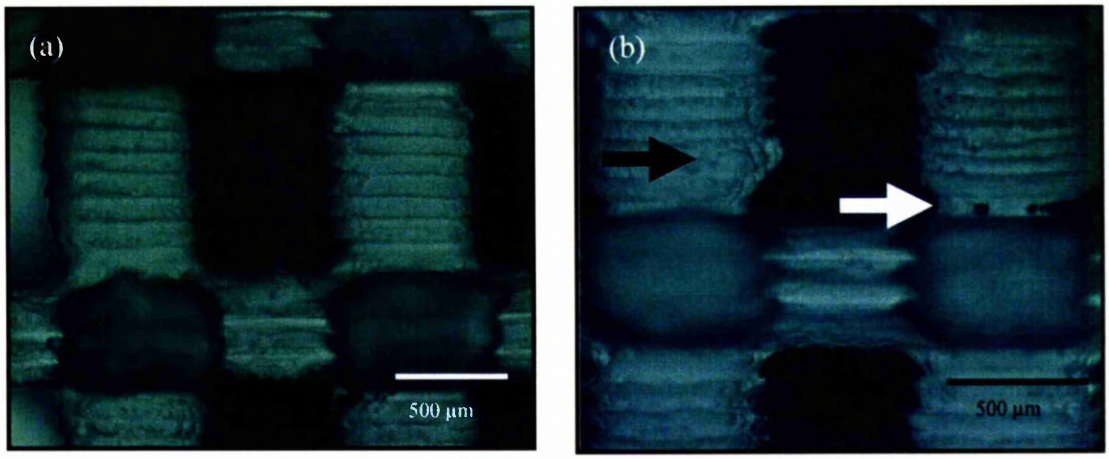

Figure 4-24 An optical image of the scaffold bonding between the layers.

Figures 4-24 (a) and (b) show optical images of the scaffolds and the bonding between each layer. Figure 4-24 (a) is a prime example of complete bonding between layers that are laser cured. In figure 4-24 (b) two anomalies can be noticed. Firstly, some over curing of the layers can be seen (black arrow), which could be a result of the resin not flowing off the surface completely, when the scaffold resurfaces after the dipping action. Secondly, the struts have not bonded completely to the horizontal layers of the scaffold (white arrow). Looking at the images it is clear that the holes in the scaffold are not cube shaped. This is because in the X and Y direction (figure 4-25 (a)), the SLA is more accurate in making a square shape, but it not very accurate in the Z direction.

4.7.1.3. SEM of Composite Scaffolds

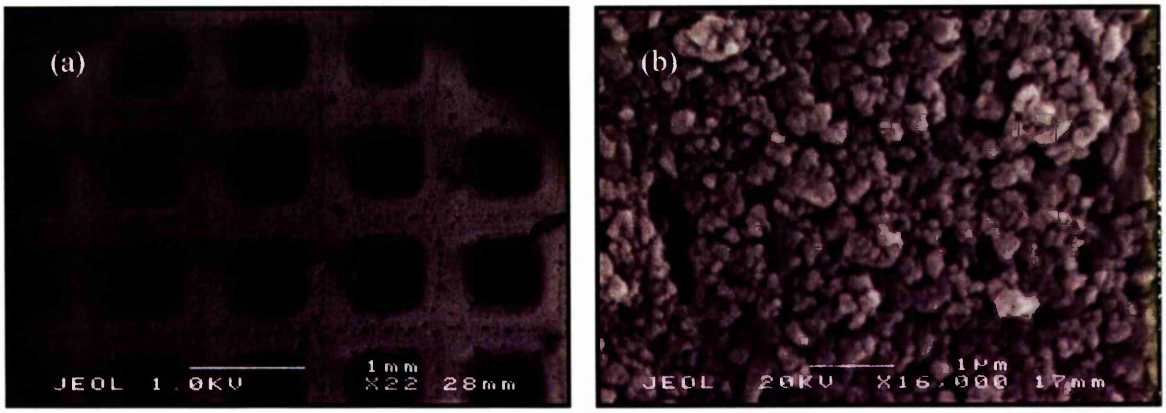

Figure 4-25 (a) the top surface of a composite scaffold and (b) higher magnification of the surface.

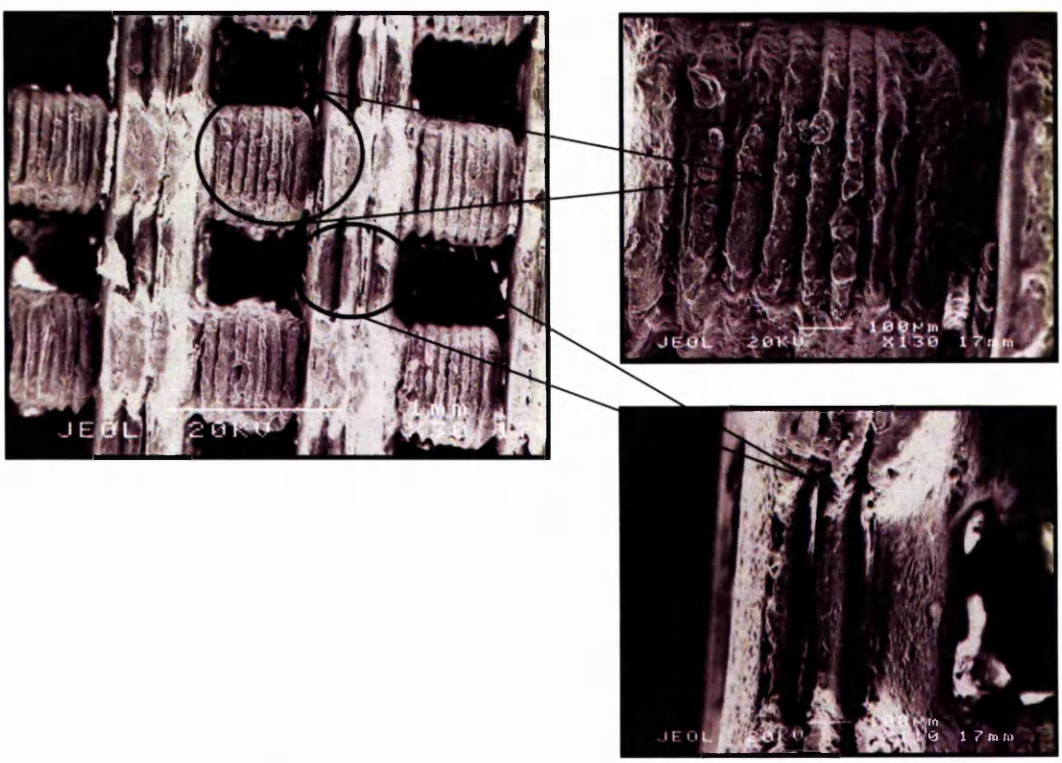

Figure 4-26 Cracking between the struts of the layers in the scaffold.

SEM of the surface of the composite scaffold is shown in figure 4-25. This shows the scaffold to have a flat surface. The holes are square with the edges not present, and the surface topography of the scaffold shows polymerisation to be completed.

Figure 4-26 is a higher magnification image that shows cracked struts and the horizontal layers. These cracks are present at several points within the scaffold, and are caused either by the cleaning process and post curing, or by the ceramic particles inhibiting the UV initiator to fully polymerise points of intersection within the scaffold. This cracking however, is unlikely to affect the structural integrity of the scaffold in service because it will be used in load bearing applications, where the scaffold would be in compression. Conversely shear forces could adversely affect the mechanical properties of the scaffold.

4.7.2. Glass-Ceramic Scaffolds

Glass-ceramic scaffolds were made by using a 1:1 ratio of IBA and PNPGDA as the binder to hold the maximum loading of bioactive glass powder. The scaffolds were made by gel casting the ceramic suspension into moulds fabricated from the SLA. Rheometry was used to determine the maximum loading of powder into the monomer. As the suspensions were to be gel cast, the viscosity of the resin did not have to be matched to that of the epoxy resin of the SLA, as for the composite scaffolds.

Rheometry in this case would show the percentage of ceramic loading that could be gel cast without problems of inhomogenity of the final scaffold.

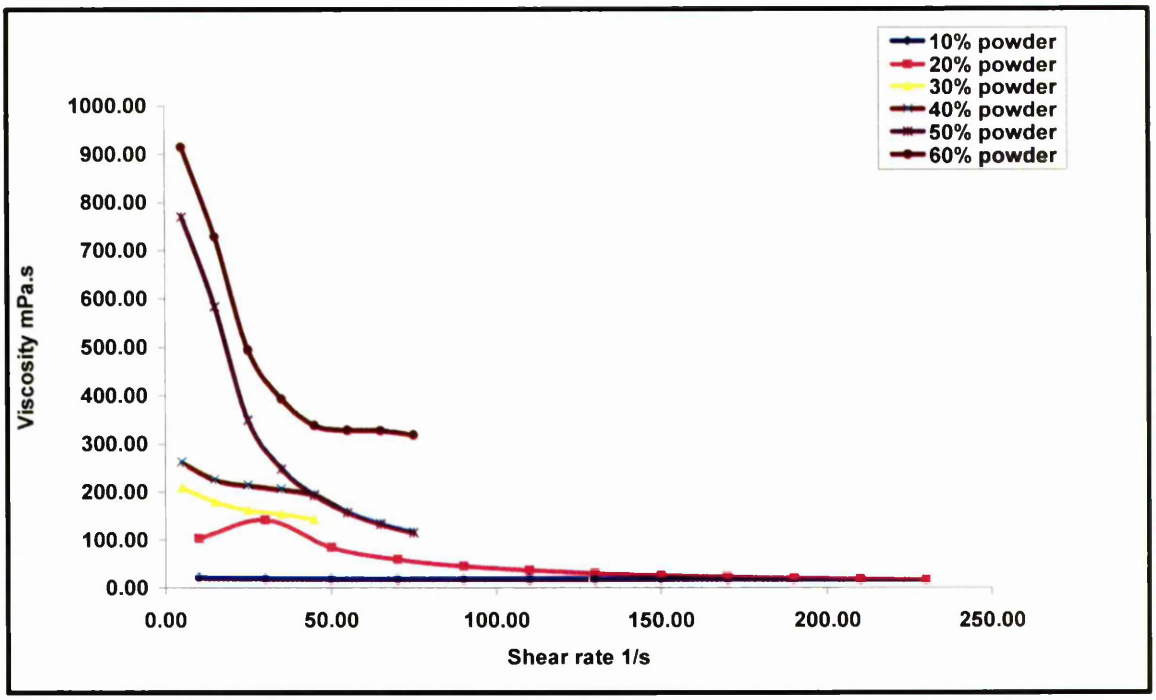

Figure 4-27 Viscosity of ceramic suspension in IBA/PNPGDA at different concentrations of glass powder.

Figure 4-27 shows the viscosity of ceramic loadings ranging from 10 – 50 vol.%. There is an increase of ~ 500 mPa.s between the viscosities of the 40 and 50% ceramic slurries. Although this was the case, 50 vol.% ceramic slurries, with 5 wt.% Variquat and 1 wt.% Benzoyl peroxide as the thermal initiator were produced to be gel cast into the moulds.

Ceramic suspensions with 50 vol.% loading was chosen to be the optimum volume fraction of ceramic powder. The reason for this was that the overall scaffold produced contained fewer defects compared to the 60 vol.% suspension and had more structural integrity than 40 vol.% ceramic suspensions, in terms of crumbling edges of the scaffold after sintering.

Two different types of glass-ceramic scaffolds were cast with 50 vol.% loading. Both had external dimensions of 7.2 mm x 7.2 mm x 6 mm, with varying size holes, i.e. 400 μm and 600 μm. The hole sizes were kept the same as the composite scaffolds to enable direct comparisons between the two types of scaffolds.

Limitations of different sized scaffolds

The SLA has proven to be very successful in making scaffolds with controlled internal and external architecture with different size pores. This technique has shown favourable results in fabricating scaffolds both using the modified SLA and using the SLA to gel cast glass-ceramic scaffolds. The machine has been capable of producing intricate shapes in a wide range of sizes. Large scaffolds, for example: 2 cm x 2 cm x 2 cm with 1 mm size holes, were produced on the SLA (figure 4-28(a)), and at the same time on the bottom range of the scale, glass-ceramic scaffolds with 100 μm holes were also fabricated (figure 4-28(b)). This indicates the range of structures that are achievable using this technique over any other method. It should be noted that these scaffolds are however, not suitable for load bearing implants and were not tested further, as pore sizes over 100 μm are required for the transportion of nutrients to the cells and for the vascularisation process.

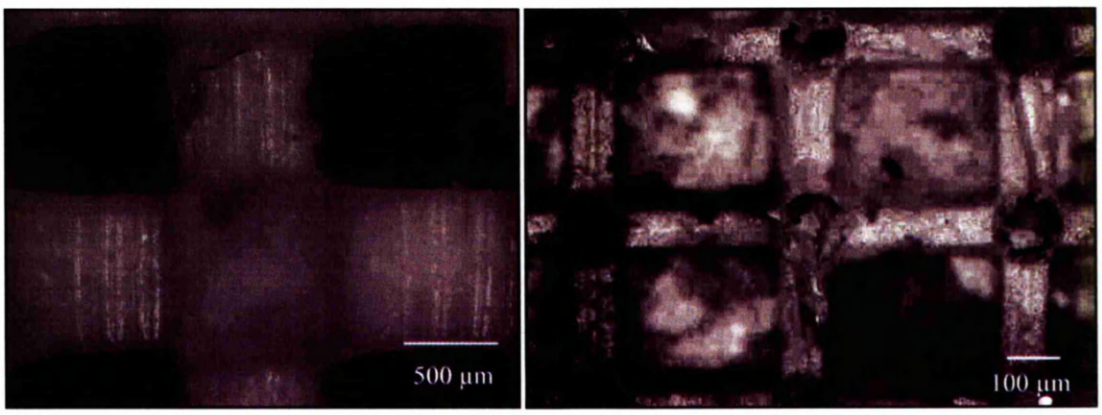

(a) (b)

Figure 4-28(a) Glass-ceramic scaffold with 1mm and (b) 100 μm holes fabricated using SLA.

These results were only observable for the fabrication of gel cast scaffolds. The method of using the modified SLA to produce composite scaffolds had a minimum range of producing 300 μm holes, as anything below this size resulted in blockage of holes during the cleaning process and overcuring of the layers within the scaffold.

Summary

SLA has proven to be a very successful technique in making scaffolds to be used as bone implants in this study. The technique has had its limitations which have for fabrication of

the composite scaffolds been the cleaning process and the removal of the excess resin lodged within the scaffold. For the glass-ceramic scaffold, there are no limitations when using the SLA, but during the gel casting of the suspensions, the de-airing process has proven difficult and the partial elimination of the air bubbles trapped within the suspensions has resulted in scaffolds that contain defects. Nevertheless, the range of geometries achievable using this technique, can be used to fabricate 3-D scaffolds for many other applications such as facial implants, knee implants, and other areas of the body.

4.7.2.1. Dilatometry

As the glass-ceramic scaffolds were made by burning off the polymer binder and the epoxy resin followed by sintering to 1200°C, there was shrinkage in the final scaffold. In order for the scaffolds to attain prescribed pore sizes after sintering, the amount of shrinkage had to be determined to calculate the correct size of moulds.

Dilatometry was used to find the reduction in volume of a cyclinder of 50 vol.% LG112 in IBA/PNPGDA upon sintering to a temperature of 1200°C.

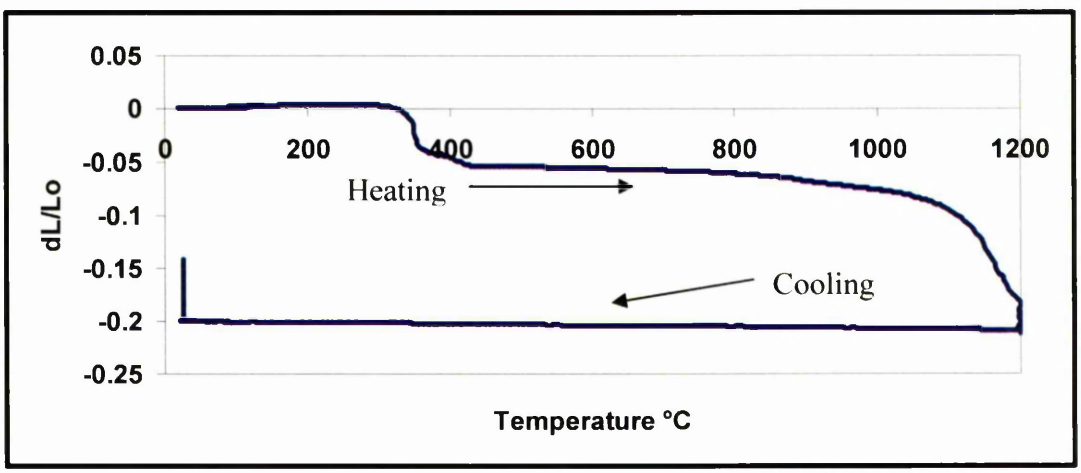

(a)

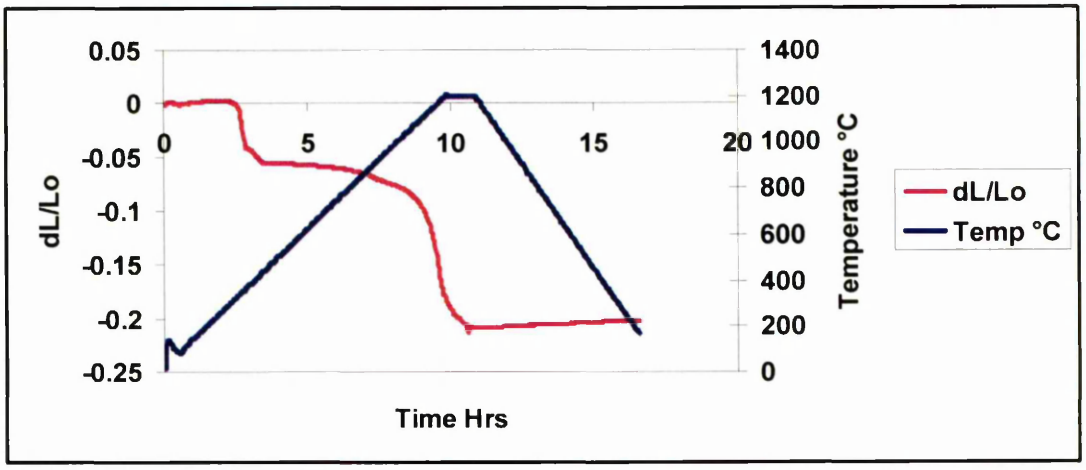

(b)

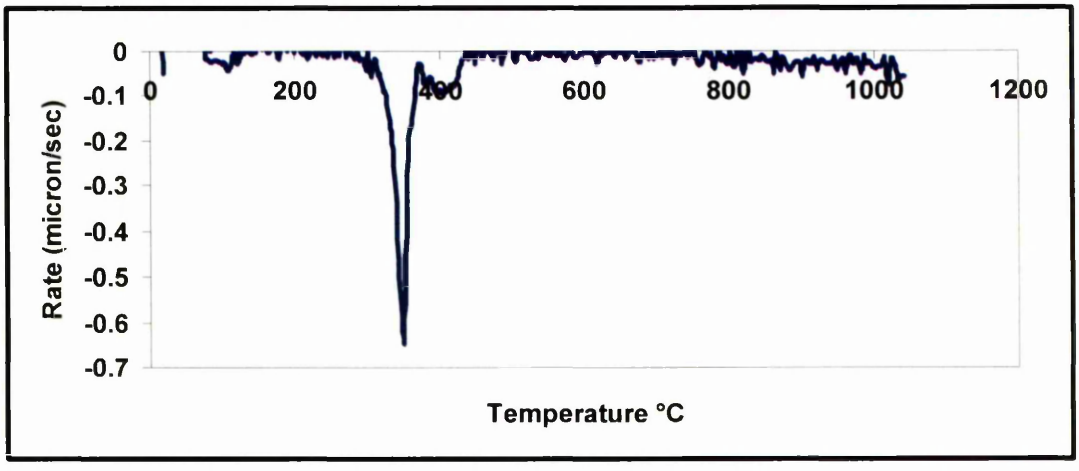

(c)

Figure 4-29 (a) Shrinkage in volume of LG112 composite with IBA/PNPGDA, (b) Rate of shrinkage, and (c) Burnout temperature of polymer binder.

Figure 4-29 (a) shows 22% shrinkage in the volume of the cylinder up to 1200°C. The time taken for most of the shrinkage is 10 hours (figure 4-29 (b)), with the burnout of the polymer binder taking place at ~ 350°C (figure 4-29 (c)).

This result was confirmed on a fabricated scaffold, by making a mould on the SLA with 500 μm holes and 500 μm struts (figure 4-30). The ceramic slurry was then gel cast into the mould, polymerised and then burnt-off to obtain a sintered scaffold. The holes and struts of the scaffold were then measured and showed a shrinkage of ~ 21%, which is consistent with the dilatometry.

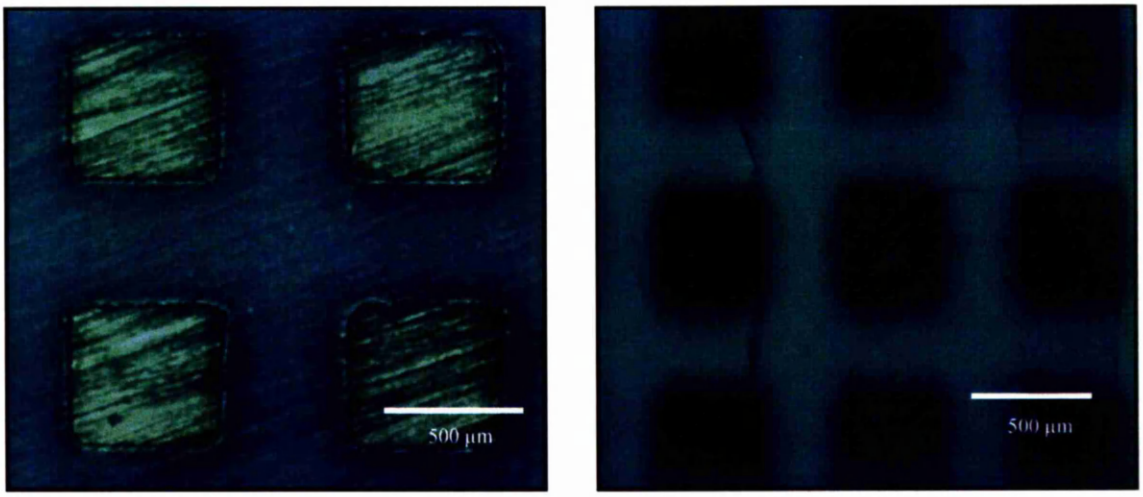

Figure 4-30 Gel cast mould (left) and the resulting scaffold (right).

4.7.2.2. Optical Microscopy

Optical microscopy was conducted on the moulds and the resulting glass-ceramic scaffolds produced.

For the scaffold with 400 µm holes, the mould was set to have struts of 512 µm and the holes to be 800 µm (figure 4-31 (a)). The resulting scaffold had 400 µm holes and 600 µm struts (figure 4-31 (b)).

For the scaffold with 600 µm holes, the mould was set to have struts of 790 µm and the holes to be 1000 µm (figure 4-32 (a)). The resulting scaffold had 600 µm holes and 800 µm struts (figure 4-32 (b)).

The uncertainty of the gel casting process and sintering to produce the correct size holes is ± 20 µm. This was determined by measuring the size of the holes on ten different scaffolds. The reason for this small discrepancy is the effect that sintering has on the ceramic. Small cracks and air bubbles can also lead to changes in the size of the holes. This technique has proven successful and was able to produce highly accurate, geometrical scaffolds on a large scale.

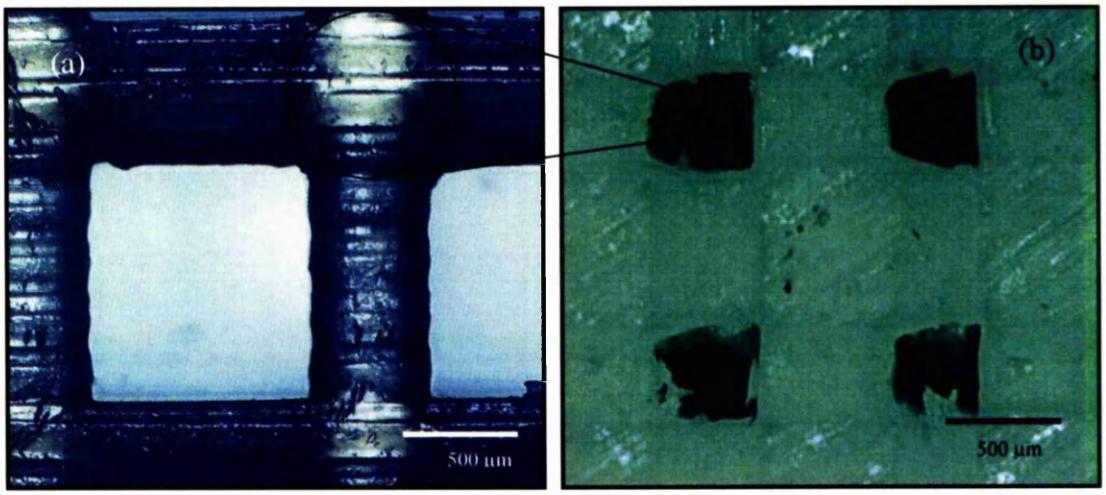

Figure 4-31 (a) the mould fabricated on the SLA and (b) the final glass-ceramic product with 400 µm holes.

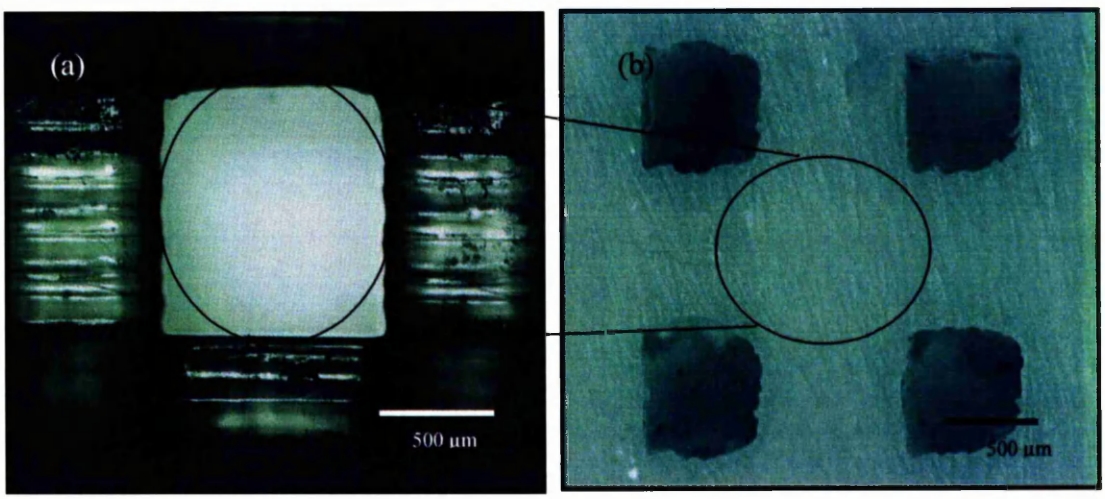

Figure 4-32 (a) the mould fabricated on the SLA and (b) the final glass-ceramic product with 600 µm holes.

The sizes of the holes when fabricating the moulds for gel casting were set to be bigger than the struts in the mould. There are two reasons for this. Firstly, when the epoxy moulds are fabricated on the SLA, the larger holes make it easier to clean and remove excess resin lodged within the mould. Blockage at any point within the mould will eventually lead to a deformed glass-ceramic scaffold with cracks and defects within it. Secondly, if the holes and struts are both the same size, upon sintering the scaffold, shrinkage would cause the holes to be too close to each other and this would lead to development of major cracks

throughout the structure. Also increasing the size of the holes on the mould leads to a greater surface area for cellular attachment and proliferation.

Figure 4-33 shows the final glass-ceramic scaffold. The build quality of the scaffold is very high, but small cracks are visible at the edge of the scaffold, which are a result of air particles trapped during the gel casting process.

These glass-ceramic scaffolds and the composite scaffolds were used for cell culture experiments.

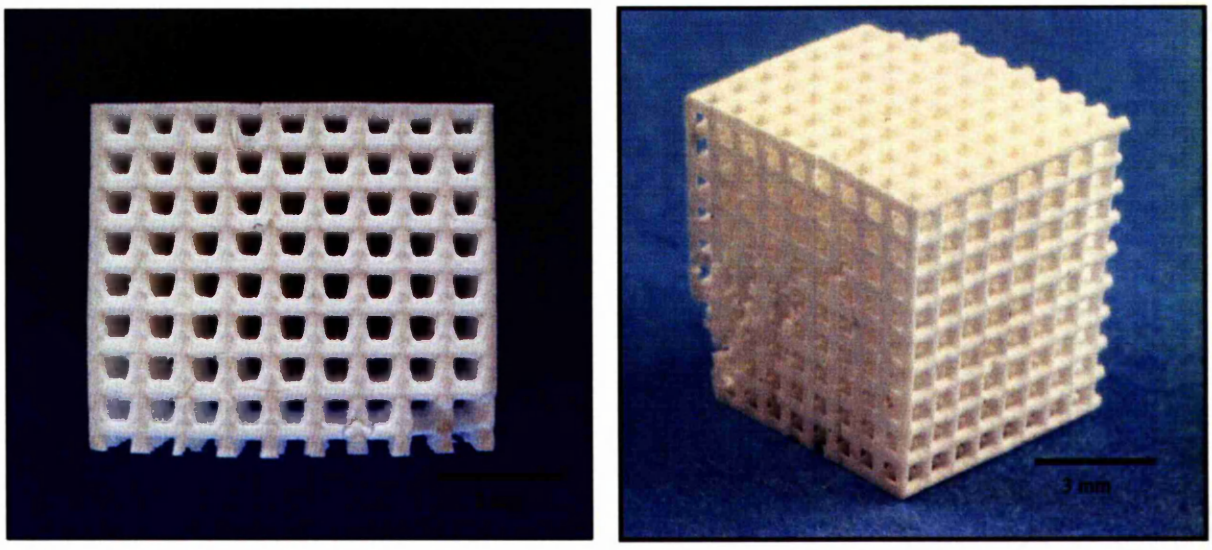

Figure 4-33 A glass-ceramic scaffold made by using the SLA and gel casting process.

4.7.2.3. SEM of Glass-Ceramic Scaffolds

SEM was conducted on the glass-ceramic scaffolds to observe the surface of the scaffold. Cracks present on the surface of the scaffold shown in figure 4-34 are caused due to the effects of shrinkage during sintering. Tiny air bubbles left within the suspension also lead to crack formation on sintering. Figure 4-35 shows a hole present at the edge of the scaffold, yet again caused by an air bubble. The image also shows directional scratching on the surface of the scaffold. These scratches are a result of the removal of the excess epoxy resin casing by grinding, after polymerisation of the suspension and prior to burn-off and sintering of the scaffold. These scratches will prove to be favourable when cells are seeded on the scaffolds, as will be shown later.

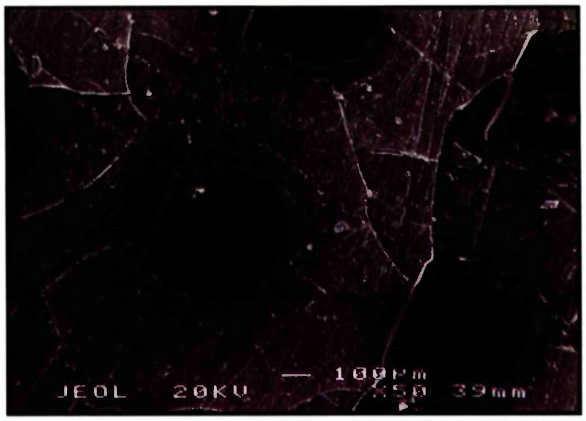

Figure 4-34 Cracks present on surface of ceramic scaffold.

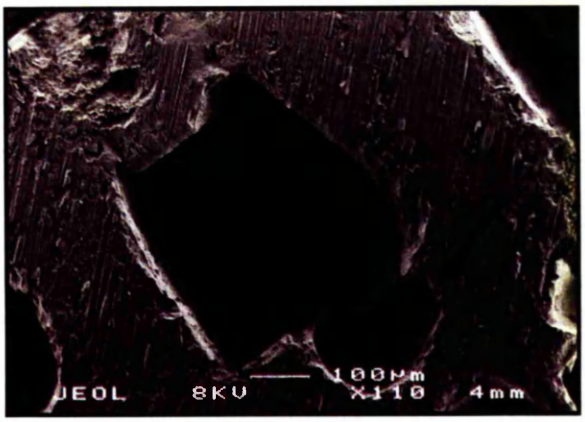

Figure 4-35 A hole (arrow) present on surface of ceramic scaffold with directional scratching.

4.7.2.4. Geometries for Cellular Studies

The geometries of the glass-ceramic scaffolds meant that cellular attachment could only be observed on the surface of the scaffolds. To observe cell behaviour within the scaffolds, different techniques were tested. The first technique tested to examine cell activity within the scaffold was histology.

Histology is the study of tissue sectioned as a thin slice, using a microtome. Cells were grown on both types of scaffolds for time periods of 7, 14 and 21 days and fixed with ethanol. After which, they were embedded into a paraffin wax. The embedded scaffolds were then ready for sectioning using a Microm HM 200. The composite scaffolds were suitable for sectioning and slices 5 µm thick could be sectioned. These sections were then stained, to observe cell morphology under a light microscope. The same process was carried out for the glass-ceramic scaffolds, but after embedding the scaffolds in the wax, sectioning them into thin slices proved very difficult. The glass-ceramic was too hard for the machine to section. Thereafter, a diamond cutter blade was used to section the glass-ceramic scaffolds, but 150 µm sections could only be cut, which were too thick for the technique of staining and observing under a light microscope.

The second technique employed to examine cell behaviour within the scaffold was X-ray tomography using X-Tek 255. The cells were seeded onto both glass-ceramic and composite scaffolds, and then stained with osmium tetroxide which has a high molecular

mass. It embeds a heavy metal directly into cell membranes, which can readily be registered by the x-rays. This technique did not prove successful, as the cells were undistinguishable from the surface of the scaffold, due to their very small size. However, this technique may be successful if the cells were stained for longer periods after seeding, showing the extent of cell proliferation throughout the scaffold.

To overcome this problem and to be able to observe cellular behaviour throughout the scaffold another type of scaffold was also fabricated to check for cell attachment. Sectioned moulds were produced on the SLA to observe cellular behaviour using sliced scaffolds (results shown in section 5.7).

Figure 4-36 shows slices of a mould made on the SLA. These slices are essentially segments of the glass-ceramic moulds that were produced previously. The sliced moulds were gel cast with the ceramic suspension and segments of scaffolds with the same external dimensions and hole size were produced. The benefit of producing these sliced scaffolds was that the segments could be placed on top of each other like a conventional scaffold (figure 4-36 (b)), cells could be seeded onto them, and then the slices could be easily taken apart to check for cell attachment and proliferation within the scaffold.

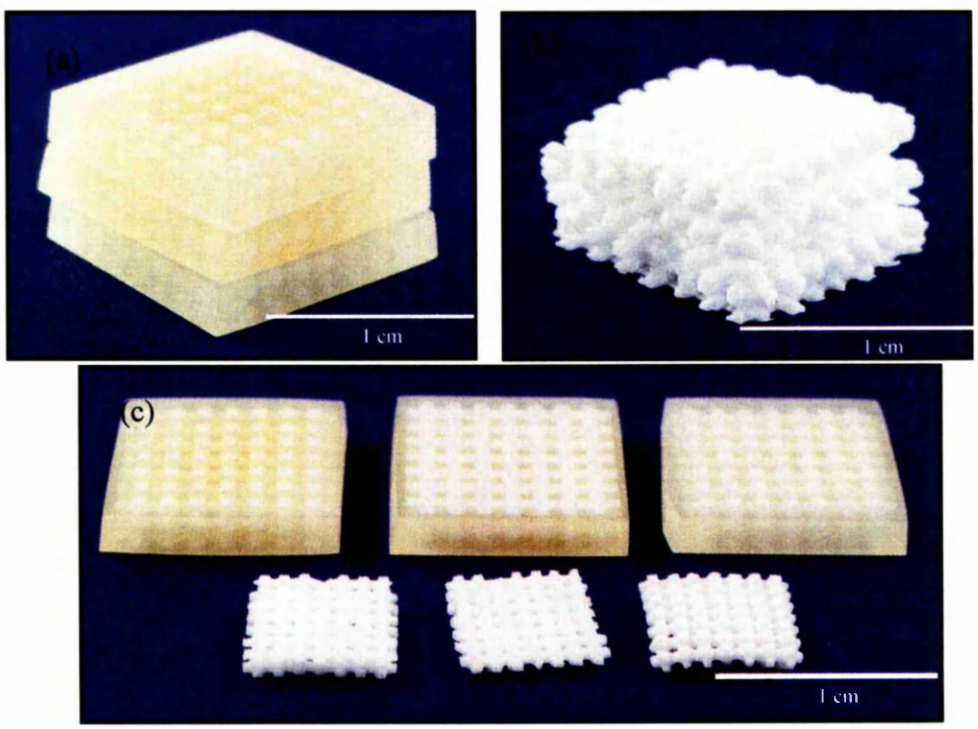

Figure 4-36 (a) gel cast sections stacked on top of each other, (b) the glass-ceramic sliced scaffold, and (c) the gel cast sections with their counterpart glass-ceramic slices.

4.8. Mechanical Testing of Scaffolds

The mechanical properties of bone scaffolds can be generally measured by way of their compressive properties. Compression is one of the prevailing loading modes they will experience *in vivo*.

A compressive force was then applied to the upper surface of the scaffolds using a 1 kN load cell at a constant crosshead displacement rate of 1 mm/min to failure. The compressive load and the sample length were recorded at 0.1 second intervals during compression. All scaffolds were tested in the direction they were fabricated in, using the SLA (figure 4-37). Using this data, the stress and strain were calculated and plotted against one another to determine the compressive strength and stiffness for each scaffold. The Elastic Modulus, an indication of the extent of compressive deformation in a scaffold for a given load, was obtained from the linear portion of the Stress versus Strain curve. Compressive strength refers to the local stress maximum after the linear elastic region of the curve.

4.8.1. Composite Scaffolds

Compressive tests were performed to evaluate the mechanical properties of these scaffolds. Gibson and Ashby (1997) summarised the compression process of a porous scaffold of a non-brittle material. Initially it exhibits linear elastic deformation at small strain, then flexure deformation for an elastic material or yielding deformation for an elastic-plastic material at large strain, followed by a plateau region and solidifying region at very large strain and extremely large strain.

Both composite scaffolds, COMP 400 and COMP 600, were tested under compressive load of 1 kN and their stress-strain curves are shown in figure 4-38 and 4-39. The external dimensions of both scaffolds were 8 mm x 8 mm x 8 mm, with varying hole sizes of 400 μm and 600 μm. This meant that COMP 400 scaffold had 10 x 10 struts present in the structure, whereas COMP 600 only had 7 x 7 struts.

Four specimens for each type of scaffold were tested in compression. Only four specimens were tested due to a shortage of specimens, and the results do show a range of values, but a good idea of their mechanical properties has been obtained.

All scaffolds tested were cube shaped with the struts being squares. The reason for the choice in scaffold geometry was because of the simplicity of the design and as this technique was being used for the first time to produce bone implants, it was a concept and feasibility study to see what kind of results were achievable by using the SLA.

Specimens which were inspected visually for minimum amount of defects were chosen for the tests, and special care was taken to make sure that the surface of the scaffolds was as flat as possible. The cross-sectional area of the scaffolds calculated for the stress-strain curves was the actual cross-sectional area excluding the area of the holes present in the scaffold. This was conducted for a more accurate representation of the scaffolds mechanical properties.

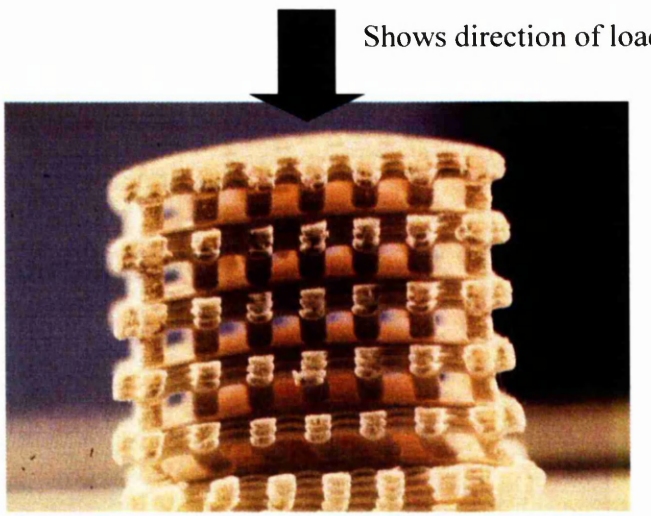

Figure 4-37 Compression loading to be in the direction the scaffold was fabricated.

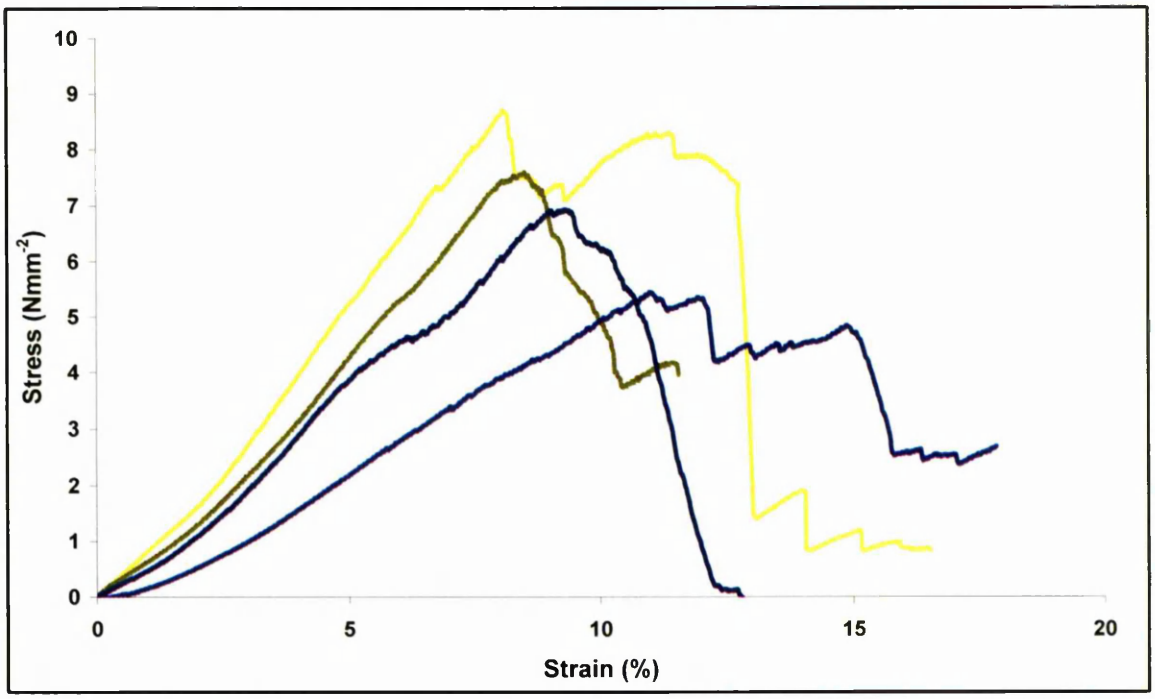

Figure 4-38 Stress-strain curve for COMP 400 scaffolds.

Four COMP 400 scaffolds were tested under compressive forces (figure 4-38). The yield strength of the scaffolds ranges from 5 – 8 MPa and the stiffness ranges from 50 – 120 MPa. The stress on the scaffolds was calculated by taking into account the load on the specimens and the cross-sectional area of the whole scaffold. The modulus of scaffolds was measured between 3 – 5 % strain. It can be seen from the graph that all four samples have different tangent slopes. The main reason for this is that although the specimens sat flat on the base of the testing rig, the top surface was not completely flat due to the shortcomings of the fabrication technique, i.e. overcuring of layers leading to a slightly convex top surface. This led in the load being placed on a small area of the scaffold, which is not a true representation of the scaffold properties. To counteract this problem, more emphasis and time needs to be spent on getting the parameters of the SLA to produce high resolution, flat surfaces when high volume fractions of ceramics are used. One of the measures that might have been done prior to testing could be to slice the scaffolds to make them completely flat, which might show better resistance of the scaffolds to compression.

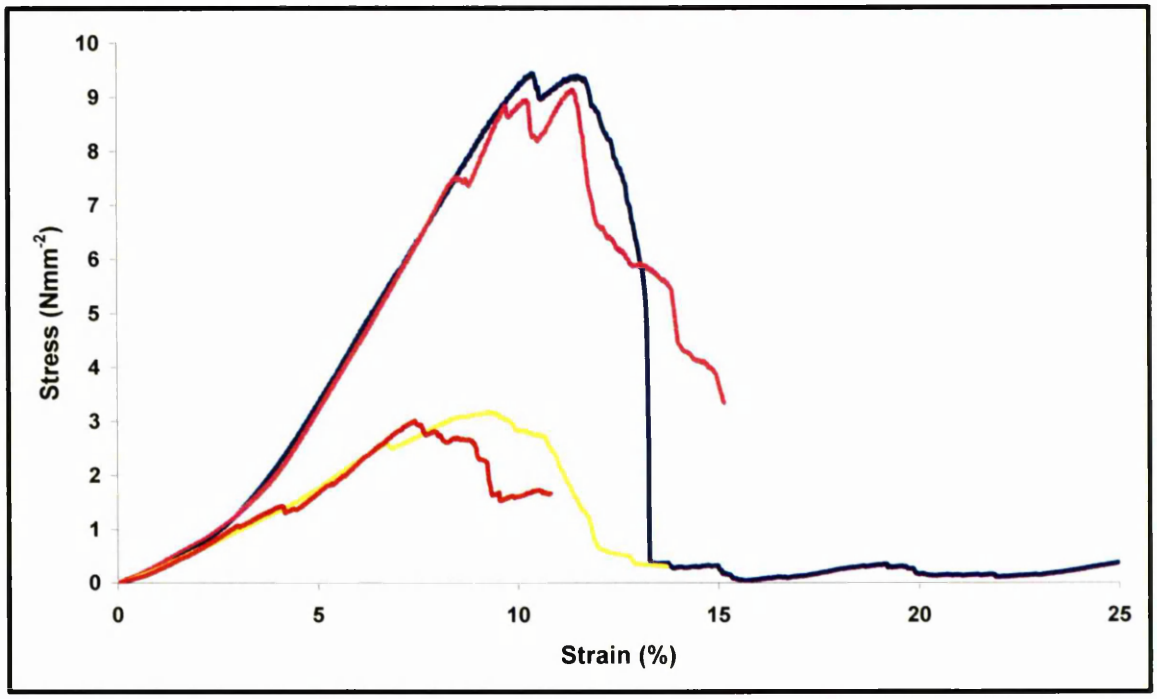

Figure 4-39 Stress-strain curve for COMP 600 scaffolds.

As compared to the COMP 400 scaffolds, COMP 600 (figure 4-39) scaffolds fall into two classes of behaviour; top ranging scaffolds and bottom ranging scaffolds. The elastic modulus of the top ranging scaffolds is approximately 125 MPa, whereas the bottom ones have a modulus of ~ 35 MPa. The modulus of the scaffolds was calculated between 4 – 6 % strain because under lower strains settling of the scaffolds was observed, which is not representative of the actual scaffold. A big difference can be seen between the yield strengths of the top and bottom ranging scaffolds. Although all scaffolds were checked for imperfections such as cracks, defects within the scaffolds could not be categorised, and these could have been the reason for the difference in the scaffolds. As scaffolds were tested in the same direction in which they were fabricated, unbonded layers of the horizontal struts would not be affected in compression. Nevertheless, a more likely cause of the inferior properties is the unbonded areas between the horizontal and the vertical struts. These points are the weak points of the structure and when under loading, the edges of the struts give way, and that particular cell collapses. Another problem noticed in the manufacturing technique is the slight shifting of the layers, as mentioned in section 4.6.1.2. Although the shifting of layers might have resulted in a flat surfaced scaffold, within the structure each vertical strut must be under compression at varying points, introducing shear stresses leading to early failure than compression and thus resulting in much lower mechanical properties. Figure 4-40 shows the horizontal struts are not flat and when the

scaffold is under compression, the centre three struts would have been taking most of the load. Due to this reason, the yield strength of the scaffolds also ranges from 2 – 8 MPa. Hence, it can be said that the primary reason for the poor resulting bottom ranging scaffolds could be that out of the 49 struts present in the scaffold, only ~ 9 (struts in the middle of the scaffold) were initially acting as supports for the structure.

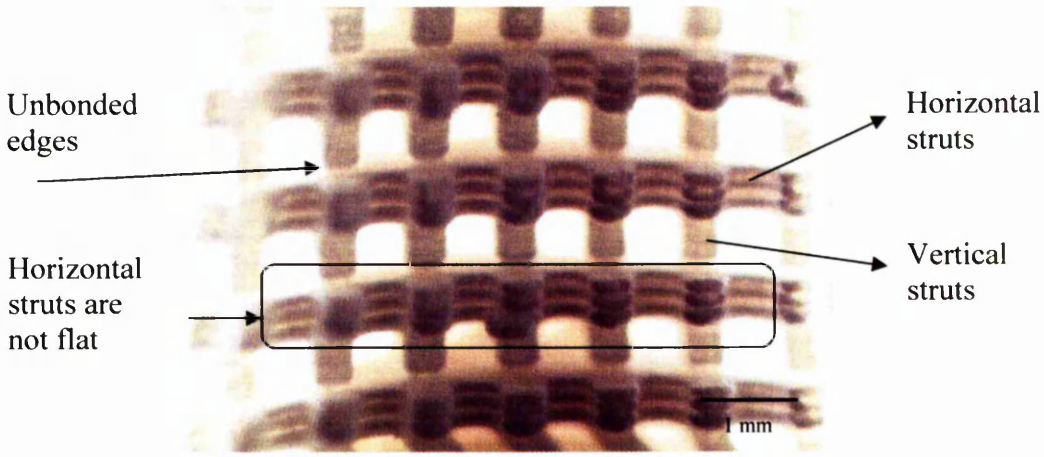

Figure 4-40 High magnification image of a composite scaffold.

Upon examination of the scaffolds during compression, the layers of the scaffolds started to delaminate (shear stress) on reaching the yield stress, after which the whole scaffold collapsed.

Comparing the two types of composite scaffolds, not much difference is evident in the mechanical properties. As mentioned in section 4.6.1.2, both scaffolds had the same size struts (500 μm) with 400 and 600 μm hole sizes. This meant that the unit cell of both scaffolds had the same dimensions (figure 4-41). However, the schematic in figure 4-42 shows view of the scaffolds on the top surface which are very different. Both scaffolds have the same external dimensions but they have differing number of struts in their structures.

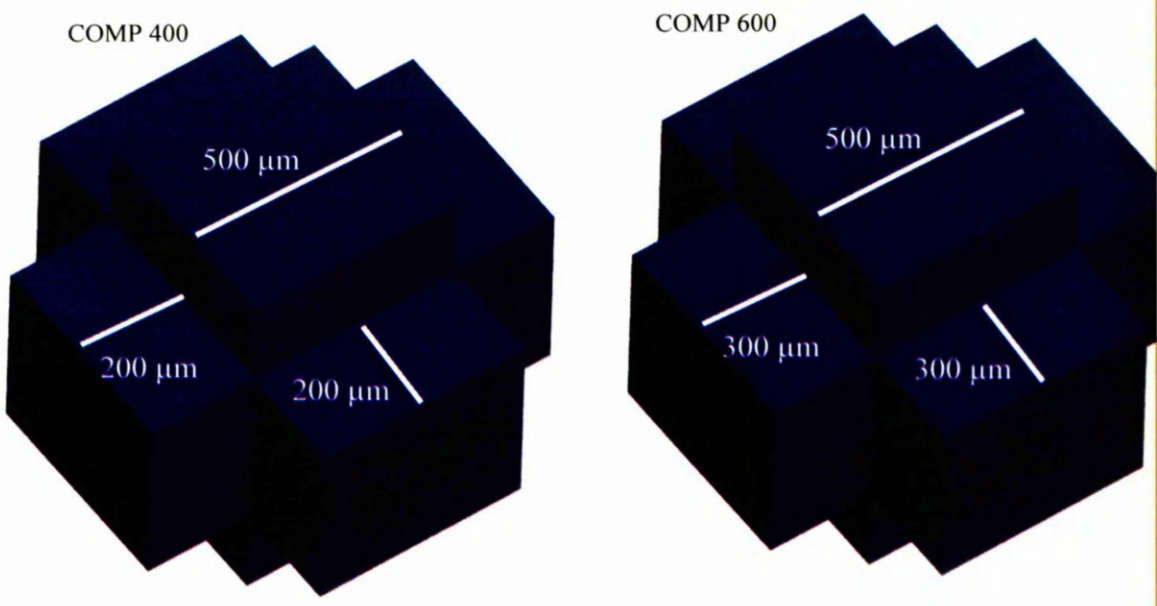

Figure 4-41 Unit cell of COMP 400 and COMP 600 scaffold.

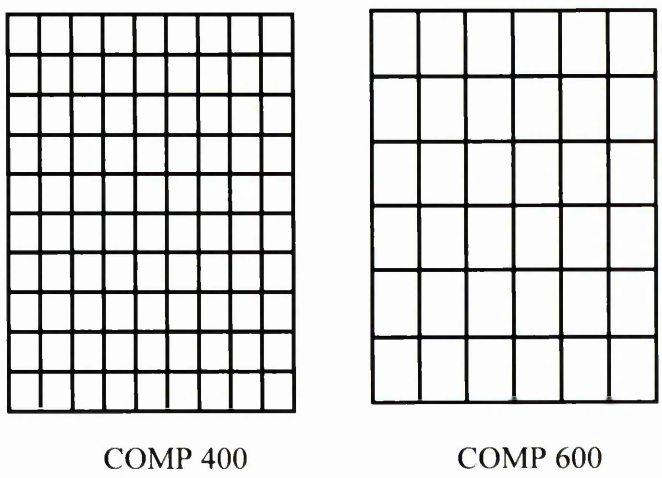

Figure 4-42 Schematic of the top surfaces of glass-ceramic scaffolds.

Apart from the bottom ranging COMP 600 scaffolds, both types of scaffold showed similar values for yield strength and modulus. As COMP 400 had 100 vertical struts compared to the 49 struts for COMP 600, it would have been expected for COMP 400 scaffold to be more stable and have superior mechanical properties to COMP 600, as they would be able to handle the load much better. However, as discussed earlier, the true number of struts present in the scaffolds might be completely different to the actual number that support the

structure in compression, before shearing and delamination of the struts causes the scaffold to fail.

4.8.2. Glass-Ceramic Scaffolds

Both types of glass-ceramic scaffolds, CER 400 and CER 600, were tested in compression and their stress-strain curves are shown in figure 4-43 and 4-44. The external dimensions of both scaffolds were 7.2 mm x 7.2 mm x 6 mm, with varying hole sizes of 400 μm and 600 μm. This meant that CER 400 scaffold had 7 x 7 struts present in the structure, whereas CER 600 only had 5 x 5 struts and the cross-sectional area of the scaffolds was the same.

Four scaffolds from each type were to be tested under compression. Great care was taken in choosing the glass-ceramic scaffolds to be tested, as a lot of cracks are present on the scaffolds due to the gel casting process (section 4.7.2.3).

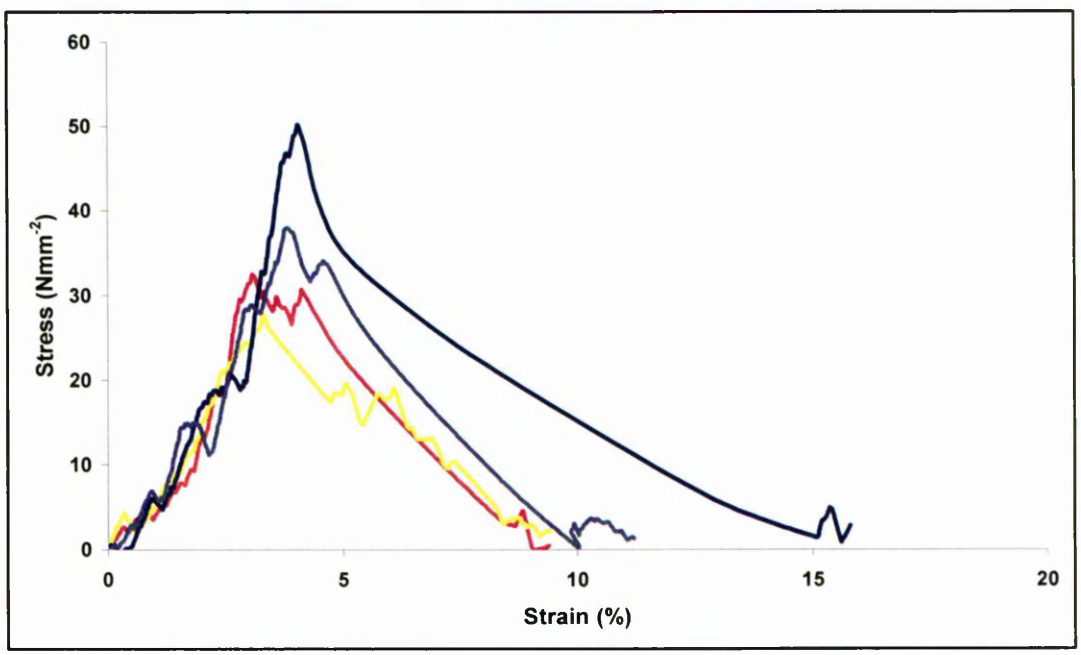

Figure 4-43 Stress-strain curve for CER 400 scaffolds.

The stress-strain curve for CER 400 scaffold (figure 4-43) shows the scaffold to have much better mechanical properties than composite scaffolds. The modulus for the scaffolds ranges from 900 – 1600 MPa with the yield stress ranging from 27 – 55 MPa. The modulus

of the scaffolds was calculated between 2 – 4 % strain. At lower strains, no region of settling is seen as all scaffolds had a flat surface. All specimens reach yield stress at a strain of ~ 4%, demonstrating consistency in the fabrication technique of the scaffold. CER 400 scaffolds demonstrated brittle fracture in compression as can be seen from the many small peaks and troughs until yield stress is reached.

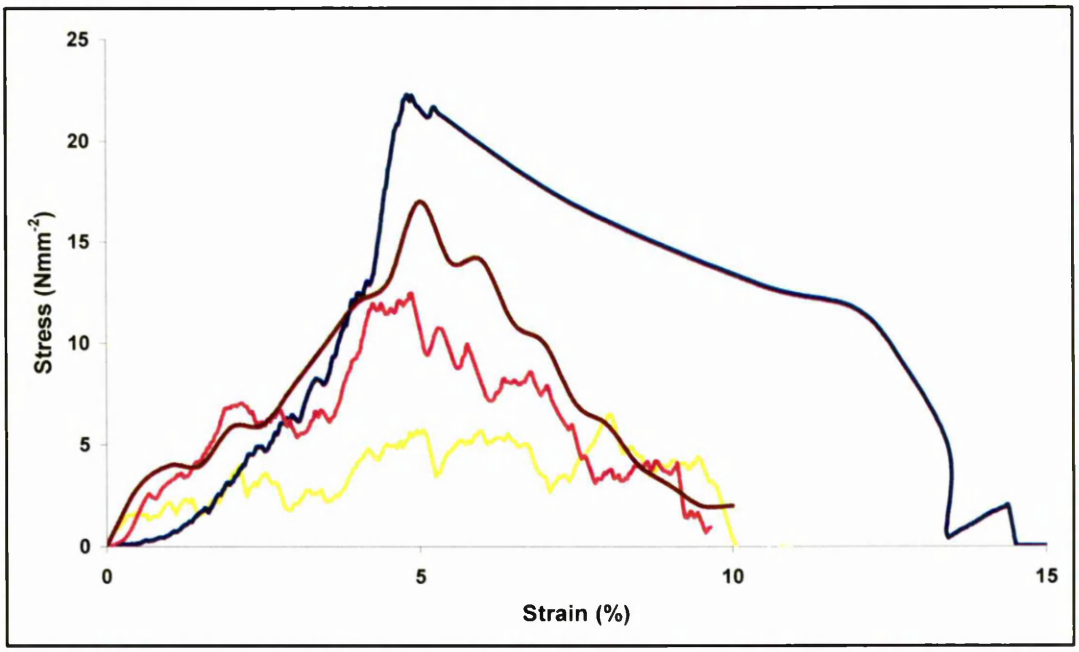

Figure 4-44 Stress-strain curve for CER 600 scaffolds.

The yield strength after testing four CER 600 scaffolds ranged from 12 – 22 MPa and the modulus ranged from 300 – 700 MPa (figure 4-44). The modulus was measured between 2 – 3 % strain. It would be safe to discard the last sample (yellow), as it clearly does not show any kind of resistance under compression and sustains approximately the same load until failure. Again, a variation can be seen in the mechanical properties of the scaffolds, which is caused by the processing techniques. As was the case with the composite scaffolds, the defects were present because layer-to-layer bonding was not complete. The glass-ceramic scaffolds had defects present within the structure but these were caused by air bubbles leading to holes during gel casting, and cracks, which were a result of shrinkage in the volume of material during sintering of the glass-ceramic.

The three glass-ceramic scaffolds all demonstrated maximum yield stress at ~ 5% yield strain, but with different modulus. This means that the change in properties of each scaffold was due to the differing amounts of small defects present within them. These

defects could have been categorised prior to compression testing using X-ray tomography. At this stage of the study, it is not possible to quantify the number of defects that would be the threshold for a scaffold to behave poorly in compression. This trend was not seen for the composite scaffolds.

A big difference can be seen in the mechanical properties of the two glass-ceramic scaffolds. The yield strength and modulus have doubled and the main reason for this result is the difference in geometry of the scaffolds. The differences in the strut size and the size of the holes have a major difference in the properties of the CER 400 and CER 600 scaffolds. As mentioned in section 4.7.2.2, the size of the holes and struts for the CER 400 were 400 μm and 600 μm respectively, whereas the CER 600 scaffold had 600 μm holes and 800 μm struts (figure 4-45). This meant that the two extra rows of struts present for the CER 400 scaffold which led to an increase in the surface area, acted as a reinforcer for the scaffold. The total surface area of the CER 400 scaffold was calculated to be 1.38 x 10^{-3} m^2, which was greater than CER 600 scaffold (1.07 x 10^{-3} m^2) (Appendix I). However, as it the cross-sectional area of the scaffold that is taken into account when scaffolds are in compression, excluding the holes meant that CER 400 (1.764 x 10^{-5} m^2) had more glass-ceramic supporting the scaffold compared to CER 600 (1.6 x 10^{-5} m^2). This demonstrates how small changes in geometry of scaffolds can have major effects on the mechanical properties. Hence, it is critical to decide on the geometry of the scaffolds in a way that not only produces a mechanically fit scaffold, but also maximises cell adhesion and protects cells when in compression *in vivo*.

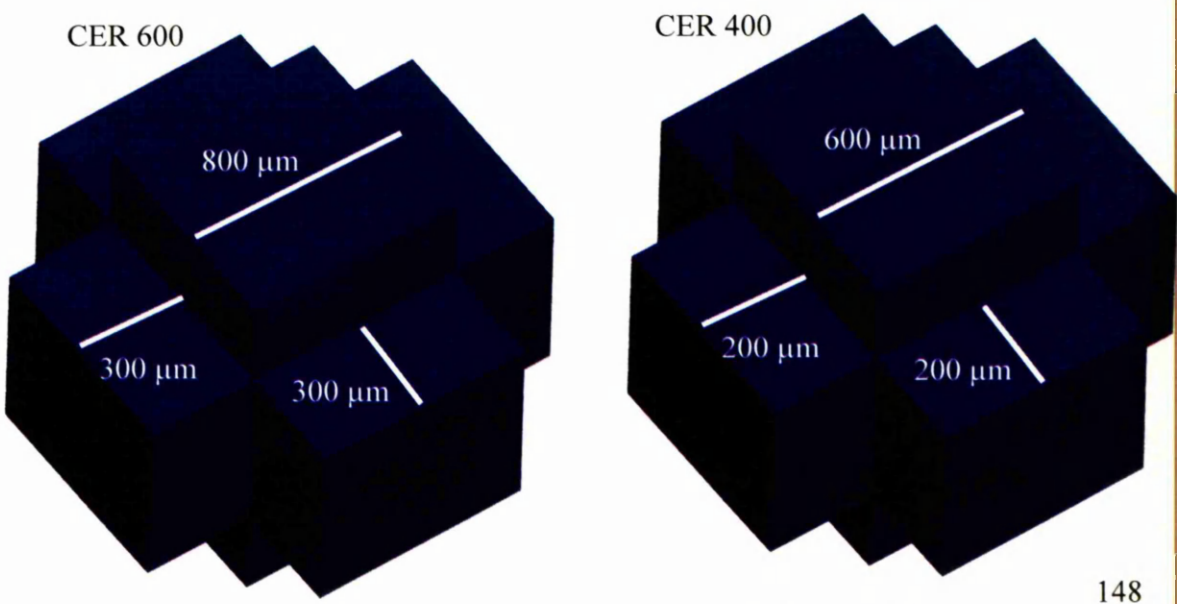

Figure 4-45 Unit cell of CER 600 and CER 400 scaffold.

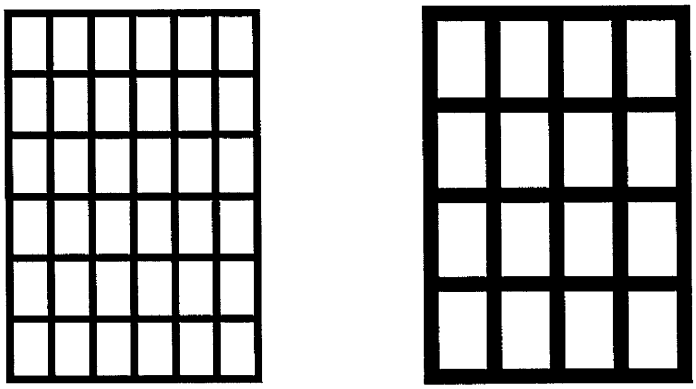

CER 400 CER 600

Figure 4-46 Schematic of the top surfaces of the glass-ceramic scaffolds.

To put things into perspective, the schematic in figure 4-46 shows a view of the scaffolds on the top surface. As can be observed both scaffolds have equal external dimensions, but CER 400 has more struts present than CER 600, and the strut size of the CER 600 is larger than that of CER 400. This difference in the geometry and the higher number of struts in the scaffold has resulted in the superior properties of CER 400. This could be further proven by calculating the densities of both scaffolds, which would provide us with important data about how much material is present in both scaffolds along with their porosities. Unfortunately, this test was not conducted during this study and would need to be performed in future studies.

4.8.3. Comparison of Scaffold Types

Table 4-2 The mechanical properties of both types of composite and glass-ceramic scaffolds.

	Compressive Modulus (MPa)	Yield Strength (MPa)
COMP 400	50 – 120	5 - 8
COMP 600	35 – 125	2 - 8
CER 400	900 – 1600	27 - 55
CER 600	300 – 700	12 - 22

The results in table 4-2 show that both composite scaffolds exhibited very similar behaviour under compression. The difference in scaffold geometry only extended as far as the change in hole sizes, which led to such comparable mechanical properties. Whereas,

the difference in the internal architecture of the glass-ceramic scaffolds led to a considerable increase in mechanical properties for CER 400. Increasing the length of the unit cell from 1 mm (CER 400) to 1.4 mm (CER 600) resulted in less stronger scaffold in compression, which was not expected.

The difference in mechanical properties of composite and glass-ceramic scaffolds is considerable. Composite scaffolds contain 40 vol.% of the ceramic, so the mechanical properties of the scaffolds would have been expected to be at least 40% of the glass-ceramic scaffolds, although this is not seen. Composite scaffolds are much more ductile due to the polymer content, but the stiffness of glass-ceramic incorporated in the composite scaffolds should have provided the scaffold with higher strength. As composite scaffolds are more ductile they have a higher strain to failure ratio as compared to glass-ceramic scaffolds, which being hard and brittle can sustain a higher load but are unable to absorb the energy, hence yield at lower strains.

Comparing the curves for the glass-ceramic and the composite scaffolds, a difference can be seen in the number of peaks that appear. This is due to the fact that as soon as the glass-ceramic scaffolds come under compression, the individual walls supporting each cell, start to collapse starting from the outside, which is represented by a dip in the curve, but as the cells collapse, the scaffolds starts to regain its strength due to the action of the walls of the scaffold, touching and supporting each other (rise in the curve). The scaffolds here showed a transition from brittle to cellular solid or trabecular bone-like stress–strain behaviour (Woodard *et al.*, 2007). In cellular solids and trabecular bone, the stress plateau is attributed to the buckling of ductile cell walls or struts, or individual trabeculae, and the stress-recovery region to the densification of the structure by the collapse of walls or struts (Gibson *et al.*, 1997; Hayes *et al.*, 1976). This occurrence does not take place for the composite scaffolds because the course of action under compression involves the delamination of layers rather than individual cells collapsing. The composite scaffolds are much more ductile; hence show a linear elastic phase at small strains. The glass-ceramic scaffolds are very brittle and have no region of elastic phase.

Table 4-3 Mechanical properties of trabecular bone and target properties of the scaffold (Ratner et al., 1996).

	Trabecular bone	Target properties of scaffold	Compact bone
Yield Strength (MPa)	5 – 10	5 – 10	131 – 224
Elastic Modulus (MPa)	50 – 100	100 – 150	17000 – 20000

Bone with a volume fraction of solids less than 70% is classified as trabecular bone and that over 70% compact (Gibson, 1985). Both glass-ceramic and composite scaffolds used in this study thus represent trabecular bone more than compact bone, so the mechanical properties expected from these scaffolds should match those of trabeculae.

Comparing table 4-2 to table 4-3, it is clear that the target properties required from the scaffold have been achieved. The composite scaffolds most resemble the modulus and yield strength of trabecular bone, whereas glass-ceramic scaffolds far surpass those properties. Blaker *et al.* (2005) tested the mechanical properties of PDLLA/Bioglass composite foams fabricated by thermally induced solid-liquid phase separation and stated the modulus of the scaffold with 15 vol.% ceramic to be 1.2 ± 0.40 MPa. Although the volume fraction of ceramic for their study is much less in the composite scaffold, the properties of the scaffold produced by this technique are quite inferior to the scaffolds fabricated in our study using the SLA. Tellis *et al* (2006). used fused deposition modelling to produce a replica of human trabecular bone using micro tomography and fabricate a scaffold made of polybutylene terephthalate. This scaffold was then subjected to compression testing and the elastic modulus was shown to be 9.43 ± 0.43 MPa. Although this technique has produced a scaffold which is stiffer than Blaker *et al.* (2005) it is still not comparable to the scaffolds produced using SLA. This was due to the drawbacks of using the technique to fabricate the scaffolds. The trabecular scaffolds matched bone samples in porosity; however, achieving physiologic connectivity density and trabecular separation required further refining of scaffold processing.

The quality of trabecular bone can be characterised by its mechanical properties, chemical composition, and microarchitecture. When endeavouring to create a biomimetic bone scaffold, a synthetic duplication of the chemical composition of bone is not yet possible. However, utilising high resolution imaging technologies, free-form fabrication techniques

such as the SLA, and a polymer or ceramic formulation with appropriate mechanical properties it is possible to closely simulate the mechanical properties and microarchitecture of trabecular bone.

In this study, composite scaffolds with 50 vol.% LG112 bioactive glass-ceramic were successfully developed using SLA. These scaffolds have a stiffness of ~ 120 MPa, and the glass particles positively reinforced the mechanical properties of the scaffolds. The strength of these scaffolds are strongly influenced by internal architecture, and many ceramic scaffolds have been produced to date exhibiting strength in the range of 10 - 30 MPa (Chu *et al.,* 2002; Bignon *et al.*, 2003; Kalita *et al.,* 2003), by manipulating the overall porosity. Given the need to replace bone with scaffolds of similar strength, the ability to modify scaffold strength by tailoring porosity becomes essential in designing scaffolds for clinical use.

In conclusion, the fabricated composite and glass-ceramic scaffolds both have enough mechanical stability to serve as a scaffold for initial cell attachment and bone tissue engineering and as an implant for bone replacement, but are not suited for carrying high forces in load-bearing regions. At this present stage of scaffold fabrication technology, an implant could provide low mechanical support for an area to be reconstructed. As bioactive glass is being used in this study because of its biocompatibility, both composite and glass-ceramic scaffolds were thereafter tested by cell seeding, and the proliferation and viability of the seeded cells was measured.

4.9. Summary

The experiments carried out in this section have demonstrated that stereolithography is a viable technique for producing scaffolds to be used as bone implants. The technique has been successful in fabricating both composite and glass-ceramic scaffolds, with controlled geometry and internal architecture, which determines the mechanical properties of the scaffold, and also determines the success of the scaffolds to be used for cell seeding. The mechanical properties of the scaffolds have shown that using SLA to produce scaffolds results in much superior properties compared to other free-form fabrication techniques.

5. Cell Results and Discussion

Cellular studies were conducted on both types of composite scaffolds and glass-ceramic scaffolds using primary human osteoblasts.

5.1. Preliminary Cell Attachment

Initial testing began by taking the four types of scaffolds and seeding osteoblasts onto their surface. These were incubated at 37 °C, 5% CO_2 for 24 hours, after which they were observed using an inverted light microscope. Observation of the culture plates showed that the culture media on the composite scaffolds had turned yellow. This meant that the medium was turning acidic as a direct result of the scaffolds, which affected cell growth.

To investigate this further, COMP scaffolds were placed in 10 ml of culture media and the solution mixed in a rotary mill for different time points ranging from 1 hour to 4 days to produce conditioned medium. Cells were seeded onto control glass cover slips and incubated, to attach for 2 hours after which, at each time point, some of the conditioned media was placed in the well plate to observe cellular behaviour.

Figure 5-1 shows the effect of the scaffolds being incubated in culture media over 4 days and it can be clearly seen from the images that the longer the composite scaffolds were left in the culture media, a more detrimental effect was observed on the osteoblasts. As time progressed, cell viability appeared to decrease, with 4 days being the worst showing clumps of dead cells and debris from the scaffold.

This behaviour of cell death was not observed for the glass-ceramic scaffolds. This meant that the processing technique used to produce the composite scaffolds was eventually leading to cell death.

Control COMP Scaffold

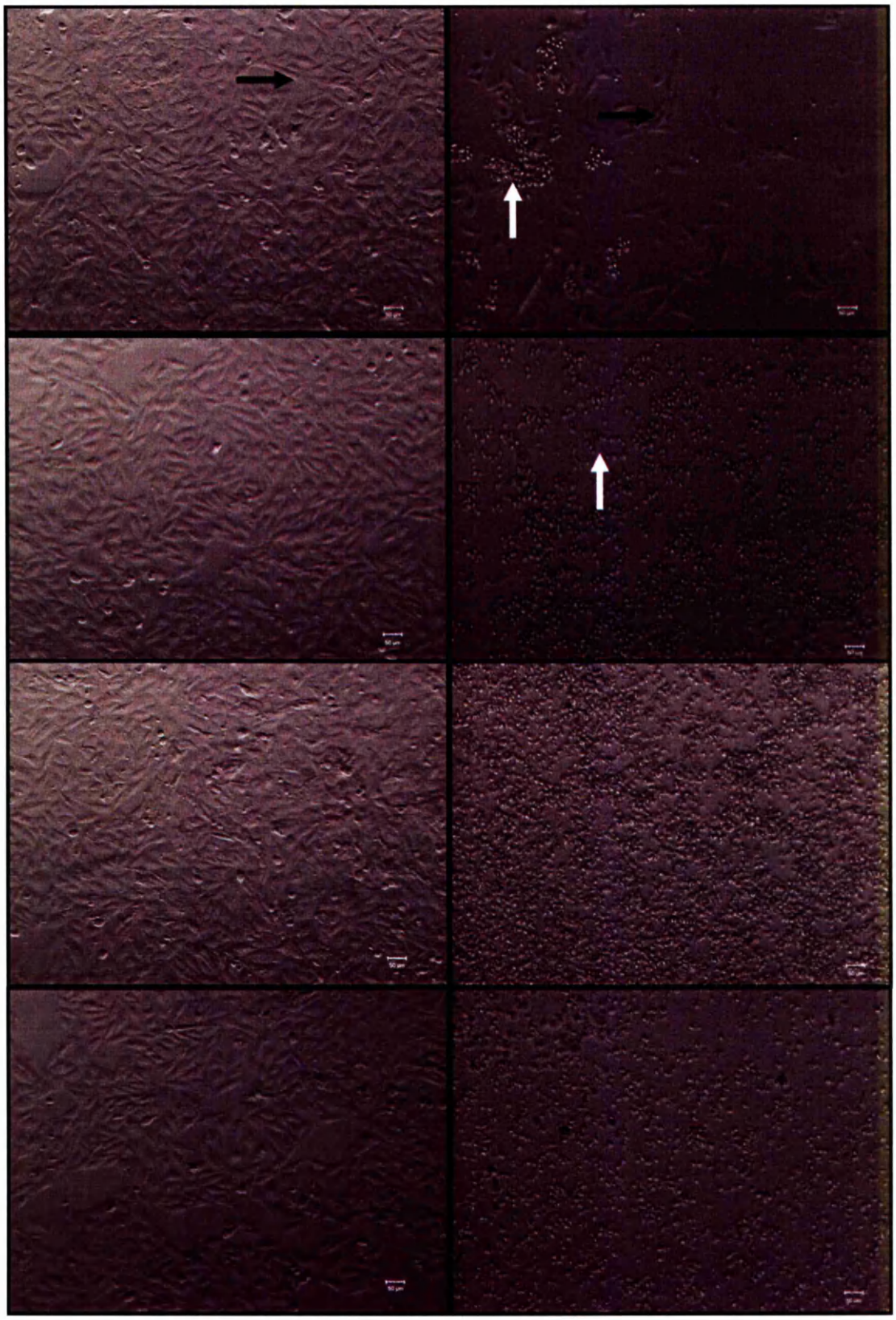

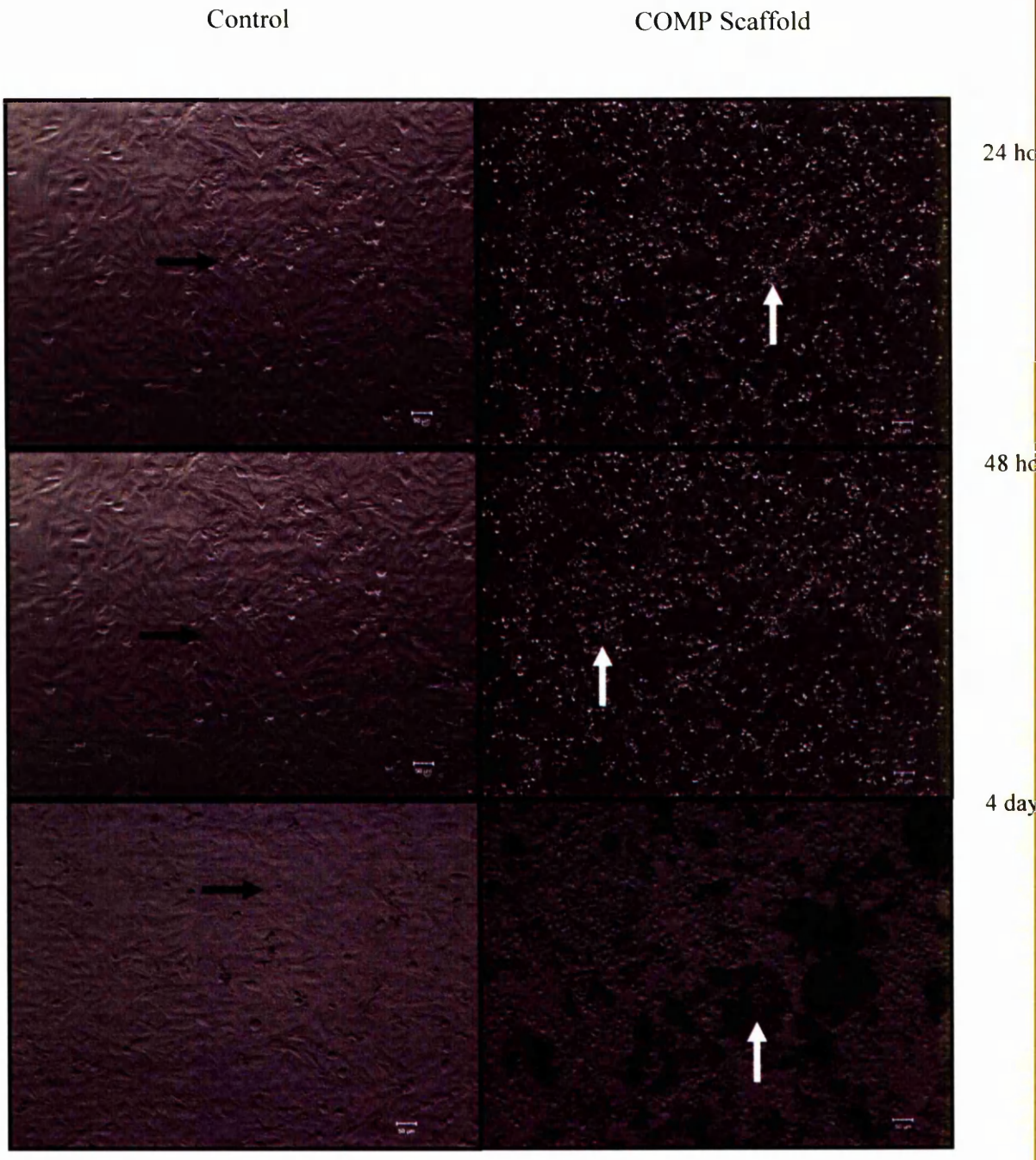

Figure 5-1 The effects of composite scaffolds incubated in media for 4 days (black arrows showing viable well spread cells and white arrows showing dead cells) (scale 50 μm) .

5.2. Cell attachment using Conditioned media

Due to the porous nature of the composite scaffolds, this affect could have been attributed to uncured monomer leaching out into the culture medium causing a toxic effect. To eliminate this theory, non-porous 2-dimensional composite slips were made on the SLA, which had just a flat surface. In addition, another 2-dimensional composite slip was also made using a conventional UV box. The 2-dimensional slips were all 1 cm^2 and were made using the same monomer and concentration of photoinitiator.

Two slips were made on the SLA, one of which was washed in PBS for 2 days, with regular rotations prior to any cell seeding. The other slip was not washed in PBS. The 2-d slip fabricated in a UV box was also washed in PBS for 2 days, along with a glass-ceramic and composite scaffold.

After washing all samples were UV sterilised for 1 hour in the laminar flow hood. These samples were then used to make conditioned media, and this was achieved by incubating all the samples in culture media for 2 days in an incubator.

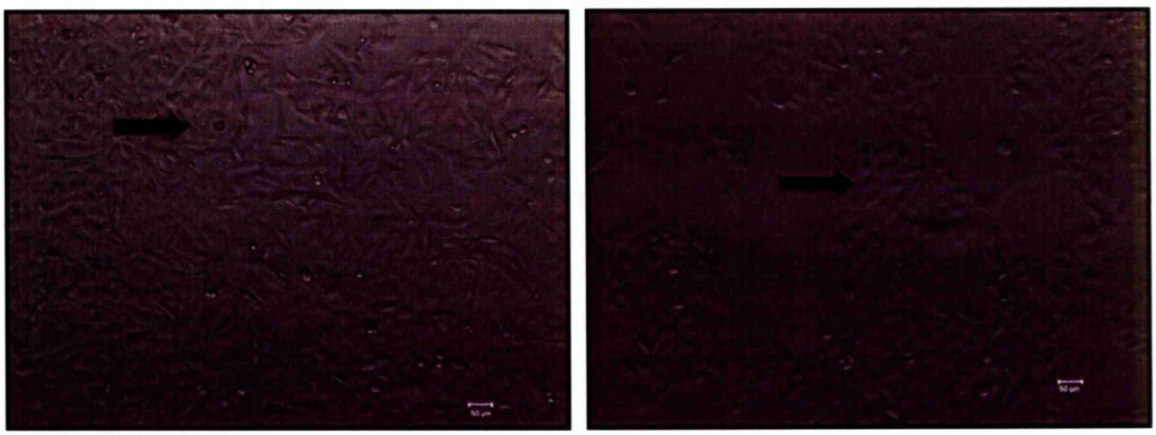

(a) (b)

Figure 5-2 (a) shows control glass slip and (b) well plate of 2-d slip of composite fabricated using a conventional UV box (scale 50 μm).

Figure 5-2 (a) shows an image through a light microscope of a control glass cover slip to ensure that cells were growing during the length of the experiment. As all scaffolds used in this study are opaque, cell attachment cannot be observed on the surfaces using a light

microscope, thus their respective well plates are studied to understand cellular behaviour. Figure 5-2 (b) shows the 2-dimensional slip of composite that was made using a conventional UV box. Over the 2 day period, the cells have attached and proliferated on the surface of the well plate (arrow). Comparing these to the 2-d composite slips fabricated on the SLA (figure 5-3) it can be observed that both slips have led to cell death (arrows), regardless of one of them being washed in PBS for 2 days prior to being used for conditioning the media.

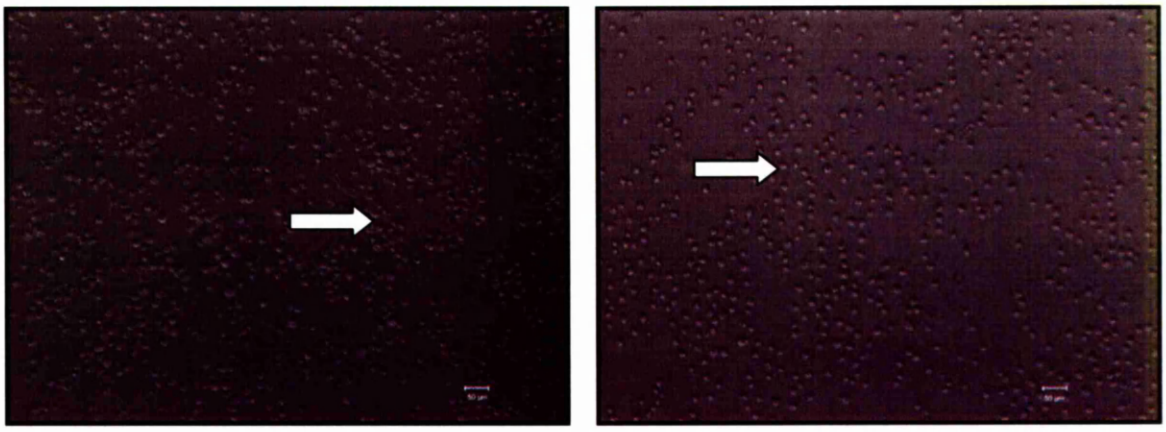

(a) (b)

Figure 5-3 (a) shows a 2-d composite slip fabricated using the SLA (washed in PBS for 2 days) and (b) shows a 2-d composite slip fabricated using the SLA (unwashed) (scale 50 μm).

This suggests that the processing technique is causing the cells to die. The different processing techniques all had the same monomer, the same concentration of initiator and the same volume fraction of ceramic loading.

As mentioned in section 4.6.1.1, the quantity of initiator used to make SLA scaffolds is higher than normal. This trend suggests that unreacted initiator present within the scaffold is leaching out and is proving to be toxic to the cells.

Figure 5-4 (a) shows the well plate of the glass-ceramic scaffold at 24 hours, where the cells have attached to the surface, and (b) cell proliferation is observed after 48 hours

(arrows). This suggests that there were no adverse effects of using conditioned media on the glass-ceramic scaffolds and no harmful toxins were leaching out.

Figure 5-5 (a) shows cell attachment on the well plate of the composite scaffold after 24 hours (black arrow), but after 48 hours the cells had died (white arrow) and the culture medium had turned yellow (b). This confirms that harmful toxins were leaching out of the composite scaffolds, which led to cell death. To substantiate this notion, HPLC was conducted on the constituents of the scaffolds to confirm the presence of toxins and their effect on cell viability.

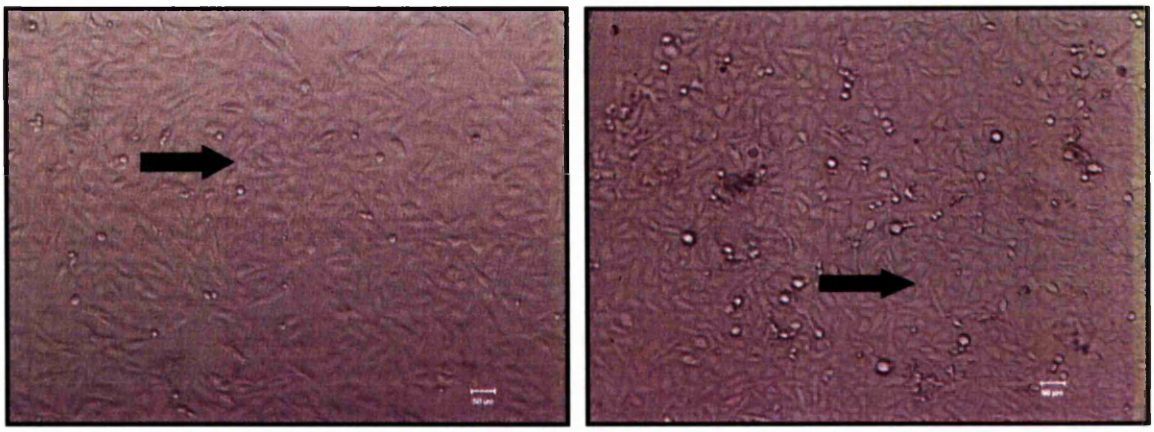

(a) (b)

Figure 5-4 (a) well plate of glass-ceramic scaffold using conditioned after 24 hours, and (b) well plate of glass-ceramic scaffold using conditioned media after 48 hours (scale 50 μm)

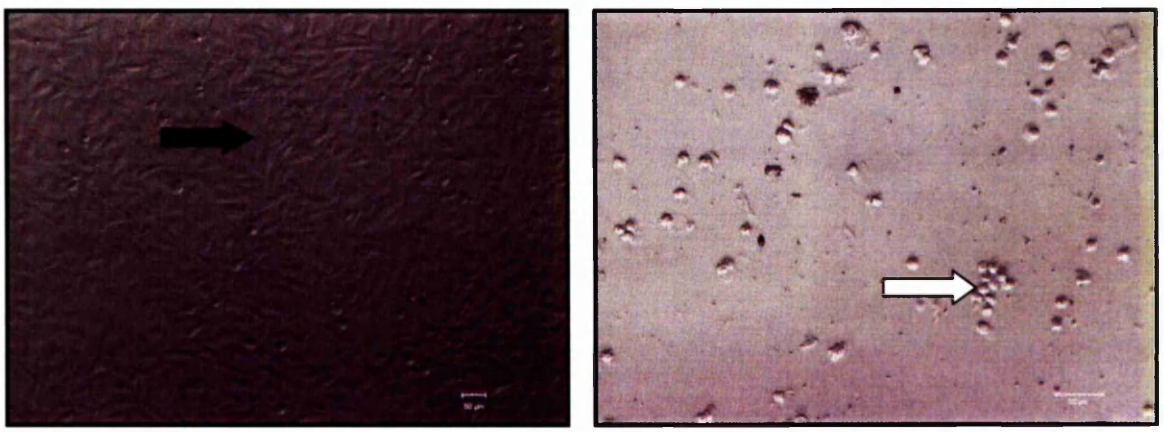

(a) (b)

Figure 5-5 (a) well plate of composite scaffold using conditioned after 24 hours, and (b) well plate of composite scaffold using conditioned media after 48 hours (scale 50 μm).

5.3. HPLC

HPLC was used to detect the presence of any leached substances that might cause the observed toxic effect on the cells. Four samples of pure initiator, pure PEGDA (258) monomer, culture media, and a solution of culture media incubated with a composite scaffold (Media Control), were used to conduct the test.

Figure 5-6 shows the relative peaks for the four samples. The initiator peaks at approximately 17.5 min and is the most prominent peak on the graph. The peaks for PEGDA monomer (~ 17 min) and the culture media (~ 20 min) are completely separated to that of the initiator. Whereas, the composite media control has a small peak present at 17.5 min, the same peak as the initiator, and no peak is seen representing the monomer. This proves that in the control media, it is solely the excess uncured photoinitiator leaching out of the scaffolds and not the monomer, which is proving toxic to cells.

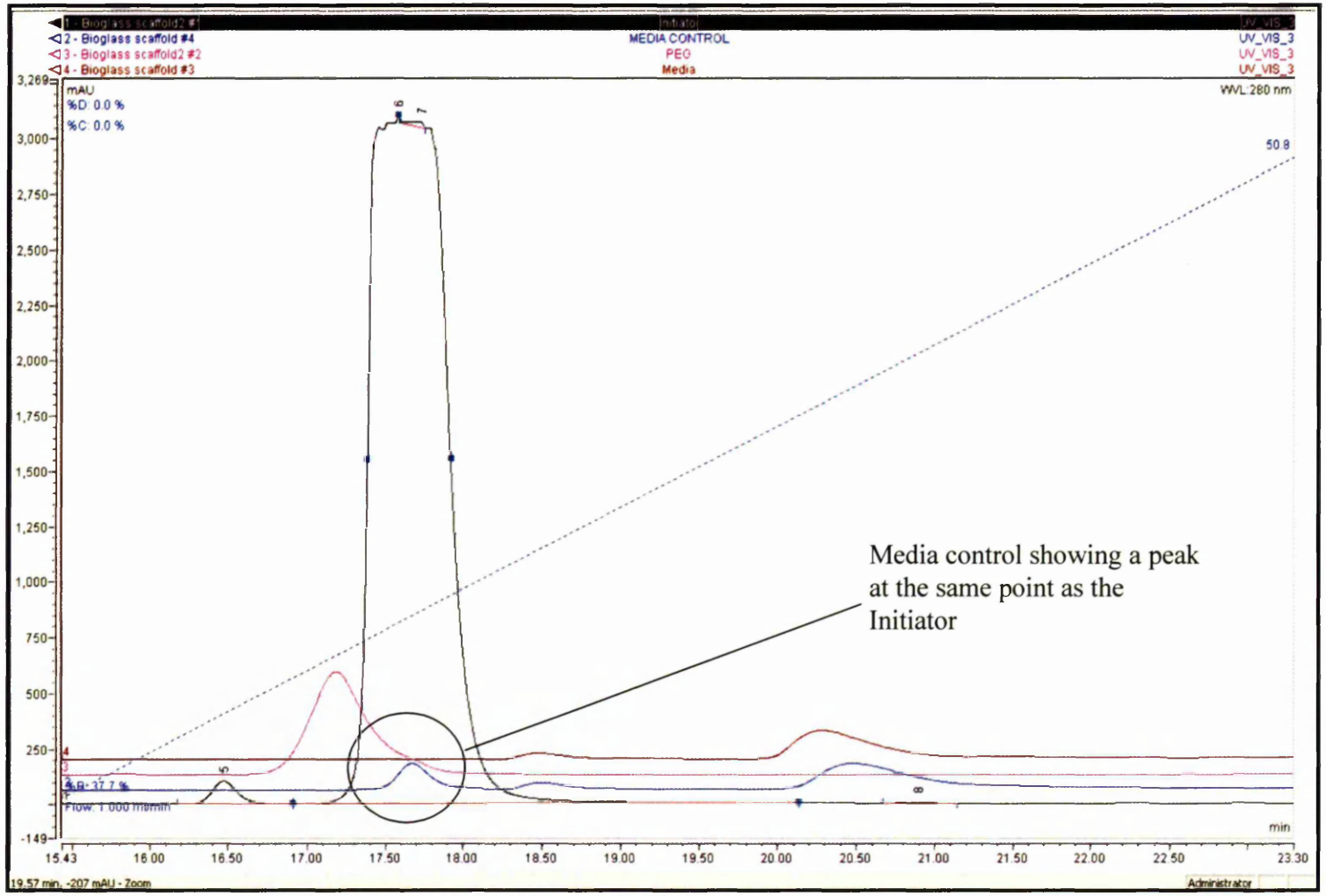

Figure 5-6 HPLC peaks for PEGDA monomer, initiator, culture media and media control.

Stereolithography has proven to be a very successful technique in producing three-dimensional geometrical scaffolds with controlled architecture and interconnected pores. But the detrimental effect of the photoinitiator on the cells means that the machine is capable of making scaffolds for load bearing applications, but these scaffolds cannot be used *in vivo* yet, due to toxicity towards the cells. This problem can be resolved by using a photoinitiator that is not toxic to cells, even at slightly higher concentrations. IRGACURE 1173 has been used in other biomedical applications and has not proven to be toxic at normal concentrations of 0.2 wt.%. But as the SLA needs a concentration of 1 wt.% to produce a scaffold with good resolution, the only alternative would be to find another cytocompatible initiator, which does not hinder cell attachment and function at higher concentrations.

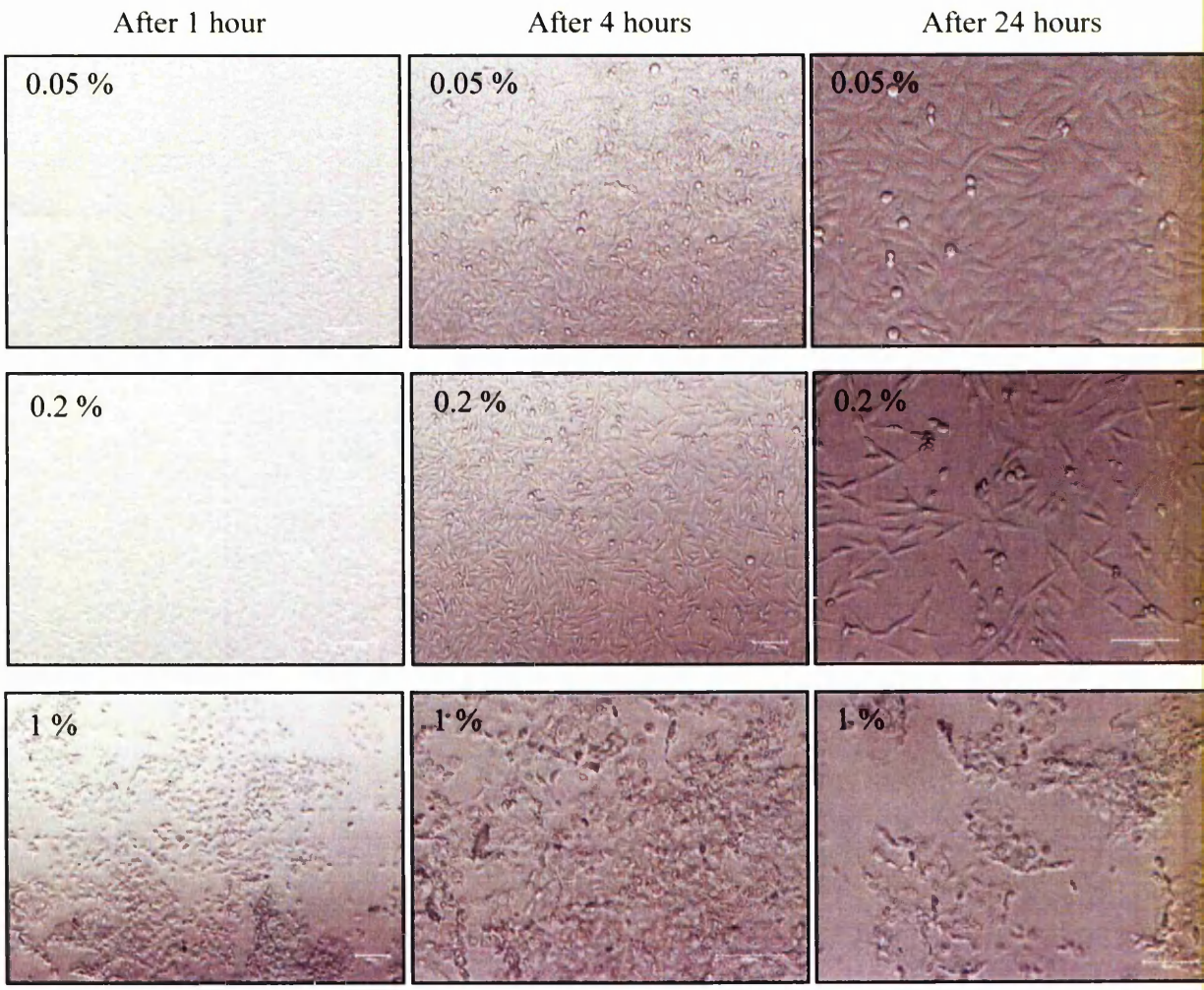

Figure 5-7 Toxic effects of different concentrations of IRGACURE 1173 seen on cells after 1 hour, 4 hours and 24 hours (scale 100 μm).

The toxicity effects of the initiator (IRGACURE 1173) were tested by seeding 4 x 10^4 cells on glass cover slips and incubating the cells for 2 days. Concentrations of photoinitiator ranging from 0.05 - 2 wt.% were mixed in culture medium and the media added to the cells. The reaction of the photoinitiator media to the cells was observed under a light microscope at 1, 4 and 24 hours. After 1 hour, at concentrations > 0.4 wt.%, the initiator had a detrimental effect on the cellular morphology causing cell death. After 4 hours, this effect could be seen on all culture wells with > 0.2 wt.% photoinitiator, and after 24 hours, only at concentrations of 0.1 and 0.05 wt.%, were the cells well attached to the glass cover slip and had sustained the effects of IRGACURE 1173. Figure 5-7 shows the effect of the photoinitiator on cells after 1, 4 and 24 hours. It is clearly visible that 1 wt.% initiator was toxic to cells from the start, with 0.2 wt.% (optimum concentration for normal polymerisations) also decreasing the number of cells attached to the surface by 24 hours. The only concentration of initiator that was stable throughout the 24 hours was 0.05 wt.%, but at such low concentrations, complete polymerisation is not achievable.

As mentioned before, the SLA needs a concentration of 1 wt.% photoinitiator to fabricate a scaffold, and upon completion of the scaffold, the post curing process should cure any unreacted initiator. After post curing, the scaffolds are washed in PBS in a rotating mixer for 2 days to remove any excess material lodged within the scaffold. The scaffolds are then used for cell culturing, and as it has not been possible to attach any cells onto the surface of the scaffolds, this could mean that the amount of photoinitiator leaching out is greater than the optimum of 0.1 wt.% as shown by the cytotoxicity results. This concludes that at least 10 % of the initiator is unreacted, and is concealed within the various layers of the scaffold and is not curable once the scaffold has been fabricated. The high surface area of the scaffolds makes it difficult to remove or cure the excess photoinitiator, whereas a 1 cm^2 slip of the same material made on the SLA has a lower surface area, which is visible for the UV light to cure the surface completely, hence cell attachment can be seen on the surface.

5.4. SEM

The opaque nature of the scaffolds and substrates meant that SEM had to be used to observe cellular attachment on the surface of the samples. This technique produced high resolution images of cellular attachment on the scaffolds as shown in figure 5-9.

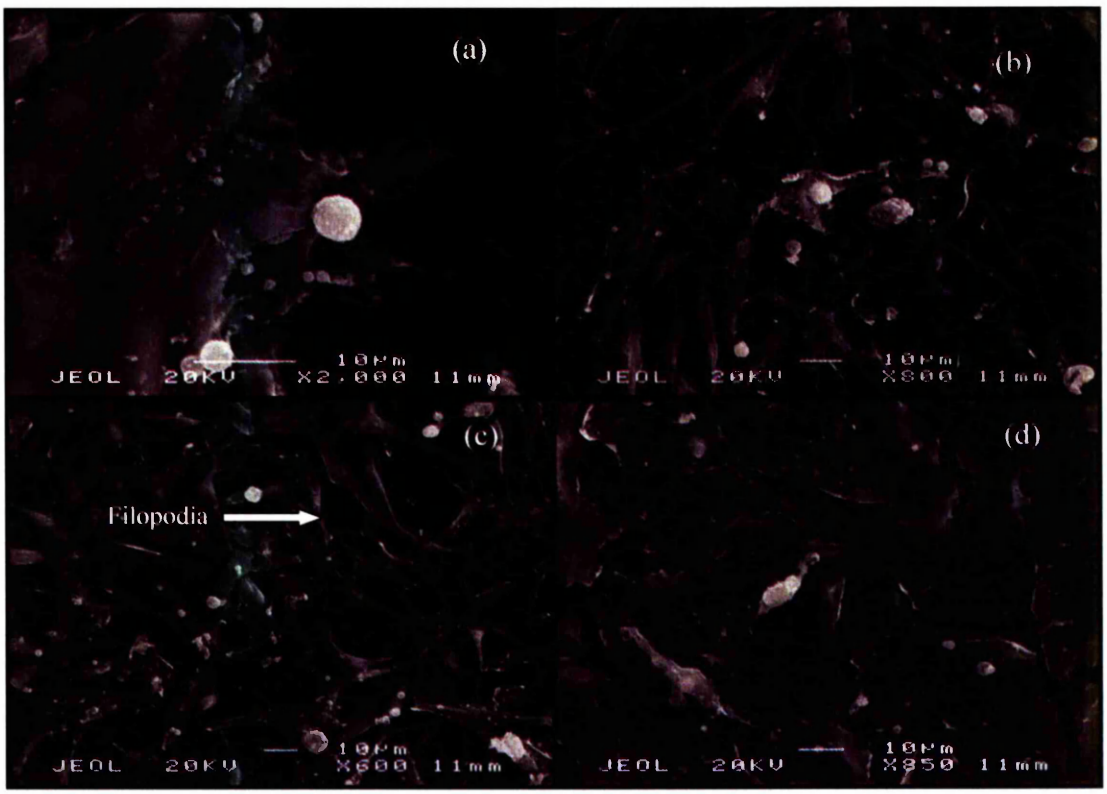

Figure 5-8 (a) to (d) Cellular attachment on control glass cover slips after 7 days.

Figure 5-8 shows the attachment of cells to the surface of glass cover slips after 7 days. The cells have a well spread polygonal morphology and these images can be used to make a comparison for the cell attachment observed on bioactive glass scaffolds.

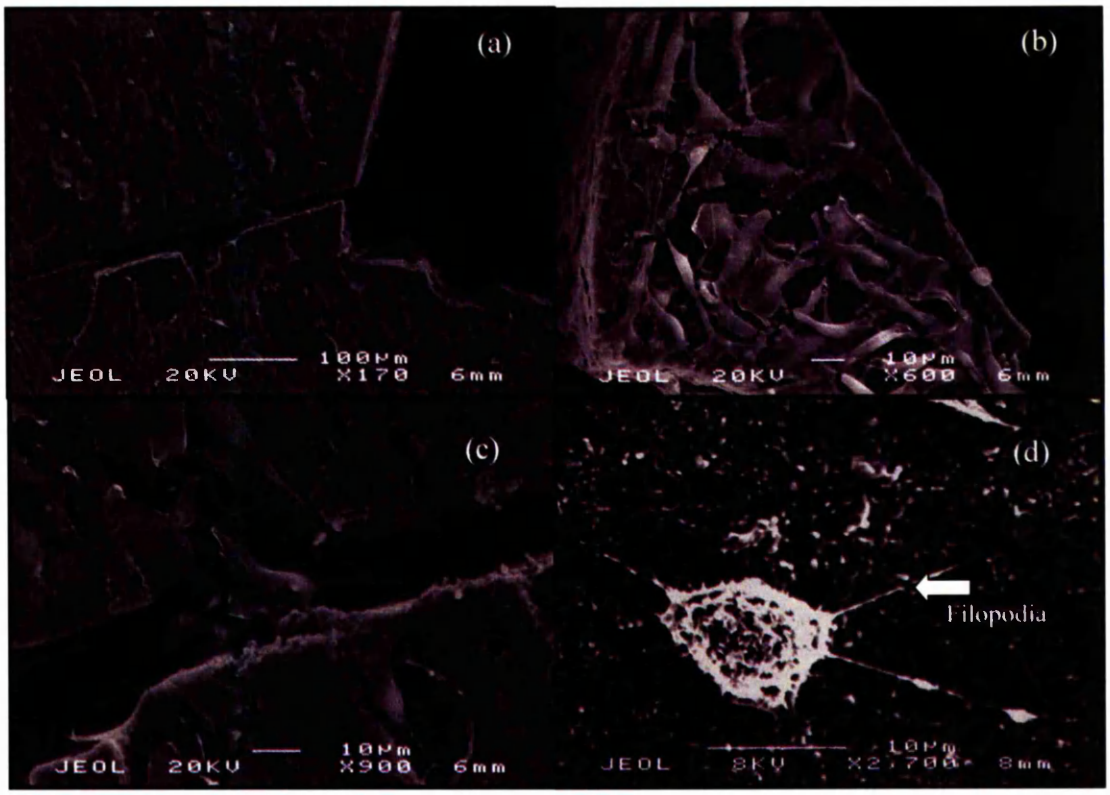

Figure 5-9 (a) to (d) Cell morphology and attachment on glass-ceramic scaffolds after 7 days.

Figure 5-9 (a) shows the surface of the glass-ceramic scaffold, with a crack going through the middle of it. Cells appear to have a well spread polygonal morphology indicating that they have an affinity for the surface. As compared to the glass cover slips after 7 days, the glass-ceramic scaffolds have fewer cells attached to the surface (figure 5-9 (b)). Figure 5-9 (c) shows a higher magnification of the crack present on the scaffold, and it can be noticed that a cell has bridged the gap. The crack is approximately 20 μm wide, and the cells have started covering any small cracks that are present on the scaffold. A single cell can be seen on the surface of the glass-ceramic with filopodia extending from the cell to the surface (figure 5-9 (d)). These contain actin filaments, which crosslink into bundles by actin-binding proteins and form the focal adhesions with the substrate (Lodish *et al.*, 2004). The cells normally use the filipodia to migrate down a pathway by extending the filipodia, then contracting the stress fibres to retract the rear of the cell to move it forwards.

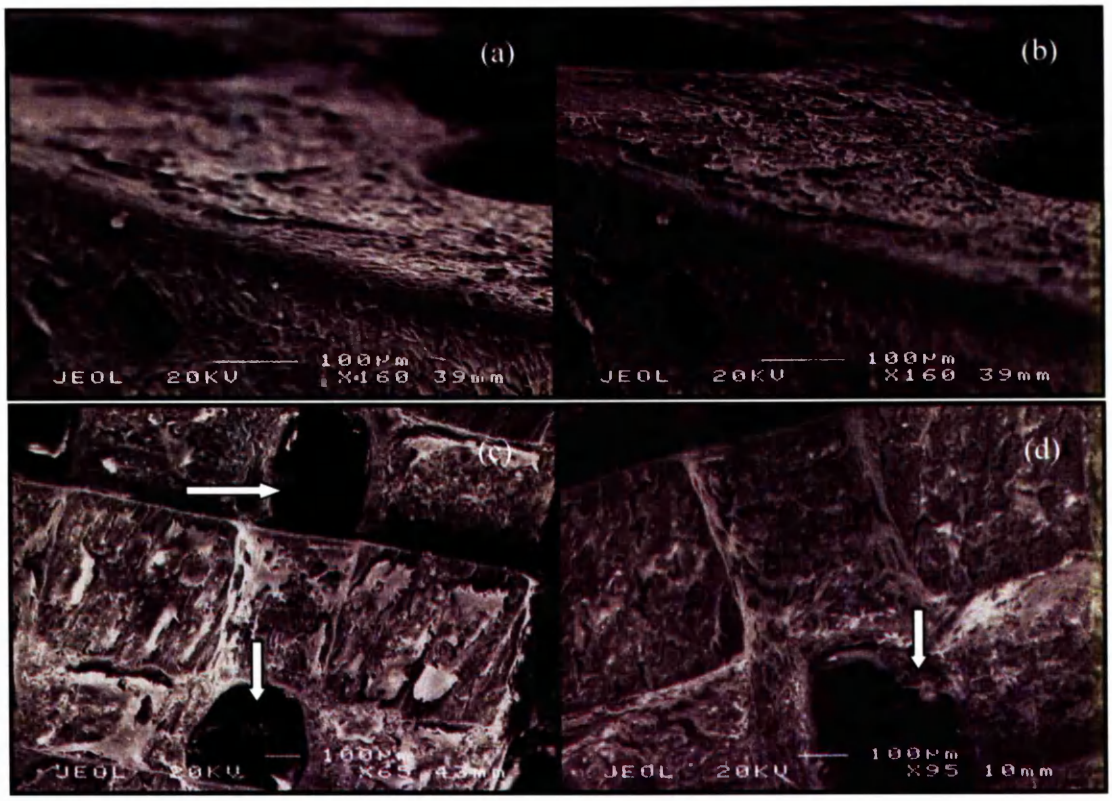

Figure 5-10 (a) and (b) The edge of a glass-ceramic scaffold, (c) and (d) show the surface of the scaffold after cell seeding for 14 days (arrows pointing to cell spreading inside the holes of the scaffold.

Figure 5-10 (a) and (b), show the edge and surface of the scaffold after 14 days of cell seeding and it can be seen that the cells have spread on both sides of the scaffold and formed a continuous monoloyer. Figure 5-10 (c) and (d) show that the cells have attached well to the scaffolds and after 14 days a confluent morphology has formed. Cells have also spread down the holes of the scaffold (arrow). For SEM, the samples have to be sputter coated with gold first, which makes it difficult to view within the holes of the sample, but cellular attachment at the edges of the holes can be clearly seen, spreading inside the holes (arrows).

Two-dimensional composite slips made in a conventional UV box were also used for cell seeding. The cells were well attached to the surface with the filpodia clearly visible (figure 5-11 (a) and (b)). Two-dimensional composite slips fabricated on the SLA were also examined for cellular attachment, but no cells were seen on the surface. The same was observed on the composite scaffolds made on the SLA. As mentioned before, the leaching

of initiator into culture media, led to the cells not attaching to the scaffolds and eventually leading to cell death.

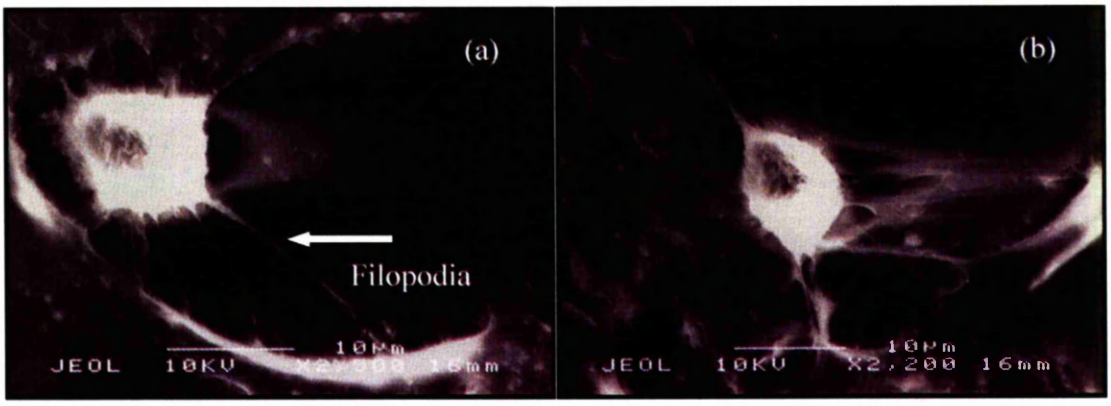

Figure 5-11 Cell attachment on 2-d composite slips fabricated in a conventional UV box.

5.5. Live/Dead Staining

Glass-ceramic and composite scaffolds were both stained for cell viability using the live/dead assay. The scaffolds were stained at two time points; 2 and 5 days. This was done because the calcein component in the assay is converted to a fluorescent product by esterases within the cytoplasm, which is a useful method to observe cell morphology. The composite scaffolds were also stained with the live/dead assay even though initial investigations had proved unsuccessful.

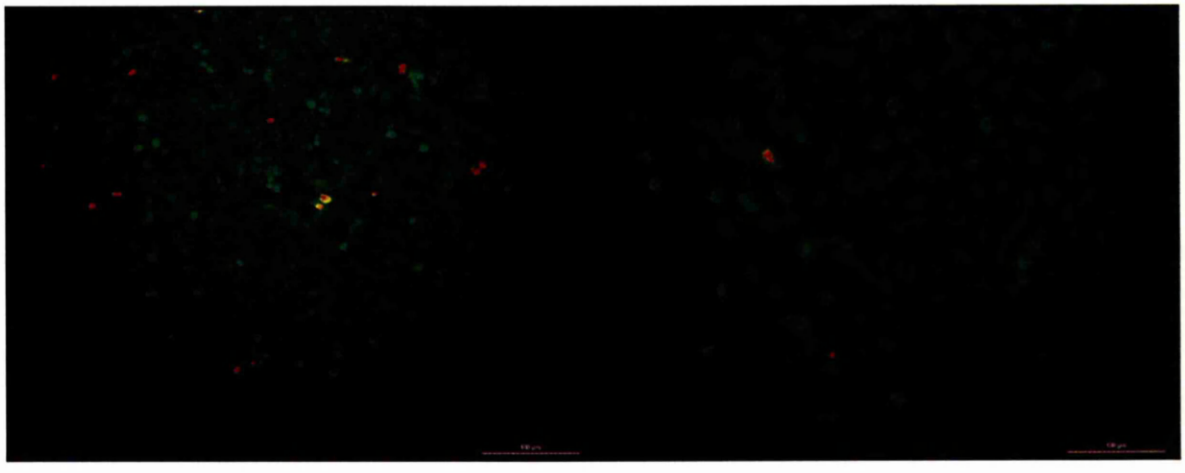

Figure 5-12 Live/dead staining on control glass cover slips after 2 days (scale 100μm).

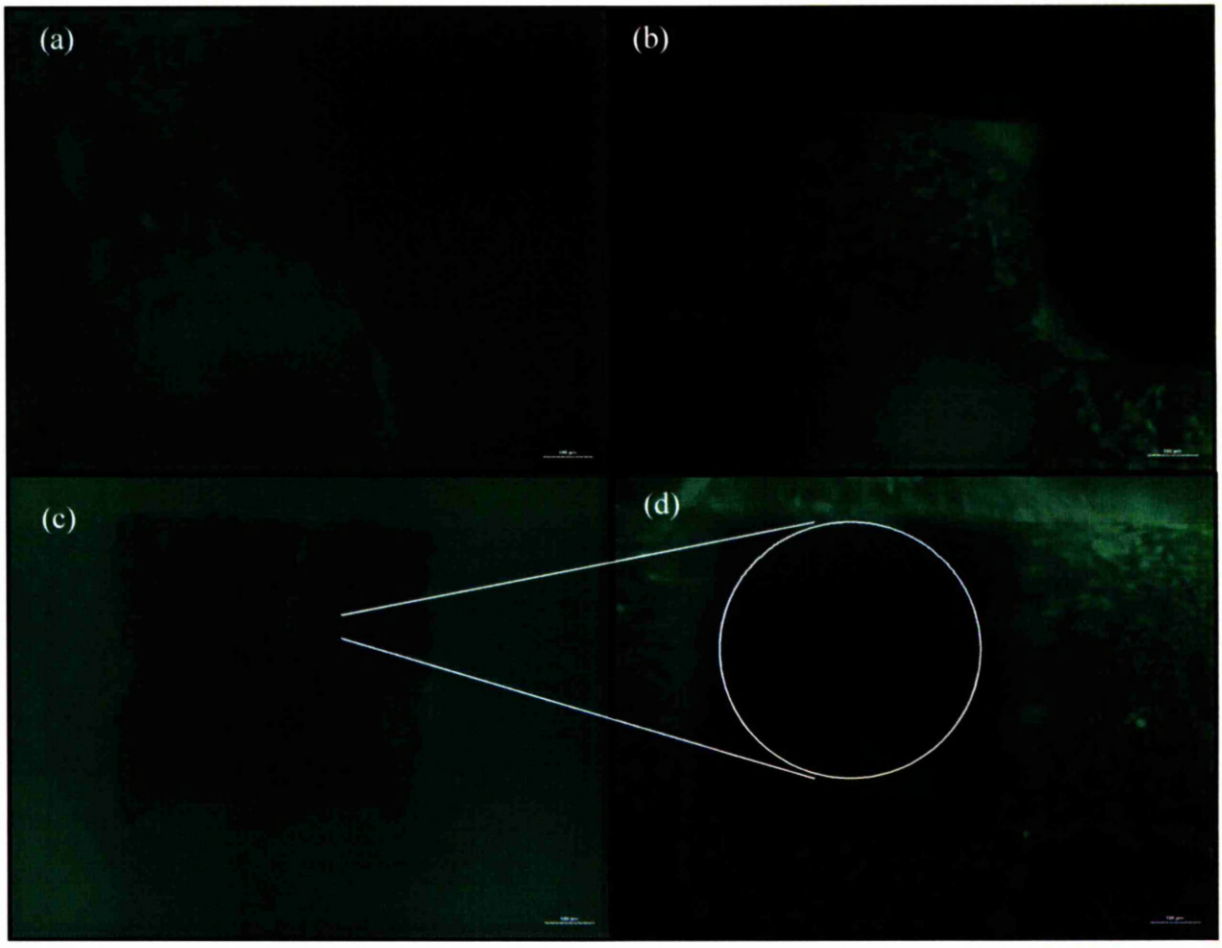

Figure 5-13 Live/dead staining on surface of glass-ceramic scaffolds (a, b and d) and on the top strut (c) which is the out of focus region in (d), after 2 days (scale 100 μm).

Live/dead staining stains the live cells green and the dead cells red. Again, the control glass cover slips (figure 5-12) were also stained with the assay to compare the scaffolds, as to how well they respond to cell attachment. Due to the fluorescing nature of bioactive glass, the surface scaffold also appears green, hence the images are not very clear. The cells have attached well to the surface of the glass-ceramic scaffolds (figure 5-13 (a)) in the middle and on the edges (figure 5-13 (b)). The same is observed throughout the top surface of the scaffold which is evident from figure 5-13 (c) and (d), which shows cells to attach on two different planes of the scaffold. Figure (c) is one of the struts of the scaffold, which is on a higher plane than the rest of the scaffold. A small crack is present on its surface, and cells have preferentially attached along it.

Normally, when live/dead staining is performed, the number of live cells are counted against the dead cells to determine percentage cell viability. Due to the fluorescing nature of bioactive glass, counting the number of cells proved difficult. However, no red stained cells were observed on the scaffold after 2 days.

Figure 5-14 Live/dead staining on composite scaffolds after 2 days (scale 100 μm).

The composite scaffolds were stained after 2 days of cell seeding and it can be seen that there are no living cells attached to the surface of the scaffold. A very low number of dead cells are present on the edges within the scaffold. This result suggests that cells did not attach to the scaffold from the beginning. If cells had attached to the scaffold, and cell death occurred due to the toxicity of the initiator, the area of the scaffold would have red staining on it. This statement could not have been made if the cells were incubated for a period of 7 days because if the cells had attached to the surface, and the toxic nature of the photoinitiator caused death, then the cells would have detached from the scaffold and no red staining would be seen in that case. The low number of red staining suggests that on seeding the cells, the surface of the PEG is unable to let the cells attach and at a later stage, after the leaching of initiator begins, the cells are killed due to its toxicity.

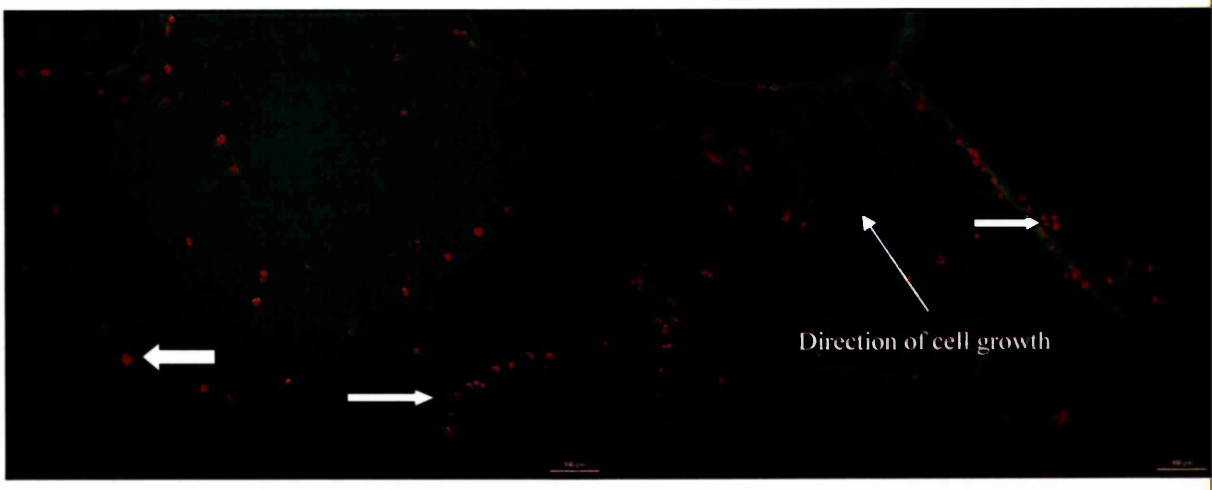

Figure 5-15 The surface of the glass-ceramic scaffolds after 5 days (scale 100 μm) with the arrows pointing the dead cells (red stain).

Live/dead staining on the glass-ceramic scaffold after 5 days shows the cells have reached confluency and covered the whole area of the scaffold. The percentage of dead cells present on the scaffolds is below 10%. These dead cells can generally be seen on the edges of the scaffold (figure 5-15). It is also observable that cells have started to grow in the direction of the scratches present on the scaffold, which were caused due to the removal of the epoxy resin casings after gel casting.

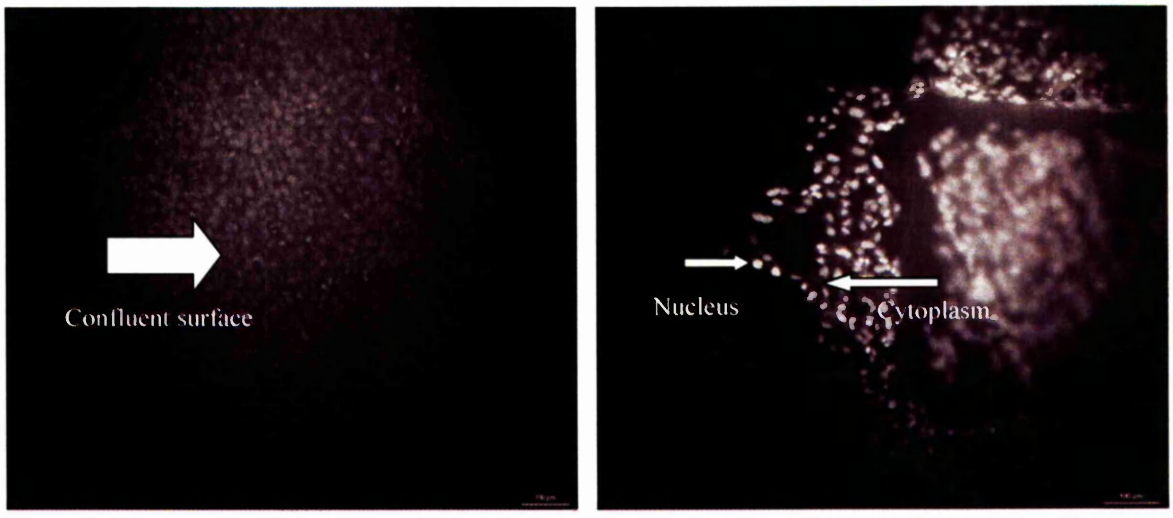

Figure 5-16 The surface of glass-ceramic scaffolds after 5 days (scale 100 μm).

Figure 5-16 shows the surface of the glass-ceramic scaffold without any filters, so that the effects of the fluorescing scaffold can be hidden and the cells are visible clearly. Unfortunately, these images could not be taken at a higher magnification due to the nature of the bioactive glass. Nevertheless, the nucleus of the cells can be clearly seen surrounded by the cytoplasm. After 5 days the cells have reached confluency on the surface of the scaffold.

5.6. Actin Cytoskeleton organisation

Actin cytoskeleton organisation was observed using Phalloidin (green labelling) of F-actin and DAPI (blue labelling) of cell nuclei on glass-ceramic scaffolds after 2 and 5 days using a fluorescence microscope. Figure 5-17 (a) shows cell attachment on the surface of the scaffolds after 2 days. It is clearly visible through the blue stain, which stains the nucleus of the cells, that the cells are present all over the scaffold. The cytoskeleton of the cells stained in green can also be seen, which shows spreading of the cells. Due to the surface topography of the glass-ceramic scaffolds, and the surface not being completely flat, focusing on the blue and green stain at one particular point proved very difficult. Thus, only a few cells can be seen with nucleus surrounded by the cytoskeleton (figure 5-17 (c) and (d)). Since the surface of glass-ceramic scaffolds are not flat, low magnification images were obtained which do not show the cytoskeleton organisation in any detail, but in actual fact, the cells had attached well to the surface of the scaffolds. Figure 5-17 (b) shows cells where the nuclei and cytoskeleton are clearly visible.

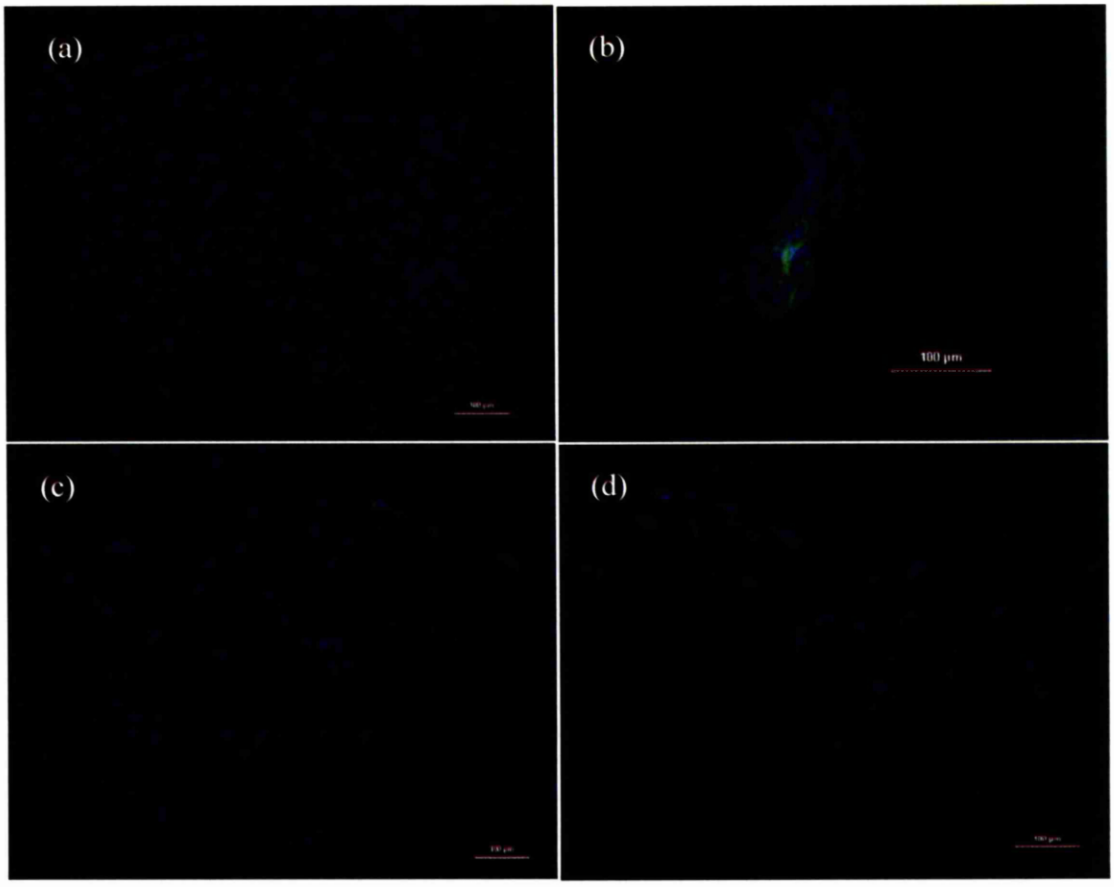

Figure 5-17 DAPI (blue) and Phalloidin (green) staining of the glass-ceramic scaffolds after 2 days (scale 100µm).

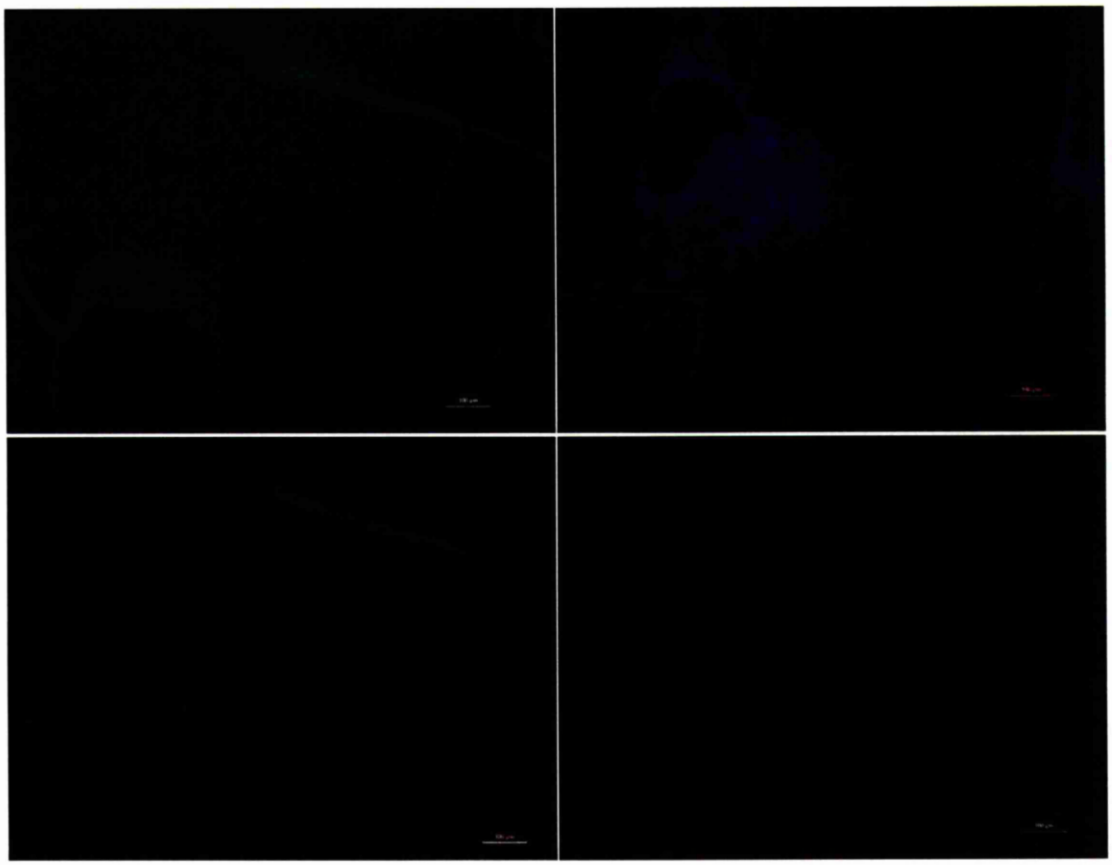

Figure 5-18 DAPI and Phalloidin staining on glass-ceramic scaffolds after 5 days (scale 100 μm).

Figure 5-18 shows the surface of glass-ceramic scaffolds being stained with DAPI and Phalloidin after 5 days. A confluent morphology is observed and the phalloidin stain demonstrates the presence of actin cytoskeleton covering the whole surface. All four images are from different regions of the scaffold displaying cell confluency. Comparing the actin cytoskeleton staining both at 2 and 5 days (figure 5-17 and 5-18) to the live/dead staining at 2 and 5 days (figure 5-13 and 5-15) for the glass-ceramic scaffolds, shows a consistent result in terms of the affinity of osteoblasts to grow on the bioactive glass surface. The initial cell morphology and attachment after 2 days, and after a high rate of proliferation, at the end of 5 days, both tests have proved the glass-ceramic surface to be highly compatible with osteoblasts.

5.7. Actin Cytoskeleton using Confocal Microscopy

Actin cytoskeleton staining on glass-ceramic scaffolds using fluorescence microscopy led to the staining of the glass-ceramic surface itself making it difficult to observe the morphology of the cells. Hence, the same stains were used (DAPI and Phalloidin) to obtain better contrast images by using a confocal microscope.

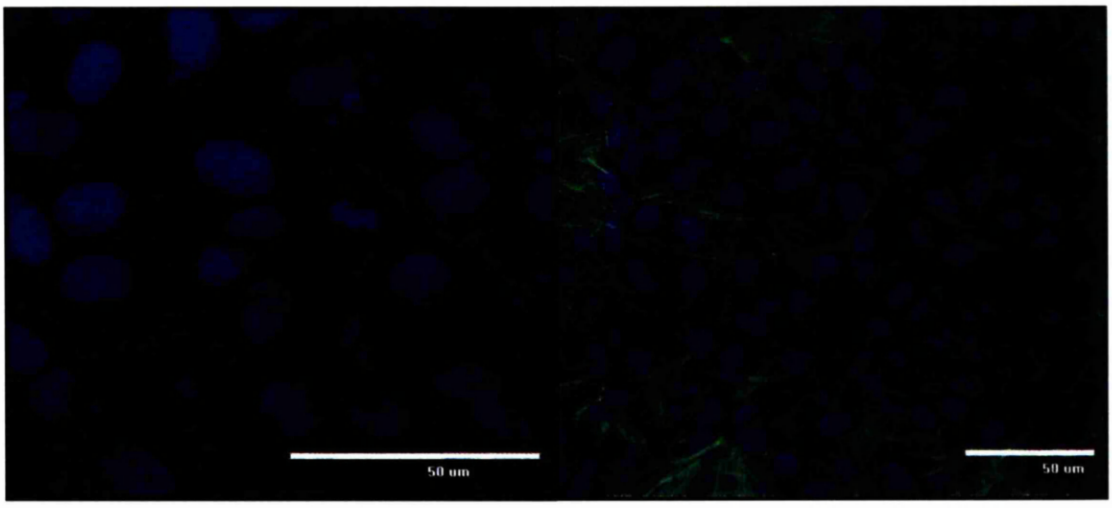

Figure 5-19 DAPI and Phalloidin staining on glass control slips after 5 days (scale 50μm).

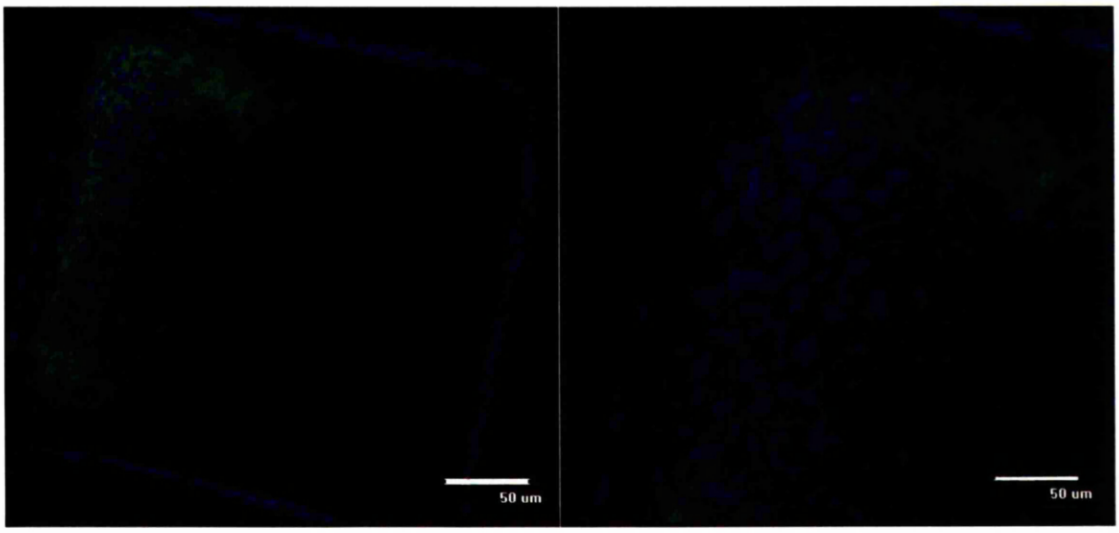

Figure 5-20 DAPI and Phalloidin staining on glass-ceramic scaffolds after 5 days (scale 50 μm).

Confocal microscopy has proven a successful imaging tool to review the morphology of the cells on the surface of the scaffolds. Comparing the control glass slips (figure 5-19) to the surface of the glass-ceramic scaffolds (figure 5-20) after 5 days, a clear similarity can be seen between the two proving the affinity of the bioactive glass surface. The nucleus of the cells is well defined, with the cytoskeleton surrounding the nucleus showing spreading.

The external dimensions of both CER 400 and CER 600 scaffolds were the same, but the surface area of the CER 400 scaffold (1.38×10^{-3} m^2) was greater than CER 600 scaffold (1.07×10^{-3} m^2) (as shown in Appendix I). This difference affects the cell population on the scaffolds and can be seen in figure 5-21 and 5-22.

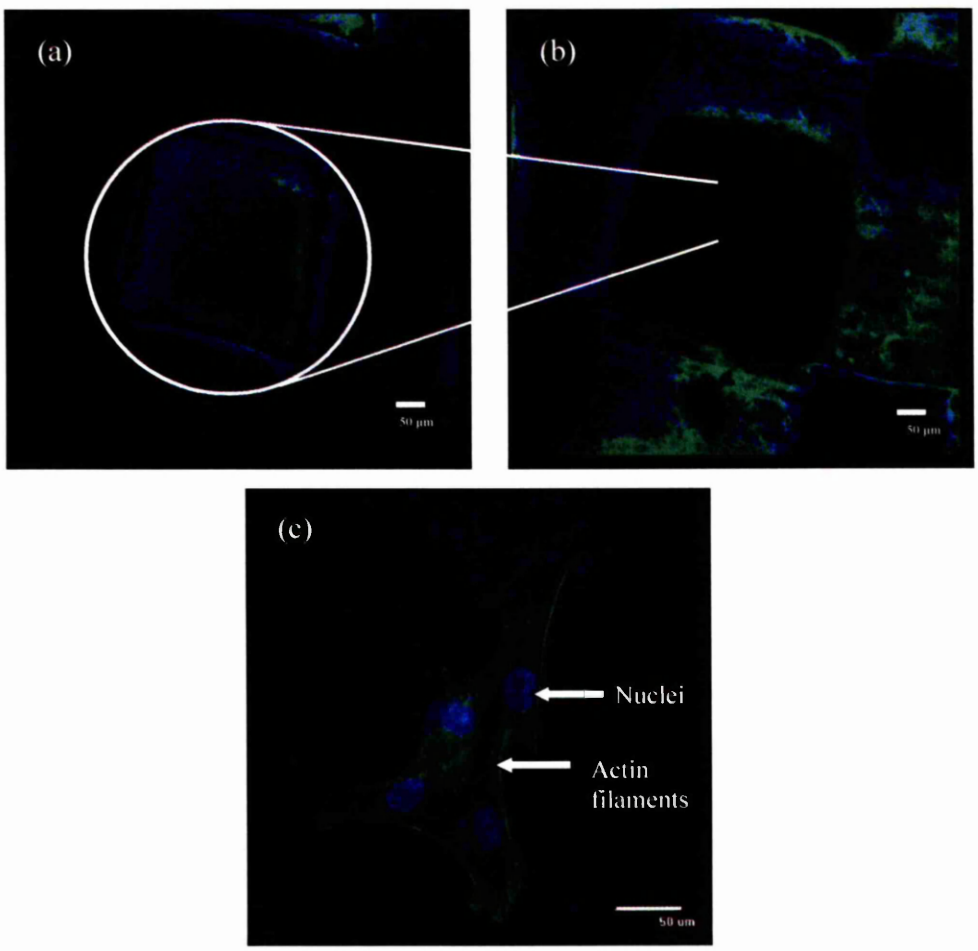

Figure 5-21 (a) The top strut of CER 600 scaffold, which is the out of focus (dark region on figure (b)), (b) surface of the CER 600 scaffold and (c) the spreading of the cells in detail (scale 50 μm) after 7 days.

Figure 5-21 (a) and (b) both show the same area of the scaffold through a confocal microscope. The images show the confluency of cells on the surface of the scaffold. As the surface of the scaffolds is not flat, the images only have certain areas in focus which show the nucleus surrounded by the cytoplasm, but in actual fact the whole surface demonstrates spreading of cells. Image (a) is the strut seen on top of the scaffold, which is on a higher plane to the rest of the scaffold as shown in image (b). Image (c) shows the nuclei surrounded by the cytoskelelton spread in all directions with the bundles of filaments showing attachment.

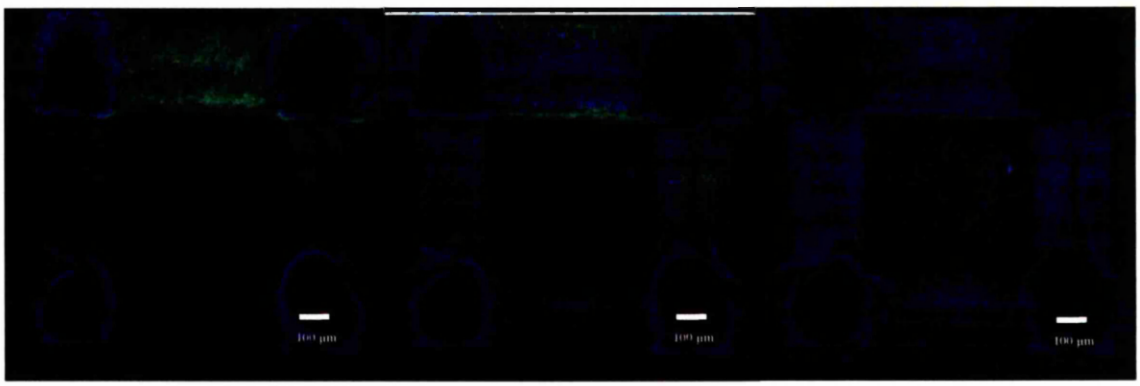

Figure 5-22 The surface of CER 400 scaffold after 7 days (scale 100 μm).

All three images shown in figure 5-22, are the same area of the scaffold, which were scanned to obtain a full image of the distribution of cells. The cells have proliferated completely over the surface of the scaffold. Comparing these to that of CER 600 (figure 5-21), it is clear that the increased surface area for the latter means more cells are present on the surface.

Although a good distribution of cells is seen on the surface of both scaffolds, this trend does not necessarily correspond to the behaviour of cells within the scaffold. For this reason, sliced glass-ceramic scaffolds were fabricated to ensure whether cells were attaching throughout the scaffold and if the rate of proliferation was the same all the way through (figure 5-24).

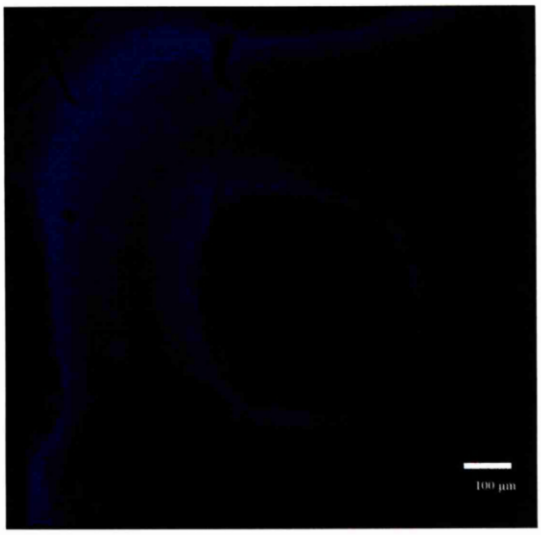

Figure 5-23 The surface of the composite scaffold (scale 100 μm).

Figure 5-23 shows an image obtained from the confocal microscope of a composite scaffold. Although the surface has stained blue, there are no cells present. This result is consistent with the results of the live/dead staining and fluorescence staining.

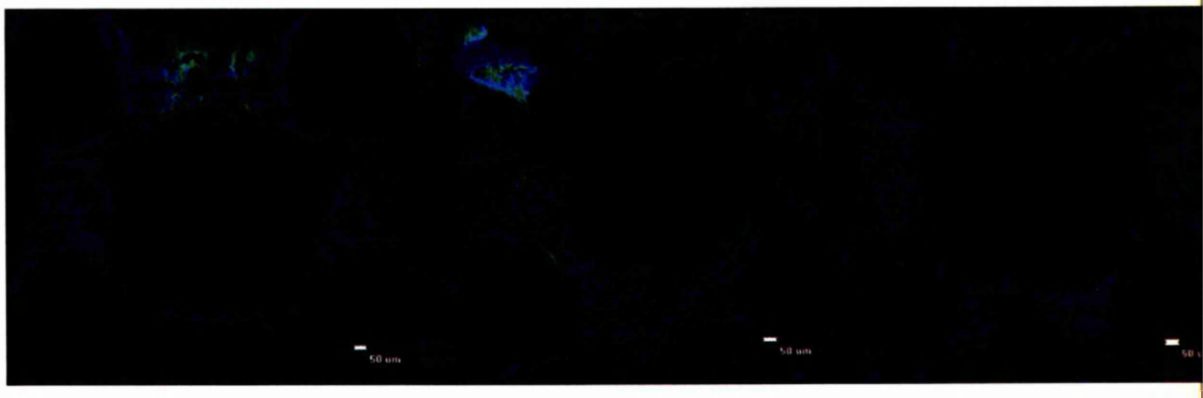

Top Slice Middle Slice Bottom Slice

Figure 5-24 Confocal images of the sliced scaffolds starting from top, middle and bottom (scale 50 μm).

Sliced scaffolds were used to observe cell behaviour throughout the structure of the scaffold. All three slices were stacked on top of each other, with the cells being seeded as they would for a normal scaffold for 7 days, after which the slices were taken apart carefully and stained with DAPI and Phalloidin. This technique proved very successful as can be seen in figure 5-24. When the cells are seeded on the scaffold, most of the cells attach to the top surface. Therefore, at the time of seeding, the cells need to be picked up

from the well plate and placed again on top of the surface to maximise the number of cells attaching to the surface of the scaffold. As can be seen from the results, after 7 days of culturing the cells are found most abundantly on the top slice where the whole surface is confluent. The middle slice has fewer cells on the surface, but the cells have attached and spread well as shown by cytoskeletal arrangement. The bottom slice of the scaffold has the least amount of cells attached to the surface, and the rate of cell proliferation is the slowest.

Osteoblasts have a tendency of attaching to the edges of surfaces, which was also observed in the case of the scaffolds. This means that the cells would grow inwards towards the centre of the scaffold. This is not considered to be a problem as cells have shown an affinity to the bioactive glass surface and the cells normally complete confluency in approximately 5 days on the top surface. This time scale gets longer as the cells work their way through the scaffold.

5.8. Alamar Blue Cell Proliferation assay

Alamar blue assay was used to calculate the number of cells that were present in the scaffold. All four types of scaffolds were used to determine a cell count within the scaffolds along with 2-d composite slips. The experiment was repeated twice to achieve accuracy and conducted with six samples of each scaffold at the same time.

Firstly, a calibration curve was plotted which was used to determine the instrumental response, to that of changing concentrations of cells to be measured (figure 5-25). The cell concentrations were increased logarithmically from 1×10^3 to 1×10^6 cells/ml and suspended homogeneously.

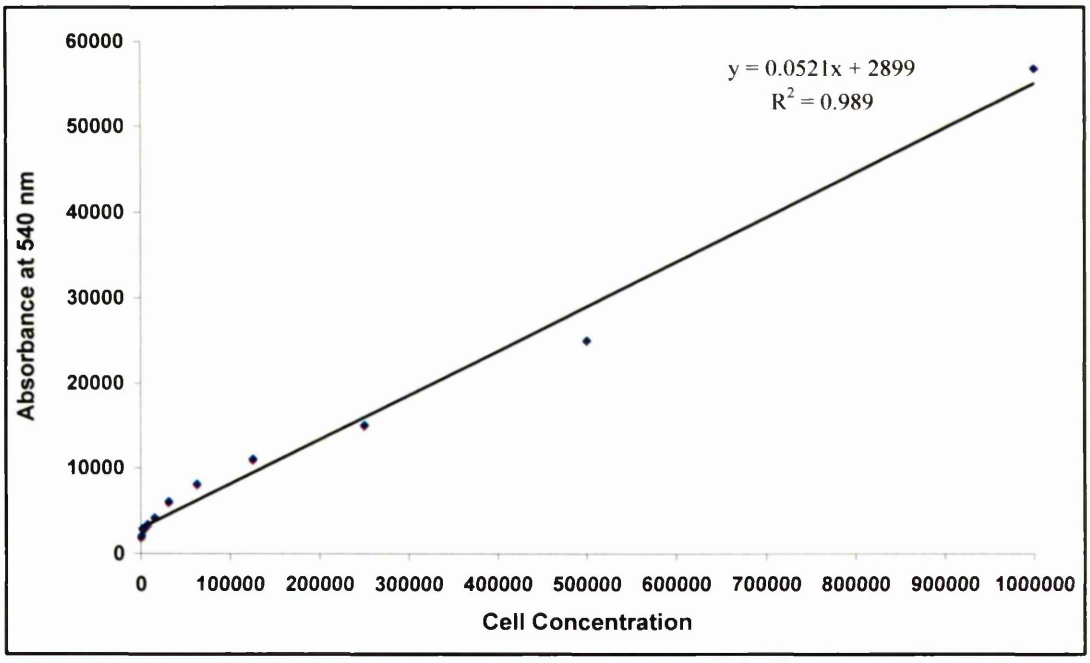

Figure 5-25 Standard curve for the Alamar blue cell proliferation assay.

The standard curve gave a R^2 value of 0.989, which was used to calculate all further cell concentrations obtained from the fluorescence reading of the scaffolds.

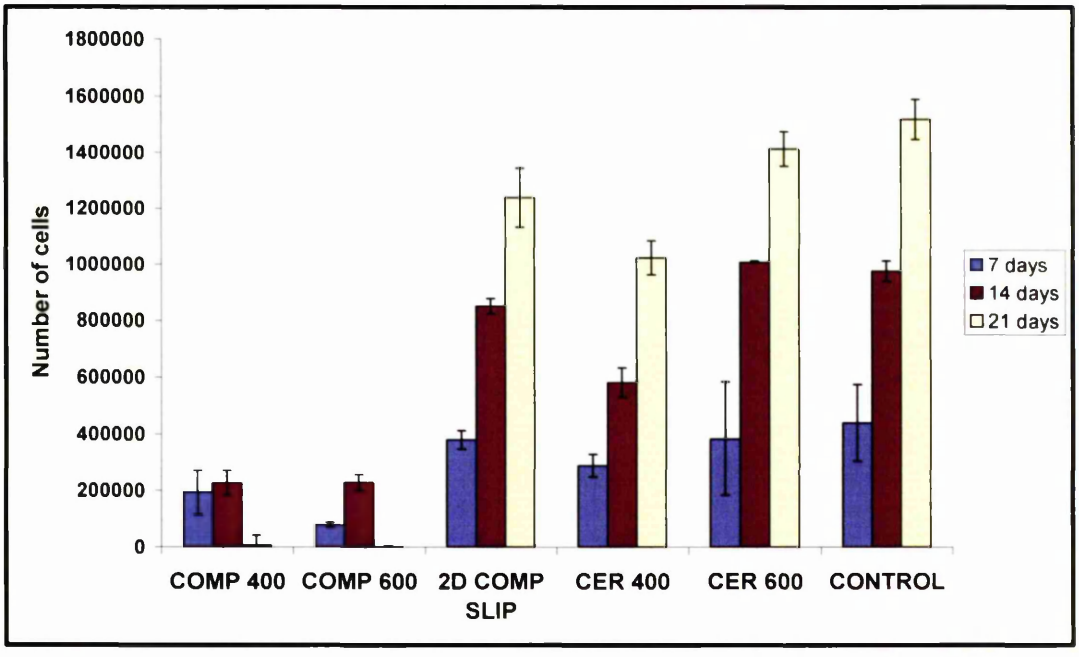

Figure 5-26 Alamar blue cell proliferation assay.

The number of cells seeded onto each substrate in the well plates was 8 x 10^4 cells. To maximise the number of cells that would attach to the scaffolds, a tight fix box was used to encapsulate the scaffolds. This box had four walls and was open both at the top and the bottom. The cells were seeded from the top, drop by drop, and then the excess lifted off from the well plate and the same procedure repeated 5 times. This procedure increased the number of cells on the scaffold, compared to normal seeding techniques.

The result shows that the composite scaffolds (COMP 400 and COMP 600) showed an increase in cell proliferation over 14 days, after which both scaffolds showed a complete decline in the number of cells on the scaffolds after 21 days. Although COMP 400 contains 2 x 10^5 cells after 7 days, and COMP 600 contains 8 x 10^4 cells after 7 days, both scaffolds reach a high of 2.5 x 10^4 cells after 14 days. It would have been expected from the COMP 400 scaffolds to reach a higher rate of proliferation, but as both scaffolds reached the same number of cells, it could be said that the cells started to die after about 12 days taking the cell count to a maximum and hence showing both scaffolds to have the same number of cells, after which both scaffolds demonstrate an aversion for the cells and show no cell count after 21 days. This effect can be due to two reasons. After 12 days the full effect of the photoinitiator leaching might be causing the cells to die, or loss of confluent monolayer during the procedure of the assay might be the reason for the decline in the number of cells, although the latter reason is less likely.

CER 400 and CER 600 show cell proliferation to increase with time. These results are comparable to the control, demonstrating very similar cell affinity to bioactive glass. Although the surface area of the CER 400 is larger than CER 600 more cells are present on the latter scaffold throughout the 21 days, and the rate of proliferation is also much higher on CER 600, as there more cells attached to the surface when seeding. This difference in cell seeding can be the main reason for this difference seen on the scaffolds.

Previous results have all shown that cells do not attach to the surface of the composite scaffolds. This has been due to the small amounts of initiators leaching out of the system. Unfortunately, the amount of initiator leaching out of a scaffold cannot be measured, as it would differ from scaffold to scaffold depending on how well the product has cured. Nevertheless, alamar blue has suggested that cells are present within the scaffold, which does not correspond to optical microscopy, SEM, DAPI and Phalloidin staining or live/dead staining. This would imply that the cells present within the scaffold, which

resemble dead cells (optical microscopy), are in fact not dead, but unable to attach to the scaffold and are thus being reduced by the action of the alamar blue. The readings received whilst doing the alamar blue test could be from a clump of cells lodged within the scaffold, which would not be a true representation of living cells. To test this hypothesis, a composite scaffold was seeded with cells for a period of 7 days after which, the whole scaffold was trypsined to check if cells were lodged within the scaffold. The scaffold was removed from the incubator and the trypsin centrifuged to see if any cells were present. This test proved negative and no cells were seen to be present in the scaffold. However, this does not establish if cells are not present within the scaffold. There could be a possibility of the cells being unable to be released by the trypsin because of the physical nature of the composite scaffolds.

T-Test analysis for two samples assuming equal variance was conducted on all samples with a confidence level of $p > 0.05$. The results are shown in table 5-1, and show if there is any significant difference between any two samples at 7, 14 and 21 days. SD represents significant difference and NSD represents no significant difference between the samples.

Table 5-1 shows the significant differences between any two samples at 7, 14 and 21 days for Alamar blue assay.

7 DAYS	COMP 400	COMP 600	2D SLIP	CER 400	CER 600	CONTROL
COMP 400		SD	SD	SD	SD	SD
COMP 600	SD		SD	SD	SD	SD
2D SLIP	SD	SD		SD	SD	NSD
CER 400	SD	SD	SD		NSD	NSD
CER 600	SD	SD	SD	NSD		NSD
CONTROL	SD	SD	NSD	NSD	NSD	

14 DAYS	COMP 400	COMP 600	2D SLIP	CER 400	CER 600	CONTROL
COMP 400		NSD	SD	SD	SD	SD
COMP 600	NSD		SD	SD	SD	SD
2D SLIP	SD	SD		NSD	SD	SD
CER 400	SD	SD	NSD		SD	SD
CER 600	SD	SD	SD	SD		NSD
CONTROL	SD	SD	SD	SD	NSD	

21 DAYS	COMP 400	COMP 600	2D SLIP	CER 400	CER 600	CONTROL
COMP 400		NSD	SD	SD	SD	SD
COMP 600	NSD		SD	SD	SD	SD
2D SLIP	SD	SD		SD	NSD	SD
CER 400	SD	SD	SD		SD	SD
CER 600	SD	SD	NSD	SD		NSD
CONTROL	SD	SD	SD	SD	NSD	

5.9. Collagen-I Antibody Staining

Collagen type I production is associated with osteoblasts. Collagen is part of the extracellular matrix of bone and hence collagen antibody staining was conducted to check for collagen production after the cells had been seeded for a length of time. The glass-ceramic scaffolds were stained with DAPI (blue) for the nucleus and a primary and secondary antibody (red) to stain the collagen present.

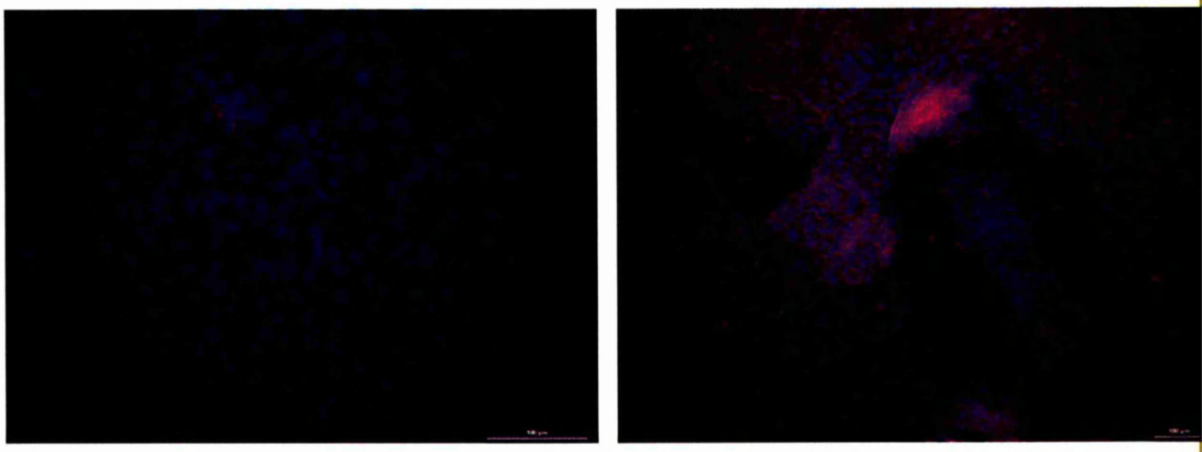

Figure 5-27 Collagen present on control glass cover slips after 7 days (scale 100 μm).

The glass cover slips in figure 5-27 are shown to give an idea of the amount of collagen that is produced after 7 days. This can be compared directly to the surface of the scaffolds. In addition, the sliced scaffold system was used to observe collagen production throughout the scaffold. Figure 5-28 shows the top slice of the glass-ceramic scaffold after 7 days. Figure 5-28 (a) is the top strut of the scaffold and it can be clearly seen that collagen (red) is present throughout the surface, and especially at the edges where fibre bundles of collagen can be seen extending at the edges. Image (b) also shows the extracellular matrix and cells growing in the direction of scratches present on the scaffold.

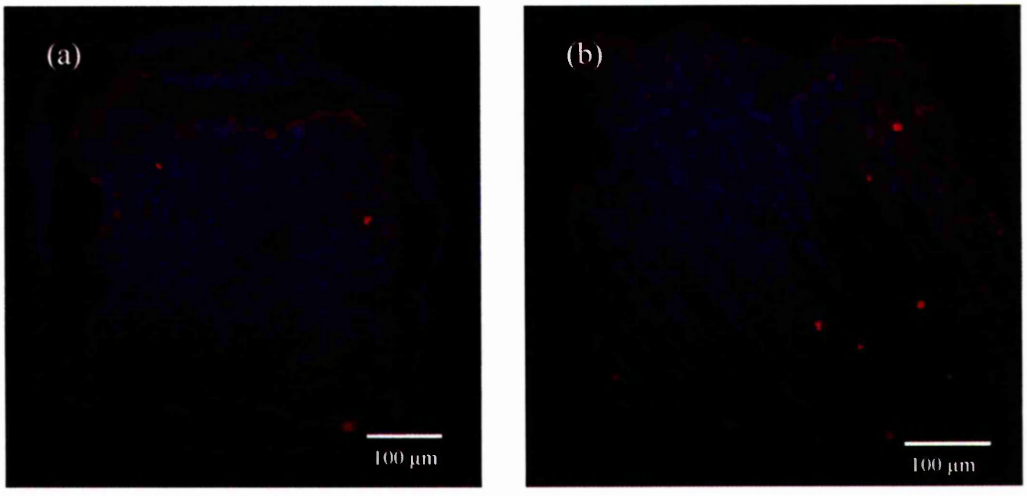

Figure 5-28 Collagen (red) on the top slice of the glass-ceramic scaffold after 7 days (scale 100 μm).

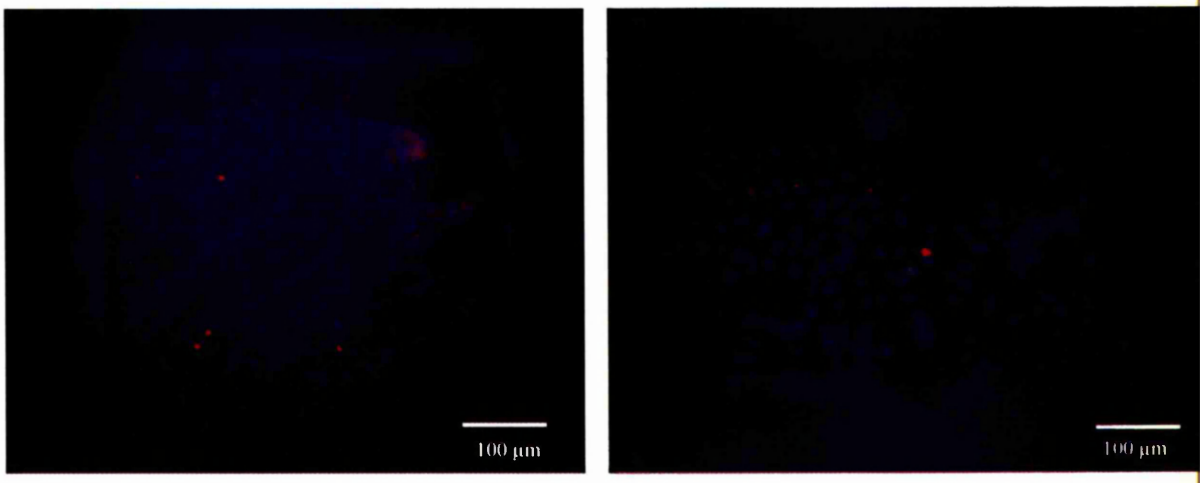

Figure 5-29 Collagen on the middle slice of the glass-ceramic scaffold after 7 days (scale 100 µm).

On the middle slice of the scaffold the density of cells has slightly decreased (figure 5-29), as was observed earlier. Cell spreading and alignment is still noticed to be directional. The phenomenon that cells elongate on the grooves of the scaffold is known as 'contact guidance' (Weiss, 1945). Matsuzaka *et al.* (2003) have concluded that microgrooves are able to influence bone-cell behaviour in various ways i.e. by determining the alignment of cells and cellular extensions, and by altering the formation and placement of focal adhesions and altering ECM production. Therefore, microgrooved surfaces maybe appropriate for bone anchored implants.

Cell distribution was observed to be better at the edges rather than down the centre of the scaffold as noticed previously.

Figure 5-30 The bottom slice of the glass-ceramic scaffold after 7 days (scale 100 µm).

Very few cells can be seen attached to the bottom slice of the scaffold and extracellular matrix can hardly be seen. The density of cells was higher at the edges, as is the case with osteoblasts, but figure 5-30 shows the surface in the middle of the bottom slice, where cells in this case have not been able to reach in 7 days. This is most probably due to mistakes during the cell seeding procedure, where the cells were not flushed through the whole scaffold. The reason cells can be seen on the edges is because during the cell seeding process, cells suspended in media first touch the top surface of the scaffold, out of which some of the suspension travels through the holes of the scaffold, while most of it overflows at the edges of the scaffold. This leads to more cells attaching at the sides and edges of the scaffold, which upon proliferation move their way inwards.

Collagen staining was also conducted on scaffolds after being seeded for 14 and 21 days, but after 7 days, osteoblasts reach confluency and then during the fixing and washing stages of collagen staining, the confluent layer of cells lift off the surface, hence not making it possible to check for collagen.

Presence of collagen is confirmed by attaching a primary antibody to the cells, but to view the production of ECM under fluorescence microscope, a secondary antibody has to be attached to the primary, which stains the collagen red.

To check that no non-specific binding of the secondary antibody is occurring and there is actual presence of collagen, a negative control was also performed, whereby the cells were cultured for 7 days, and the scaffold was just stained with the secondary antibody (figure 5-31).

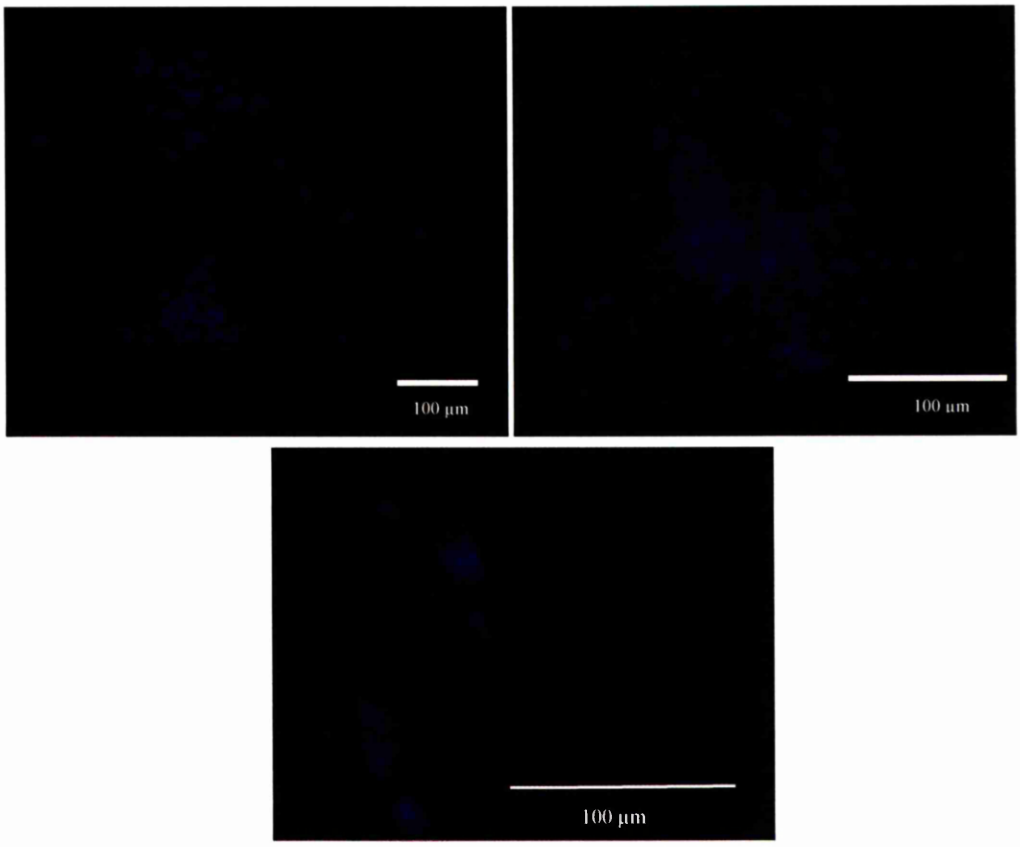

Figure 5-31 Negative control for collagen staining (scale 100 µm).

For the negative control, cells were seeded on to glass-ceramic scaffolds for 7 days, and during the antibody staining stage only the secondary antibody was used. As can be clearly observed from the images, there is no red stain present on the surface of the scaffolds, proving that collagen was present on the surface of the scaffolds when both antibodies were used.

5.10. Collagen assay

Collagen assay was conducted on all four types of scaffolds. It quantifies the amount of acid-soluble collagen released into culture medium. The scaffolds were cultured with osteoblasts for 7, 14 and 21 days and their respective amounts of collagen were measured using a spectrophotometer.

A calibration standard curve was also plotted for the collagen assay. The standard curve gave a R^2 value of 0.9806, which was used to calculate the amount of collagen produced by the scaffolds (figure 5-32).

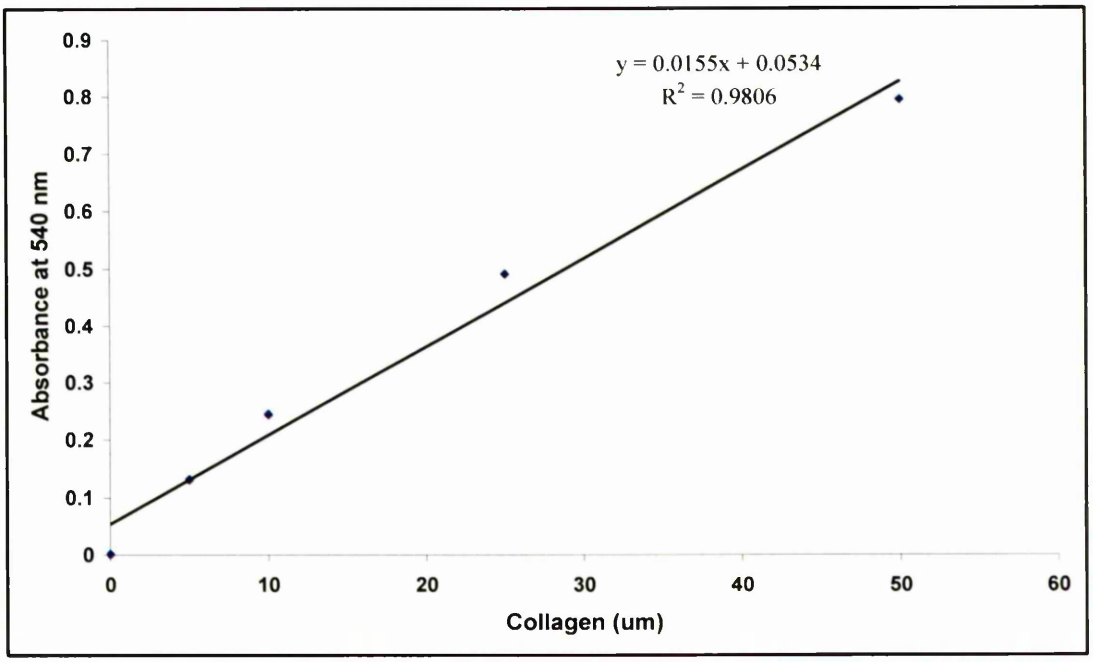

Figure 5-32 Standard curve for the soluble collagen assay.

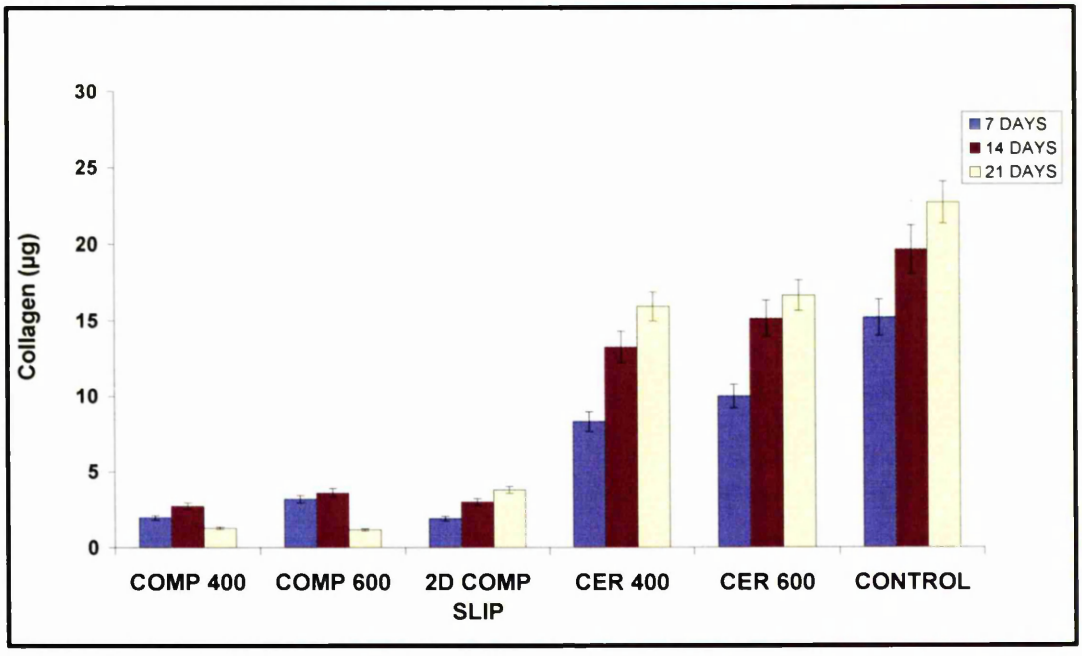

Figure 5-33 Collagen-I assay.

Collagen assay (figure 5-33) has clearly demonstrated that collagen production on CER 400 and CER 600 increases as time after cell seeding increases. These results are quite

comparable with control glass slip, once again proving the affinity of the bioactive material for cells. The COMP scaffolds both show very little collagen production on the scaffolds as expected, since cell attachment is very poor on the surface of the scaffolds, hence making it difficult to lay down any extracellular matrix. Comparing these results to the 2-D composite slips, it can be observed that relatively more collagen is produced on the surface of the slips, as the surface area of the composite slip is ~ 1.5 times less than that of the scaffolds.

T-Test analysis for two samples assuming equal variance was also conducted on all samples with a confidence level of $p > 0.05$. The results are shown in table 5-2, and show if there is any significant difference between any two samples at 7, 14 and 21 days. SD represents significant difference and NSD represents no significant difference between the samples.

Table 5-2 shows the significant differences between any two samples at 7, 14 and 21 days for collagen assay.

7 DAYS	COMP 400	COMP 600	2D SLIP	CER 400	CER 600	CONTROL
COMP 400		SD	NSD	SD	SD	SD
COMP 600	SD		SD	SD	SD	SD
2D SLIP	NSD	SD		SD	SD	SD
CER 400	SD	SD	SD		SD	SD
CER 600	SD	SD	SD	SD		SD
CONTROL	SD	SD	SD	SD	SD	

14 DAYS	COMP 400	COMP 600	2D SLIP	CER 400	CER 600	CONTROL
COMP 400		SD	SD	SD	SD	SD
COMP 600	SD		SD	SD	SD	SD
2D SLIP	SD	SD		SD	SD	SD
CER 400	SD	SD	SD		SD	SD
CER 600	SD	SD	SD	SD		SD
CONTROL	SD	SD	SD	SD	SD	

21 DAYS	COMP 400	COMP 600	2D SLIP	CER 400	CER 600	CONTROL
COMP 400		NSD	SD	SD	SD	SD
COMP 600	NSD		SD	SD	SD	SD
2D SLIP	SD	SD		SD	SD	SD
CER 400	SD	SD	SD		SD	SD
CER 600	SD	SD	SD	SD		SD
CONTROL	SD	SD	SD	SD	SD	

5.11. Alizarin Red S assay

Alizarin Red S assay was used to find out the extent of calcification that occurs on the bioactive surfaces of the scaffolds after a period of 10 days. As a control, a pellet of LG112 bioactive glass powder was used, but no cells were seeded onto the surface. The substrate was stained with alizarin red just as the glass-ceramic and composite scaffolds to compare the amount of mineralisation that had occurred as a result of cell seeding and due to the already present calcium in the bioactive glass.

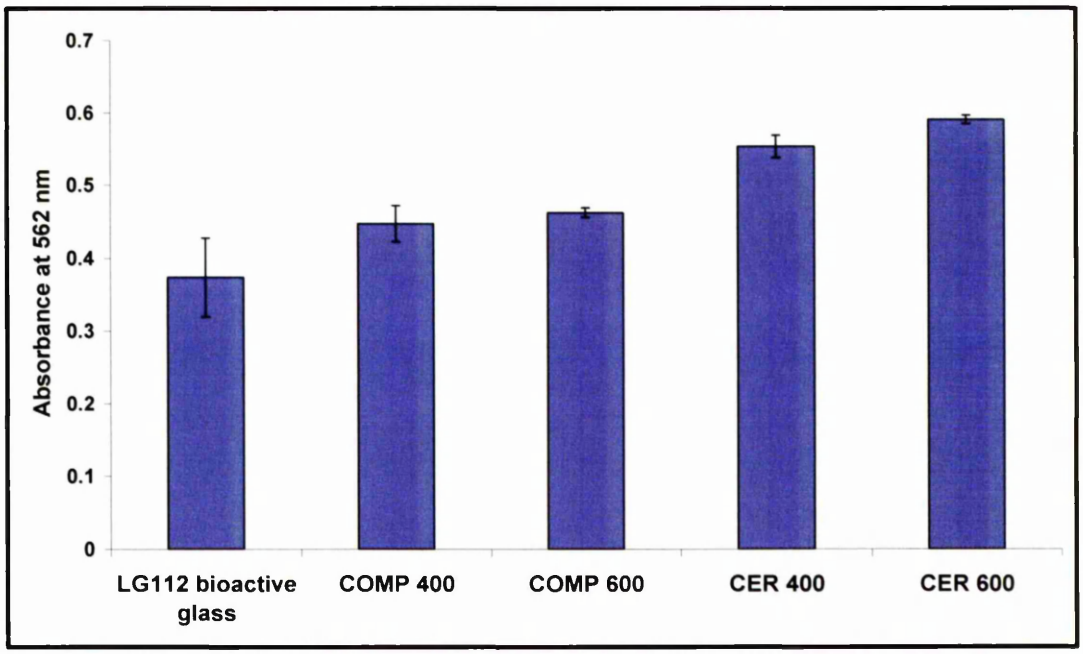

Figure 5-34 Absorbance of alizarin red on all scaffolds.

The results (figure 5-34) show that in the control specimen there is some mineralisation detected, but is less than those present on the scaffolds which had been seeded with osteoblasts. CER 600 demonstrates the highest amount of mineralisation on the scaffolds, with CER 400 following very closely. Again, cell seeding should be maximised to achieve accurate results. The composite scaffolds COMP 400 and COMP 600 both had very similar amounts of mineralisation detected on them. This effect is quite surprising if all previous factors are considered. No cell attachment has been observed before apart from the results obtained from the alamar blue assay. Hence, if there are no cells present on the composite scaffolds, the question of mineralisation being higher than the control specimen (100 % bioactive glass) seems to be an odd result.

The onset of mineralisation in studies conducted with hydroxyapatite starts around 6 to 8 days after the culture process by the expression of osteocalcin in the culture medium, and the rise in detectable calcium in the cell layer (Chang *et al.*, 2000). It was also indicated in this study that an elevated concentration of calcium and phosphate is vital for initiation of mineralisation.

It has been demonstrated that LG112 bioactive glass bulk nucleates to principally give fluorapatite ($Ca_5(PO_4)_3F$), which is analogous to the hydroxyapatite phase of bone (Freeman *et al.* 2003). Hence mineralisation was tested on the scaffolds after 10 days.

Figure 5-35 shows that alizarin red has only stained the surface of the sample where the cells were seeded, and attached, not the underside, where no cells were present. This demonstrates the accuracy of the technique in providing a true representation of the results.

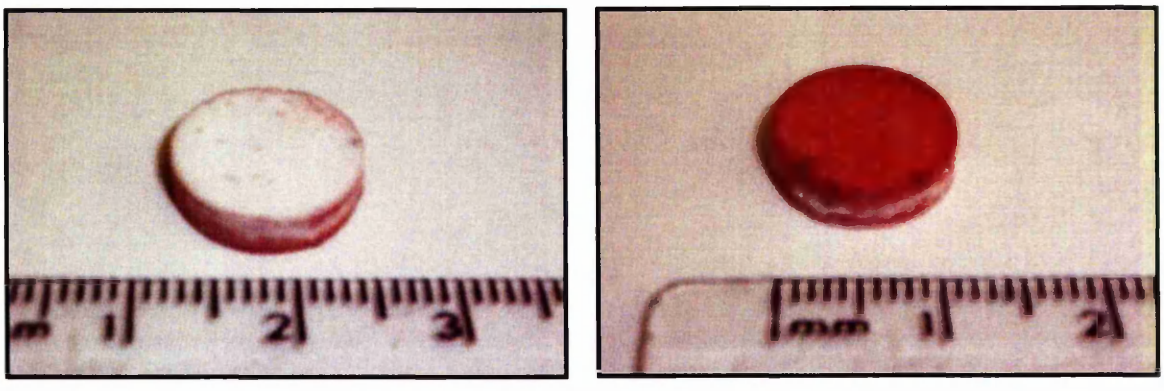

Figure 5-35 (a) underside of bioactive glass sample, and (b) the top side of bioactive glass sample which has stained red.

To check for actual mineralisation on the surface of the scaffolds, EDAX was performed to determine the chemical composition after cell seeding for 10 days. This technique proved very difficult as the machine could not distinguish between the calcium content of the bioactive glass and the mineralisation caused due to the osteoblasts.

Gough *et al.* (2004) tested for mineralisation on bioactive foamed scaffolds, and due to the composition of bioactive glass already containing calcium, the nodules on the scaffolds were trypsinised from the surface and then fixed and stained. This was done as calcium is already present in the material making it difficult to get a true representation of the

mineralisation that has taken place. This technique proved successful for their work (Gough *et al.* 2004).

However, this technique proved hard to conduct on the CER and COMP scaffolds, as it could not be established successfully due to the opaque nature of the scaffold, if the nodules had been removed from within the scaffold, or indeed if there were any nodules present. SEM conducted on the surface of the glass-ceramic scaffolds showed the very little signs of nodule formation, even though the cells were spread all over the surface after 14 days. Hence, the best method of proving the onset of mineralisation was to conduct the quantitative assay, where the cells were seeded onto the scaffolds in the presence of an additional chemical; dexamethasone which promotes mineralisation.

Another supplement which can also be used is β-glycerophosphate. These supplements can be used in conjunction with each other or independently. Jones *et al.* (2007) showed that for bioactive glass 70S30C the addition of either supplement did not appear necessary for osteoblast culturing, but these supplements were necessary for osteoblasts cultured on most other materials such as HA or polymer matrices to produce mineralised matrix (Schiller *et al.* 2001; Coelho *et al.* 2000; Ohgushi *et al.* 1996).

Work carried out on 58S bioactive glass (60 mol% SiO_2, 36 mol% CaO, 4 mol% P_2O_5) stimulated human osteoblasts to form mineralised bone nodules within 10 days of culture without dexamethasone and β-glycerophosphate. There was a possibility that phosphate leaching from the glass may have stimulated the process (Gough *et al.* 2004), and as LG112 has a high concentration of phosphate, this may also contribute to the production of a mineralised matrix.

T-Test analysis for two samples assuming equal variance was conducted on all samples with a confidence level of $p > 0.05$. The results are shown in table 5-3, and show if there is any significant difference between any two samples after 10 days. SD represents significant difference and NSD represents no significant difference between the samples.

Table 5-3 shows the significant differences between any two samples at 7, 14 and 21 days for Alamar blue assay.

	COMP 400	COMP 600	CER 400	CER 600	LG112 GLASS
COMP 400		NSD	SD	SD	SD
COMP 600	NSD		SD	SD	SD
CER 400	SD	SD		SD	SD
CER 600	SD	SD	SD		SD
LG112 GLASS	SD	SD	SD	SD	

5.12. Summary

Both composite and glass-ceramic scaffolds were tested to assess the biocompatibility of the scaffolds. Composite scaffolds fabricated directly using the SLA did not show positive results as toxic chemicals leaching out of the scaffold led to cell death. This resulted in the scaffold proving not suitable for implantation in the body. Glass-ceramic scaffolds demonstrated good cell viability and proliferation of cells leading to extracellular matrix production and eventually resulting in the onset of mineralisation. These scaffolds would be ideal materials to be tested *in vivo*.

6. Conclusion and Suggestions for Future Work

6.1. Summary and Conclusion

Stereolithography has proven to be a successful technique for fabricating three-dimensional composite and glass-ceramic scaffolds. In comparison to other fabrication methods the SLA has shown the ability to produce precise and intricate shapes, without any major drawbacks. This technique has also proved the ability to fabricate products at a large scale in relatively less time than other fabrication methods.

In this study, SLA was used to fabricate scaffolds to be used as load-bearing implants. Composite scaffolds were fabricated with 40 vol.% glass-ceramic loading and showed comparable strength and stiffness to trabecular bone. These scaffolds were fabricated directly using the SLA and the only drawback of this technique was that there were a range of holes present in the structure. The original hole sizes to be present in the scaffold were 400 and 600 μm, but this was supplemented with + 150 μm in certain regions of the scaffold, due to the cleaning process, which distorted the holes present in the scaffold. Glass-ceramic scaffolds were prepared using gel casting technique in conjunction with SLA. This technique proved to be more precise in obtaining the preferred hole sizes than by direct fabrication using the SLA. The glass-ceramic scaffolds had a much higher strength and modulus as compared to the composite scaffolds, but due to their brittle nature, glass-ceramic scaffolds are not yet proficient enough to be used as load-bearing implants. However, these scaffolds proved the technique to be a viable method in producing bioactive scaffolds which could be used in other non-load bearing applications.

As these scaffolds were being produced to be used *in vivo*, both types had to be tested for cell viability. Both composite and glass-ceramic scaffolds were tested for cell viability using human osteoblasts. All scaffolds were subjected to various tests and assays to prove their affinity within the body and if they had any cytotoxic effects. During the fabrication of the composite scaffolds directly from the SLA, some of the unreacted photoinitiator was still present within the scaffolds, and due to this reason cells were unable to attach to the surface of the composite scaffolds and proved to be cytotoxic. This deemed the composite scaffolds unfit for use *in vivo* at this stage. This problem can be rectified by further testing to find a cytocompatible photoinitiator.

The glass-ceramic scaffolds had no initiator present and therefore the scaffolds showed good cell viability on the surface and within the scaffold, and produced extracellular matrix. The bioactivity of the glass-ceramic has also been proven by the fact that onset of mineralisation was also observed on the scaffolds. These scaffolds are fit to be used *in vivo*, for non-load bearing applications at this stage.

6.2. Future Work

The conclusions drawn from this study have inevitably led to a body of further work and improvements; as such this section will acknowledge the improvements required and identify areas of advancement for this technique.

6.2.1. Fabrication of Scaffolds

- Extensive tests to be conducted to obtain a non-toxic and cytocompatible photoinitiator, which can be used with the SLA to obtain high quality scaffolds. This test also needs to conclude how closely the cure depths need to be actually matched to the window panes test.
- The procedures for removal and cleaning excessive resin lodged within the scaffolds need to be addressed more seriously and other methods need to be considered in achieving a scaffold free of uncured suspensions.
- Density measurements of both types of scaffolds need to be conducted to obtain the macroporosities of the scaffolds. These measurements will give a clearer idea about the stiffness of scaffolds changing with the density.
- Higher quality glass-ceramic scaffolds with the least amount of internal defects would have been achieved if de-airing during the gel casting process was improved.
- For a more comprehensive study of mechanical properties of scaffolds under compression, further repetitions of both types of scaffolds are required. The sample set used in this study was small and therefore the results obtained were not completely representative.
- Compression testing in the transverse direction would also prove helpful in providing better understanding of how the struts within the scaffold behave under compression.

6.2.2. Cellular studies

- Cell viability needs to be tested again on the composite scaffolds after a suitable cytocompatible photoinitiator has been used in the fabrication of the scaffolds.
- Microtoming of composite scaffolds to check for cell attachment and proliferation within the scaffold.
- A further comprehensive study is required on the glass-ceramic scaffolds to see the extent of mineralisation and nodule formation.
- Potential inflammatory responses – based on macrophage culture on the scaffolds needs to be addressed.
- Studies showing ways to prove angiogenesis is possible in the scaffolds is vital if the scaffolds are to be used as implants.
- Different polymers to be tested for fabrication of composite scaffolds – ones that are more prone to cell adhesion.
- Comparison of LG112 bioactive glass to other bioactive glasses in fabrication and cellular studies.

6.3. Future Advancement

This research topic has shown great potential in fabricating three-dimensional scaffolds and the next step would be to consider the future advancements that can be taken to make this a more comprehensive study.

- Further analysis of bioactive glass LG112 for crystallisation temperatures needs to be conducted, with different phase transformations and the effects of the constituents within the glass needs to be examined.
- Analysis of differing mechanical properties and the reaction of cells to different geometries of scaffolds with varying pore sizes of different shapes.
- Pore sizes to be reduced to < 350 μm in accordance with various studies to see the effects of transportation of nutrients to the cells and removal of waste products.
- Sectioning of composite and glass-ceramic scaffolds to observe cell attachment within the scaffolds.
- Direct printing of cells on the scaffolds could also be an option for ensuring maximum cell density is achieved.

- Tailoring PEGDA's surface properties to achieve high degree of cell adhesion whilst optimising the rate of cell migration.
- Eventually all tests will lead to in *vivo* testing of scaffolds.

References

- *Alexis F, Factors affecting the degradation and drug-release mechanism of poly(lactic acid) and poly[(lactic acid)-co-(glycolic acid), Polymer international, vol. 54, 1, 36-46, 2005.*
- *Amprino R, Investigations fo some physical properties of bone tissue. Acta Anatomica (34), 161-186, 1958.*
- *Anselme K, Osteoblasts adhesion on biomaterials, Biomaterials 26 (7), 667-681, 2000.*
- *Athanasiou K.A, Schmitz J.P, Agarwal C.M, The Effects of Porosity on in Vitro Degradation of Polylactic Acid–Polyglycolic Acid Implants Used in Repair of Articular Cartilage, Tissue Engineering, 4(1): 53-63, 1998.*
- *Bauer T.W, Schils J, The pathology of total joint orthroplasty II, Mechanisms of implant failure, Skeletal Radiology, 28, 483-497, 1999.*
- *Berthet-Colominas, White S.W, Miller A, 'Structural study of the calcifying collagen in turkey leg tendons', Journal of molecular biology (134), 431-445, 1979.*
- *Bignon A, J. Chouteau, J. Chevalier, G. Fantozzi, J-P. Carret and P. Chavassieux, Effect of micro- and macroporosity of bone substitutes on their mechanical properties and cellular response, J Mater Sci Mater Med 14 (12), pp. 1089–1097, 2003.*
- *Blaker J.J, V. Maquet, R. Jérôme, A.R. Boccaccini, and S.N. Nazhat, Mechanical properties of highly porous PDLLA/Bioglass® composite foams as scaffolds for bone tissue engineering, Acta Biomaterialia, Volume 1, Issue 6, Pages 643-652, 2005.*
- *Boyd D.C, Thompson D.A. Glass ceramics, Kirk-Othmer Encyclopedia of Chemical Technology, 11, 3rd edition, 809, 1980.*
- *Boyd J.D, Claire, W.G, Hamilton W.J, Appleton A.B, Textbook Human Anatomy, McMillian, 1996.*
- *Breme J, V.Biehl, Metallic biomaterials, Handbook of Biomaterial Properties, 1998.*
- *Bronzino J.D, The Biomedical Engineering Handbook, 532-609, 1995.*
- *Brown B.H, Smallwood R.H, Barber D.C, Hose D.R, Medical physics and biomedical engineering. IOP Publishing Ltd, 1999.*
- *Burnstein A.H, D.T.Reilly, M.Martens Aging of bone tissue: Mechanical properties, J.Bone Jt. Surg., (58A), 82, 1976.*
- *Callister W.D, Materials Science and Engineering: An Introduction, Fifth Ed., 2000.*
- *Campanelli S, Bohez E.L.J, Computer aided design, Statistical analysis of the SLA process to improve accuracy, 39, 80-86, 2007.*
- *Cao W, L.L.Hench, Bioactive materials, Ceramics International, (22), 493-507, 1996.*
- *Cehreli M, Sahin S, Akca K, Role of mechanical environment and implant design on bone tissue differentiation; current knowledge and future contexts, Journal of Denstistry, 32, 2004.*
- *Chang Y.L, C.M. Stanford and J.C. Keller, Calcium and phosphate supplementation promotes bone cell mineralisation: implications for hydroxyapatite (HA)-enhanced bone formation, J Biomed Mater Res **5**, pp. 270–278, 2000.*
- *Chartier T, C.Chaput, M.Loiseau, Stereolithography of structural complex ceramic parts, Journ of materials science 37, 3141-3147,2002*
- *Chen C.S., Alonso J.L, Ostuni E, Whitesides G and Ingber D.E. "Cell Shape Provides Global Control of Focal Adhesion Assembly." Biochem. Biophy res. CO. 307, 355–361,2003.*
- *Chu T.M, J.W.Hollaran, S.J.Hollister, S.E.Feinberg, Hydroxyapatite implants with designed internal architecture, Journal of Materials Science: Materials in medicine, (12), 471-478, 2001.*

- *Chu T-M.G, D.G. Orton, S.J. Hollister, S.E. Feinberg and J.W. Halloran, Mechanical and in vivo performance of hydroxyapatite implants with controlled architectures, Biomaterials 23, (5), pp. 1283–1293, 2002.*
- *Chu, T. M. G. and Halloran, J. W., Curing of highly-loaded ceramic suspensions in acrylates, http://msewww.engin.umich.edu, 2002.*
- *Cima L.G , J.P.Vacanti, Tissue eng in cell transplantation using degradable polymer substrates, J.Biomech. Eng. (113), 143.1991.*
- *Clifford A, R.Hill, A.Rafferty, P.Mooney, D.Wood, S.Matsuya, The influence of calcium to phosphate ratio on the nucleation and crystallisation of apatite glass ceramics, 2001.*
- *Coelho and M.H. Fernandes, Human bone cell cultures in biocompatibility testing. Part II: effect of ascorbic acid, beta-glycerophosphate and dexamethasone on osteoblastic differentiation, Biomaterials 21 (11), pp. 1095–1102, 2000.*
- *Cohen S, T.Yoshioka, Controlled delivery systems for proteins based on Poly(lactic/glycolic acid) microspheres, Pharm Res, (8), 713, 1991.*
- *Cooper G.M and Hausman R.E, The Cell: A molecular approach, 3rd edition, 2004.*
- *Cooper J.A., Effects of Cytochalasin and Phalloidin on Actin. J. Cell Biol. 105 (4): 1473-1478, 1987.*
- *Crawford R.H., R H. Barlow, J W. Beaman, J J. Bourell, D L, "Replacement of Biological Parts Using Solid Freeform Fabrication Technologies", ASME Advances in Bioengineering, 36, 1997.*
- *Currey J, 'Mechanical Adaptations of bone', 1984.*
- *Damien C.J, Parsons J.R, Bone graft and bone graft substitutes: a review of current technology, J. Appl. Biomaterials, 2, 187-208, 1990.*
- *Decker C, Photoinitiated crosslinking polymerisation, Prog. Polym. Sci. (21), 593-650, 1996.*
- *Deligianni D.D, Missirlis Y.F, Tanner K.E and Bonfield W., Mechanical behaviour of trabecular bone of the human femoral head in females, Journal of Materials Science: Materials in Medicine, Volume 2, Number 3 / July, 1991.*
- *Delmotte C. Cambier F, Manufacturing of complex ceramic parts by selective curing of pastes, Euroceramics VIII, Proceedings of the 8th ECerS Conference, 2003.*
- *Dufuad O, Corbel S, Stereolithography of PZT ceramic suspensions, Rapid prototyping journal, 8, 89-90, 2002.*
- *Flautre B, M.Descamps, Porous HA ceramic for bone replacement: Role of the pores and interconnections, Journ. of Mater Sci: Materials in Medicine (12), 679-682, 2001.*
- *Freeman C.O, I. M. Brook, A. Johnson, P. V. Hatton, R. G. Hill and K. T. Stanton Crystallization modifies osteoconductivity in an apatite–mullite glass–ceramic, Journal of Materials Science: Materials in Medicine, Volume 14, Number 11, 2003.*
- *Gibson L., The mechanical behaviour of cancellous bone, Journal of Biomechanics 18, pp. 317–328, 1985.*
- *Gibson L.J. and M.F. Ashby, Cellular solids: structure and properties (2nd ed), Pergamon Press, Oxford (1997)*
- *Goodhew P.J, F.J. Humphreys, "Electron Microscopy and Analysis", 2001.*
- *Goodridge R, Ohtsuki C, Kamitakahara M, Wood D, Dalgarno K.W., Fabrication of Bioactive Glass-ceramics by selective laser sintering, Key Engineering Materials, Vol 309-311, 289-292, 2006.*
- *Gough J.E, Julian R. Jones and Larry L. Hench, Nodule formation and mineralisation of human primary osteoblasts cultured on a porous bioactive glass scaffold, Biomaterials Volume 25, Issue 11, May 2004, Pages 2039-2046.*

- *Gregory C.A, D.Prockop, An alizarin red based assay of mineralisation by adherent cells in culture: comparison with CPC extraction, Analytical Biochemistry, 329, 77-84, 2004.*
- *Griffith C, Dautenbach J, McMillian S, Desktop manufacturing – LOM vs. Printing, American Ceramic Society, Ceramic Bulletin, 73, 1994.*
- *Griffith C, Dautenbach J, McMillian S, Solid freeform fabrication of functional ceramic components using LOM technique, SFF symp proc, 1995.*
- *Griffith C, J. Dautenbach, S. McMillin, "Desktop Manufacturing – LOM vs. Pressing," Am. Ceram. Soc. 'Ceram Bulletin' 73, 1994.*
- *Griffith C, J. Dautenbach, S. McMillin, "Solid Freeform Fabrication of Functional Ceramic Components Using Laminated Object Manufacture Technique," SFF Symp. Proc. 1995*
- *Griffith M, Halloran, Scattering of ultraviolet radiation in turbid suspensions, J. Appl Phys, 81(6), 1997.*
- *Griffith M.L and Holloran J.W, Freeform fabrication of ceramics via stereolithography, Journ. Of American Cer Soc, 79 (10), 1996.*
- *Grotte, J.J, Am J Otol. Sep;19(5):565-8., Results of Cavity construction with hydroxyapatite implants after 15 years, 1998.*
- *Guida A, Hill R.G, Evans S, Fluoride release from model glass ionomer cements, Journ of Materials Science: Materials in medicine, 13, 645-649, 2002.*
- *Harris J.M, Introduction to Biotechnical and Biomedical Applications of Poly(ethylene Glycol), Poly(Ethylene Glycol) Chemistry: Biotechnical and Biomedical applications, 1992.*
- *Hayes W. and D.R. Carter, Postyield behavior of subchondral trabecular bone, J Biomed Mater Res 10 (4), pp. 537–544, 1976.*
- *Hench L.L, Bioactive Glasses: Mechanisms of Bioactive bonding, www.bg.ic.ac.uk/Lectures/Hench/bioglass/cal3.htm*
- *Hench L.L, Bioactive Glasses: theory and clinical applications, Bioceramics 7, 3-14, 1994.*
- *Hench L.L, Bioactive Materials: The potential for tissue regeneration, Founders award society for Biomaterials, 24th Annual meeting, 511-518, 1998.*
- *Hench L.L, Bioceramics: From concept to clinic. J. Am.Ceram.Soc. (74)7, 1487-1510, 1991.*
- *Hench L.L, R.J.Splinter, W.C.Allen, Bonding mechanisms at the interface of ceramic prosthetic materials, Journal of Biomed. Mates. Res, (2) [1], 117-141, 1972.*
- *Hill R.G, M.Patel, D.J.Wood, Preliminary Studies on castable apatite-mullite glass ceramics, In Bioceramics 4, edited by W.Bonefield, G.W.Hastings and K.E. Tanner, 79-86, 1991.*
- *Hing K.A, Best S.M, Bonefield W, Journal of materials Science, Materials in medicine, 30, 1999.*
- *Hoffman A, Applications of synthetic polymeric biomaterials in medicine and biotechnology, Polymeric biomaterials, 1986.*
- *Holand W, Beall G, Glass-Ceramic Technology, The American Ceramic Society, 2002.*
- *Howlett CR, Evans MDM, Walsh WR, Johnson G, Steele JG. Mechanism of initial attachment of cells derived from human biodegradable polymer/HA composites 485 bone to commonly used prosthetic materials during cell culture. Biomaterials 1994;3:213–222.*
- *http://mse.iastate.edu/microscopy/path.html*
- *http://web.mit.edu/tdp/www/whatis3dp.html*
- *http://www.bris.ac.uk/depts/Synaptic/info/imaging/figs/fluomicro.gif).*

- *http://www.malvern.com/ProcessEng/images/diagrams.gif*
- *http://www.matscieng.sunysb.edu/Berndt/Berndt-NP42/Slide078.JPG*
- *http://www.umanitoba.ca/faculties/science/biological_sciences/lab13/images/bonex40.jpeg*
- *Hutmacher D.W, Scaffold design and fabrication technologies for engineering tissues-state of the art and future perspectives, Journ. of Biomat. Sci. Polymer Edition (12)1, 107-124, 2001.*
- *Ishaug-Riley S.L, Crane G.M, Mikos A.G, Bone formation by marrow stromal osteoblasts transplantation using poly (D,L-lactic co-glyceric acid) foams implanted into rat mesentry, J.Biomed Mater Res, 36, 1-8, 1997.*
- *Jakubauskas H.L and E. I. DuPont de Nemours & Co, Use of A-B block polymers as dispersant for non-aqueous coating systems, 3(2), 1997.*
- *Jallot E, H.Benhayoune, L.Kilian, J.L.Irigaray, Surface and Interface Analysis, STEM and EDXS characterisation of physiochemical reactions at the interface between a bioglass coating and bone, (29), 314-320, 2000.*
- *Janney M.A, Gelcasting, In Rahaman Edition, The handbook of ceramic engineering, 1998.*
- *Jarcho M, Calcium phosphate ceramics as hard tissue prosthesis, Clin Orthop Rel Res, 1981.*
- *Jones D.W and Rizkalla A.S, Fracture toughness of bioglass™/ceramic systems, Bioceramic materials and applications (2nd ed.),Ceramic transactions, 63, 87–91, 1995.*
- *Jones J.R, L.L.Hench, Biomedical materials for new millennium: perspective on the future, Materials Science and Technology, (17), 891, 2001.*
- *Jones J.R, Olga Tsigkou, Emily E. Coates, Molly M. Stevens, Julia M. Polak and Larry L. Hench, Extracellular matrix formation and mineralization on a phosphate-free porous bioactive glass scaffold using primary human osteoblast (HOB) cells, Biomaterials, Volume 28, Issue 9, March 2007, Pages 1653-1663.*
- *Kalita S.J, S. Bose, H.L. Hosick and A. Bandyopadhyay, Development of controlled porosity polymer–ceramic composite scaffolds via fused deposition modeling, Mater Sci Eng, 23 (5), pp. 611–620,2003.*
- *Katz E.P and Shi Tung Li, 'Structure and function of bone collagen fibres', Journal of molecular biology (80), 1-15, 1973.*
- *Katz J, Developments in medical polymers for biomaterials applications, Biomaterials, 2001.*
- *Kawahara H, Kawahara D, Hayakawa M, Osseointegration under Immediate Loading: Biomechanical Stress-Strain and Bone Formation-Resorption, Implant Dentistry, 12(1):61-68, 2003.*
- *Keene D.R, L.Y.Sakai and R.E.Burgeson, Human bone contains type III collagen, type IV collagen and fibrillin: Type III collagen is present on specific fibres that may mediate attachment of tendons, ligaments and periosteum to calcined bone cortex, J. Histochem.Cytochem. (39), 59-69, 1991.*
- *Klawitter J.J, S.F.Hulbert, Applications of Porous Ceramics for the attachment of Load bearing Orthopaedic applications, Journal of Biomed. Mater.Res.Symp, (2), 161, 1971.*
- *Klosterman D, Chartoff R, Osborne N, Rodrigues S, Curved layer LOM of ceramics and composites, Solid freeform fabrication symposium proceedings, University of Texas,671-680, 1998.*

- *Kneser U, P.M.Kaufmann, Hepatocyte transplantation using biodegradable matrices in ascorbic acid-deficient rats: comparison with heterotopically transplanted liver grafts, Transplantation, 71(9):1226-31, 2001.*
- *Kodama H, Automatic method of fabricating 3D plastic model with photohardening polymer, Review of Scientific Instruments, 1981.*
- *Kohn D.G, Sarmadadi M, Effects of pH on human bone marrow stromal cells in vitro: Implications for tissue engineering of bone, Journ Biomed Mater Res, 60, 292-299, 2002.*
- *Kokubo T, A/W Glass-Ceramic: Processing and Properties, in An Introduction to Bioceramics, Edited by Hench and Wilson, 75-88, 1993.*
- *Kokubo T, M.Shigematsu, Y.Nagashima, M.Tashiro, Apatite and Wollastonite-Containing glass-ceramics for prosthetic application, Bull. Inst. Chem. Res, Kyoto University, (60), 260-268, 1982.*
- *Lee M, Dunn J and Benjamin W, Scaffold fabrication by indirect three-dimensional printing, Biomaterials, 26 (20), 4281-4289, 2005.*
- *Levy R.A, Chu T.G.M, Holloran J.W. Hollister S, CT generated porous hydroxyapatite orbital floor prosthesis as a prototype bioimplant, American Journ of Neurosadiol, 18, 1522-1525, 1997.*
- *Limpanuphap S, B.Derby, Manufacture of biomaterials by a novel printing process, Journal of materials Science: Materials in Medicine (13), 1163-1166, 2002.*
- *Limpanuphap S, Manufacture of Biomaterials by a Novel printing process, PhD thesis for University of Manchester, 2004.*
- *Liu C, Xia Z, Czernuszka J.T., Design and Development of Three-Dimensional Scaffolds for Tissue Engineering, Pharmaceutical Engineering, Vol 85, 1051-1064, 2007.*
- *Lodish, Berk, Matsudaira, Kaiser, Krieger, Scott, Zipursky, Darnell, Molecular Cell Biology Fifth Edition Lodish pg. 821, 823 2004.*
- *Lowenstein H.A, Minerals formed by organisms Science (211), 1126-1131, 1981.*
- *Lu L, A.G.Mikos, The importance of new processing techniques in tissue engineering, MRS Bull, Nov 29, 1996.*
- *Maquet V, A.R.Boccaccini, L.Pravata, Porous poly(α-hydroxyacid)/Bioglass composite scaffolds for bone tissue engineering: preparation and in vitro characterisation, Biomaterials 2003.*
- *Martin R.B, Bone as a ceramic composite material, Mat Sci. Forum, 293, 5-16, 1999.*
- *Martini, 'Fundamentals of anatomy and physiology – 4th Edition', 1998.*
- *Maskill S.A, 'Micro-mechanisms of failure in natural composite materials', PhD thesis, University of Leeds,1999.*
- *Matsuda T, Mizutani M, Liquid acrylate-endcapped biodegradable PCL, Computer aided sterelithographic microarchitectural surface photocontructs, J.Biomed Mater Res, 62, 395-403, 2002.*
- *McAteer, J.A, Davis J, Basic cell culture technique and maintainence of cell lines, Basic Cell Culture, 2nd Edition, 2002.*
- *McCalden R.W, J.A.McGeogh, M.B.Baker, J.Bone.Jt.Surg., (75A), 1193, 1993.*
- *McElhaney J.H, Journal of Applied Physiology, (21), 1231-1236,1966.*
- *McMillian P.W, Glass-Ceramics, 2nd Edition, 1979.*
- *Mikos A.G, Preparation and characterisation of poly(L-lactic acid) foams, Polymer, (35)5, 1068-1077,1994.*

- *Mooney D.J, Baldwin D.F, Langer R.C, Novel approach to fabricate porous sponges of poly (D,L-lactic co-glyceric acid) without the use of organic solvents, Biomaterials 17, 1417-1422, 1996.*
- *Mooney D.J, C.L.Mazzoni, C.Breuer, J.P.Vacanti, R.Langer, Stabilised PLGA fibre based tubes for tissue engineering, Biomaterials, (21), 2529-2543, 2000.*
- *Nelson J.C, N. K. Vail, J. W. Barlow, J. J. Beaman, D. L. Bourell, H. L. Marcus, "Selective Laser Sintering of Polymer Coated SiC Powder," Ind. Eng. Chem. Res., 34, [5], 1995.*
- *NIH consensus conference: Total hip replacement. NIH Consensus Development Panel on Total Hip Replacement, Vol. 273 (24), 1995.*
- *O'Brien J, I. Wilson, Investigation of the Alamar Blue (resazurin) fluorescent dye for the assessment of mammalian cell cytotoxicity, Eur. J. Biochem, 267, 5421-546, 2000.*
- *Ohgushi, Y. Dohi, T. Katuda, S. Tamai, S. Tabata and Y. Suwa, In vitro bone formation by rat marrow cell culture, J Biomed Mater Res 32 (3), pp. 333–340, 1996.*
- *Okano J, Mechanism of cell attachment from temperature modulated hydrophilic and hydrophobic polymer surfaces, Biomaterials, 16 (4), 297-303, 1995.*
- *Omatete O.O, M.A.Janney, R.A.Strehlow, Gelcasting – A new ceramic forming process, Ceramic bulletin, (70)10, 1641-1649, 1991.*
- *Park J.B and R.S.Lakes, 'Biomaterials: An Introduction – 2nd Edition', 1992.*
- *Paul L.C, Chronic rejection of organ allografts: Magnitude of the problem, Transplantation Proceedings, 2404-2406, 1992.*
- *Piekarski K, 'Analysis of bone as a composite material', Int.J.Eng.Sci (11), 557, 1973*
- *Piekarski K, Journal of Applied physics, (41), 215-223, 1970.*
- *Pierre S.J, J. C. Thies, A. Dureault, N. R. Cameron, J. C. M. van Hest, N. Carette, T. Michon, R. Weberskirch, Covalent Enzyme Immobilization onto Photopolymerized Highly Porous Monoliths, Advanced Materials, Vol 18 (14), 1822-1826, 2006.*
- *Private communication with K.T.Stanton.*
- *Rafferty A, A.Clifford, R.Hill, D.Wood, Influence of Fluorine content in apatite-mullite glass-ceramics, J.Am.Ceram.Soc., (83)11, 2833-38, 2000.*
- *Ramay H.R, M.Zhang, Preparation of porous hydroxyapatite scaffolds by combination of the gelcasting and polymer sponge methods, Biomaterials (24), 3293-3302, 2003.*
- *Ratner B.D, A.S.Hoffman, F.J.Schoen, J.E.Lemons, Biomaterials Science : An Introduction to materials in medicine, Elsevier Science, ISBN 0-12-582461-0, 1996.*
- *Rawlings R.D, Bioactive Glasses and Glass-Ceramics, Clinical Materials,(14),155-179,1993.*
- *Riden K, Worrall SF, Corrigan AM. UK National Third Molar project: the initial report. British Journal of Oral & Maxillofacial Surgery 36: 14-18, 1998.*
- *Rilley D.T, A.H.Burstein, V.H.Frankel, Journal of Biomechanics, (7), 271-275, 1974.*
- *Rimmer S, C. Johnson, B. Zhao, J.Collier, L. Gilmore, S. Sabnis, P. Wyman, C. Sammon, N. J. Fullwood and S. MacNeil, Epithelialization of hydrogels achieved by amine functionalization and co-culture with stromal cells, Biomaterials, Volume 28(35), 5319-5331, 2007.*
- *Rizzi S.C, Heath D.J, Biodegradable polymer/hydroxyapatite composites: Surface analysis and initial attachment of human osteoblasts, Journal of Biomedical Materials ResearchVolume 55, Issue 4 , Pages 475 – 486,1999.*
- *Sachlos, E., Czernuszka, J.T., "Making tissue engineering scaffolds work. Review on the application of solid freeform fabrication technology to the production of tissue engineering scaffolds", European Cells and Materials, Vol. 5 pp.29-40, 2003.*
- *Sarikaya M, 'Biomimetics: Materials fabrication through biology', Proc.of Nat. Amer.Studies (96), 14183-14185,1999.*

- *Schiller P.C, G. D'Ippolito, W. Balkan, B.A. Roos and G.A. Howard, Gap-junctional communication is required for the maturation process of osteoblastic cells in culture, Bone 28 (4), pp. 362–369, 2001.*
- *Specchia N, Greco F, Effect of hydroxyapatite porosity on growth and differentiation of human osteoblast-like cells, Journal of Materials Science, Volume 37, Number 3, 1 February 2002, pp. 577-584.*
- *Stand Z, Role of the glass phase in bioactive glass-ceramics, Biomaterials (13)5, 1992.*
- *Stanulis-Preger, B.M, Cellular senescence revisted: A review, Mech Ageing Dev, 38, 1-48, 1987.*
- *Stewart D.R, Concepts of glass-cermaics, In Pye, Stevens, La Course, Introduction to glass science, New York: Plenum Press: 237-271.*
- *Subramanion K, N. K. Vail, J. W. Barlow, H. L. Marcus, "Selective Laser Sintering of Alumina with Polymer Binders," J. Rapid Prototyping, 1, [2], 1995.*
- *Swanson S.A.V, 'Biomechanical Characteristics of bone', Adv.Bio.Eng (1), 137-181, 1971.*
- *Tellis B.C, Szivek JA, Bliss CL, Margolis DS, Vaidyanathan RK, Calvert P. Trabecular scaffolds created using micro ct guided fused deposition modeling, Journal Materials Science and Engineering, Part C. April, 2006.*
- *Thompson D.A and D.C.Boyd, "Glass Ceramics", Kirk-Othmer Encyclopedia of Chemical Technology, Vol. 11, 3rd Edn (Wiley, New York, 1980) p. 809*
- *Trainer M, The Effects of Particle Shape on Particle Size Resolution using Angular Scattering Measurements, Pittsburgh Conference, 2001.*
- *Verrier S, J.J.Blaker, V.Maquet, L.Hench, PDLLA/Bioglass composites for soft tissue and hard tissue engineering: an in vitro cell biology assessment, Biomaterials (25), 3013-3021, 2004.*
- *Vert M, SM Li, G Spenlehauer, P Guerin - Journal of Materials Science: Materials in Medicine, Recent advances in bone tissue engineering, 1992.*
- *Vincent J.F, 'Structural Biomaterials', 1982.*
- *Vrouwenvelder W.C.A, Journal of Biomedical Materials Res, (27), 465-475, 1993.*
- *Wainwright, Biggs, Currey, Gosline, 'Mechanical Design in Organisms', 1976.*
- *Wang M, L.L.Hench, W.Bonfield, Bioglass/high density polyethylene composite for soft tissue applications: Preparations and evaluation, 1998.*
- *Weiner S, Traub W, Organisation of hydroxyapatite crystals within collagen fibres, Lett 206, 262-266, 1986.*
- *Whang K, E.Healy, Engineering bone regeneration with bioabsorbable scaffolds with novel microarchitecture, Tissue Eng (5), 679-682, 2001.*
- *Wiener S, Wagner H.D, The material bone: structure-mechanical function relations, The Annual review of materials science, 28, 1998.*
- *Williams C, J. Elisseeff, Variable cytocompatibility of six cell lines with photoinitiators used for polymerizing hydrogels and cell encapsulation, Biomaterials, 26, 1211-1218, 2005.*
- *Williamson M, Black R, PCL–PU composite vascular scaffold production for vascular tissue engineering: Attachment, proliferation and bioactivity of human vascular endothelial cells, Biomaterials, 19, 2006.*
- *Wilson J, L.L.Hench, Introduction to Bioceramics, 1993.*
- *Wilson L.W, L.L.Hench, Surface-Active Biomaterials, Science (226), 630, 1984.*
- *Woodard J.R., Amanda J. Hilldore, Sheeny K. Lan, C.J. Park, Abby W. Morgan, Jo Ann C. Eurell, Sherrie G. Clark, Matthew B. Wheeler, Russell D. Jamison and Amy J. Wagoner Johnson, The mechanical properties and osteoconductivity of hydroxyapatite*

bone scaffolds with multi-scale porosity, Biomaterials Volume 28, Issue 1, Pages 45-54, 2007.

- *Wright T.M, W.C.Hayes, Fracture mechanics parameters for compact bone –effects of density and specimen thickness, Journal of Biomechanics, 10(7), 419-430, 1977.*
- *Wu K.C, Solomon M.J, Halloran, Prediction of ceramic Stereolithography resin sensitivity from theory and measurement of diffusive photon transport, Journal of Applied Physics, 98, 2005.*
- *Yanpeng J, Zonghua L, Changren Z and Fuzhai C,Formation of bone-like apatite on poly(L-lactide) to improve osteoblast-like compatibility in vitro and in vivo , Frontiers of material science, Vol 1(2), 2007.*
- *Yaszemski M.J, R.G.Payne, W.C.Hayes, R.Langer, A.G.Mikos, Evolution of bone transplantation: molecular, cellular and tissue strategies to engineer human bone, Biomaterials (17), 175-185, 1996.*
- *Yeong W.L and Lee M, Indirect fabrication of collagen scaffold based on inkjet printing techniques, Rapid prototyping journal, 12(4), 2006.*
- *Yetkin H, Atik OS, Sener E, Altun NS, Cila E. Biodegradable implants for fixation of fractures. Tur J Arthrop Arthros Surg 4(6): 26-29, 1993.*
- *Yetkin H, Senkoylu A, Biodegradable Implants in Orthopaedics and Traumatology, Turk J Med Sci, 30,297–301, 2000.*
- *Zakaria F.A, Development of Carbonated Apatite for Possible Biomedical Purposes, SIRIM link, 2007.*
- *Zhou D.H, Chen C, Parametric process optimization to improve the accuracy of rapid prototyped stereolithography parts, International journal of machine tools and manufacture, 40, 1-17, 1999.*

Appendix I

Surface Area of CER 400 scaffold

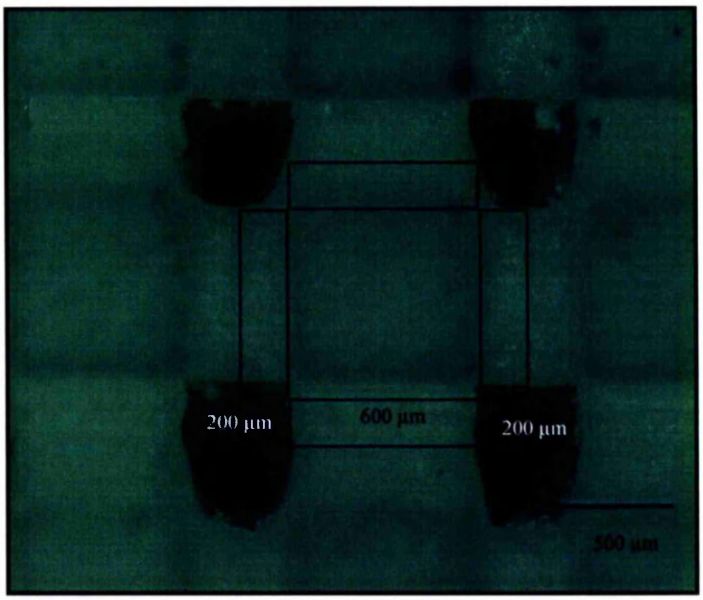

Dimensions of scaffold
= 6mm x 7.2mm x 7.2mm

Unit cell is shown in the image
Struts – 600 x 600 x 600 µm

There are 6 struts and each strut has 4 faces visible for cell attachment

Total number of faces = 6 x 4 = 24

$$\text{Area} = 6 \times 4 \times d\,(a-d)^2$$

where,
a = full length = 1000µm
d = one strut thickness = 600µm

$$= 6 \times 4 \times (6 \times 10\text{-}4)\,(1 \times 10\text{-}3 - 6 \times 10\text{-}4)^2$$

= 2.88 x 10-6 m2

$$\text{Volume} = 6 \times d2 \times (a-d)^2 + d3$$

$$= 6\,(6 \times 10\text{-}4)2 \times 2 \times 10\text{-}4 + (6 \times 10\text{-}4)3$$

$$= 6.48 \times 10\text{-}10\ m3$$

SA : Volume ratio

$$= \frac{2.88 \times 10\text{-}6}{6.48 \times 10\text{-}10} = 4444$$

Total volume of scaffold = (6 x 10-3) (7.2 x 10-3)2
= 3.11 x 10-7 m3

Total surface area scaffold = SA x Total volume
V
= 3.11 x 10-7 x 4444

= 1.38 x 10-3 m2

Total no. of cells seeded = 80,000
No. of cells per unit area = 80000 = 57.88 x 106 cells/m2
1.38 x 10-3
= 80000 = 5.797 x 10-5 cells/μm2
1.38 x 109

There is 1 cell every 1 = 17250 μm2
5.797 x 10-5

Which means √17250 = 131 μm

Therefore meaning there is 1 cell every 131 μm.

Surface Area of CER 600 scaffold

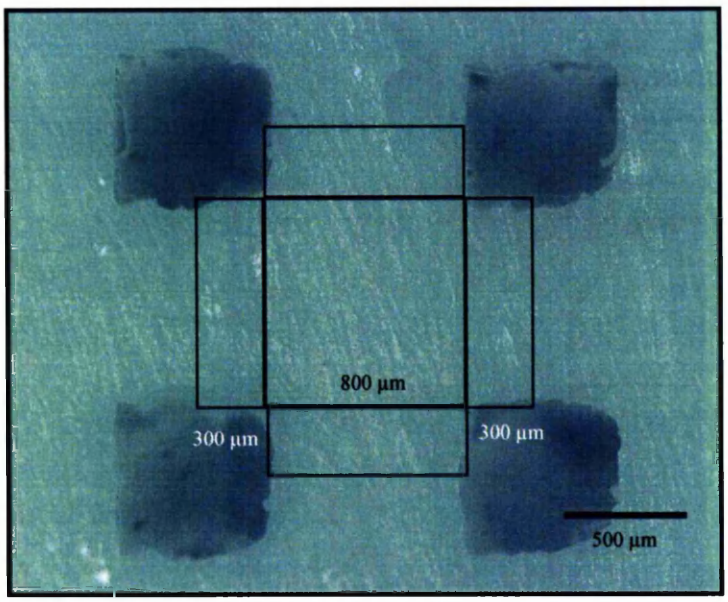

Dimensions of scaffold
= 6mm x 7.2mm x 7.2mm

Unit Cell is shown in the image
Struts - 800 x 800 x 800 µm

There are 6 struts and each 4 faces visible therefore there are 24 faces.

Area = 6 x 4 x d (a-d)
2
= 6 x 4 x (8 x 10-4) x (1.4 x 10-3 – 8 x 10-7)
2
= 5.76 x 10-6 m2

Volume = 6 x d2 x (a-d) + d3
2
= 1.664 x 10-9 m3

SA: Volume ratio

= 5.76 x 10-6 = 3461
1.664 x 10-9

Total volume of scaffold = 3.11 x 10-7 m3

Total surface area of scaffold = SA x Total Volume
V
= 3.11 x 10-7 x 3461

= 1.07 x 10-3 m2

Total number of cells seeded = 80,000
Therefore number of cells per unit area = 80000 = 7.48 x 10-5 cells / µm2
1.07 x 10-9

Therefore there is 1 cell every $\frac{1}{7.48 \times 10\text{-}5} = 13375$

$\sqrt{13375} = 116\mu m$

Therefore meaning that there is 1 cell present every 116μm.